



Freddy Ignacio Rojas Rodriguez

**Real-time aging of ethylene-propylene-diene rubber inside
jacket layer of Electrical Submersible Pump Cables
under actual operating conditions**

Dissertação de Mestrado

Dissertação apresentada como requisito parcial para obtenção do grau de Mestre pelo Programa de Pós-graduação em Engenharia de Materiais e de Processos Químicos e Metalúrgicos, do Departamento de Engenharia Química e de Materiais da PUC-RIO.

Orientador: Prof. Bojan Marinkovic

Rio de Janeiro
December 2020

PONTIFÍCIA UNIVERSIDADE CATÓLICA
DO RIO DE JANEIRO



Freddy Ignacio Rojas Rodriguez

**Real-time aging of ethylene-propylene-diene rubber inside
jacket layer of Electrical Submersible Pump Cables
under actual operating conditions**

Disertation presented to the Programa de Pós-graduação em Engenharia de Materiais e de Processos Químicos e Metalúrgicos of PUC-Rio in partial fulfillment of the degree of Mestre em Engenharia de Materiais e de Processos Químicos e Metalúrgicos. Approved by the Examination Committee.

Prof. Bojan Marinkovic

Advisor

Departamento de Engenharia Química e de Materiais – PUC-Rio

Prof. José Roberto Moraes d'Almeida

Departamento de Engenharia Química e de Materiais – PUC-Rio

Profa. Paula Mendes Jardim

Departamento de Engenharia Metalúrgica e de Materiais UFRJ

Prof. Marcio da Silveira Carvalho

Coordenador Setorial do Centro

Técnico Científico – PUC-Rio

Rio de Janeiro, December 17th, 2020.

All rights reserved.

Freddy Ignacio Rojas Rodriguez

Degree in chemistry at Universidad Central de Venezuela (Caracas– Venezuela, 2010). He has experience in in evaluating polymeric matrix composites through kinetic analysis and mechanical properties.

Bibliographic data

Freddy Ignacio Rojas Rodriguez

Real-time aging of ethylene-propylene-diene rubber inside jacket layer of Electrical Submersible Pump Cables under actual operating conditions / Freddy Ignacio Rojas Rodriguez; advisor: Bojan Marinkovic.–Rio de Janeiro: PUC-Rio, Departamento de Engenharia Química e de Materiais, 2020

278 f.: il. (color.); 30 cm

Tese (mestrado)– Pontifícia Universidade Católica do Rio de Janeiro, Departamento de Engenharia Química e de Materiais, 2020.

Inclui bibliografia

1. Engenharia Química e de Materiais –Teses. 2. Envelhecimento EPDM in real time. 3. Energia de ativação aparente pelo método CKA-ic I. Marinkovic, Bojan. II. Pontifícia Universidade Católica do Rio de Janeiro. Departamento de Engenharia Química e de Materiais. III. Título.

CCD: 620.11

To my daughter Jennifer.

Acknowledgments

To my advisor, Professor Bojan Marinkovic, for the care, guidance, kindness and time dedicated to our project. I am grateful for your valuable teachings in the classroom. Thank you for trusting and for the incentive to continue growing personally and professionally. My respect and admiration for a great person.

To our research group. To Anja Dosen, Juliana Viol, Yuri dos Santos for their patience with the characterization. To Lucas Almeida, Alison Madrid, Tamires Martinhão, Esteban Moreno and Fabián Orozco for their great teamwork and for their great friendship.

To the Technological Institute of PUC-RIO (ITUC) especially for the Technical Manager Eng. Mec. M. Sc Adrian Giassone for the contribution in mechanical tests.

To my friends who are a family of the Aqueous Solutions Injection Expertise (PISA), for listening to my request for help to get out of a very difficult situation in my native country. To Jose Manuel Alvarez, Amaury Marin, Larry Chacon, Caroline Romero, Arjan Kamp, Elena Escobar, Reinaldo Angulo, Angel Rico, Maria Busolo, Eduardo Manrique, Clara Hernandez, Alfredo Pérez, Raul Moreno, Marisol Garcia, Brigida Meza, Mary Pérez and many others who contributed to my trip to Brazil. To José Manuel's children who helped raise funds with their friends for my original trip.

To Maria Luisa Arnal and Evis Penott for their friendship and encouragement in the GPUSB and USB.

To EDQM, its staff and group of teachers who have helped me. In to her Secretary of Post Graduate Carmem Façanha, who dedicates her life to her work.

To Alison Madrid who in these times of isolation became my company across the distance, showing me understanding. Unconditional love.

To Graciela and my daughter Jennifer who are striving to support me at all times. A great love.

This study was financed in part by the Coordenação de Aperfeiçoamento de Pessoal de Nível Superior – Brasil (CAPES) – Finance Code 001.

To Equinor Brasil Energia Ltda. through contract 21123-3 and Agência Nacional de Petróleo (ANP) for financing and providing the study samples.

Abstract

Rojas Rodriguez, Freddy Ignacio; Marinkovic, Bojan (advisor). Real-time aging of ethylene-propylene-diene rubber inside jacket layer of Electrical Submersible Pump Cables under actual operating conditions. Rio de Janeiro, 2020. 278p. Dissertação de mestrado –Departamento de Engenharia Química e de Materiais, Pontifícia Universidade Católica do Rio de Janeiro

The effect of aging in real time on the mechanical, chemical and kinetic properties of copolymer ethylene propylene diene monomer rubber (EPDM) was quantified, after being exposed to real operating conditions in the artificial petroleum lift system, from the Peregrino field. (managed by Equinor Brasil Ltda.). The EPDM rubber was collected from part of the mechanical protection cover (Jacket) of the electrical supply cables of the electro-submersible pumps (ESP). The study involves samples from 0, 2 to 4.8 years old and with depths ranging from 0, 760 to 2170 m below sea level. The aging was followed by studies of infrared spectroscopy techniques by Fourier transform (FTIR) assisted with attenuated total reflection (ATR), SEM electron microscope, along with energy dispersion X ray spectrometer (EDX), simultaneous thermal analyzer (STA), reticulation fraction measurement, hardness (Shore D scale), uniaxial traction tests and adsorption tests in the protection fluid (Parker-fluid+safe-Scan). The stability of EPDM rubber was studied by non-isothermal methods such as: Kissinger-Murray-White (KMW), Ozawa-Flynn-Wall (OFW), Friedman (FR), combined kinetic analysis (CKA) and correction of the combined kinetics analysis by isoconversion (CKA-ic). A 5 % oscillation in the apparent activation energy ($E=248$ kJ/mol) during the thermal degradation of the material in N_2 , shows a reaction that produced a reaction order ($n=0.93$), a pre-exponential factor ($A=\ln(40 /\text{min}^{-1})$) and indicates that the material does not suffer hydrolytic attack or oxidation degradation observed in aging tests in the presence of water and compression. On the other hand, the properties of the uniaxial tensile test show sensitivity to the depth of the samples, which may well indicate degradation of amorphous areas of EPDM, a product of high temperatures and pressures in the deposit.

Keywords

Real-time aging EPDM, Degradation Activation Energy, Correction of the isoconversion CKA method (CKA-ic).

Resumo

Rojas Rodriguez, Freddy Ignacio; Marinkovic, Bojan. **Envelhecimento em tempo real da borracha de etileno-propileno-dieno dentro da camada de revestimento dos cabos das bomba eletro-submersível sob condições operacionais reais.** Rio de Janeiro, 2020. 278p. Dissertação de mestrado – Departamento de Engenharia Química e de Materiais, Pontifícia Universidade Católica do Rio de Janeiro

O efeito do envelhecimento em tempo real nas propriedades mecânicas, químicas e cinéticas da borracha de copolímero de copolímero etileno-propileno-dieno não conjugado (EPDM) foi quantificado, após ser exposto a condições reais de operação no sistema artificial de elevação de petróleo, do campo de Peregrino (administrado pela Equinor Brasil Ltda.). A borracha EPDM foi coletada de parte da camada de proteção mecânica (Jacket) dos cabos de alimentação elétrica das bombas eletro-submersíveis (ESP). O estudo envolve amostras de 0, 2 a 4.8 anos e com profundidades que variam de 0, 760 a 2170 m abaixo do nível do mar. O envelhecimento foi acompanhado por estudos de técnicas de espectroscopia de infravermelho por transformada de Fourier (FTIR) assistida por reflexão total atenuada (ATR), microscópio eletrônico de MEV, juntamente com espectrômetro de dispersão de energia (EDX), analisador térmico simultâneo (STA), medição da fração de reticulação, dureza (escala Shore D), testes de tração uniaxial e testes de adsorção no fluido de proteção (Parker-fluido+safe-Scan). A estabilidade da borracha EPDM foi estudada por métodos não isotérmicos como: Kissinger-Murray-White (KMW), Ozawa-Flynn-Wall (OFW), Friedman (FR), análise cinética combinada (CKA) e correção da cinética combinada análise por isoconversão (CKA-ic). Uma oscilação de 5 % na energia de ativação aparente ($E=248$ kJ/mol) durante a degradação térmica do material em N_2 , mostra uma reação que produziu uma ordem de reação ($n=0.93$), um fator preexponencial ($A=\ln(40/\text{min}^{-1})$) e indica que o material não sofre ataque hidrolítico ou degradação por oxidação, comparando com os observada nos testes de envelhecimento na presença de água e compressão. Por outro lado, as propriedades do teste de tração uniaxial mostram sensibilidade à profundidade de as amostras, o que pode muito

bem indicar degradação de áreas amorfas de EPDM, produto de altas temperaturas e pressões no depósito.

Palavras-chave

Envelhecimento em tempo real EPDM, Energia de Ativação de Degradação, Correção do método de isoconversão CKA (CKA-ic).

Tables of contents

1 Introduction	1
2 Literature review	5
2.1. Copolymer of "ethylene + propylene + unconjugated diene"	5
2.2. Aging	8
2.3. Differential thermal analysis (DTA)	10
2.4. Kinetic fundamentals	12
2.4.1. Rate of reaction	13
2.4.2. Isoconversion approach	15
2.4.3. Free Kinetic Model (MFK)	17
2.4.3.1. Kissinger model (KMW)	17
2.4.3.2. Ozawa-Flynn-Wall model (OFW)	18
2.4.3.3. Friedman model (FR)	19
2.4.4. Combined Kinetic Analysis model (CKA)	20
2.4.4.1. Combined Kinetic Analysis by Isoconversion model (CKA-i)	21
2.5. Uniaxial Tensile Tests	21
2.6. Shore Hardness	22
2.7. Adsorption	23
3 Objectives	24
3.1. General Objective	24
3.2. Specific objectives	24
4 Materials and methods	26
4.1. Studied material	26
4.2. Solvent and fluids	27
4.3. Elastomer characterization	28
4.3.1. Fourier Transform Infrared (FTIR) spectroscopy	28
4.3.1.1. Rubber samples for FTIR	28
4.3.1.2. Waste samples from STA analyzed by FTIR	29
4.3.2. Simultaneous Thermal Analyzer (STA)	29

4.3.2.1. Thermo-degradation up to 570 °C	29
4.3.2.2. Thermo-degradation up to 900 °C	29
4.3.3. Shore D Hardness	30
4.3.3.1. Shore D hardness test samples	30
4.3.4. Tensile test	31
4.3.4.1. Uniaxial Tensile Test Samples	32
4.3.5. Scanning Electron Microscope (SEM) coupled with energy dispersive X-ray spectrometer (EDX)	32
4.3.6. Crosslinked content	33
4.3.7. Absorption in Packer-Fluid+Safe-Scan	34
4.3.7.1. Absorption samples	34
5 Results and discussions	35
5.1. FTIR	35
5.1.1. Classification of Rubber samples by FTIR	35
5.1.2. Identification of the polymer in the Rubber samples by FTIR	37
5.1.3. FTIR Interpretation of Group 1	39
5.1.3.1. Additional evidence to verify the identification of Metakaolin	41
5.1.4. FTIR Interpretation of Group 2	42
5.1.4.1. Additional evidence to verify identification of Kaolin	43
5.1.5. FTIR aging study	44
5.2. STA of the Rubbers	46
5.2.1. Thermo-degradation up to 570 °C	46
5.2.2. Thermo-degradation up to 900 °C	48
5.3. Preselection/refinement of data for the non-isothermal kinetic study of the elastomer	50
5.3.1. Kissinger model (KMW)	53
5.3.2. Ozawa-Flynn-Wall (OFW) model	54
5.3.3. Friedman model (FR)	59
5.3.4. Combined Kinetic Analysis model (CKA)	63
5.3.4.1. Reaction order for CKA	64
5.3.4.2. Activation energy by CKA	67
5.3.4.3. Application of the isoconversion principle on the CKA method (CKA-i)	69

5.3.4.4. Correction of the isoconversion CKA method (CKA-ic)	71
5.4. Kinetic triplet	76
5.5. Mechanical proprieties	82
5.5.1. Shore D Hardness	82
5.5.2. Tensile test	84
5.6. Scanning Electron Microscope (SEM) coupled with energy dispersive X-ray spectrometer (EDX)	88
5.7. Crosslinked content	89
5.8. Absorption of Packer-Fluid+Safe-Scan	91
6 Conclusions and future works	93
6.1. Conclusions	93
6.2. Future works	94
7 References	96

List of Figures

Figure 1 Peregrino Field, Level 2, Dual Lateral Completion. Modified image from Ranjeva et al.,[7] Multilateral level-5 dual long horizontal openhole gravel pack completion on the peregrino field, Proc. - SPE Annu. Tech. Conf. Exhib. 4 (2014) 2964–2979.....	3
Figure 2 Cable ESP Baker Hughes Incorporated.....	4
Figure 3 Molecular structures of EPDM whit different diene a) 2-ethylidene-5-norbornene (ENB), b) dicyclopentadiene (DCPD), c) 5-vinyl-2-norbornene (VNB).	5
Figure 4 Schematic representation of Shore hardness measurement.....	23
Figure 5 a) Digimess equipment for Shore D hardness. b) Schematic description of the tip identification image adapted from ASTM D2240 "Standard Test Method for Rubber Property-Durometer Hardness" [67]..	30
Figure 6 Shore D hardness test samples.	31
Figure 7 Universal testing machine Instron 5500R.....	31
Figure 8 Nominal shape and dimensions of the test bodies for uniaxial tensile tests with it dimensions: a=18, b= 110 and c=4 mm.	32
Figure 9 SEM TM3000 da Hitachi.	33
Figure 10 Apparatus used for cross-linkages determination through ASTM D2765 [71].....	33
Figure 11 Absorption test bodies shaped to a 50 mm long cylinder.	34
Figure 12 FTIR spectra for Rubber I, II, III and VI samples. Group 1 (Appendix B1 to B3 and B6).....	36
Figure 13 FTIR spectra for Rubber IV and V samples Group 2 (Appendix B4 to B5).....	36
Figure 14 FTIR spectra of Rubber I (Group 1) and Rubber V (Group 2). ..	37
Figure 15 Spectra of ATR Rubber I (Group 1) and Rubber V (Group 2). The signs in blue color highlight the EPDM bands.	39
Figure 16 FTIR spectra from Rubber Waste I and VI after thermal treatment at 900 °C under synthetic air condition.....	41
Figure 17 FTIR of STA waste for Rubber IV and V samples (Group 2)....	44

Figure 18 Amplification of the ATR for Rubber I and II. The figure shows the calculation of carbonyl index group ($IC_{1455/1740}$) using the peaks at 1740 cm^{-1} for carbonyl and 1455 cm^{-1} for EPDM.	45
Figure 19 TGA and DTG for Rubber I at $20\text{ }^{\circ}\text{C min}^{-1}$ with N_2 at 20 ml min^{-1}	47
Figure 20 TGA and DTG at $25\text{ }^{\circ}\text{C min}^{-1}$ for rubbers from Group 1 in N_2 at 20 ml min^{-1} from $30\text{-}570\text{ }^{\circ}\text{C}$ and synthetic air 20 ml min^{-1} from $570\text{-}900\text{ }^{\circ}\text{C}$...	49
Figure 21 TGA curves of EPDM degradation region in Rubber I at 20 ml min^{-1} , under N_2 atmosphere with different heating rates.	51
Figure 22 Conversion of EPDM degradation in Rubber I, at 20 ml min^{-1} , under N_2 atmosphere with different heating rates.	52
Figure 23 Kissinger plots for the 6 rubbers, under N_2 atmosphere at 20 ml min^{-1} and non-isothermal conditions at heating rates 5, 10, 15, 20, 30 and $40\text{ }^{\circ}\text{C min}^{-1}$	53
Figure 24 OFW plots for all rubbers under N_2 atmosphere at 20 ml min^{-1} and non-isothermal conditions at heating rates 5, 10, 15, 20, 30 and $40\text{ }^{\circ}\text{C min}^{-1}$. Analyzed under isoconversion condition.	55
Figure 25 OFW plots for Rubber I, under N_2 atmosphere at 20 ml min^{-1} and non-isothermal conditions at heating rates 5, 10, 15, 20, 30 and $40\text{ }^{\circ}\text{C min}^{-1}$. Analyzed under isoconversion condition (Appendix G1 to G7).	56
Figure 26 a) Behavior of activation energy and frequency factor at different conversions. b) variation of activation energy with frequency factor. For Rubber I, obtained with the OFW method in non-isothermal conditions at heating rates 5, 10, 15, 20, 30 and $40\text{ }^{\circ}\text{C min}^{-1}$. Analyzed under isoconversion condition	58
Figure 27 Friedman's method plot for all rubbers, under N_2 atmosphere at 20 ml min^{-1} , in non-isothermal conditions at heating rates 5, 10, 15, 20, 30 and $40\text{ }^{\circ}\text{C min}^{-1}$. Analyzed under isoconversion condition.....	60
Figure 28 Friedman's method plot for Rubber I, under N_2 atmosphere at 20 ml min^{-1} and non-isothermal conditions at heating rates 5, 10, 15, 20, 30 and $40\text{ }^{\circ}\text{C min}^{-1}$. Analyzed in the range of 0.2 to 0.95 conversion.....	60
Figure 29 Friedman's method for Rubber I, under N_2 atmosphere at 20 ml min^{-1} , under non-isothermal conditions at heating rates 5, 10, 15, 20, 30 and $40\text{ }^{\circ}\text{C min}^{-1}$. Analyzed under the condition of isoconversion.....	61

Figure 30 Friedman's method plotting for Rubber, under N ₂ atmosphere at 20 ml min ⁻¹ , under non-isothermal conditions at heating rates 5, 10, 15, 20, 30 and 40 °C min ⁻¹ . Analyzed under the condition of isoconversion. Corresponding to the overlap in Figure 28 and 32.	61
Figure 31 a) Behavior of activation energy and frequency factor at different conversions. b) variation of the activation energy with the frequency factor. For Rubber I, obtained with Friedman's method in non-isothermal conditions at heating rates 5, 10, 15, 20, 30 and 40 °C min ⁻¹ . Analyzed under the condition of isoconversion.	63
Figure 32 CKA method plot for calculating the reaction order of the thermo degradation of Rubber I, under N ₂ atmosphere at 20 ml min ⁻¹ and non-isothermal conditions at heating rates 5, 10, 15, 20, 30 and 40 °C min ⁻¹ ..	65
Figure 33 CKA method plot for calculation of the reaction order of all rubbers, under N ₂ atmosphere at 20 ml min ⁻¹ , in non-isothermal conditions at heating rates 5, 10, 15, 20, 30 and 40 °C min ⁻¹	65
Figure 34 CKA method plot for calculating the activation energy of the thermo-degradation reaction of Rubber I in an atmosphere of N ₂ at 20 ml min ⁻¹ and non-isothermal conditions at heating rates 5, 10, 15, 20, 30 and 40 °C min ⁻¹	67
Figure 35 CKA-i method plot for the thermo-degradation reaction of Rubber I in an atmosphere of N ₂ at 20 ml min ⁻¹ and non-isothermal conditions at heating rates 5, 10, 15, 20, 30 and 40 °C min ⁻¹	70
Figure 36 CKA method plot for Rubber I in an atmosphere of N ₂ at 20 ml min ⁻¹ , under non-isothermal conditions at heating rates of 5, 10, 15, 20, 30 and 40 °C min ⁻¹ . Analyzed under the isoconversion condition. Corresponding to the overlay of Figure 34 and Figure 35.	72
Figure 37 Comparison of OFW (a) with CKA-I (b) for the degradation of Rubber I in an atmosphere of N ₂ at 20 ml min ⁻¹ , under non-isothermal conditions at heating rates of 5, 10, 15, 20, 30 and 40 °C min ⁻¹	73
Figure 38 a) behavior of the activation energy and frequency factor at different conversions. B) variation of the activation energy with the frequency factor. For Rubber I. Obtained with the CKA-ic method under non-isothermal conditions at heating rates of 5, 10, 15, 20, 30 and 40 °C min ⁻¹ . Analyzed under the isoconversion condition.	75

Figure 39 Summary plot of the apparent activation energies obtained by the different methods for the degradation of the 6 EPDM rubbers, under N ₂ atmosphere, evaluated under non-isothermal conditions.	77
Figure 40 Apparent preexponential factor of degradation obtained by the different methods for the degradation of the 6 EPDM rubbers, under N ₂ atmosphere, evaluated under non-isothermal conditions.	79
Figure 41 Shore D Hardness EPDM rubbers.	83
Figure 42 Stress-strain curve of Rubber I samples.	84
Figure 43 Young's modulus of EPDM rubbers.	85
Figure 44 Yield Strength of EPDM rubbers.	86
Figure 45 Tensile Strength of EPDM rubbers.....	86
Figure 46 Maximum strain of EPDM rubbers.....	87
Figure 47 EDX Results for Aluminum and Silicon.	89
Figure 48 Cross-link fraction for EPDM rubbers.	90
Figure 49 Percentage variation of mass for the all rubber immersed in Packer-Fluid+Safe-scan.	91

List of Tables

Table 1 Example of EPDM rubber formulations.	8
Table 2 EPDM samples and source information	27
Table 3 Description of fluid for adsorption tests (Packer-Fluid+Safe-Scan).28	
Table 4 -EPDM Bands [73]-[19].	38
Table 5 Metakaolin bands in Group 1 rubber.[19]-[79].....	40
Table 6 Kaolin bands in Group 2 rubbers [77][84][85][86][87].	43
Table 7 Average TGA results for rubbers after being evaluated at 7 heating rates (5,10,15, 20, 25, 30 and 40 °C min ⁻¹) with N ₂ at 20 ml min ⁻¹ from 30-570 °C (Appendix C19 to C20).....	48
Table 8 TGA results at 25 °C min ⁻¹ for the rubbers in the synthetic air stage at 20 ml min ⁻¹ from 570-900 °C	49
Table 9 Heating rates validation in the experiments.....	52
Table 10 Results of the kinetic data obtained by the KMW method for the 6 rubbers, under N ₂ atmosphere at 20 ml min ⁻¹ and non-isothermal conditions at heating rates 5, 10, 15, 20, 30 and 40 °C min ⁻¹	54
Table 11 Results of the OFW method for Rubber I, under N ₂ atmosphere at 20 ml min ⁻¹ and non-isothermal conditions at heating rates 5, 10, 15, 20, 30 and 40 °C min ⁻¹ , assuming n=1. Analyzed under isoconversion condition.	57
Table 12 Results of the OFW method to conversion $\alpha = 0.65$ in non-isothermal conditions at heating rates of 5, 10, 15, 20, 30 and 40 °C / min. Analyzed under the isoconversion condition. (Appendix G7 to G12).	59
Table 13 Results of Friedman's method for Rubber I, under N ₂ atmosphere at 20 ml min ⁻¹ and non-isothermal conditions at heating rates 5, 10, 15, 20, 30 and 40 °C min ⁻¹ , assuming n=1. Analyzed under isoconversion condition.	62
Table 14 Results of the CKA method for the calculation of the reaction order of Rubber I in an atmosphere of N ₂ at 20 ml min ⁻¹ and non-isothermal conditions at heating rates of 5, 10, 15, 20, 30 and 40 °C min ⁻¹	66
Table 15 Summary of the average order of reaction obtained by CKA	66

Table 16 Results of the CKA method for calculating the reaction order of Rubber I in an atmosphere of N ₂ at 20 ml min ⁻¹ and non-isothermal conditions at heating rates of 5, 10, 15, 20, 30 and 40 °C min ⁻¹	68
Table 17 Results for the 6 Rubbers by the CKA method in a N ₂ atmosphere at 20 ml min ⁻¹ and non-isothermal conditions at heating rates of 5, 10, 15, 20, 30 and 40 °C min ⁻¹	69
Table 18 Results of the CKA-i method for the thermo-degradation reaction of Rubber I in an atmosphere of N ₂ at 20 ml min ⁻¹ and non-isothermal conditions at heating rates 5, 10, 15, 20, 30 and 40 °C min ⁻¹	71
Table 19 CKA-ic results for Rubber I considering the isoconversion principle for the thermo-degradation reaction in an atmosphere of N ₂ at 20 ml min ⁻¹ and non-isothermal conditions at heating rates of 5, 10, 15, 20, 30 and 40 °C min ⁻¹	74
Table 20 Summary of the apparent activation energies obtained by the different methods for all the EPDM rubbers extracted from the jackets.	78
Table 21 Summary of the apparent preexponential factor of degradation obtained by the different methods for all the EPDM rubbers extracted from the jackets.	81
Table 22 Shore D Hardness for all EPDM samples.....	83
Table 23 A summary of mechanical properties evaluated by tensile tests.....	85
Table 24 Majority elemental composition determined by EDX	88
Table 25 Cross-link fraction all rubbers.	89
Table 26 Percentage end absorbed weight all rubbers.	92

List of Equations

(1).....	13
(2).....	13
(3).....	14
(4).....	14
(5).....	14
(6).....	14
(7).....	14
(8).....	14
(9).....	14
(10).....	15
(11).....	15
(12).....	15
(13).....	15
(14).....	16
(15).....	16
(16).....	16
(17).....	16
(18).....	16
(19).....	16
(20).....	17
(21).....	17
(22).....	18
(23).....	18
(24).....	18
(25).....	18
(26).....	18
(27).....	18
(28).....	19
(29).....	19
(30).....	19

(31).....	19
(32).....	19
(33).....	20
(34).....	20
(35).....	20
(36).....	20
(37).....	20
(38).....	21
(39).....	21
(40).....	22
(41).....	22
(42).....	23
(43).....	54
(44).....	58
(45).....	58

List of Appendix

Appendix A Supplementary material to support Chapter 4.

A1	109
A2	110
A3	110
A4	111
A5	111
A6	112
A7	112

Appendix B Supplementary material to support Chapter 5.1.1.

B1	113
B2	114
B3	115
B4	116
B5	117
B6	118

Appendix C Supplementary material to support Chapter 5.2.1

C1	119
C2	120
C3	121
C4	122
C5	123
C6	124
C7	125
C8	126
C9	127
C10	128
C11	129
C12	130
C13	131

C14	132
C15	133
C16	134
C17	135
C18	136
C19	137
C20	138
Appendix D Supplementary material to support Chapter 5.2.2	
D1	139
D2	140
D3	141
D4	142
D5	143
D6	144
Appendix E Supplementary material to support Chapter 5.3	
E1	145
E2	146
E3	147
E4	148
E5	149
E6	150
Appendix F Supplementary material to support Chapter 5.3.1	
F1	151
F2	152
F3	153
Appendix G Supplementary material to support Chapter 5.3.2	
G1	154
G2	155
G3	156
G4	157
G5	158
G6	159
G7	160

G8	161
G9	162
G10	163
G11	164
G12	165
G13	166
G14	167
G15	168
G16	169
G17	170
G18	171
Appendix H Supplementary material to support Chapter 5.3.3	
H1	172
H2	173
H3	174
H4	175
H5	176
H6	177
H7	178
H8	179
H9	180
H10	181
H11	182
H12	183
H13	184
H14	185
H15	186
H16	187
H17	188
H18	189
H19	190
H20	191
H21	192

H22	193
H23	194
H24	195
Appendix I Supplementary material to support Chapter 5.3.4.1	
I1	196
I2	197
I3	198
I4	199
I5	200
I6	201
I7	202
I8	202
I9	203
I10	203
I11	204
I12	204
Appendix J Supplementary material to support Chapter 5.3.4.2	
J1	205
J2	206
J3	207
J4	208
J5	209
J6	210
J7	211
J8	211
J9	212
J10	212
J11	213
J12	213
Appendix K Supplementary material to support Chapter 5.3.4.3	
K1	214
K2	215
K3	216

K4	217
K5	218
K6	219
K7	220
K8	221
K9	222
K10	223
K11	224
K12	225
Appendix L Supplementary material to support Chapter 5.3.4.4	
L1	226
L2	227
L3	228
L4	229
L5	230
L6	231
L7	232
L8	233
L9	234
L10	235
L11	236
L12	237
L13	238
L14	239
L15	240
L16	241
L17	242
L18	243
Appendix M Supplementary material to support Chapter 5.5.2	
M1	244
M2	245
M3	246
M4	247

M5	248
M6	249

List of abbreviations and symbols

Symbol	Description
$\frac{d\alpha}{dt}$	Reaction rate
A	Conversion
α_i	Conversion in isoconversion
α_m	Conversion in T_m
T	Time
K	Speed constant
f(α).	Conversion function or reaction model
f(α_i)	Conversion function or reaction model in isoconversion
A	Constant effective frequency factor or pre-exponential factor
A_{α_i}	Constant effective frequency factor or pre-exponential factor in isoconversion
\bar{A}	Average constant effective frequency factor or pre-exponential factor
E	Activation energy
E_{α_i}	Activation energy in isoconversion
\bar{E}	Average activation energy
T	Temperature
T_m	Maximum temperature in graph $\frac{d\alpha}{dT}$ vs. T
T_α	Temperature in Isoconversion
Tg	Glass transition temperature
R	Universal gas constant
n	Order of reaction
n th	Umpteenth order reaction
W_T	Non-converted mass-fraction
w_0	Initial mass
w_T	Mass at temperature T

w_{∞}	Final mass
$\phi = \frac{dT}{dt}$	Heating rate
ϕ_{True}	True heating rate
$g(\alpha)$	Integral function
$P(x)$	temperature integral
$x=E/RT$	Change of variable of the temperature integral
ϵ	Engineering strain
ΔL	Variation in length
L_0	Original length
σ	Unitary stress
F	Uniaxial force
S_0	Original surface
σ_y	Yield Strength
UTS	Ultimate Tensile Strength
SH	Shore Hardness
PD	Penetration Distance
% W_{ab}	Liquid absorption percentage
ΔW_{ab}	Variation in mass
W_{0ab}	Original mass
γ	Uncertainty
N/A	Not applicable
EPDM	Ethylene-Propylene-Diene Monomer
FPSO	Floating Production Storage and Offloading
FTIR	Fourier Transform Infrared spectroscopy
ATR	Attenuated Total Reflection
STA	Simultaneous Thermal Analyzer
DSC	Differential Scanning Calorimetry
TGA	Thermal Gravimetric Analysis
DTG	Derivative of TGA
SEM	Scanning Electron Microscope
EDX	Energy Dispersive X-ray
DTA	Differential thermal analysis

EVA	Poly (ethylene-vinyl acetate)
CSM	chlorosulfonated polyethylene rubber
EBN	2-ethylidene-5-norbornene
DCPD	dicyclopentadiene
VNB	5-vinyl-2-norbornene
ν_{sy}	Symmetrical stretch
ν_{asy}	Asymmetric stretch
δ_{sy}	Symmetrical angular deformation in plane
δ_{asy}	Asymmetric angular deformation in the plane
δ_p	Asymmetric angular deformation off plane
δ	Deformation
IC	Carbonyl group index
MFK	Free Kinetic Model
KMW	Kissinger-Murray-White
OFW	Ozawa-Flynn-Wall
FR	Friedman
CKA	Combined Kinetic Analysis model
CKA-i	Combined Kinetic Analysis by Isoconversion model
CKA-ic	Correction of the isoconversion CKA
KAS	Kissinger-Akahira-Sunose
CAGR	compound annual growth rate
R^2	Coefficient of determination
—	Average of any variable
C-LF	Cross-Link Fraction
ESC	Environmental Stress Cracking
Z	Atomic numbers

1 Introduction

Ethylene-propylene-diene rubber (EPDM) is a thermoplastic polymer and it achieved great importance in applications of electro-submersible pump cables (ESP), due to its electrical/mechanical stability at temperatures from 245 to 450 K and background pressure of 1800 PSI [1]. Due to these qualities, it is widely used as insulation and/or protection of power cables in ESP.

Mano [2] described EPDM as synthetic rubber with a copolymer of "ethylene + propylene + non-conjugated diene" elaborated by Ziegler-Natta catalysis, which can be vulcanized if required. It is generally reinforced with carbon black and possesses, at least, 2 wt.% of the diene. Some authors such as Mahapatra et al.,[3] reported a diene content of 4 to 8 wt.% and in this case these are 2-ethylidene-5-norbornene (ENB), dicyclopentadiene (DCPD) or 5-vinyl-2-norbornene (VNB). This last author, extends the EPDM concept by indicating that the content ethylene, can vary from 45 to 87 wt.%. In this sense, it seems that the term EPDM is commercially applied to a family of copolymer formulations which are considered rubbers and which properties can obviously be unique according to the formulation obtained.

In Brazil, from 2000 to 2018, the National Agency of Petroleum, Natural Gas and Biofuels registered that the oil production doubled in this period. One of the reasons for this improved production is due to the efficiency of new technologies, such as the use of modern Electrical Submersible Pumps (ESP). Statistics for 2019 agreed that ESP are responsible for 60% of world oil production[1]. On the other hand, D. Harris et al.,[4] reported that 20% of failures are attributed to cable problems with 2 years of operation and when studying the incidents in offshore installations with 10 years of operation the percentage rises from 30 to 48%.

The decoupling of modern society from oil as an energy source depends on population growth, the policies being adopted by each country or region, the feasibility of access to new technologies, and cost-effectiveness. In this context, the

IAE (International Agency for Energy) in "World Energy Outlook 2019"[5] states that the demand for black gold will increase by about 1x106 bbl/d on average each year until 2025 while will report a drop in demand by 2040. Although this information is based on current statistics and geopolitical scenarios, it can be agreed that oil will continue to be a necessary commodity in the world's supply.

In the specific case being studied here, Equinor shares with Sinochem the management of an offshore oil field, located 85 km off the coast of Cabo Frio, southeast of Rio de Janeiro/Brazil, in Campo Basin[6][7]. The field is called Peregrino and has been operating since 2008 with oil of 13 to 15 °API, its reserve is 2.5 billion barrels and an average production of 1 x 105 bbl/day. In this field, the ESP systems support the reservoir from 30 oil production wells and 7 water re-injection wells. On the surface the field contemplates two drilling-capable wellhead platforms and Floating, Production, Storage and Offloading (FPSO). While below the water level (depth over 95 meters) the wells are operating by artificial oil lifting.

Under the surface of the seabed there are complex completion systems, used to manage production/pressure maintenance of the reservoir, integrated by several sets of parts that are assembled by sections. As an example, Figure 1 shows a completion design installed in Peregrine field reported by Ranjeva et al.,[7]. In this same image, the basic elements that make up the ESP system, such as the pump and its cable (originally represented in blue in the image), are highlighted within the red circle.

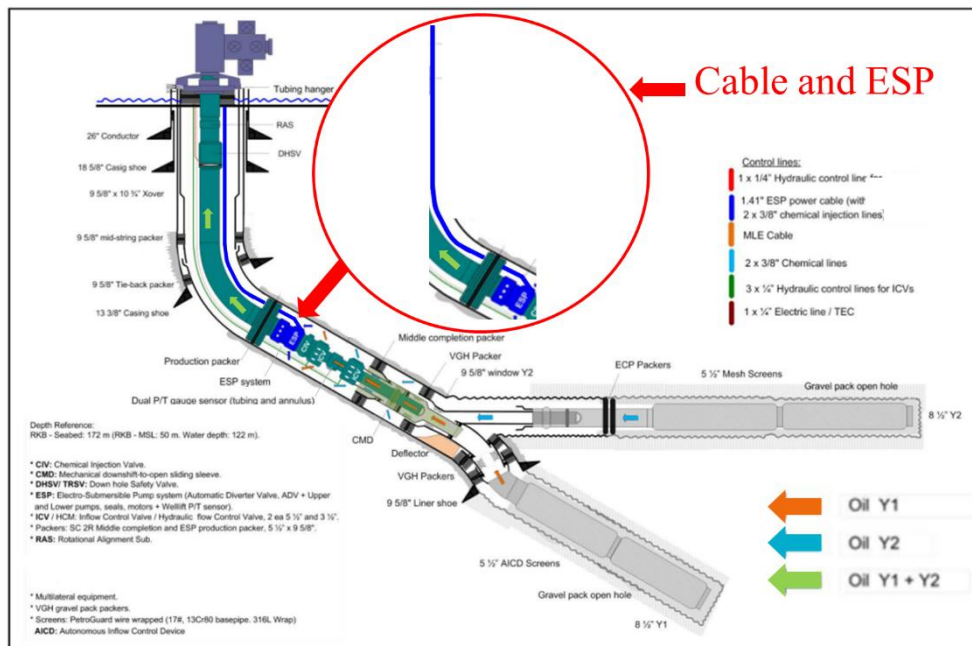


Figure 1 Peregrino Field, Level 2, Dual Lateral Completion. Modified image from Ranjeva et al.,[7] Multilateral level-5 dual long horizontal openhole gravel pack completion on the peregrino field, Proc. - SPE Annu. Tech. Conf. Exhib. 4 (2014) 2964–2979.

Honório et al.,[8] described the type of cable used in the Peregrino deposit, corresponding to 3 metallic copper conductors with thickness to 1 AWG (Appendix A1) and containing the following components: a) metallic conductor responsible for transmitting the current (copper conductors), b) insulating layer in contact with the metallic conductor which decreases the leakage of current and is manufactured with EPDM CL-90, c) waterproofing cover with high dielectric constant made of polytetrafluoroethylene (PTFE), d) Jacket or mechanical protection layer, a second layer of EPDM, with the formulation CL-185, e) metallic armor made from galvanized or stainless steel. Up to this point, the cable has been described as such, but it is also common to find attached elements such as lines for fluid injection or hydraulic control. As shown in Figure 2, it is feasible to adapt the cable to the required applications, turning it into an umbilical cord between the surface and the bottom of the well.

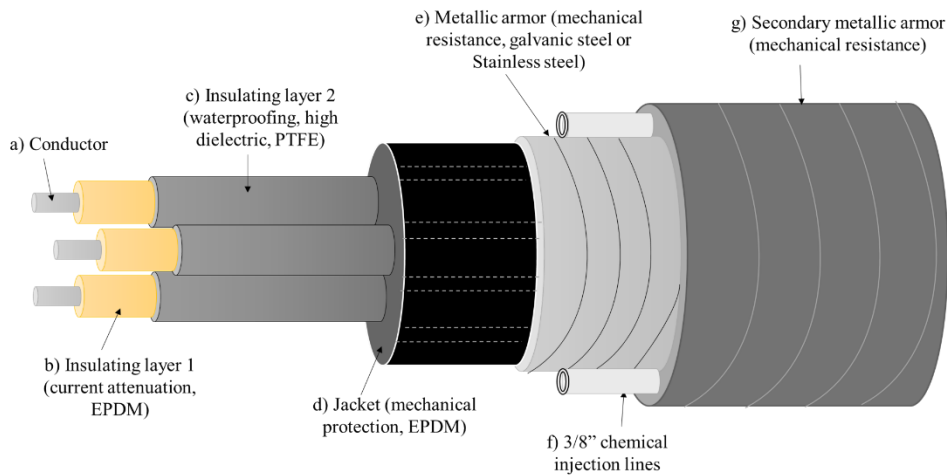


Figure 2 Cable ESP Baker Hughes Incorporated.

Williams et al.,[9] argue that the oil industry wants to extend the life of their ESPs. Authors agreed that in extreme conditions as those of a field, the absence of information about ESP aging presents a challenge for oil industry.

The objective of this work is to analyze the effects of aging suffered by the rubber of the mechanical protection cover or the cover of the ESP cable. Rubber used in operating conditions of 2 and 4.8 years in the Peregrine field in wells A-29 and B-17. Furthermore, the challenge is to quantify the change in its properties due to aging and to predict the life of the material exposed to similar conditions. In this way, we can provide accurate information for ESP technology, capable of being used as a basis for planning maintenance or preventive replacement of ESP cables, making the best possible investment budget and maximizing production.

2 Literature review

2.1. Copolymer of "ethylene + propylene + unconjugated diene"

Formally, when the acronym EPDM is used, it refers to the copolymer of "ethylene + propylene + unconjugated diene", which is composed of the three polymers, falls within the group of terpolymers (Figure 3)[2]. The placement of various additives that can vary as colorant, stabilizer or filler is common in all polymers. The need for the placement of additives is linked to the stage of processing or use for which the material or application is required. For example, in the processing stage, auxiliary additives may be required to stabilize the material or improve its finish by making the final product more attractive, while UV additives are typical for purposes where the material is exposed to the environment specifically to sunlight. or radiation with this similar wavelength[10].

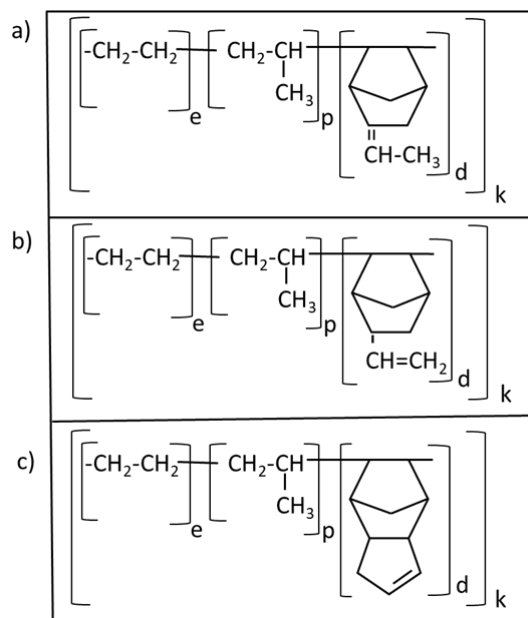


Figure 3 Molecular structures of EPDM with different diene a) 2-ethylidene-5-norbornene (ENB), b) dicyclopentadiene (DCPD), c) 5-vinyl-2-norbornene (VNB).

The variety of additives on the market involves products to help release molds, odors, colors, antistatic, slip and much more variety with specific uses such as blowing agents, fillers, magnets, heat stabilizers, degradation accelerators and even other polymers. The selection of the additive is the task of the producer and/or processing agent, they know the level of specialization that the polymeric material requires. Fillers are controversial additives that are added to reduce the volume of polymeric material, but sometimes a correct design and selection of this filler complements and improves the properties of the material. These latter materials with significant filling proportions enter the field of composite materials. It is possible to find additives with multiple qualities such as carbon black that gives it a dark color, serves as a filler in the polymer matrix, reducing costs, but when used with EPDM it increases some mechanical properties[11].

EPDM rubbers are among the three most commercially important synthetic rubbers in the world, along with styrene-butadiene and butadiene rubbers[3]. In 2017, a market size of USD 3.90 billion was estimated and a compound annual growth rate (CAGR) of 6.5% is projected for 2018-2025[12]. The fields in which EPDM is used are varied: construction, cables, electricity and electronics, plastic modifications, automotive, tires and tubes, among others. The most prominent field in its use is in automobiles where it is used as window and door seals, hydraulic brake system seals, belts, and lubricant additive to improve performance. Among the qualities that make the material attractive as seals or membranes is its low permeability to oxygen and ozone as a result of the unsaturation present in the side chains. In the field of cable sheathing, vehicle construction and manufacturing, properties such as flexibility, weather resistance, resistance to heat and UV radiation make the material attractive and competitive[3][13].

The synthesis of EPDM is carried out by heterogeneous catalysis with Ziegler Natta type catalysts that randomly incorporate blocks of polyethylene, polypropylene and a diene forming the main chain[14]. The continuity of the polyethylene and polypropylene blocks gives the material the ability to crystallize, facilitating resistance to organic solvents and resistance to heat. Non-polar polyolefin chains when crystallized provide resistance to organic and inorganic acids in addition to increasing mechanical strength. Whereas the random incorporation contributes to form amorphous zones. Among the dienes reported in

the literature are (ENB), dicyclopentadiene (DCPD) or 5-vinyl-2-norbornene (VNB)[3].

EPDM is typically a thermoplastic elastomer that, with the support of the additive processing and placement step, can be vulcanized to become a thermoset material. EPDM is versatile due to properties that come into conflict and can be characterized as a thermoplastic or thermoset material. The boundary property that allows predicting the predominance of the thermoplastic character is the ability to flow when heated, this same property is extended to its ability to become dissolved by solvents. The condition that a manufacturer uses to control thermostability is the degree of vulcanization of the rubber. In cases with low or non-existent degree of vulcanization the heated material can flow as a liquid (Thermoplastic). On the other hand, the high degree of vulcanization turns the material into a three-dimensional network that at temperatures higher than the melting temperature of EPDM, preventing the displacement of sections of the material chain from occurring as they are tied by atomic bonds as a consequence of the crosslinking of the polymeric chains (thermostable). By including cross-linking within the polymer matrix through the vulcanization process, some properties are modified[15]. P. Sutanto et al.,[16] show the variation of mechanical properties such as: hardness, elongation at break, compression and tensile strength with the degree of vulcanization

The diversity of EPDM copolymers are feasible consequences of the preparation of copolymers by changing the individual content of polyethylene, polypropylene or diene chains[17]. Another way to prepare different EPDM copolymers is to vary the monomer content, each with its unique properties[18]. PE content controls the EPDM crystallinity, whereas the decrease in crosslinking density and the increase in chain scissions are consequences of a higher PP content. Moreover, the higher the diene content, the higher is the crosslink density.

Under the commercial approach or in less formal language, the term EPDM is used to refer to the rubber applications of this terpolymer regardless of the variety or quantity of additives with which they are mixed. Table 1 shows the varieties of EPDM rubber formulations used by various authors, showing formulations with a high content of the EPDM terpolymer where logically the name EPDM rubber is used for obvious reasons, but the formulation with 26 % of the EPDM copolymer and 61 % by weight of filler which is still known as EPDM rubber despite containing a small proportion of the polymer.

Table 1 Example of EPDM rubber formulations.

Autor	% EPDM	% Additives	% Carbon black	% Oil	Other filler
S. Mitra et al.[19]	93	7			
T. Nakamura et al.[20]	62	2	36		
Q. Zhao et al.[21]	52	6	31	11	
Y. Seo et al.[22]	48	18		2	32
D. Bouguedad et al.[23]	26	13			61

2.2. Aging

The term aging is associated with the change of properties of a substance as a consequence of the passage of time. These property changes can occur when the material is exposed to an environment, radiation source, mechanical process, or its own instabilities. Changes in the properties of a substance are attributed to irreversible physicochemical change processes such as: oxidation, ionization, decrease in free volume, de-vulcanization, formation or breaking of atomic bonds and various phenomena that modify the original substance over time. The aging processes can extend to the degradation or transformation of the material to complete disintegration. Temperature, as in any chemical process, plays a fundamental role in accelerating the transformations that matter undergoes.

The aging process is evaluated in real time or in accelerated time. The first real-time condition is achieved by exposing the material to real conditions, evaluating the change in properties over time. The second accelerated time condition is achieved by exposing a material to simulated conditions with greater intensity than the real ones, causing the degradation to occur more quickly and therefore the time is shorter. The preference of the industry or different authors is to use accelerated time experiments since the results are obtained much more quickly. Real-time experiments are rarer due to the cost of time to expose the samples.

Physical aging commonly occurs in polymers with excess free volume when finding the material below its glass transition temperature (T_g), the chain sections remain rigid, therefore the material is a glass that is not in Balance. With increasing temperature, the kinetically constrained polymer chains relax as a result of the

movement of chain segments that are commonly concentrated at separate points in the material block. Ultimately, this causes portions of the material to randomly decrease their free volume causing non-uniform densification in the material. Therefore, the random decrease in free volume induces failures, stress concentrators, irregularities ranging from surface imperfections to mechanical failures[24].

Seo Y. et al.,[22] reported differences of 30% in the activation energy in thermo-oxidative processes after aging at different times and temperatures. The aging of the EPDM samples was reproducing refrigerant fluid leaks from nuclear power plants that use the material in electrical cables and where the EPDM rubber material is extracted in cable covers. They also report that elongation at break tends to decrease with increasing temperature as a result of aging.

Studies on the aging of EPDM gaskets were carried out by C. Li et al.,[25] when exposing the material to stress by thermo-oxidation and compression, highlighting that the phenomenon of thermo-oxidation produces carbonyl groups, and that of the separation of the compression phase between the polymeric matrix and the carbon black. In high temperature tests (150 °C) they reported that crosslinking reactions dominate over chain cleavage reactions. Their data revealed that aging is more severe with higher temperatures and compressions, showing in particular that thermo-oxidation reactions cause an increase in Tg and a decrease in free volume, while the effect of compression aging induces the opposite effect (decrease in Tg and increase in free volume). Kömmling et al.,[26] agree that chain cleavage and crosslinking reactions are simultaneous phenomena during material aging and that it is almost impossible to differentiate which phenomenon has the greatest influence at temperatures below 125 °C for EPDM.

Q. Zhao et al.,[21][27] expose EPDM samples in meteorological cameras and simulated ultraviolet radiation with a maximum of 90 days, reporting an increase in Links. They also propose a plausible mechanism for the formation of carbonyl groups by keeping the material under UV radiation and an oxidizing environment. Confirming C=O groups by FTIR with bands at 1734 cm⁻¹ and whose concentration increases with time. The formation of C-O-C groups on the surface of the material was followed by bands at 1159 and 1050 cm⁻¹. Furthermore, they exhibit increases in tensile strength with increasing cross-links reaching a maximum that drops sharply with the progress of degradation

T. Šarac et al.,[28] experienced the aging of a mixture of EPDM/EVA/filler with a composition of 40/10/50 % by weight, under oxidizing atmosphere and N₂ at different temperatures and gamma radiation dose. Reporting different behaviors of mechanical properties after aging. With the particularity that thermogravimetric analyzes show dependence with temperature and the dose of gamma radiation only in oxidizing atmosphere, while in N₂ it remains constant.

Aging in an EPDM sample with only 7% crosslinking additives (peroxides and process accelerators) was carried out by chemical attack with a highly oxidizing mixture (Cr(VI)/H₂SO₄ at 20% w). S. Mitra et al.,[19] experiment for 12 weeks resulting in a decrease in cross-links, according to reports of an increase in carbonyl groups and an increase in some mechanical properties like tensile strength. On the other hand, they conclude that the higher molar masses and the higher level of branching of the chain facilitate degradation by hydrolytic attack or chemical degradation.

T. Nakamura et al.,[20] evaluated the aging in real conditions of the seals of the water systems made with EPDM rubbers and used for 3 years at temperatures of 20 to 45 °C produced water . The EPDM chain structure underwent oxidation and polymer chain breaking, likely resulting in carbonyl groups, esters, and double bonds. As a consequence of the degradation, the crosslink content and the surface hardness were reduced by half.

M. Kalae et al.,[29] show an unexpected effect when varying the proportion, morphology and size of the zinc oxide particles used as fillers for EPDM rubbers. They reported that the activation energies and reaction order for thermodegradation in the presence of N₂ varied from case to case. Activation energy values can even double due to better reinforcement of the nano-sized zinc oxide particles. Show that the degradation of the material is linked to both the terpolymer and the additives present in the mixture.

2.3. Differential thermal analysis (DTA)

Differential thermal analysis begins by quantifying over time the variation of the physical properties of a material. In particular, thermogravimetry makes it possible to evaluate the change in mass of a material with temperature at different heating rates. Although Roberts-Austen has reported DTA since 1899, it was not until the mid-20th century that it became commercial[30]. Over the years, technology and various methods are developed, in the field of kinetics isothermal and non-isothermal methods are proposed. Researchers such as: T. Akahira et al., 1925[31], H. Kissinger 1956[32], H. Friedman 1964[33], A. COATS et al., 1964[34], T. Ozawa 1965[30], M. Starink 2003[35] and other have worked on non-isothermal methods for calculating the energy of activation, reaction order and pre-exponential factor magnitudes required to make the kinetic description of a process.

The use of parameters such as the Arrhenius activation energy to estimate durability or stability of polymeric materials is proposed by S. Ding et al.,[36] reporting that the activation energy of degradation in thermal processes is related to the rate of brittleness of the material.

F. Shehzad et al.,[37] synthesized 2 different polyethylene, showing how the new product prepared with Hybrid Graphite-LDH supported zirconocene presents higher thermal stability compared to the traditional preparation without zirconocene catalytic support. The higher thermal stability of the product in the new synthesis is evidenced by its higher activation energy, which is calculated using the non-isothermal Starink method. Both the Starink method and the Kissinger method use the peak temperature of the DTA graph and both agree that a higher peak temperature implies a greater thermal stability and therefore a greater activation energy.

J. Badia et al.,[38] works with multiple reprocesses by extruding a virgin polyethylene terephthalate (PET) in the presence of oxygen. As PET is a material susceptible to oxidative thermodegradation, it is shown that there is a decrease in activation energy with chain breakage as a consequence of the thermal, mechanical and chemical process. The kinetic parameter calculation method was performed under non-isothermal conditions evaluating 6 methodologies: Ozawa-Flynn-Wall (OFW), Kissinger - Akahira - Sunose (KAS), Vyazovkin, Master-Curves, Perez-Maqueda and Coats - Redfern. During each reprocessing stage, organic substances with evidence of decomposition such as benzaldehyde, aldehyde, CO₂ and CO are recorded.

C. Gamlin et al.,[39] present evidence of how the thermal stability of EPDM rubbers is affected by varying the ethylene/propylene ratio in the copolymer. Showing greater stability to thermal degradation by increasing the ethylene content. They reported values for the activation energies obtained by OFW for each mixture in a range of 144 to 203 kJ mol⁻¹.

The mechanical, viscoelastic behavior and kinetic properties of chlorosulfonated polyethylene rubber (CSM) and ethylene propylene diene terpolymer (EPDM) are evaluated and compared by T. Naruse et al.,[40] using Arrhenius equation methods and OFW are able to study degradation energies in a range of 80 to 120 °C. As the activation energies are reported in the isoconversion condition, the phenomenon of dependence between the activation energy is observed and conversion. Furthermore, they report that the fatigue resistance was in agreement with the activation energy of thermogravimetry

2.4. Kinetic fundamentals

Vyazovkin et al., [41] consider that the adequate description of a reaction kinetic depends on the triple kinetic, referring to the following 3 parameters: activation energy, pre-exponential factor and order of reaction.

In other terms and applied to this study, it is being indicated that kinetic parameters such as activation energy, pre-exponential factor and order of reaction are essential elements to build a kinetic model, capable of expressing the aging of EPDM rubbers extracted from ESP cable jackets.

Taking advantage of the potential offered by a kinetic model to predict the useful life of a material, allowing us to have well founded criteria to order the maintenance or replacement works of the material, in operational conditions of the reservoir, where each intervention on a well represents a high monetary cost. It is necessary to use the kinetic method that contemplates the kinetic triplet.

In this section of kinetic fundamentals, a summary of concepts, principles and mathematical developments used in kinetic methods based on non-isothermal

conditions are presented. Additionally, a proposal for non-isothermal kinetic studies by the Combined Kinetic Analysis (CKA) method under isoconversion conditions are introduced.

2.4.1. Rate of reaction

The starting point for the analysis of the kinetics of a reaction is exposed by equation (1) [42]. It describes the variation of the conversion (α) with respect of the time (t) showing its dependence with the product of 2 terms $k(T)$ and $f(\alpha)$.

$$\frac{d\alpha}{dt} = k(T) f(\alpha) \quad (1)$$

The first term of equation (1), identified as the speed constant ($k(T)$) is defined by S. A. Arrhenius by equation (2)[43]. In the Arrhenius model is grouped the influence of effective collisions, dependent on direction and area of contact, with the number of clashes between the agents that come into contact. In this way, it is presented the recognized constant effective frequency factor or pre-exponential factor (A). On the other hand, Arrhenius equation indicates the existence of a minimum energy (activation energy= E) necessary for the fraction of agents coming into contact to be transformed into a product at an absolute temperature (T). Finally, completing the dimensional changes of the units using the universal gas constant R.

$$k(T) = A e^{-\frac{E}{RT}} \quad (2)$$

The second term of equation (1), $f(\alpha)$ is identified as the conversion function or reaction model. Reaction model is considered the mathematical interpretation of the instantaneous variation of the amount of reacting agents involving the chemical process executed by them to transform. Additionally, from this conversion function it can be understood how the reagents are affected by the mechanism with which they transformation to products. In several non-isothermal kinetic studies this $f(\alpha)$ is omitted, as it is described in the research of Friedman[33]. For other authors such as Coats et al.,[34] it is indispensable to indicate an adequate reaction model for a correct computation of the kinetic parameters.

Equation (3) is a characteristic expression applied in solid state reactions. Gamlin et al.,[39] use it in the degradation of EPDM. Identifying the variables:

n =order of reaction, W_T =the non-converted mass-fraction at any time or temperature and α =the conversion.

$$f(\alpha) = (1 - \alpha)^n = W_T^n \quad (3)$$

The transformation to conversion (α) of the mass data is easily done by equation (4). Defining its variables: initial mass (w_0), mass at temperature T (w_T) and final mass (w_∞).

$$\alpha = \frac{w_0 - w_T}{w_0 - w_\infty} \quad (4)$$

Alternatively, equation (5) is proposed when the complete consumption of the analyzed material occurs or an isolated transformation phenomenon is studied.

$$\alpha = \frac{w_0 - w_T}{w_0} = 1 - \frac{w_T}{w_0} = 1 - W_T \quad (5)$$

Returning to the kinetic deductions, equation (2) is substituted in (1) to generate equation (6), which is the basis of the approaches for kinetic studies under isothermal conditions. Defining the change in the amount ($d\alpha$) of a reaction agent over time (t).

$$\frac{d\alpha}{dt} = A e^{-\frac{E}{RT}} f(\alpha) \quad (6)$$

It is viable to make the transformation of equation (6) to non-isothermal conditions based on the fact that temperature and time are varying simultaneously. Using the heating rate (ϕ) to perform the transformation, as expressed in equation (7).

$$\phi = \frac{dT}{dt} \quad (7)$$

Including equation (7) in equation (6), it describes the basis of the non-isothermal models in equation (8).

$$\frac{d\alpha}{dT} = \frac{A}{\phi} e^{-\frac{E}{RT}} f(\alpha) \quad (8)$$

Starting from equation (8), kinetic studies have focused on two classical trends[42]:

-Derived methods. Taking advantage of the mathematical properties of the logarithm and applying on the equation (8) it is possible to deduce the equation (9).

$$\ln \frac{\phi d\alpha}{dT} = \ln A f(\alpha) - \frac{E}{RT} \quad (9)$$

-Integral methods. Organizing variables of the equation (8) and looking for the diverse solutions for the defined integrals, the integral function ($g(\alpha)$) was

deduced in the equation (10)[44]. Culminating in equation (11), estimation that compensates by approximation the reaction model ($f(\alpha)$). With the purpose of finding the solution of the temperature integral ($P(x)$), which is not solved analytically.

$$g(\alpha) = \int_0^\alpha \frac{d\alpha}{f(\alpha)} = \frac{A}{\phi} \int_{T_0}^T e^{-\frac{E}{RT}} dT \quad (10)$$

$$g(\alpha) = \frac{AE}{\phi R} P(x) \quad (11)$$

Commonly, the first step in solving equation (11) is to approximate $P(x)$ to a polynomial form. Doyle[45], proposed to do the following consideration: $x=E/RT$ and applying expansions of asymptotic series, as below in equation (12).

$$P(x) \cong \frac{e^{-x}}{x^2} \quad (12)$$

Budrugaec [46] experimented with $\text{CaC}_2\text{O}_4\text{-H}_2\text{O}$ dehydration and compared the results of derived and integral methods publishing differences between the obtained results and reports discrepancies that can range from 20 to 70% in the computation of activation energies.

2.4.2. Isoconversion approach

Vyazovkin et al.,[47] agreed that it is possible to predict the variation in conversion with respect to time under non-isothermal conditions. They maintaining as a basis that the reaction rate is a function only of temperature at a constant conversion (α_i). This approach is known as the isoconversion approach.

Particularly, the differential methods of isoconversion approach is supported by applying logarithm in equation (6). So that, developing equation (13) as following[48].

$$\ln \frac{d\alpha}{dt} = \ln k(T) + \ln f(\alpha) \quad (13)$$

Proceeding with the partial derivative with respect to $(1/T)$ of equation (13) in the isoconversion condition leads to equation (14).

$$\left[\frac{\partial \ln \frac{d\alpha_i}{dt}}{\partial T^{-1}} \right]_{\alpha_i} = \left[\frac{\partial \ln k(T)}{\partial T^{-1}} \right]_{\alpha_i} + \left[\frac{\partial \ln f(\alpha_i)}{\partial T^{-1}} \right]_{\alpha_i} \quad (14)$$

Vyazovkin et al.,[49] agrees with Friedman[33], who considers $f(\alpha_i)$ as a constant in the temperature range and by definition this term is replaced by zero giving the equation (15).

$$\left[\frac{\partial \ln \frac{d\alpha_i}{dt}}{\partial T^{-1}} \right]_{\alpha_i} = \left[\frac{\partial \ln k(T)}{\partial T^{-1}} \right]_{\alpha_i} \quad (15)$$

Based on the Arrhenius model (equation (2)) and deriving again by the inverse of the temperature ($1/T$), the equation (16) is deduced.

$$\left[\frac{\partial \ln k(T)}{\partial T^{-1}} \right]_{\alpha_i} = \left[\frac{\partial \ln A e^{-\frac{E}{RT}}}{\partial T^{-1}} \right]_{\alpha_i} = -\frac{E_{\alpha_i}}{R} \quad (16)$$

Introducing equation (16) in (14), leads to equation (17), which describes the dependence of conversion with time under isothermal conditions.

$$\left[\frac{\partial \ln \frac{d\alpha_i}{dt}}{\partial T^{-1}} \right]_{\alpha_i} = -\frac{E_{\alpha_i}}{R} \quad (17)$$

Including the definition of heating rate of equation (7) within equation (17) is presented the model developed for non-isothermal conditions for the methods derived from equation (18).

$$\left[\frac{\partial \ln \phi \frac{d\alpha_i}{dT}}{\partial T^{-1}} \right]_{\alpha_i} = -\frac{E_{\alpha_i}}{R} \quad (18)$$

Budrugaac et al.,[50] summarize with equation (19) the equivalent isoconversion computation model for integral methods.

$$\left[\frac{\partial \ln \frac{g(\alpha)}{A} + \frac{E_{\alpha_i}}{TR}}{\partial T^{-1}} \right]_{\alpha_i} = \frac{E_{\alpha_i}}{R} \quad (19)$$

2.4.3. Free Kinetic Model (MFK)

Starink[35] explains the MFK model, which has been used in the literature to group kinetic methods by derived and integral methods under non-isothermal conditions where reaction models $f(\alpha)$ are excluded. Friedman[33] considers that the reaction model is independent of the temperature, while other authors such as Ozawa[51] include approximations in the integral methods to mathematically compensate the use of $f(\alpha)$.

2.4.3.1. Kissinger model (KMW)

This method also known as Kissinger-Murray-White[52] (KMW), adding the contributions of the researchers who developed this integral method, proposes the following mathematical model of the equation (20) [53].

$$\ln\left(\frac{\phi}{T_m^2}\right) = -\frac{E}{RT_m} + \ln\frac{AR}{E} + \ln[n(1 - \alpha_m)^{n-1}] \quad (20)$$

KMW proposed a maximum temperature (T_m) for each particular heating speed, acquiring its absolute value in Kelvin from the graph $\frac{d\alpha}{dT}$ vs. T , reported in the condition of $\frac{d^2\alpha}{dT^2}=0$. Similarly, α_m is the corresponding conversion at maximum temperature, deductible from the TGA graphs. Pal et al.,[54] reported that it is typical to observe the variation of the conversion at the maximum reaction speed, changed into individual values of the heating rate.

An important condition of this model is the order of reaction $n=1$ according to Farjas et al.,[55] in order to reduce the equation (20) to a linear model as shown in equation (21).

$$\ln\left(\frac{\phi}{T_m^2}\right) = -\frac{E}{RT_m} + \ln\frac{AR}{E} \quad (21)$$

In the cases where the reaction order $n \neq 1$ has been found, the solution for the integral function ($g(\alpha)$) is invariable at a fixed conversion. This is equivalent to including in the term $\ln[n(1 - \alpha_m)^{n-1}]$ a single value of the reaction order (n) and a fixed conversion (α), resulting in consequence that $\ln[n(1 - \alpha_m)^{n-1}]$ is constant. Changing the equation (21) in the equation (22).

$$\ln\left(\frac{\phi}{T_m^2}\right) = -\frac{E}{RT_m} + \ln\frac{AR}{Eg(\alpha)} \quad (22)$$

Balart et al.,[48] agree to the term $\ln\frac{AR}{Eg(\alpha)}$ a constant to reduce the equation (22) to the equation (23), this allows to obtain the tangent of the line hence the activation energy. But it is not always possible to solve for the frequency factor

$$\ln\left(\frac{\phi}{T_m^2}\right) = -\frac{E}{RT_m} + \mathbf{Constant} \quad (23)$$

According to equation (22) Akahira-Sunose[31] applied the isoconversion to the integral method of KMW. They studied by this way integrals defined in the calculation and develop what is known as KAS (Kissinger-Akahira-Sunose). Useful technique to obtain the profile behavior of the activation energy by the isoconversion approach.

2.4.3.2.

Ozawa-Flynn-Wall model (OFW)

Ozawa's[51] developed a comprehensive method under isoconversion conditions using Flynn-Wall's P(x) approximation (equation (24)).

$$\log P(x) = -2.315 - 0.4567x \quad (24)$$

Further adjustments as recommended in ASTM E698[56] change the approximation to that shown in equation (25).

$$P(x) = (x + 2)^2(x^{-1})(e^{-x}) \quad (25)$$

Equation (26) shows the proposal of T. Ozawa[48].

$$\log \phi = -\frac{0.4567E}{RT_\alpha} - \log g(\alpha) - 2.315 + \log \frac{AE}{R} \quad (26)$$

Equation (26) takes a form of a line, considering equation (27) where T_α is also the temperature in Kelvin read at a constant conversion at different heating rates.

$$\log \phi = -\frac{0.4567E}{RT_\alpha} + \mathbf{Constant} \quad (27)$$

Standard ASTM E698[56] sets out additional procedures for computing activation energy with corrections. Additionally, Standard ASTM E698 indicates

that equation (28) can be applied to obtain the frequency factor assuming an order of reaction of 1.

$$A = \frac{\phi E e^{\frac{E}{RT}}}{RT^2} \quad (28)$$

2.4.3.3. Friedman model (FR)

Friedman [33] started directly from the derived method shown in equation (9) fix variables and apply logarithm. Report the equation (29), with which it achieves linear plots "if" is applied on the straight line at constant conversion. Thus Friedman obtains data from a straight line (slope) by plotting the following mathematical expression

$$\ln \frac{\phi d\alpha_i}{dT} = \ln A_{\alpha_i} f(\alpha_i) - \frac{E_{\alpha_i}}{RT} \quad (29)$$

A formal proposition of the Friedman proposition is understood by equation (30). As can be seen, it is only possible to evaluate the activation energy.

$$\left[\frac{\partial \ln \frac{\phi d\alpha_i}{dT}}{\partial T^{-1}} \right]_{\alpha_i} = \left[\frac{\partial \left(\ln A_{\alpha_i} + f(\alpha_i) - \frac{E_{\alpha_i}}{RT} \right)}{\partial T^{-1}} \right]_{\alpha_i} = -\frac{E_{\alpha_i}}{R} \quad (30)$$

Friedman evaluated through equation (31) the order of reaction and the frequency factor. He indicated that his model would have a linear behavior but his own results show deviations from this behavior at the edges of the plotted data.

$$\ln A_{\alpha_i} f(\alpha_i) = \ln A - n \ln \left(\frac{w_T - w_{\infty}}{w_0} \right) \quad (31)$$

Budruga et al.,[50][57] indicated that the results of the activation energy obtained by the Friedman method can be affected by the conversion, resulting in different values when compared with the results of activation energies computed by OFW. Proving his statement with equation (32)

$$E_{FR} = E_{FWO} + 0.052E_{FWO} - R \left(\frac{\partial \ln \frac{d\alpha}{dT}}{\partial T^{-1}} \right) \quad (32)$$

2.4.4. Combined Kinetic Analysis model (CKA)

This model is based on methods derived from calculations under non-isothermal conditions. Unlike MFK, the CKA method proposed a starting reaction model $f(\alpha)$. Its development begins by applying logarithm directly to equation (8) thus developing equation (33).

$$\ln\left(\phi \frac{d\alpha}{dT}\right) = -\frac{E}{RT} + \ln f(\alpha) + \ln A \quad (33)$$

Some recommendations of several authors such as Šesták et al.,[58] to select an $f(\alpha)$ reaction model to use in CKA, start by using the proposals reported in previous isothermal studies. Gamlin et al.,[59] directly use the simple model for n^{th} order $f(\alpha) = (1 - \alpha)^n$ for n^{th} order (n), described in equation (3). Incorporating in equation (33) therefore, equation (34) is developed.

$$\ln\left(\phi \frac{d\alpha}{dT}\right) = -\frac{E}{RT} + \ln(1 - \alpha)^n + \ln A \quad (34)$$

This equation is very useful depending on how it can be manipulated mathematically, getting the two following expressions. The calculation of the order of the reaction is reported by Gu et al.,[53] using the equation (35).

$$\ln\left(\frac{\phi \frac{d\alpha}{dT}}{e^{-\frac{E}{RT}}}\right) = n \ln(1 - \alpha) + \ln A \quad (35)$$

On the other hand, Balar et al.,[48] introduced equation (36) for the calculation of the activation energy

$$\ln\left(\frac{\phi \frac{d\alpha}{dT}}{(1 - \alpha)^n}\right) = -\frac{E}{RT} + \ln A \quad (36)$$

To complete the analysis by this method, an internal calculation process can be proposed for the values of n and E as shown in equation (37)

$$\ln\left(\frac{\phi \frac{d\alpha}{dT}}{(1 - \alpha)^n}\right) + \frac{E}{RT} = \ln\left(\frac{\phi \frac{d\alpha}{dT}}{e^{-\frac{E}{RT}}}\right) - n \ln(1 - \alpha) \quad (37)$$

2.4.4.1. Combined Kinetic Analysis by Isoconversion model (CKA-i)

A novel calculation proposal is born by applying the isoconversion approximation to equation (36) expressing this modification as shown in equation (38).

$$\left[\frac{\partial \ln \left(\frac{\phi \frac{d\alpha}{dT}}{(1-\alpha)^n} \right)}{\partial T^{-1}} \right]_{\alpha_i} = \left[\frac{\partial \left(-\frac{E}{RT} + \ln A \right)}{\partial T^{-1}} \right]_{\alpha_i} = -\frac{E_{\alpha_i}}{R} \quad (38)$$

Equation (38) unlike the Friedman method (equation (30)) is clearly including the reaction model. To be more formal, we could rewrite in a more general way substituting $(1 - \alpha)^n$ for $f(\alpha)$ as seen in equation (39). Opening the probability to study other proposals of reaction models

$$\left[\frac{\partial \ln \left(\frac{\phi \frac{d\alpha}{dT}}{f(\alpha)} \right)}{\partial T^{-1}} \right]_{\alpha_i} = \left[\frac{\partial \left(-\frac{E}{RT} + \ln A \right)}{\partial T^{-1}} \right]_{\alpha_i} = -\frac{E_{\alpha_i}}{R} \quad (39)$$

2.5. Uniaxial Tensile Tests

When studying a body subjected to a static or quasi-static load, a deformation is originated in that volume. The amount of deformation caused is determined by the mechanical properties of the substance. By applying this load in only one direction, the changes produced by the load can be represented using normal stresses and deformations. This allows to have an estimate of the mechanical behavior of the material. Uniaxial tensile tests allow a substance with known shape and dimensions to be subjected to a tensile load in only one direction.

Uniaxial tensile tests are known to provide the behavior of the studied material starting from the elastic region where the deformations are reversible, passing through a possible plastic region (non-reversible deformations) and ending

at points of rupture or maximum deformation. At each point of these tests the following parameters are computed:

- Engineering strain (ϵ) is known as the change in size in one direction quantified as the computed fraction of the ratio of the variation in length (ΔL) of the deformed body divided by the original length (L_0).

$$\epsilon = \frac{\Delta L}{L_0} \quad (40)$$

- Unitary stress (σ) Computed as the quotient of the uniaxial force (F) applied on the body under study divided by the original surface (S_0).

$$\sigma = \frac{F}{S_0} \quad (41)$$

It is classic to transform the tensile test results into stress transformation curves where various parameter values are displayed, such as: Young's Modulus, Yield Strength (σ_y), Ultimate tensile Strength (UTS), Breaking Strain, Fracture Point and many other parameters such as Proportional Limit.

2.6. Shore Hardness

Hardness is a parameter that allows describing the mechanical characteristics of a material. At present this magnitude is very striking due to its speed and ease of execution[60]. When evaluating the plastic deformation located on a surface, the parameter known as hardness can be quantified, with a relationship where the hardness is inversely proportional to the footprint produced or the penetration distance (Figure 4).

Gent[61] explains that for Shore hardness(SH) the penetration distance(PD) of a rigid indenter with a specific geometry and a constant load on the surface of the material is measured. The Shore hardness is calibrated to measure the penetration depth of the indenter and owes its name to Albert Ferdinand Shore who developed this instrument in 1920.

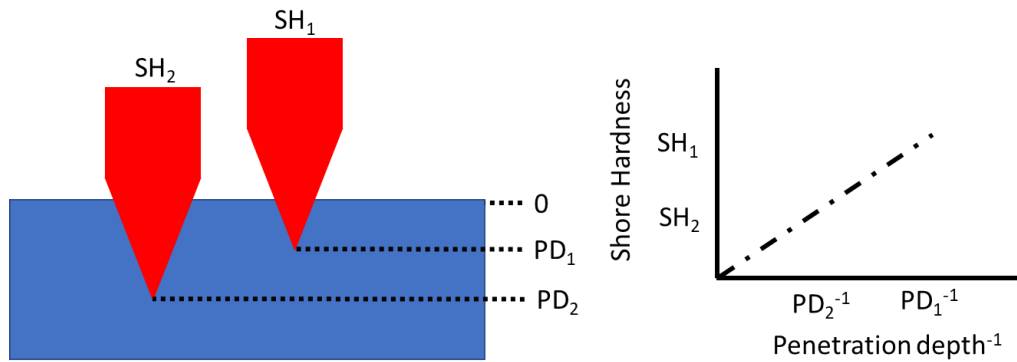


Figure 4 Schematic representation of Shore hardness measurement.

2.7. Adsorption

Among the possible interactions that exist between a liquid and a polymeric material we have the phenomenon of adsorption. This process occurs when a portion of the liquid that is in contact with the polymer invades the volume of the material and begins to swell.

Hansen[62] comments that when a liquid is absorbed by a polymer, various phenomena occur depending on the degree of adsorption. At low degrees of adsorption, it begins by observing softening and ends in failures due to environmental stress cracking (ESC). While high degrees of retention of the liquid could occur the dissolution of the material.

Vlastos[63] comments that there is a drastic deterioration in the performance of EPDM rubber insulation by adsorbing water when exposed to the environment. Sundararajan[64] explains that when aging EPDM chains can separate hydrophobic methyl groups, transforming into groups with hydrophilic polarity that make the material more suitable for the absorption of polar substances.

In this case, the liquid absorption percentage ($\%w_{ab}$) is measured as the quotient of the variation in mass (Δw_{ab}) of the polymeric material with respect to its original mass (w_{0ab}).

$$\%w_{ab} = \frac{\Delta w_{ab}}{w_{0ab}} \quad (42)$$

3 Objectives

3.1. General Objective

The objective is to quantify the variation in mechanical and kinetic properties as a consequence of aging under real operating conditions in EPDM rubbers originally extracted from the mechanical protection layer (Jacket) of ESP cables from the Peregrino field.

3.2. Specific objectives

- Qualitative assessment of the components of the EPDM jacket layer using the FTIR (Fourier-transform infrared) technique.
- Quantify the mass loss as a function of temperature using the TGA (Thermogravimetric analysis) technique. Assign temperature intervals for each event in order to define the stage, with which it is possible to methodically compare the compositions in mass % of the rubbers extracted from each cable
- Study the results of the kinetic models in non-isothermal conditions by Kissinger, Ozawa-Flynn-Wall and Combined kinetic analysis to develop kinetic models of the degradation of the composite material that is extracted from the jacket layer of the 6 ESP cables.
- Evaluation of the effect of aging on the mechanical properties of the EPDM-based composite extracted from the jacket layer from six ESP cables aged in different conditions.
- Evaluate the adsorption properties at room temperature of the EPDM-based composite from the jacket layer from six ESP cables aged in different conditions.

To evaluate by distillation of recirculated toluene the consequences of the aging process on the crosslinking content in the EPDM-based compound of the coating layer of six ESP cables that were aged under different conditions.

4 Materials and methods

4.1. Studied material

In this investigation, elastomer was EPDM-based composite originated from the mechanical protection cover (Jacket) of 6 ESP cables, which include: 2 ESP cables kept in warehouse and 4 used cables that were subjected to real field conditions for 2 to 4.8 years at different depths. The ESP cables were commercialized by Baker Hughes Company and kindly supplied by Equinor Company, Brazil.

The portion of cables stored in the warehouse that remained outside the well operating conditions for practical purposes will be considered as reference samples. Although the storage conditions and the time that the warehouse cables remained in these conditions outside the well are unknown. The warehouse ESP cables were supplied by Equinor and commercialized by Baker Hughes Company with similar characteristics to those installed in the wells of Peregrino field.

The ESP cable group that was used in the A-29 and B-17 oil wells, both in the Peregrino field, were operating for 738 days (2 years) and 1752 days (4.8 years), respectively. The initial reservoir conditions are 78°C at 2300 m (7550 feet Total Measured Depth) and the pressure varying from 740 to 3,350 Psia (can be calculated as a function of hydrostatic pressure)[65]. The depths, times and information raised are shown in Table 2. In order to stabilize the cables along the pipeline that connects the top of the well with the point where the ESP is located, the cables are surrounded by a packing fluid known as Packer-Fluid+Safe-Scan.

The information of the technical data sheet offered by Baker Hughes Company is presented in (Appendix A1), revealing that the elastomer of the mechanical protection layer or jacket corresponds to the formulation EPDM CL-185, without giving more details. This CL-185 code is an internal assignment handled as know-how of Baker Hughes Company and is not of public access.

Table 2 EPDM samples and source information (Appendix A2 to A7)

Rubber	I	II	III	IV	V	VI
Supplier	Baker	Baker	Baker	Baker	Baker	Baker
company	Hughes	Hughes	Hughes	Hughes	Hughes	Hughes
Serial	103471	N/A	1031583	N/A	105216	1074616
Cable	3401		396		726	298
Depth (m)	0	0	760	917	1927	2170
Well			B17	A29	A29	B17
Time (days)	0	0	1752	738	738	1752
Note	Ware-house cable	Ware-house cable	82 °C 234.9 bars	82 °C 235 bars	82 °C 235 bars	82 °C 234.9 bars

*N/A not applicable.

** Rubber I is protected with stainless steel. Rubbers II to VI are covered by galvanized steel.

4.2. Solvent and fluids

The gases for the STA experiments are supplied by the company Air Products Brazil Ltda. and are described below:

-Nitrogen (N₂) 99% purity

-Synthetic air with the typical mixture of 72% N₂, 28% O₂ and traces of other gases.

The toluene solvent in the determination of cross-linked content is from Merck KGaA with ACS Reagent purity, ≥ 99.7 suggested for analysis.

Packer-Fluid + Safe-Scan is described as a water-based solution containing oxygen scavenger, and anti-emulsifiers[66]. This solution is used as a packing liquid inside oil wells to contain ESP cables and it is described in Table 3. The Packer-Fluid + Safe Scan was delivered by Equinor-Brazil.

Table 3 Description of fluid for adsorption tests (Packer-Fluid+Safe-Scan).

Product	Function	Concentration
Industrial Glycerol/ Water 75 to 80 % w/w	Diluent	Quantum satis
Sodium Chloride	hydration of the formation clay formation	$\leq 6 \%$ (w/w)
Glutaraldehyde	Bactericide	1%
Ultrawt 70	Anti-Emulsifier	$\lesssim 1 \%$ (w/w)
Sodium bisulfite	Oxygen scavenger	200 ppm

4.3. Elastomer characterization

4.3.1. Fourier Transform Infrared (FTIR) spectroscopy

The technique of Fourier Transform Infrared (FTIR) spectroscopy with a coupled Attenuated Total Reflection (ATR) sensor was used as a method to obtain qualitative information on the functional groups of the molecules and inter-atomic bonds present in the jacket layer.

For the FTIR-ATR analysis, a Spectrum Two model equipment from the company Perkin-Elmer was used. The wavenumber sweeps were performed in the range of 4000 to 500 cm^{-1} , with 4 cm^{-1} resolutions and 20 consecutive measurements.

4.3.1.1. Rubber samples for FTIR

The samples of each elastomer are obtained by removing a small specimen of about 1 cm^3 from each jacket layer. At the moment of evaluating it, a thin layer was removed from one side of the specimen with a blade. The flat surface created by the cut was placed directly on the FTIR equipment.

4.3.1.2. Waste samples from STA analyzed by FTIR

Rubber waste obtained in the STA experiment (described later) was used to for FTIR as well. The procedure consists in collecting each of the scraps after being subjected to the procedure indicated in section 4.3.2.2 and placing the powdered material on the sample holder of the equipment.

4.3.2. Simultaneous Thermal Analyzer (STA)

Differential Scanning Calorimetry (DSC) and Thermal Gravimetric Analysis (TGA) tests were performed on the Perkin-Elmer Corporation's Simultaneous Thermal Analyzer (STA 6000) using a platinum crucible. The material samples were cut in sizes of approximately 1 mm. The experiments were conducted primarily under two conditions as shown in the following 2 subsections.

4.3.2.1. Thermo-degradation up to 570 °C

Analyses in non-oxidizing atmosphere were evaluated with a N₂ flow at 20 ml min⁻¹ and a mass of the material ranging from 12 to 15 mg. For each of the 6 elastomer samples, independent experiments were executed with a set of 6 heating rates (\emptyset): 5, 10, 15, 20, 30 and 40 °C min⁻¹. The temperature range evaluated was 30 to 570 °C.

4.3.2.2. Thermo-degradation up to 900 °C

Experiments were conducted with a single heating rate (\emptyset) of 25 °C min⁻¹ for each one elastomer sample. The material mass was 12 to 15 mg of elastomer. The complete heating program was from 30 to 900 °C which was divided in 2 stages. The first stage is summarized within the temperature range from 30 to 570 °C in N₂ gas atmosphere with a flow rate of 20 ml min⁻¹. In the second stage, maintaining the heating rate at 25 K min⁻¹, the atmosphere was modified to synthetic air with a flow rate of 20 ml min⁻¹ and extending the test from 570 to 900 °C.

4.3.3. Shore D Hardness

Penetration resistance measurement was performed with a durometer calibrated in the Shore D hardness range from Digimess manufacturer. The apparatus includes a metal tip with a very specific geometry (Figure 5) and a mass of 5 kg to keep the load constant. This equipment was integrated into a bench stand that helps to ensure the correct application of the load and feeds the instrument perpendicularly to the test surface. All tests were performed at room temperature of 25 °C with air humidity between 70-80 %. Four samples were prepared per specimen of the rubber, measuring 15 points per flat face, for a total of 30 measurements on each test body.

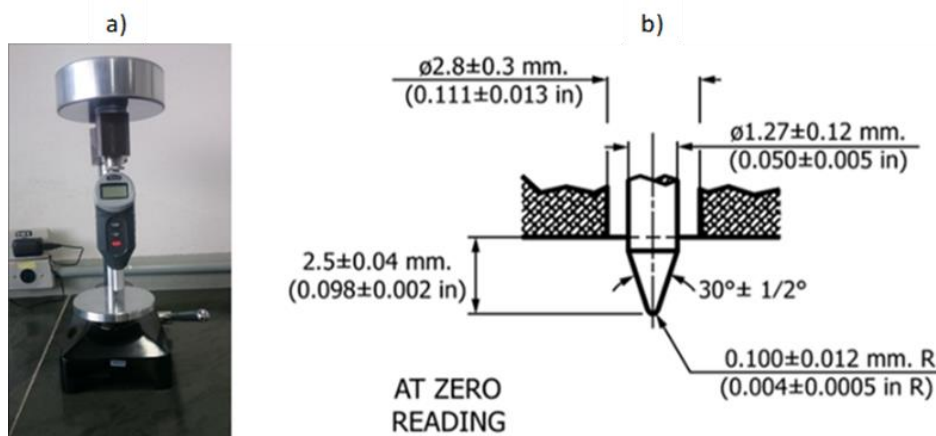


Figure 5 a) Digimess equipment for Shore D hardness. b) Schematic description of the tip identification image adapted from ASTM D2240 "Standard Test Method for Rubber Property-Durometer Hardness"[67].

4.3.3.1. Shore D hardness test samples

Following the indications described in ASTM D2240[67] "Standard Test Method for Rubber Property-Durometer Hardness", a cylindrical test body was manufactured with nominal dimensions of 34.0 mm in diameter and 10.0 mm in height, which allowed a transversal evaluation of the hardness of the 6 EPDM elastomers, measuring with the instrument only on the transversal face of the

mechanical protection cover. Figure 6 shows an example of the design of the test bodies.



Figure 6 Shore D hardness test samples.

4.3.4. Tensile test

The tensile tests were performed on an Instron Machine 5500R universal testing machine, with a 100 kN load sensor, 6 mm jaws at an ambient temperature of ($24\text{ }^{\circ}\text{C} \pm 2\text{ }^{\circ}\text{C}$). At least 5 test bodies of each elastomer sample at a speed of 10 mm min^{-1} [68] were used. The initial test section length was 42 mm. Figure 7 shows a picture of a universal testing machine. The experiments were based on the standard of ASTM D412 "Standard Test Methods for Vulcanized Rubber and Thermoplastic Elastomers-Tension"[69].



Figure 7 Universal testing machine Instron 5500R.

4.3.4.1. Uniaxial Tensile Test Samples

The samples for the uniaxial tensile tests were manufactured in two steps. The first step was the removal by cutting of the jacket layer of each cable, following the section of the jacket layer along the longitudinal axis. Consequently, the second step was a process of mechanical wear of the EPDM elastomer, providing the shape of a rectangular prism. For this purpose, all the faces were to smooth down, except the external face which has a serrated surface. The recommendations to this procedure are presented in the British Standard EN 60811-1-1 [70]. Figure 8 shows the nominal shape and dimensions of each test body of: $a = 18$, $b = 110$ e $c = 4$ mm.

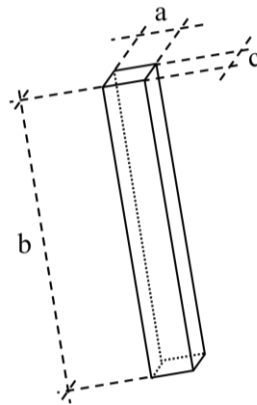


Figure 8 Nominal shape and dimensions of the test bodies for uniaxial tensile tests with it dimensions: $a = 18$, $b = 110$ and $c = 4$ mm.

4.3.5. Scanning Electron Microscope (SEM) coupled with energy dispersive X-ray spectrometer (EDX)

The images of the surface of the material were obtained with a SEM equipment developed by Hitachi, model TM3000, which has been coupled to an energy dispersive X-ray spectrometer also produced by Hitachi, model SwiftED3000 that allows the identification of atoms by emitting X-ray radiation patterns, characteristic of each element. The analyses were performed at 15.0 kV, with variable magnification. The relevance of this experiment is to study the surface of the EPDM elastomer at a microscopic level and the elemental characterization of samples. Figure 9 shows a picture of this equipment.



Figure 9 SEM TM3000 da Hitachi.

4.3.6. Crosslinked content

In order to characterize the 6 EPDM elastomers of the jacket layer of the 6 cables the soluble fraction was extracted by dissolution in toluene, at its boiling point, using the guidelines defined in ASTM D2765 "Standard Test Methods for Determination of Gel Content and Swell Ratio of Cross-linked Ethylene Plastics" [71]. A schematic diagram of the assembly used in this experiment is shown in Figure 8. For this particular test, 0.4 g of the elastomer was used in 350 ml of toluene for 48 hours, repeating the test 3 times per sample of EPDM rubber.

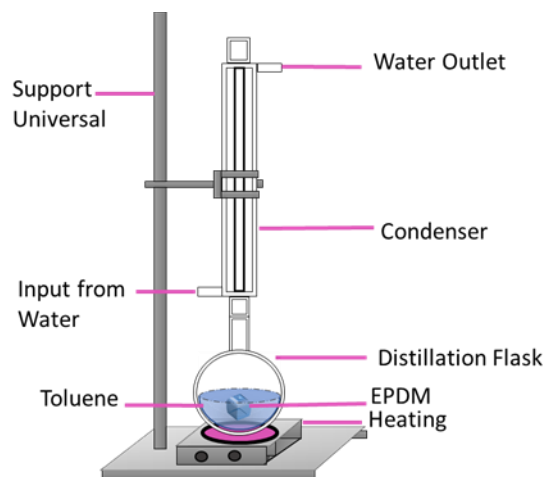


Figure 10 Apparatus used for cross-linkages determination through ASTM D2765 [71].

4.3.7. Absorption in Packer-Fluid+Safe-Scan

The absorption tests were conducted in a Becker with three samples, immersed in 500 ml of the solution (Packer-Fluid+Safe-scan). The test temperature was (25°C) for a period of 88 days, recording the mass variations with time on a Shimadzu balance model AY220 with 4 decimal places. The procedures used were extracted from ASTM D570 [72].

4.3.7.1. Absorption samples

The samples exposed in the Packer-fluid + Safe-scan fluid were manufactured maintaining the nominal external diameter of 34 mm the original mechanical cable protection cover. Subsequently, cross cuts were made, which allowed for a part shaped approximately to a 50 mm long cylinder. Each piece was mechanically removed from all internal and external material not belonging to the mechanical protection cover, leaving a whole piece of this cover intact. The void space in the center corresponds to the volume occupied by the other internal and mechanically removed elements (metal wire, insulation covers). Figure 11 shows images of the shape of the samples in this experiment.



Figure 11 Absorption test bodies shaped to a 50 mm long cylinder.

5 Results and discussions

5.1. FTIR

Taking into account sparse information on chemical composition of EPDM CL-185 rubber, it was proposed to carry out studies using the FTIR technique, to determine chemical composition of this composite material. On the other hand, the data collected by FTIR are useful to search for possible chemical alterations of the material product of aging in real operating conditions.

The fact that commercial rubbers are actually a composite material represents a challenge, since they are made by mixing a polymer with various components such as: fillers, processing oils, colorants and other additives [2]. The FTIR signals produced by each spectrum obtained were studied to deduce each of the elements that compose it and finally compare the rubbers used with each other and the references in the literature.

As expected, FTIRs present various limitations as a consequence of the rubber signals as they are superimposed with the presence of other bands (additives to the mixture) at similar wavelengths.

5.1.1. Classification of Rubber samples by FTIR

Figure 12 and Figure 13 show the first overview of the FTIR for the 6 rubbers samples from which the mechanical protection covers (jacket layer) are made.

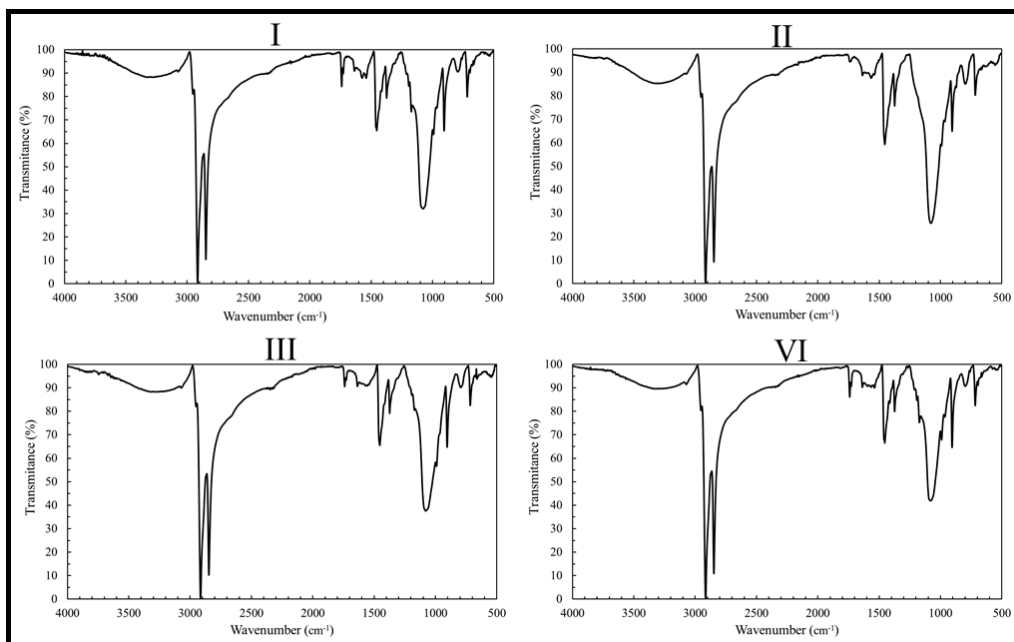


Figure 12 FTIR spectra for Rubber I, II, III and VI samples. Group 1 (Appendix B1 to B3 and B6).

The direct qualitative comparison of these results reflects similarity of the spectra of the samples of Rubber I, II, III and VI (Figure 12). Demonstrating that the samples of the industrial preparation have similar chemical composition between them.

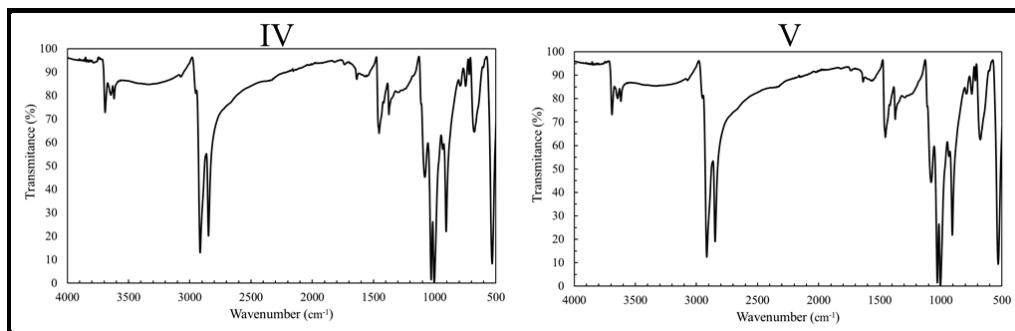


Figure 13 FTIR spectra for Rubber IV and V samples Group 2 (Appendix B4 to B5).

Similarly, it is verified that the Rubber IV and V samples (Figure 13) agree on their signal response during the infrared scan, indicating that it is the same material.

This evidence reveals the presence of 2 different materials that are catalogued in 2 sets: Group 1 (Rubber: I, II, III and VI) and Group 2 (Rubber: IV and V).

Figure 14 was constructed to better appreciate the differences and similarities between the responses to the FTIR signal.

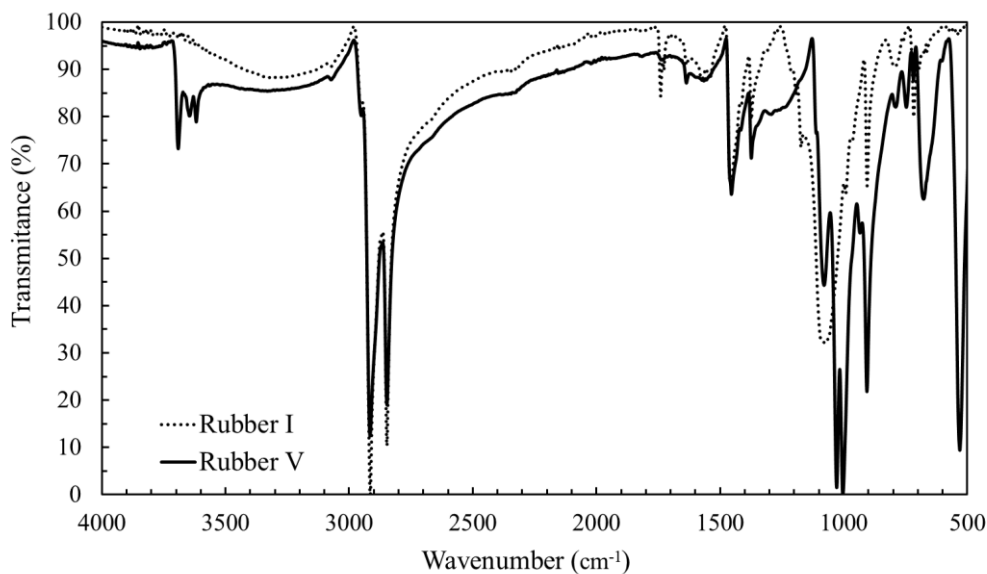


Figure 14 FTIR spectra of Rubber I (Group 1) and Rubber V (Group 2).

Figure 14 shows the bands which vibrates in the 3700-3600 cm^{-1} regions. These bands appeared in the spectra of the Rubber V samples and are absent in Rubber I. In the 1300-500 cm^{-1} zone, within the fingerprint zone for FTIR, the multiple peaks with particular shape and intensity certify that the spectra of the rubbers belong to 2 materials with different structure.

5.1.2. Identification of the polymer in the Rubber samples by FTIR

The first part of the interpretation of the FTIR to be considered concerns the bands of the EPDM polymer that, as shown in Table 4, are interpreted as belonging to the EPDM. This result is compared with literature reports by various authors such as Lopes, Coates, Nakamura, ASTM International, Riba and Mitra[20][73][74][75][76].

In Figure 15, the Rubber I and V samples are again shown as an example of each material. In blue, the bands identified by authors such as Riba et al., [76] (Table 4). At values of 2957 cm^{-1} has the small band of a stretch, ($\nu_{asy}SP^3 C - H$). Later,

2915 and 2848 cm^{-1} corresponding to asymmetric and symmetric C-H stretches present in CH_2 and CH_3 . Other peaks are those near of 1455 and 1374 cm^{-1} , which explained in literature as asymmetric and symmetric C-H deformations in CH_2 and CH_3 . Finally, the existence of the asymmetric balance outside the plane originated by a number greater than or equal to 4 continuous CH_2 groups is evidenced by the bordering peak at 720 cm^{-1} .

Therefore, the results certified the presence of EPDM as one of the components of the commercial formula of the rubber used to prepare the 6 samples of the mechanical protection cover. However, the analysis and interpretation of the FTIR spectra indicates the coexistence of other materials that will be described below.

Table 4 -EPDM Bands [19][20][73][76][77].

Band (cm^{-1})	Interpretation	Description
3075	$\nu_{\text{sy}}\text{SP}^2 = \text{C} - \text{H}$	Symmetrical stretch C-H
2957	$\nu_{\text{asy}}\text{SP}^3 \text{C} - \text{H}$	Asymmetric stretch C-H
2915	$\nu_{\text{asy}}\text{SP}^3 \text{C} - \text{H}_3$	Asymmetric stretch C-H
	$\nu_{\text{asy}}\text{SP}^3 \text{C} - \text{H}_2$	
2848	$\nu_{\text{sy}}\text{SP}^3 \text{C} - \text{H}_3$	Symmetrical stretch C-H
	$\nu_{\text{sy}}\text{SP}^3 \text{C} - \text{H}_2$	
1455	$\delta_{\text{asy}}\text{SP}^3 \text{C} - \text{H}_3$	Asymmetric angular deformation in the plane CH_3
	$\delta_{\text{sy}}\text{SP}^3 \text{C} - \text{H}_2$	Symmetrical angular deformation in plane (Scissor) CH_2
1374	$\delta_{\text{sy}}\text{SP}^3 \text{C} - \text{H}_3$	Symmetrical angular deformation in the plane (Umbrella) CH_3
709	$\delta_{\text{p}}\text{SP}^3 \text{CH}_2$	Asymmetric angular deformation off plane (Wagging) $n_{\text{CH}_2} \geq 4$

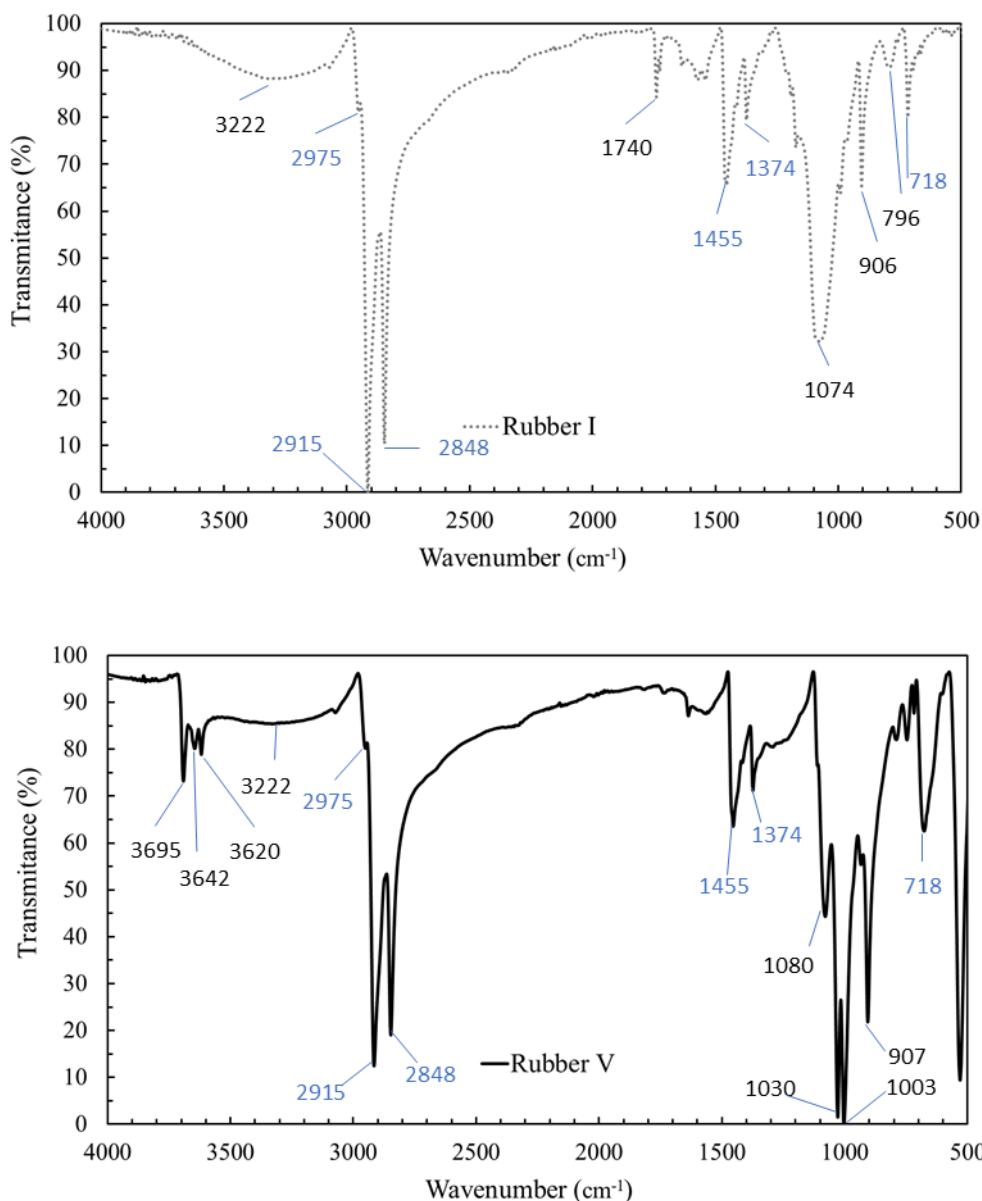


Figure 15 Spectra of ATR Rubber I (Group 1) and Rubber V (Group 2). The signs in blue color highlight the EPDM bands.

5.1.3. FTIR Interpretation of Group 1

Table 5 presents the description and interpretation of the additional vibration bands observed in the rubbers from the Group I that cannot be identified as EPDM.

By comparing them with the reports of Ilić et al.,[78] these bands fit with Metakaolin (reference pattern produced by the author by the thermal decomposition of kaolinite).

Elimbi et al.,[79] admits the presence of water in aluminosilicate geopolymers up to 550 ° C, giving the basis for the presence of water in the mixture of industrial origin. Coinciding with water bands at 3100-3800 cm⁻¹.

Table 5 Metakaolin bands in Group 1 rubber.[19][78][79][80][81][82]

Band (cm ⁻¹)	Interpretation	Description
3100-3850	δ H – O – H	Angular deformation H ₂ O or
	ν_{asy} – OH	Symmetrical stretch OH
1638	δ_{sy} H ₂ O	Symmetrical angular deformation in plane (Scissor) H ₂ O
900-1100	ν_{asy} Si – O – Si	Symmetrical and Asymmetric stretch of SiO ₂ or
	ν_{asy} Si – O – Al	Si-O-Al amorphous
800	δ Al – OH	Deformation Al-O Change of Al octahedral to tetrahedral

The prominent band by its shape and intensity at above 3000 cm⁻¹ is reported by several authors Mitra, Ilić, Bansod, Puligilla et al., [19][78][77][81][82]. Their articles agree that broad bands in the vicinity of 3100-3850 cm⁻¹ refer to the coexistence of water, which absorbs in the infrared region by a deformation ($\delta_s H - O - H$). Another signal that is reported occurs in parallel, is at 1640 cm⁻¹ assigned to scissor-type angular deformations ($\delta_s H_2 O$). Although water is not part of the structure of aluminosilicate or EPDM, its presence is reported in the FTIR spectra of the original rubbers. This liquid is justified in the inter- or intramolecular trapped aluminosilicate load [78].

Metakaolin is reported by Elimbi and López et al.,[79][80] agreeing that the band at 900-1100 cm⁻¹ is a consequence of the asymmetric stretching of amorphous SiO₂ or structures of the Si-O-Al type. The works of Ilić, López et al., [78][80] establish that the increase of Al-O to the tetrahedral form produces vibrations close to 800 cm⁻¹.

With what is stated in this section, the presence of Metakaolin and traces of water trapped in rubbers I, II, III and VI are confirmed. Additional evidence isolating and reaffirming Metakaolin is set forth in the following paragraphs.

5.1.3.1. Additional evidence to verify the identification of Metakaolin

The convolution of the signals due to the multiple components of an industrial preparation represents a challenge in FTIR analysis, and in many opportunities their separation is required to later purify and obtain a valid result. Noting that STA inorganic residues after 900 °C in synthetic air oxidant atmosphere are abundant and they are separated from all organic components by the decomposition process. EDS confirm the presence of Si and Al in these residues. Evaluating this alternative step facilitated the validation of Metakaolin as one of the components of the rubber taken from the mechanical protection cover. FTIR scans (Figure 16) were made to stable STA residues (section 4.3.2.2). Therefore, confirming the presence of a silicon geopolymer reported as Metakaolin in the mix, the rubbers of Group 1 (I, II, III and VI).

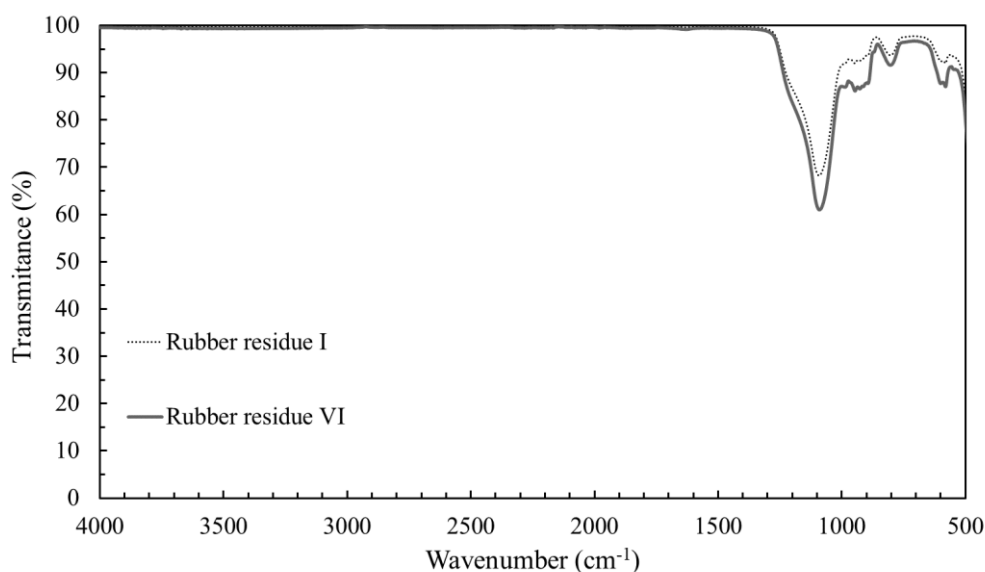


Figure 16 FTIR spectra from Rubber Waste I and VI after thermal treatment at 900 °C under synthetic air condition.

Spectra shown in Figure 16 match up well with those reported by Ilić et al., [78] where they analyzed the transformation of Kaolin into Metakaolin by heat treatment. The unlabeled FTIR signals in Figure 16 are being considered as trace

contaminants because the source of the Metakaolin is unknown. Other inorganic additives could also be incorporated in the industrial formula, which are not discarded, such as zinc oxide, which can present signals in regions close to the silicates. The latter typically added in industrial or laboratory formulations as mentioned in research by Zaharescu et al.,[83] to improve properties in rubbers.

5.1.4. FTIR Interpretation of Group 2

Therefore, the objective of this section is to label the peaks that have not been discussed and to help identify the substances that cause the difference in Group 2.

Table 5 summarizes the Kaolin bands that have been identified in the mixture with EPDM rubber. Reports of the works of Ilić, Jianwen, Zulfiqar, Zhu, Leśniak et al.,[78][84][85][86][87] confirm these results.

The more formal reading of the bands assigns the 3100-3850 cm^{-1} ($\delta_s H - O - H$) signal to water. Around 3620, 3642 and 3695 cm^{-1} we have a signal with very striking triple bands that are assigned to Si-OH and Al-OH stretching that Zhu et al., [86] mention as typical of Kaolin. These authors propose that there is a double band of 3670 and 3651 cm^{-1} , in our case they seem to be superimposed giving only the band of 3642 cm^{-1} .

Asymmetric SiO_2 or amorphous Si-O-Al stretches are found in 1080 cm^{-1} [86]. A double band in the area of 1050-1000 cm^{-1} matches with report of Zhu et al.,[48] as Si-O-Si stretch in 1030 cm^{-1} and Si-O-Al stretch 1003 cm^{-1} . In 907 cm^{-1} there is a deformation by bending of OH groups and 794 cm^{-1} a stretching of Al-OH groups are exposed the literature of Ilić et al., [78].

Stretches of Si-O in 697 cm^{-1} is commented by Zhu et al.,[86] ending with O-Si-O or Al-O deformations are labeled by the same authors. Thus, completing the ATR reading for Group 2 spectra, identifying a geopolymer containing Kaolin as part of the EPDM mixture.

Table 6 Kaolin bands in Group 2 rubbers [78][84][85][86][87].

Band (cm ⁻¹)	Interpretation	Interpretation
3620, 3642 e	ν Si – OH	OH stretch
3995	ν Al – OH	
1080	ν_{asy} Si – O – Si	Asymmetric stretch of SiO ₂ or Si-O-
	ν_{asy} Si – O – Al	Al amorphous
1030-1003	ν Si – O – Si	Stretch of Si-O-Si ou Si-O-Al
	ν Si – O – Al	
907	δ – OH	OH deformation
784	δ Al – OH	Deformation of Al-OH Change of Al octahedral to tetrahedral
718	ν Si – O – Al	Stretch of Si-O-Al ou Si –O
	ν Si – O	
697	ν Si – O	O-Si-O stretch
540	δ O – Si – O	Deformation of O-Si-O or Al-O
	δ Al – O	

5.1.4.1.**Additional evidence to verify identification of Kaolin**

Repeating the experience of analyzing the residues of the rubber samples originated by using the STA tests at 900 °C in synthetic air. The presence of Kaolin can be checked by an indirect route. in accordance to Ilić et al.,[78] it is possible to transform Kaolin into Metakaolin by heat treatment at 650 °C. Based on the premise that Kaolin was identified by the signals already discussed in FTIR and that the samples were exposed to 900 °C to ensure the degradation of organic substances it can be inferred that the isolated material in this methodology is a Metakaolin, which

source is Kaolin. Figure 17 shows the FTIR results of this experience, which are compared with the reference offered by Ilić et al.,[78].

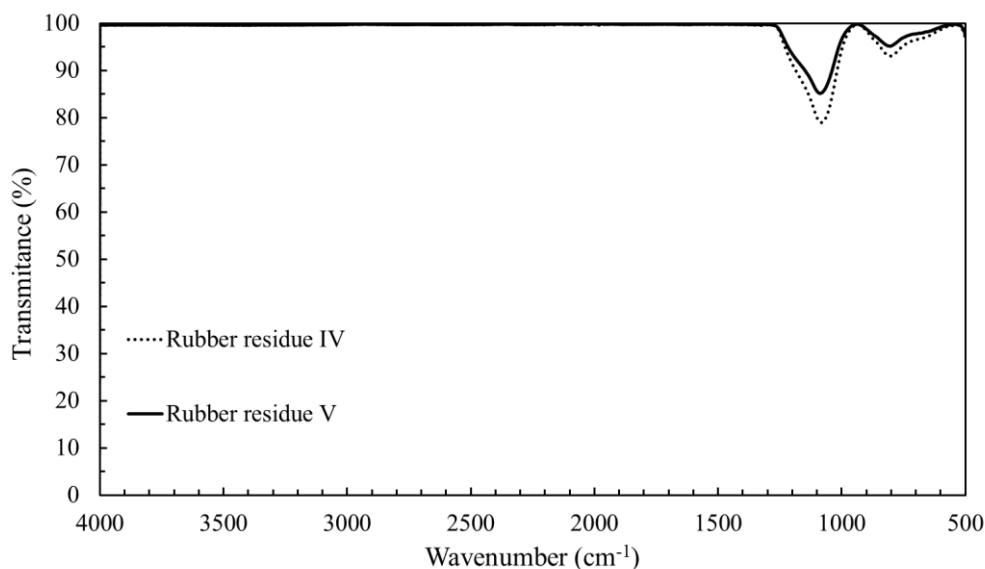


Figure 17 FTIR of STA waste for Rubber IV and V samples (Group 2).

5.1.5. FTIR aging study

The FTIR technique is typically used to study aging in many polymers. Mitra and Bouguedad et al.,[48][52][60][61] observed in the region of 1710 to 1800 cm^{-1} band that is normally assigned to the symmetric stretching of the carbonyl group ($\nu_{\text{Si}} \text{C} = \text{O}$). The carbonyl group signal intensity is used for carbonyl group index (IC) calculations, this last magnitude is proportional to the amount of carbonyl groups that appear during the aging of a material. By constructing a calibration curve of IC versus aging time, it is possible to observe the dependence of these 2 parameters. The calculation is made using relative intensities in ranges where a response proportional to the concentration is found. But as shown in Figure 18 an enlargement on the FTIR spectra for Rubber I and II (both new samples used for the control) the $\text{IC}_{1455/1740}$ obtained are 2.25 and 13.57 respectively.

Because rubbers I and II are new samples that have not been subjected to reservoir conditions, the $\text{IC}_{1455/1740}$ results for both cases are expected to be close to

each other and close to zero. Additionally, the variation of the $IC_{1455/1740}$ between both samples should report closer values. But the results show, this large variation of the $IC_{1455/1740}$ (13.57 and 2.25 for rubber I and II respectively) of the theoretically non-degraded samples outside of well conditions makes it impossible to make a proportional correlation of time with $IC_{1455/1740}$. When observing that there is no proportionality between the IC and the concentration, other possible sources are being considered as those responsible for the intensity of the C=O vibrations.

Although it can be theorized that early degradation events occurring in the EPDM extrusion/vulcanization process are responsible for the vibrations of the C=O groups, it is equally sensible to assume that the carbonyl group is present in some low molecular weight additive. S. Mitra et al.,[19] report stearic acid as a curing agent. N.D. Bansod et al.,[81] report that maleic anhydride is positioned to functionalize silicon particles with nonpolar chain sections of the EPDM molecules. P. Sutanto et al.,[16] report that additives such as ZDBC (Zinc Diethyldithiocarbamate) and ZDMC (Zinc Dibutyldithiocarbamate) are accelerating agents added to control vulcanization and produce resonance in this region.

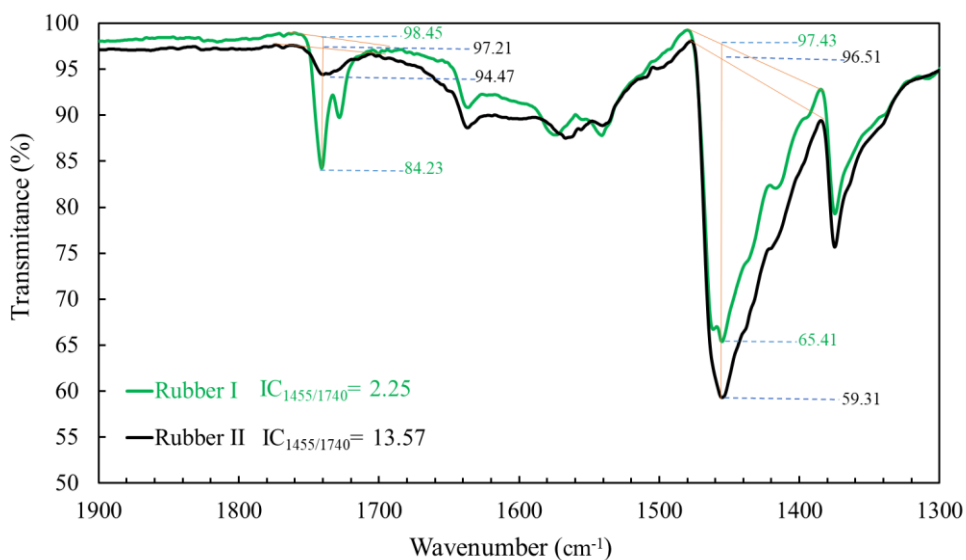


Figure 18 Amplification of the ATR for Rubber I and II. The figure shows the calculation of carbonyl index group ($IC_{1455/1740}$) using the peaks at 1740 cm^{-1} for carbonyl and 1455 cm^{-1} for EPDM.

5.2. STA of the Rubbers

The STA technique represents another key point in the characterization of the rubbers extracted from the jacket of the ESP cables. With the loss of mass in the temperature range, it is possible to establish the compositions used by the manufacturer at the time of preparation of the EPDM composite. On the other hand, it is feasible to establish stages in which thermal events such as evaporation or degradation.

Based on the procedures of Maurer and Liang et al., [88][89] the use of 2 different atmospheres is necessary to quantify the type of charges such as: carbon black and CaCO_3 . The first atmosphere is nitrogen gas, a non-oxidizing gas, from 30 to 570 °C. This method allowed evaluation of the degradation of EPDM and mass loss of low molecular weight substances, as investigated by Petrović et al.,[90]. The second synthetic air atmosphere was used by Liang et al.,[89] for its ability as an oxidant to quantify the content of substances such as carbon black.

5.2.1. Thermo-degradation up to 570 °C

By contributions of Bouguedad, Liang, Gamlin et al.,[23][90][91] it is known that the thermal decomposition of EPDM is reported in the range of 410 to 550 °C under nitrogen atmosphere. Additionally, Gamlin et al.,[91] agreed that different low molecular weight oils and additives are present at 310 to 390 °C. And as concluded from the FTIR analyses there are substances like water trapped in samples.

In Figure 19 the TGA result is illustrated for Rubber I, showing that 3 different mass loss ranges can be summarized with the help of the first derivative of mass loss curve (DTG). These ranges normally defined thermal phenomena of evaporation and/or degradation. The decrease in mass per stage can be attributed as follows: 30 to 250 °C loss of water (stage 1), 250 to 410 °C extender or processing oils (stage 2) and 410 to 570 °C the thermal decomposition of the EPDM copolymer

(step 3). This information is later used to indicate the composition of the mixture with which the EPDM rubber was prepared and will be completed with the results of the experience up to 900 °C (section 5.2.2) since over the 3 stages of mass loss only about 70% of the material is consumed.

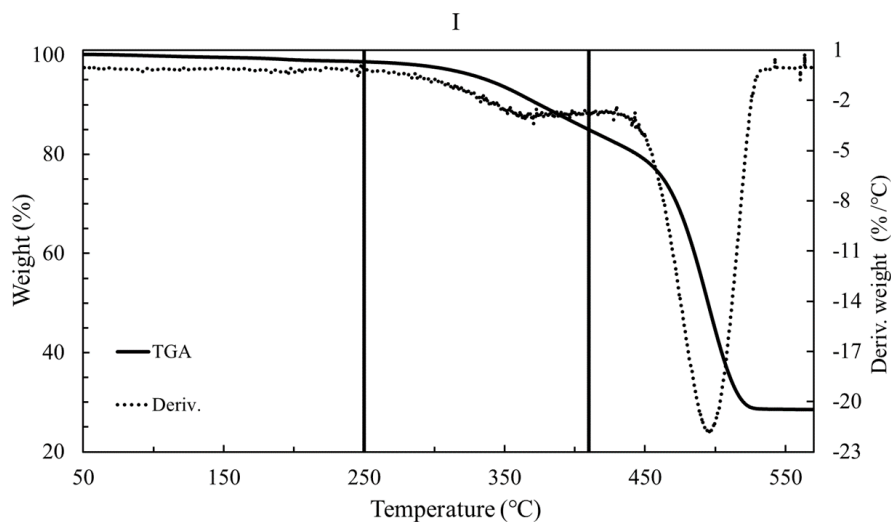


Figure 19 TGA and DTG for Rubber I at 20 °C min⁻¹ with N₂ at 20 ml min⁻¹.

Table 6 summarized temperature ranges described above for each elastomer sample after they were evaluated at all heating rates and the information were obtained from the TGA curves (Appendix C1 to C18).

Relying on the TGA results of Table 7 and what is discussed in section 5.1.1 new evidence of the differences between Group 1 and 2 is shown. The first one is the EPDM terpolymer content (% Weight lost 410-570 °C), presents a difference of approximately 2.2% between the 2 sets of materials. Often this difference is attributed to the control processes during production and is usually neglected. The relevant is that the composite material has a portion of EPDM that ranges from 54.1 to 56.3%.

Another peculiarity in the samples of Group 1 is that they have a higher percentage of water (1,47%) compared to Group 2 (0.67%). Based on the fact that Metakaolin is an aluminosilicate with an amorphous structure (L. Caraballo et al.,[92]) with more free space available to be occupied by the liquid in contrast to Kaolin that is organized as crystal (D. Bish et al.,[93]), a higher mass of water is hypothetically expected in Group 1.

Table 7 Average TGA results for rubbers after being evaluated at 7 heating rates (5,10,15, 20, 25, 30 and 40 °C min⁻¹) with N₂ at 20 ml min⁻¹ from 30-570 °C (Appendix C19 to C20).

Group	Rubber	Depth (m)	Well	Time (days)	%Weight lost 30-250 °C (Water)	%Weight lost 250-410 °C (Oil)	%Weight lost 410-570 °C (EPDM)
1	I	0		0	1.449	13.840	56.343
	II	0		0	1.373	14.131	55.795
	III	760	B-17	1752	1.421	13.081	55.754
	VI	2170	B-17	1752	1.640	14.747	56.255
	Average				1.471	13.950	56.037
	Standard deviation				0.101	0.599	0.264
2	IV	917	A-29	738	0.739	13.648	54.606
	V	1927	A-29	738	0.610	13.799	54.102
	Average				0.675	13.724	54.353
	Standard deviation				0.065	0.075	0.251

A similarity present in the 6 composite materials analyzed refers to the content of additives, in particular extender oils shown in Table 7. The quality shown are close and are within the standard deviation when quantifying their presence from 250 to 410 °C.

In summary, the composition of the composite material is as follow: a minimum of 54.3% EPDM, 13.7% processing oils, and 1.5 to 0.7% water were found.

5.2.2. Thermo-degradation up to 900 °C

Figure 20 is used to illustrate TGAs with the extended methodology with synthetic air oxidizing atmosphere (Appendix D1 to D6) to determine carbon black content and aluminosilicates within rubbers. In this particular case, the samples of Group 1 are presented with Metakaolin represented by stable masses above 900 °C. The carbon black values are calculated by the differences in mass at the beginning of the methodology at 570 °C, temperature at which all the EPDM is considered completely degraded, and the final mass, excepting that the final mass is due to the stable residue of aluminosilicate above this temperature.

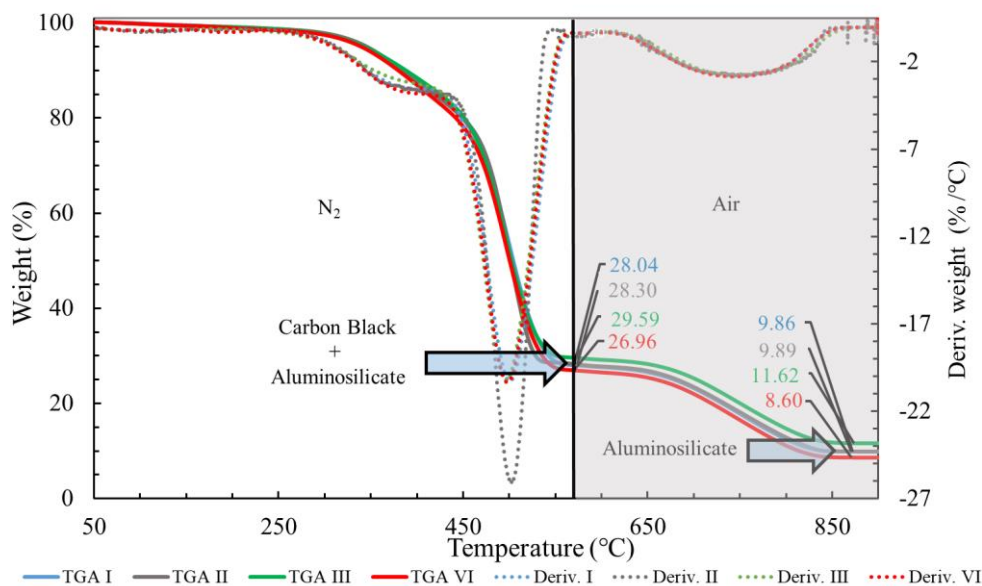


Figure 20 TGA and DTG at 25 °C min⁻¹ for rubbers from Group 1 in N₂ at 20 ml min⁻¹ from 30-570 °C and synthetic air 20 ml min⁻¹ from 570-900 °C.

Table 8 summarized weight and weight loss during TGA analysis at 25 °C min⁻¹, in synthetic air 20 ml min⁻¹ from 570-900 °C (Attachment 35).

Table 8 TGA results at 25 °C min⁻¹ for the rubbers in the synthetic air stage at 20 ml min⁻¹ from 570-900 °C

Group	Rubber	Depth (m)	Well	Time (days)	% Weight 570 °C (Carbon black + Aluminosilicate)	% Weight lost 570-900 °C (Carbon black)	% Weight 900 °C (Aluminosilicate)
1	I	0		0	28.046	18.185	9.861
	II	0		0	28.300	18.408	9.892
	III	760	B-17	1752	29.591	17.973	11.618
	VI	2170	B-17	1752	29.965	18.367	8.598
	Average					28.266	18.233
Standard deviation					0.934	0.172	1.074
2	IV	917	A-29	738	30.815	16.955	13.860
	V	1927	A-29	738	31.254	17.177	14.077
	Average					31.035	17.066
Standard deviation					0.220	0.111	0.109

Table 7 shows a new peculiarity between Groups 1 and 2. For the first one, the % mass of Metakaolin 9.99 was quantified, while for the second one, it corresponds to the % mass of Kaolin 13.97. This heterogeneity of values could impact on the properties of the material. Another subtle variation is the carbon black content which varies between 18.23wt.% to 17.07 wt.%.

Summarizing of the thermal degradation results, the 6 EPDM rubbers show 54 to 56.5 wt.% of the EPDM as a matrix. The charges include carbon black (17 to 18 wt.%) and an aluminosilicate (10 wt.% Metakaolin Group 1 and 14 wt.% Kaolin Group 2). Approximately 14 wt.% of extender or processing oils were added to its preparation and 1.5 to 0.7 wt.% water.

This information is important when studying mixtures with this set of heterogeneities due to the impact on all final properties: gas adsorption (S. Rutherford et al.,[94]), mechanical properties (E. Redline et al.,[95]), flammability (X. Wen et al.,[96]), electrical, de-vulcanization (H. Le et al.,[97]) and aging (Z. Petrović et al.,[90])

5.3. Preselection/refinement of data for the non-isothermal kinetic study of the elastomer

Before studying the results of the kinetic triplet (E, A and n) and proposed models (KMW, OFW, Friedman, CKA and CKA-i) it is important to present the preselection/refinement of the data and the criteria that justify this selection. This will allow making decisions which model is the most appropriate in the present investigation.

First, the kinetic study of the degradation of EPDM rubber is proposed, starting at 410 °C, based on works by Bouguedad et al.,[23]. At this temperature, the polymer pyrolysis process begins in an N₂ atmosphere allowing to consider STA data only in the interval from 410 to 570 °C. Figure 21 illustrates this temperature range.

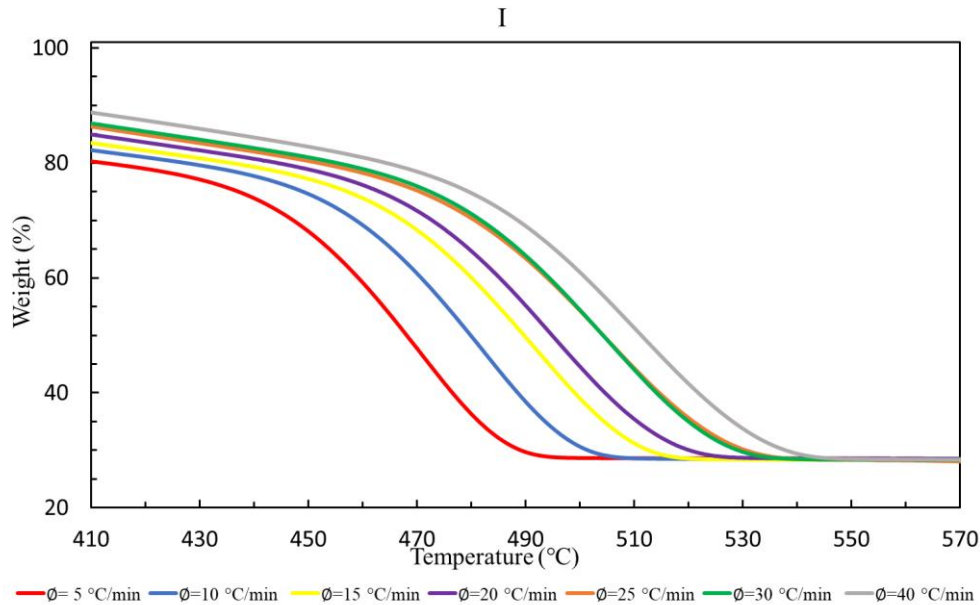


Figure 21 TGA curves of EPDM degradation region in Rubber I at 20 ml min^{-1} , under N_2 atmosphere with different heating rates.

The transformation from mass data (wt.%) to conversion data (α) is easily done by equation (4). Conversion results are plotted in Figure 22, used as an example. The individual trend of the data plot at each speed exhibits a pattern behavior and does not present irregularities in the results. But when analyzing the conversion plot at the 7 proposed speeds ($5, 10, 15, 20, 25, 30$ and 40 °C min^{-1}) for the 6 EPDM rubbers (Appendix E1 to E6), it is repeatedly observed that overlap occurs from the data obtained at the heating rate of 25 °C min^{-1} and 30 °C min^{-1} . This behavior is considered atypical and to solve this phenomenon it is proposed to exclude one of the 2 heating speeds.

The discarding of the 25 °C min^{-1} data was based on the fact that the conversion plot with the 7 heating speeds are constructed with data obtained under 2 different types of experiments at specific conditions. The first experiment contemplates the heating rates $5, 10, 15, 20, 30$ and 40 °C min^{-1} in a range of 30 to 570 °C in a N_2 atmosphere (section 4.3.2.1). The second experiment uses only 25 °C min^{-1} divided into 2 steps, which start with the range of 30 to 570 °C in N_2 followed by temperatures of 570 to 900 °C in Ar (section 4.3.2.2). Therefore, it is proposed to exclude the data at the heating rate of 25 °C min^{-1} from the conversion plot and these data are excluded for the kinetic analyzes.

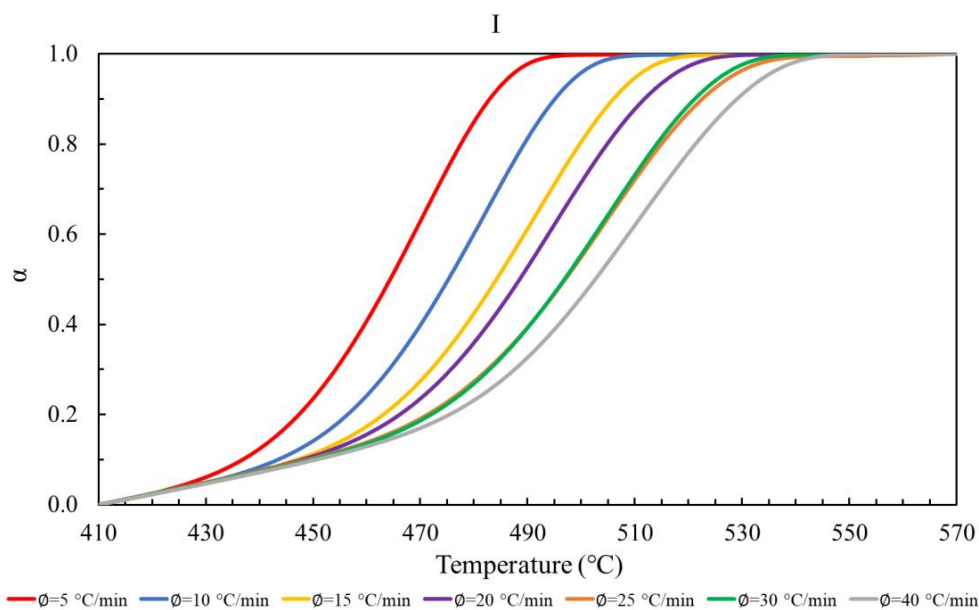


Figure 22 Conversion of EPDM degradation in Rubber I, at 20 ml min^{-1} , under N_2 atmosphere with different heating rates.

To validate the heating rates (ϕ) in which the experiments were carried out, calculations of the temperature variation divided by the time variation $\phi = \frac{dT}{dt}$ were made in the range from 410 to 570 °C. Obtaining real values of said heating rate (ϕ_{True}), with the latter the kinetic calculations are carried out individually. Table 8 presents the nominal values of the heating rates (ϕ) and the true values of the heating rate (ϕ_{True}) for each rubber.

Table 9 Heating rates validation in the experiments.

ϕ (K/min)	Rubber					
	I	II	III	IV	V	VI
ϕ_{True} (K/min)						
5	4.90	4.89	4.88	4.89	4.90	4.90
10	9.87	9.88	9.88	9.88	9.87	9.88
15	14.96	14.91	14.93	14.90	14.93	14.92
20	20.09	20.06	20.08	20.00	19.95	20.05
30	30.33	30.33	30.39	30.31	30.25	30.34
40	40.58	40.65	40.68	40.71	40.57	40.65

*the uncertainty of the calculation ranges between the second and third decimal places.

5.3.1. Kissinger model (KMW)

From equation (21) implemented by Kissinger, it was possible to obtain a linear relationship in the graphs as shown in Figure 23

$$\ln\left(\frac{\phi}{T_m^2}\right) = -\frac{E}{RT_m} + \ln\frac{AR}{E} \quad (21)$$

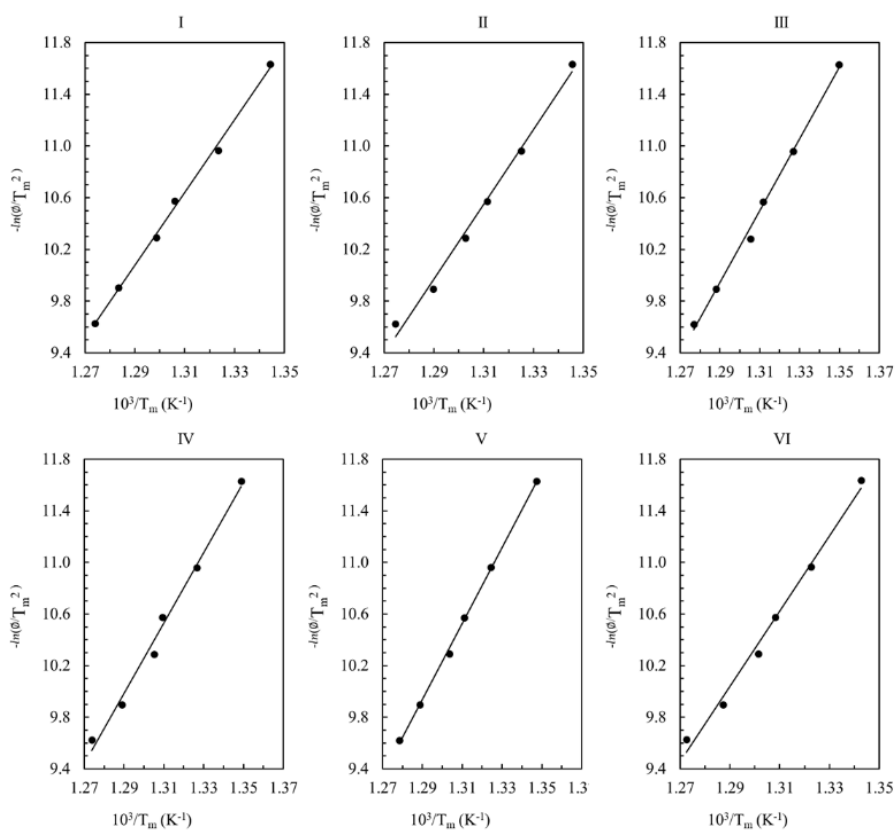


Figure 23 Kissinger plots for the 6 rubbers, under N₂ atmosphere at 20 ml min⁻¹ and non-isothermal conditions at heating rates 5, 10, 15, 20, 30 and 40 °C min⁻¹.

With the outcomes of Figure 23 it is feasible to present kinetic models like the one proposed below for Rubber I in equation (43), just by substituting A and E values, selecting temperature(T) in Kelvin and under n=1 assumption.

$$k = 6.8305 \times 10^{15} \text{min}^{-1} e^{-\frac{233914 \frac{\text{J}}{\text{mol}}}{8.314 \frac{\text{J}}{\text{mol K}} T \text{K}}} \quad (43)$$

The results for the 6 samples are shown in Table 9. Note the R² variation for the 6 trend lines from 0.9891 to 0.9990. Interpreting in the lowest case 98.91 % of the data match the linear model, supporting this theory. Another relevant result are the inaccuracies of the activation energy values, which differ from 4 to 12 kJ/mol (1 to 5 %) of the reported value (Appendix F1 to F3).

Table 10 Results of the kinetic data obtained by the KMW method for the 6 rubbers, under N₂ atmosphere at 20 ml min⁻¹ and non-isothermal conditions at heating rates 5, 10, 15, 20, 30 and 40 °C min⁻¹.

Rubber	R ²	E (kJ/mol)	γ _E	ln(A /min ⁻¹)	γ _{lnA}
I	0.9974	234	6	36	11
II	0.9920	240	11	38	11
III	0.9959	231	7	36	10
IV	0.9891	227	12	35	10
V	0.9990	245	4	38	11
VI	0.9908	243	12	37	11

5.3.2. Ozawa-Flynn-Wall (OFW) model

Figure 24 shows the results of the OFW method for the 6 elastomers based on equation (27).

$$\log \phi = -\frac{0.4567E}{RT_{\alpha}} + \text{Constant} \quad (27)$$

Each plot in Figure 24 results in the projection of a flat surface made up of several lines. These lines present similar behaviors in their direction. The R^2 of the lines varies from 0.9919 to 0.9995, which supports the approach to straight lines (Appendix G1 to G12). Validating the OFW model application in the kinetic study. OFW plots are applying the isoconversion approximation for α fluctuating from 0.2 to 0.95. The arbitrarily proposed separation between the lines is $\Delta\alpha=0.05$ with the mean of projecting a surface formed by multiple lines at constant conversions (α_i). The maximum number of feasible lines to draw is limited by the appreciation of the equipment at maximum speed. In these experiments the appreciation is close to $\Delta\alpha=0.0003$. With such a small separation of α , the graph would be saturated and appreciating the linearity of the model when examined at a constant α . Therefore, a separation of $\alpha = 0.05$, was proposed to allow visualizing the alignment pattern and its linearity.

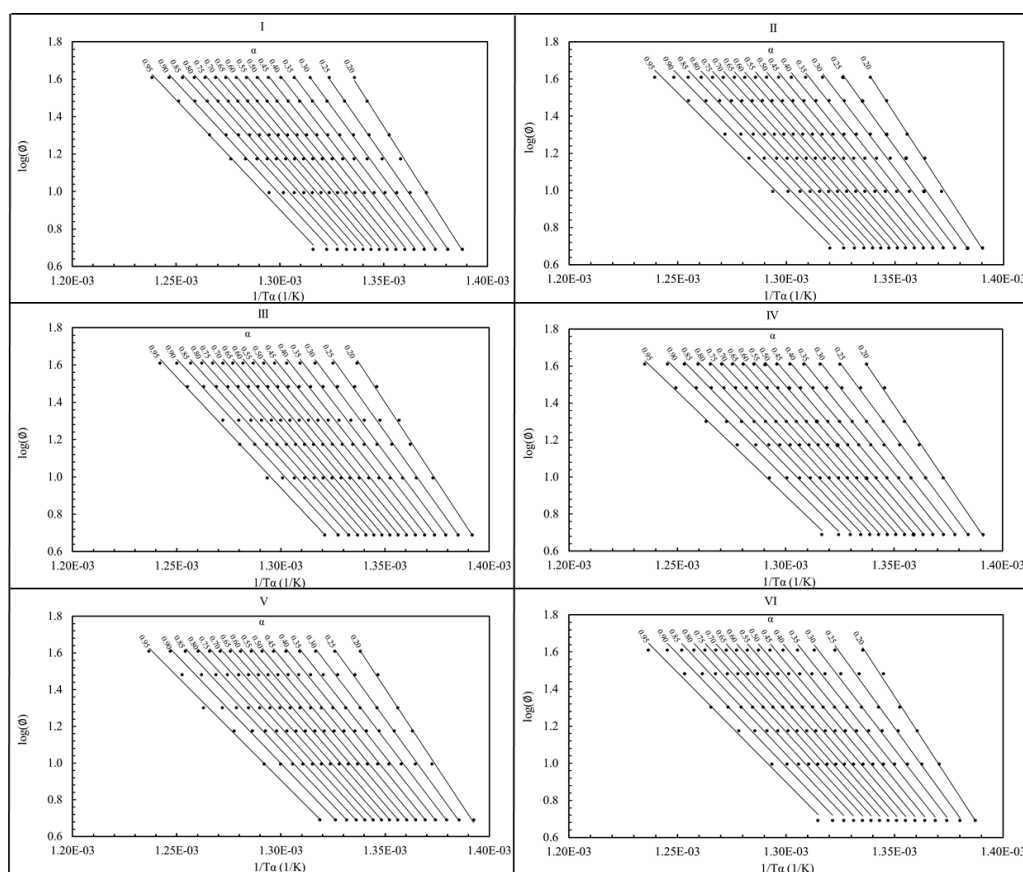


Figure 24 OFW plots for all rubbers under N_2 atmosphere at 20 ml min^{-1} and non-isothermal conditions at heating rates $5, 10, 15, 20, 30$ and $40 \text{ }^\circ\text{C min}^{-1}$. Analyzed under isoconversion condition.

Figure 25 shows the $\log(\phi)$ dependence with the inverse of the absolute temperature for Rubber I at the 6 proposed heating rates using the method developed by Ozawa under isoconversion condition. The special feature is the lower edge of the surface, which is well aligned with the axis of the abscissa. Understanding there is an equivalence of $1/T$ with the conversion.

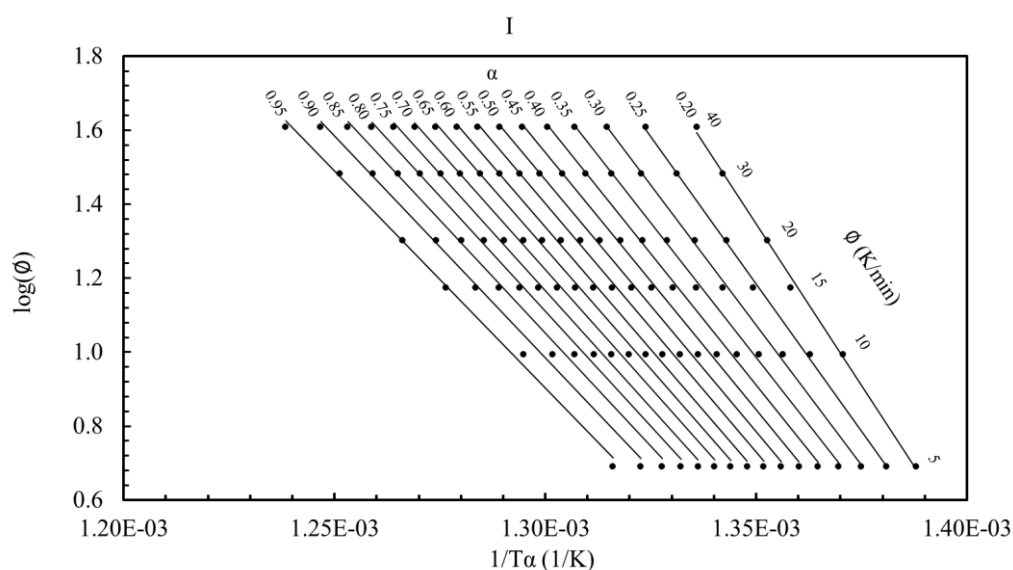


Figure 25 OFW plots for Rubber I, under N_2 atmosphere at 20 ml min^{-1} and non-isothermal conditions at heating rates 5, 10, 15, 20, 30 and $40 \text{ }^\circ\text{C min}^{-1}$. Analyzed under isoconversion condition (Appendix G1 to G7).

Table 13 shows the data obtained from the OFW model in Figure 25, regarding the tendency to the linear behavior of the model with minimum $R^2 = 0.9964$ showing values according to the linearity. The linearity behavior is repeated in all samples (Appendix G7 to G12).

A behavior profile between activation energy, frequency factor, and conversion is shown in Figure 26. E vs A graphs show a linearity, confirming their parallel responses with the variation of the conversion. This pattern is similar for the other six rubbers (Appendix G13 to G18).

Figure 26a illustrates the data from Table 11, which corresponds to the trend between the frequency factor (A) and the activation energy (E) along the conversion axis. It could be theorized that at low conversions, the amount of material available to react is the greatest, opening a maximum interaction of the reactive atoms. On the other hand, at high conversions there is little material left to transform, therefore, the number of interactions of the reactive atoms also decreases.

Additionally, in Figure 26b helps to perceive the existence of the approximately linear dependence of the amount of activation energy and the frequency factor. This behavior shows that the greater the number of effective collisions of the reactants, a greater amount of activation energy is required. Both quantities E and A decrease in parallel in the course of the reaction due to the evident consumption of the reactants.

Table 11 Results of the OFW method for Rubber I, under N₂ atmosphere at 20 ml min⁻¹ and non-isothermal conditions at heating rates 5, 10, 15, 20, 30 and 40 °C min⁻¹, assuming n=1. Analyzed under isoconversion condition.

α	R ²	E (kJ mol ⁻¹)	γ_E	ln(A /min ⁻¹)
0.20	0.9979	322	7	53
0.25	0.9986	293	5	48
0.30	0.9986	277	5	45
0.35	0.9985	266	5	43
0.40	0.9984	259	5	41
0.45	0.9983	253	5	40
0.50	0.9981	248	5	39
0.55	0.9980	244	5	38
0.60	0.9978	240	6	38
0.65	0.9976	237	6	37
0.70	0.9974	233	6	36
0.75	0.9973	230	6	35
0.80	0.9971	226	6	35
0.85	0.9969	222	6	34
0.90	0.9968	218	6	33
0.95	0.9964	213	6	32
Average	\bar{E} (kJ mol ⁻¹)	249	$\gamma_{\bar{E}}$	28
	ln(\bar{A} /min ⁻¹)	39	$\gamma_{\ln\bar{A}}$	5

Málek[98] reported similar responses of activation energy and frequency factor. In which 2 magnitudes are correlated by the equation (44). Defining “a” and “b” as a constant value results from the graph.

$$\ln A_{\alpha_i} = a + bE_{\alpha_i} \quad (44)$$

Budrugaec et al.,[99] reported the change of the activation energy with the progress of the reaction and report its behavior by equation (45) where E_0 and E_1 are constant parameters of the regression.

$$\ln A_{\alpha_i} = a + bE_{\alpha_i} \quad (45)$$

Budrugaec et al.,[50] reported that the variation of the activation energy with the progress of the reaction is reported for complex chemical processes, such as chemical reactions: parallel, successive or reversible.

A summary of the results for all Rubber is shown in Table 12 for $\alpha = 0.65$ with R^2 minimum 0.9945 exposing the linearity of the results to this conversion.

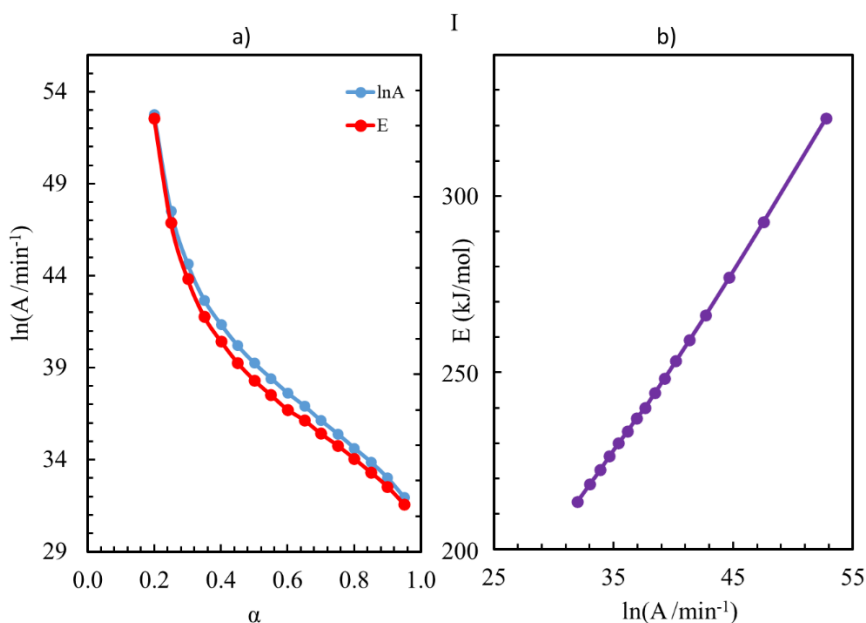


Figure 26 a) Behavior of activation energy and frequency factor at different conversions. b) variation of activation energy with frequency factor. For Rubber I, obtained with the OFW method in non-isothermal conditions at heating rates 5, 10, 15, 20, 30 and 40 °C min⁻¹. Analyzed under isoconversion condition

Table 12 Results of the OFW method to conversion $\alpha = 0.65$ in non-isothermal conditions at heating rates of 5, 10, 15, 20, 30 and 40 °C / min. Analyzed under the isoconversion condition. (Appendix G7 to G12).

Rubber	R ²	\bar{E} (kJ mol ⁻¹)	$\gamma\bar{E}$	$\ln(\bar{A} / \text{min}^{-1})$
I	0.9976	237	6	37
II	0.9953	240	8	37
III	0.9969	239	7	37
IV	0.9994	235	3	37
V	0.9967	235	7	37
VI	0.9945	239	9	37

5.3.3. Friedman model (FR)

The Friedman model proposed in 1964 [100] as one of the first differential methods where the isoconversion approximation was considered is based on equation (29). It is presented in Figure 27 for the 6 Rubbers in the study (Appendix H1 to H6). Showing lines that are parallel but that when aligned form a surface with a curvature.

$$\ln \frac{\phi d\alpha_i}{dT} = \ln A_{\alpha_i} + f(\alpha_i) - \frac{E_{\alpha_i}}{RT} \quad (29)$$

Figure 28 shows for Rubber I the behavior at 6 heating speeds of the results without applying the isoconversion condition (equation (33) without applying the isoconversion approximation). This image makes it possible to better appreciate the origin of the curvature of the surface formed by drawing the lines that join each heating rate in the isoconversion condition. This last condition is shown in Figure 29, being the common presentation of the results.

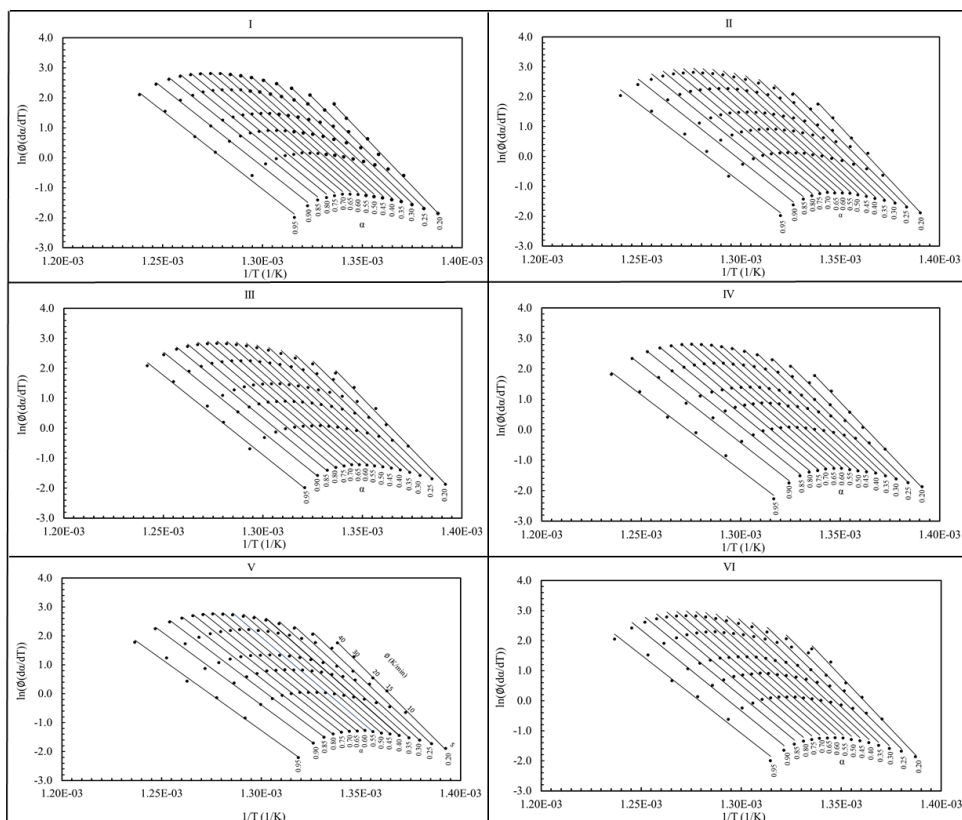


Figure 27 Friedman's method plot for all rubbers, under N_2 atmosphere at 20 ml min^{-1} , in non-isothermal conditions at heating rates $5, 10, 15, 20, 30$ and $40 \text{ }^\circ\text{C min}^{-1}$. Analyzed under isoconversion condition.

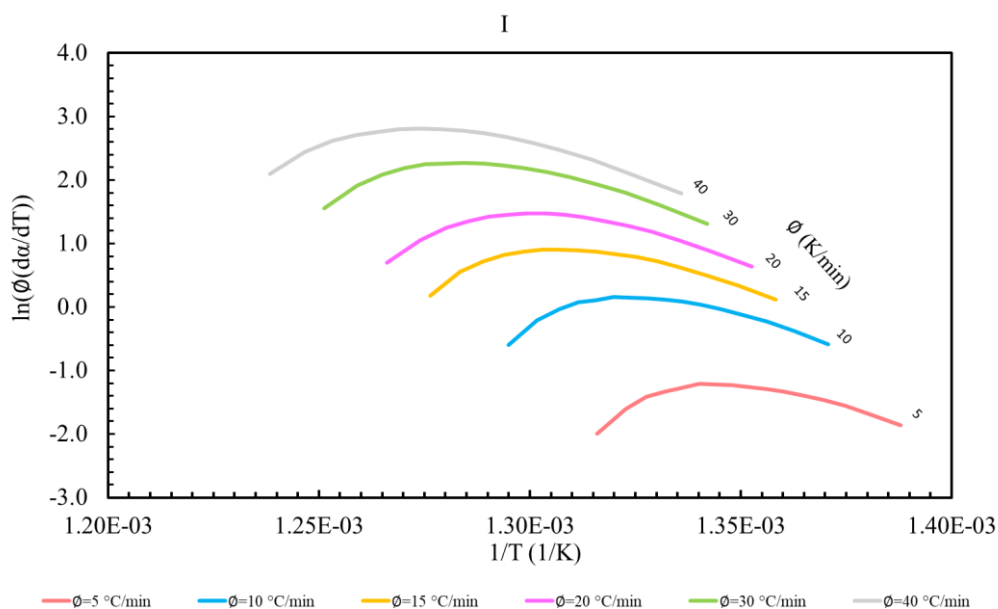


Figure 28 Friedman's method plot for Rubber I, under N_2 atmosphere at 20 ml min^{-1} and non-isothermal conditions at heating rates $5, 10, 15, 20, 30$ and $40 \text{ }^\circ\text{C min}^{-1}$. Analyzed in the range of 0.2 to 0.95 conversion.

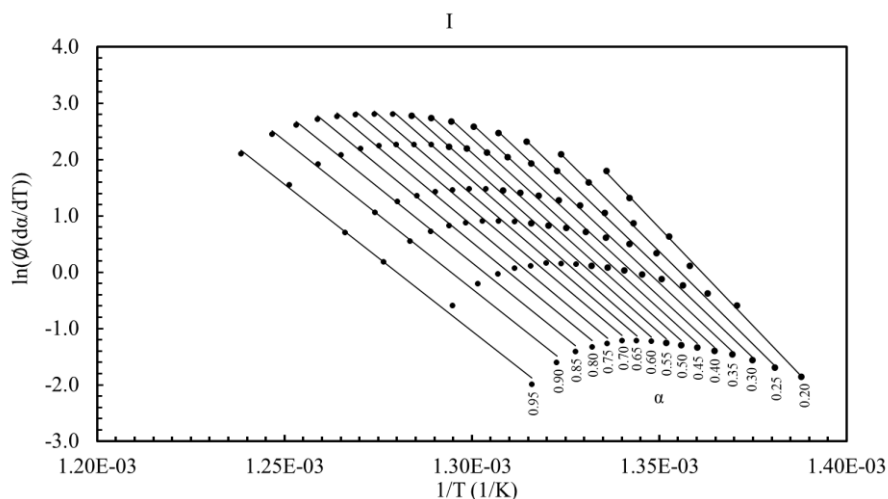


Figure 29 Friedman's method for Rubber I, under N_2 atmosphere at 20 ml min^{-1} , under non-isothermal conditions at heating rates $5, 10, 15, 20, 30$ and $40 \text{ }^\circ\text{C min}^{-1}$. Analyzed under the condition of isoconversion.

Figure 30 presents the superposition of Figure 28 and Figure 29 exposing the complete appearance of the Friedman method. In the Appendix H7 to H12, the results for the 6 Rubbers are shown showing a similar behavior

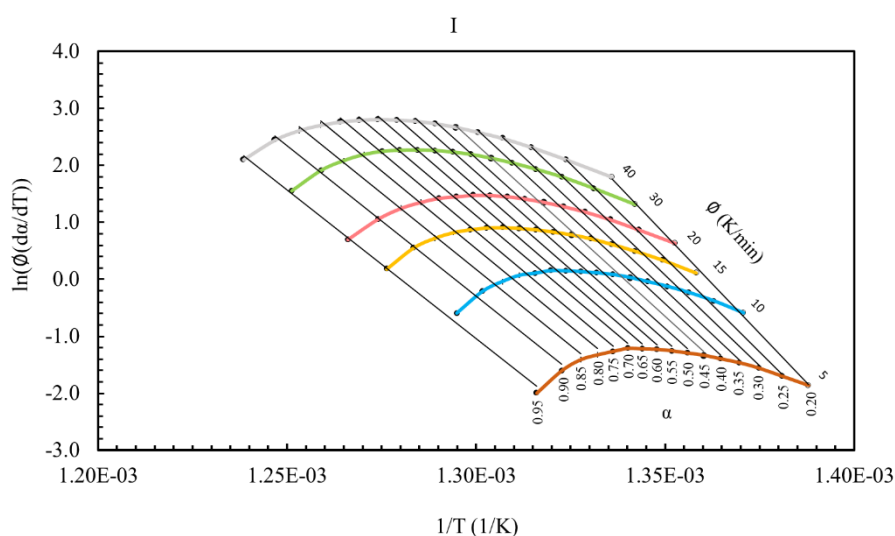


Figure 30 Friedman's method plotting for Rubber, under N_2 atmosphere at 20 ml min^{-1} , under non-isothermal conditions at heating rates $5, 10, 15, 20, 30$ and $40 \text{ }^\circ\text{C min}^{-1}$. Analyzed under the condition of isoconversion. Corresponding to the overlap in Figure 28 and 32.

The activation energy and frequency factor obtained by the Friedman method are presented in Table 13. Emphasizing the activation energy data, which varies from 578 to 433 kJ mol^{-1} in the range of 0.2 to 0.95 conversion. The average

value is $489 \pm 40 \text{ kJ mol}^{-1}$ and the logarithm of the frequency factor presents a variation with the conversion, with 78 ± 8 as an average. In both cases the resulting data doubles the magnitudes when compared with OFW and KMW. This difference can be explained by P. Budrugeac's contribution to the equation (32). Or as the same author explains when comparing equation (18) and (19) the results of the activation energy computed by the differential method and by the integral methods are not equal.

$$E_{FR} = E_{FWO} + 0.052E_{FWO} - R \left(\frac{\partial \ln \frac{d\alpha}{dT}}{\partial T^{-1}} \right) \quad (32)$$

$$\left[\left[\frac{\partial \ln \frac{d\alpha_i}{dt}}{\partial T^{-1}} \right]_{\alpha_i} = -\frac{E_{\alpha_i}}{R} \right]_{\text{Differential}} \neq \left[\left[\frac{\ln \frac{g(\alpha)}{A} + \frac{E_{\alpha_i}}{TR}}{\partial T^{-1}} \right]_{\alpha_i} = \frac{E_{\alpha_i}}{R} \right]_{\text{Integral}} \quad (18)\&(19)$$

Table 13 Results of Friedman's method for Rubber I, under N₂ atmosphere at 20 ml min⁻¹ and non-isothermal conditions at heating rates 5, 10, 15, 20, 30 and 40 °C min⁻¹, assuming n=1. Analyzed under isoconversion condition.

α	R ²	E (kJ mol ⁻¹)	γ_E	ln(A /min ⁻¹)	$\gamma_{\ln A}$
0.20	0.9982	578	12	95	2
0.25	0.9981	547	12	89	2
0.30	0.9979	530	12	86	2
0.35	0.9977	518	12	84	2
0.40	0.9977	511	12	82	2
0.45	0.9974	502	13	81	2
0.50	0.9970	497	14	80	2
0.55	0.9971	490	13	78	2
0.60	0.9969	482	13	77	2
0.65	0.9966	474	14	76	2
0.70	0.9965	465	14	74	2
0.75	0.9962	461	14	73	2
0.80	0.9955	453	15	71	2
0.85	0.9958	444	14	70	2
0.90	0.9953	438	15	68	2
0.95	0.9951	433	15	67	2
Average	\bar{E} (kJ mol ⁻¹)	489	$\gamma_{\bar{E}}$	40	
	ln(\bar{A} /min ⁻¹)	78	$\gamma_{\ln \bar{A}}$	8	

Figure 31 shows the graphical representation of data from Table 13. In the plot indicates that the activation energy and frequency factor vary with conversion. Displaying that both magnitudes vary in parallel with the progress of the conversion, making both values almost behave linearly with each other.

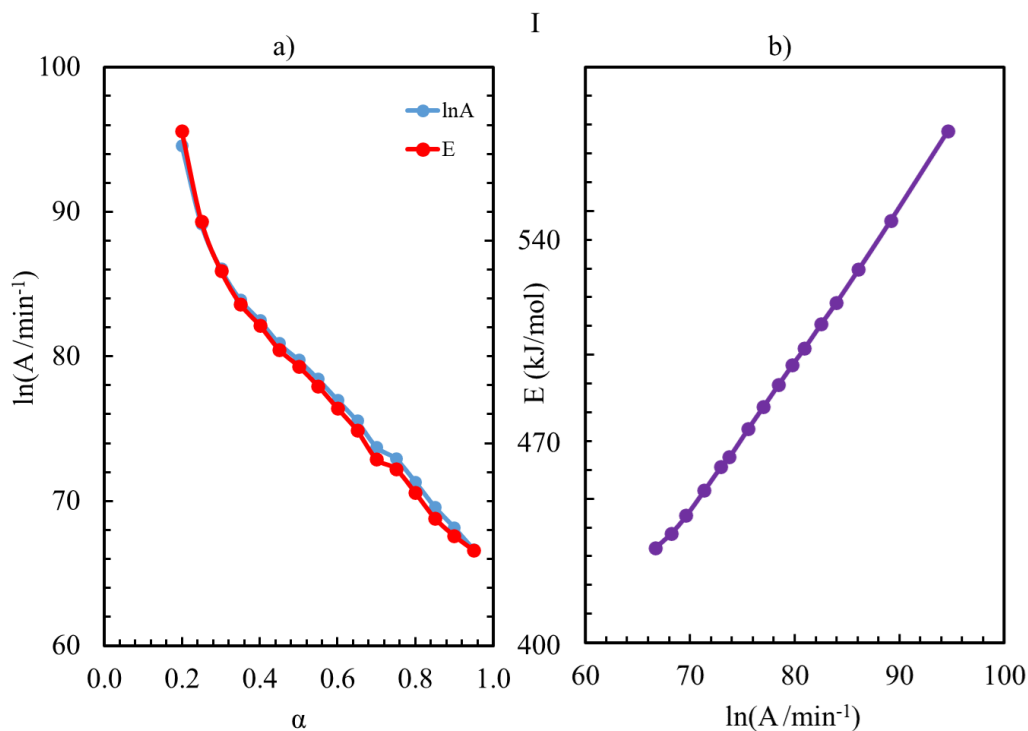


Figure 31 a) Behavior of activation energy and frequency factor at different conversions. b) variation of the activation energy with the frequency factor. For Rubber I, obtained with Friedman's method in non-isothermal conditions at heating rates 5, 10, 15, 20, 30 and 40 °C min⁻¹. Analyzed under the condition of isoconversion.

The activation energy and frequency factor variation results for the 6 Rubber are presented individually in Appendix H13 to H24 showing similar results to those shown in Table 13 and Figure 31 for Rubber I.

5.3.4. Combined Kinetic Analysis model (CKA)

5.3.4.1. Reaction order for CKA

Following the approach for the computation of the reaction order by the CKA model (equation (39)).

$$\ln \left(\frac{\phi \frac{d\alpha}{dT}}{e^{-\frac{E}{RT}}} \right) = n \ln(1 - \alpha) + \ln A \quad (35)$$

Figure 32 the result for Rubber I evaluated under non-isothermal conditions is presented. Each line represents the results obtained at a single heating rate individually identified by a color. Appreciating the tendency of the different lines to project almost parallel to each other. The small deviations of the slope of each line or of the reaction order in this case, could be attributed to the errors in the experimental measurements. Additionally, the separation and order of presentation of each line in the graph stand out, which does not have any linear relationship of separation or propensity with the increase in the heating rate, so the use of a mean value seems to be the most indicated for report an end of the reaction order.

Figure 33 shows for the 6 rubbers analyzed how the response pattern is repeated when determining the reaction order of the EPDM degradation, in the conversion interval from 0.2 to 0.95. For more detail on these figures see Appendix I1 to I6

Table 16 reflects the typical results using Rubber I as an example in Figure 35. Showing the linearity obtained with R^2 greater than 0.9991 and slopes with uncertainties with maximum value in the third decimal place. The average of the order of reaction is 0.87 with a standard deviation of 0.05, exposing the proximity of the values.

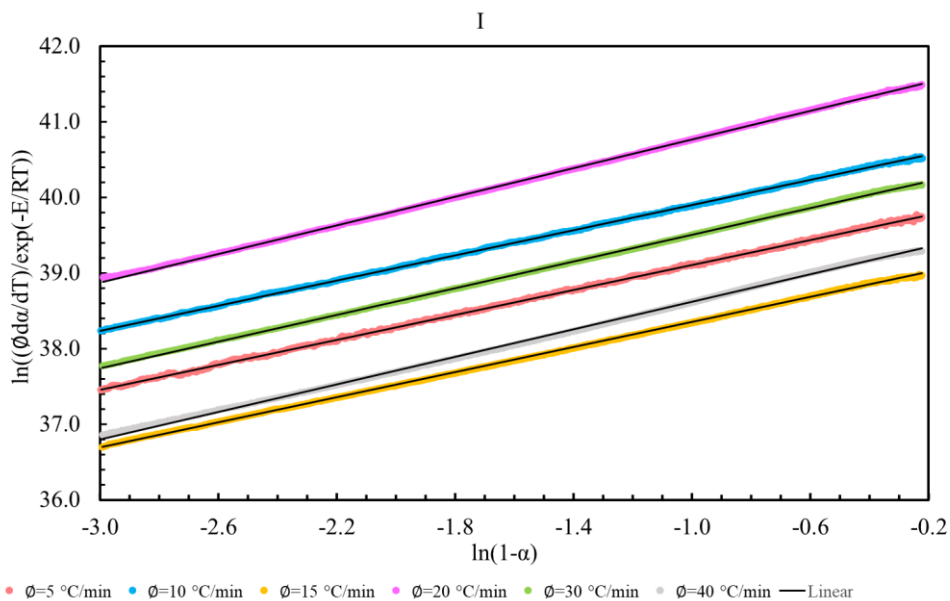


Figure 32 CKA method plot for calculating the reaction order of the thermo degradation of Rubber I, under N_2 atmosphere at 20 ml min^{-1} and non-isothermal conditions at heating rates $5, 10, 15, 20, 30$ and 40 °C min^{-1} .

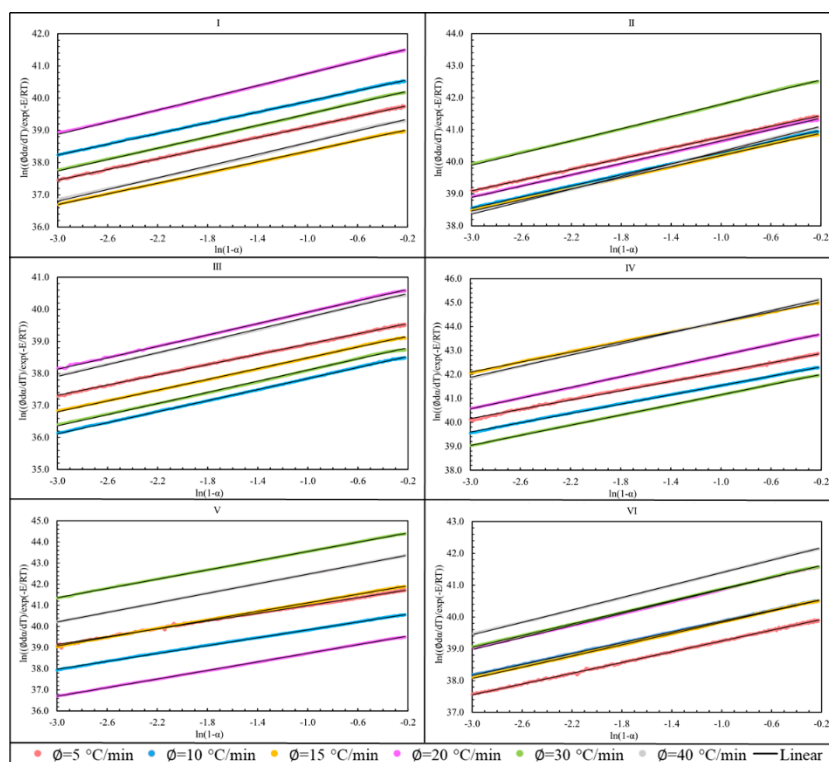


Figure 33 CKA method plot for calculation of the reaction order of all rubbers, under N_2 atmosphere at 20 ml min^{-1} , in non-isothermal conditions at heating rates $5, 10, 15, 20, 30$ and 40 °C min^{-1} .

Table 14 Results of the CKA method for the calculation of the reaction order of Rubber I in an atmosphere of N₂ at 20 ml min⁻¹ and non-isothermal conditions at heating rates of 5, 10, 15, 20, 30 and 40 °C min⁻¹.

\emptyset (K/min)	n	γ_n	$\ln(A / \text{min}^{-1})$	$\gamma_{\ln A}$	R ²
5	0.8251	0.0002	39.9350	0.0003	0.9997
10	0.8303	0.0003	40.7301	0.0003	0.9998
15	0.8301	0.0004	39.1810	0.0005	0.9996
20	0.9468	0.0005	41.7139	0.0006	0.9997
30	0.8832	0.0005	40.3928	0.0007	0.9997
40	0.9107	0.0010	39.5320	0.0013	0.9991
\bar{n}	0.87	$\gamma_{\bar{n}}$	0.05		
$\ln(\bar{A} / \text{min}^{-1})$	40.2	$\gamma_{\ln \bar{A}}$	0.8		

Table 17 collects the averages of the individual reaction order results for each material obtained from the CKA method (Appendix I7 to I12). It is appreciated that the values are very close to unity. However, there is a subtle difference separating Rubbers I, II, III and VI (Group 1 with Metakaolin filling) from Rubbers IV and V (Group 2 with Kaolin filling). This difference in reaction orders is not very significant when considering the uncertainty in the calculations, but it is indicative that the material of group 2 reacts more quickly to degradation processes when compared to group 1.

Table 15 Summary of the average order of reaction obtained by CKA

Rubber	\bar{n}	$\gamma_{\bar{n}}$
I	0.87	0.05
II	0.90	0.05
III	0.86	0.04
IV	1.05	0.07
V	1.02	0.08
VI	0.90	0.05

These results for n and R² also confirm that the reaction model $f(\alpha) = (1 - \alpha)^n$ considered describes the thermodegradation of EPDM very well.

5.3.4.2. Activation energy by CKA

Figure 34 confirms the trend to linearity of the CKA model for the calculation of the activation energy (equation (36)) in the conversion range from 0.2 to 0.95, at the proposed heating rates. The behavior of the lines is similar to that of lines parallel to each other. The existence of a sequential pattern is noted in the order of the lines obtained with the heating rate.

$$\ln \left(\frac{\phi \frac{d\alpha}{dT}}{(1-\alpha)^n} \right) = -\frac{E}{RT} + \ln A \quad (36)$$

As shown in equation (36) this algorithm sets a single activation energy value (E) for a fixed heating rate (ϕ). In this case, it can be seen that for each reaction speed there is a displacement of the lines when modifying their cut-off point, but there is a clear tendency for the tangents of the data obtained to be parallel and independent of the heating rate. For subsequent analysis, we will continue to assign the CKA code to these lines obtained by equation (36).

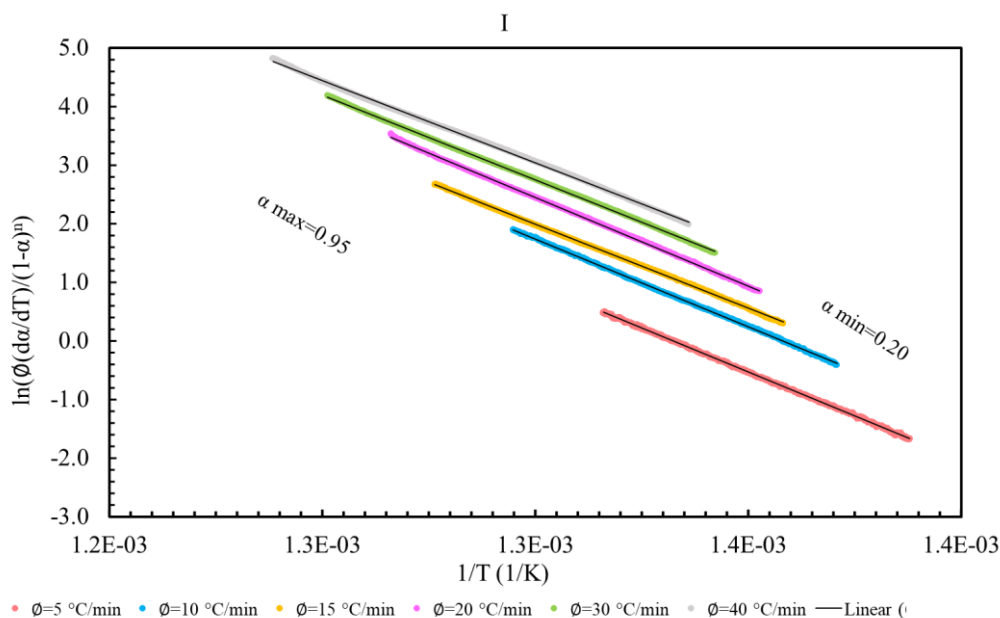


Figure 34 CKA method plot for calculating the activation energy of the thermo-degradation reaction of Rubber I in an atmosphere of N_2 at 20 ml min^{-1} and non-isothermal conditions at heating rates 5, 10, 15, 20, 30 and 40 °C min^{-1} .

Table 18 shows the calculated magnitudes of Figure 34. Noting that the minimum value of R^2 is 0.9994, indicating a fit very close to that of a line with the inverse of temperature. The individual values of the activation energy listed are a reflection of the tendency of the lines to be almost parallel to each other, as they are computed from the slopes of each line. The average activation energy is 244 kJ mol^{-1} with an uncertainty of 7 kJ mol^{-1} which is approximately 3 % of the absolute value.

Table 16 Results of the CKA method for calculating the reaction order of Rubber I in an atmosphere of N_2 at 20 ml min^{-1} and non-isothermal conditions at heating rates of 5, 10, 15, 20, 30 and $40 \text{ }^\circ\text{C min}^{-1}$.

\emptyset (K/min)	E (kJ mol ⁻¹)	γ_E	$\ln(\bar{A} / \text{min}^{-1})$	$\gamma_{\ln A}$	R^2
5	249.2	0.1	39.94	0.01	0.9997
10	249.3	0.1	40.73	0.01	0.9998
15	237.9	0.1	39.18	0.02	0.9997
20	251.1	0.1	41.71	0.02	0.9997
30	240.7	0.1	40.39	0.02	0.9998
41	233.4	0.2	39.53	0.03	0.9994
\bar{E} (kJ mol ⁻¹)	244	$\gamma_{\bar{E}}$	7		
$\ln(\bar{A} / \text{min}^{-1})$	40.2	$\gamma_{\ln \bar{A}}$	0.8		

Table 19 presents a general summary of the average of the results obtained calculated by the CKA method (Appendix J1 to J12) for each rubber sample. Degradation energies are reported with a maximum uncertainty of 9 kJ mol^{-1} (approximately 4%). Appreciating that they are obtained from the slopes of the CKA model in a range of heating rates from 5 to 40 K min^{-1} . The linear behavior and a propensity to be ordered almost in parallel within the limits studied stands out. On the other hand, the average of the frequency factor expressed as $\ln(\bar{A} / \text{min}^{-1})$ oscillates close to 42 and have a maximum uncertainty of 2 (close to 4%) giving very close values despite being calculated by the intercept of the straight at each speed.

Table 17 Results for the 6 Rubbers by the CKA method in a N₂ atmosphere at 20 ml min⁻¹ and non-isothermal conditions at heating rates of 5, 10, 15, 20, 30 and 40 °C min⁻¹.

Rubber	\bar{n}	$\gamma_{\bar{n}}$	\bar{E} (kJ mol ⁻¹)	$\gamma_{\bar{E}}$	$\ln(\bar{A} / \text{min}^{-1})$	$\gamma_{\ln\bar{A}}$
I	0.87	0.05	244	7	40.2	0.8
II	0.90	0.05	251	5	41.6	0.6
III	0.86	0.04	240	5	39.7	0.8
IV	1.05	0.07	265	7	44	1
V	1.02	0.08	255	9	42	2
VI	0.90	0.05	250	2	41.3	0.8

5.3.4.3.

Application of the isoconversion principle on the CKA method (CKA-i)

It is typical to observe in literature that the isoconversion principle is discussed for differential methods only by the Friedman equation. The application of the isoconversion principle in the CKA model with 0.05 separation interval in the conversion, projects a series of lines with behavior that approximates straight lines, whose behavior in global projects a surface as shown in Figure 38. For further analysis, we assign the CKA-i code to the straight lines obtained under the isoconversion condition. The formal proposal of this method is in equation (42) which we recall below.

$$\left[\frac{\partial \ln \left(\frac{\phi \frac{d\alpha}{dT}}{(1-\alpha)^n} \right)}{\partial T^{-1}} \right]_{\alpha_i} = \left[\frac{\partial \left(-\frac{E}{RT} + \ln A \right)}{\partial T^{-1}} \right]_{\alpha_i} = -\frac{E_{\alpha_i}}{R} \quad (38)$$

As can be seen in equation (42), the effect of including a reaction model in the computation of the differential method still allows the calculation of the activation energy. Comparing Figure 35 of CKA-i with Figure 29 of the Friedman

method, the difference is that the projected surface when joining the multiple lines is flat for CKA-i and a curved plane for Friedman. In Appendix K1 to K6 can visualize the CKA-i plots for the 6 Rubbers.

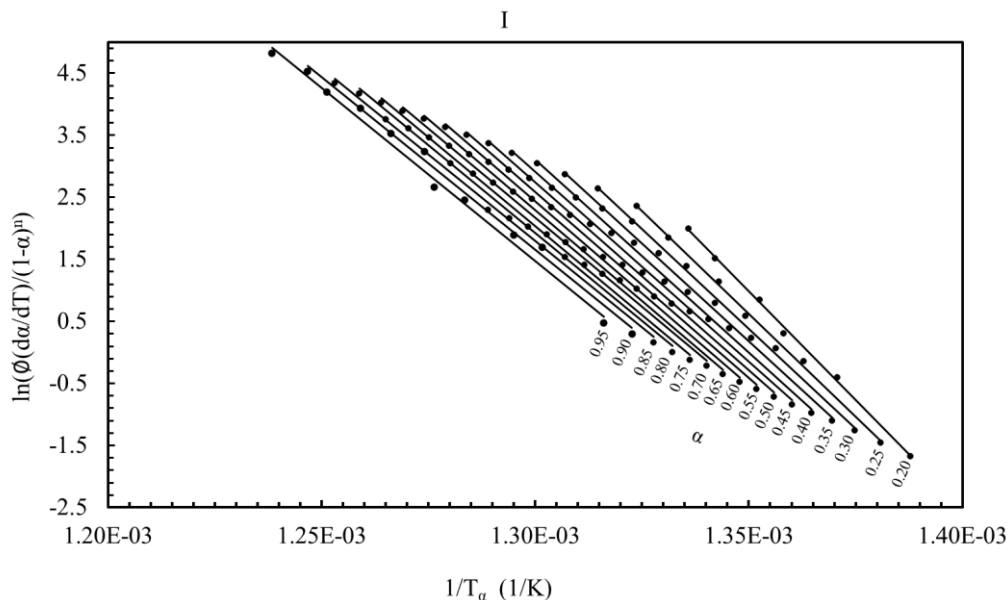


Figure 35 CKA-i method plot for the thermo-degradation reaction of Rubber I in an atmosphere of N_2 at 20 ml min^{-1} and non-isothermal conditions at heating rates 5, 10, 15, 20, 30 and $40 \text{ }^\circ\text{C min}^{-1}$.

The differences in values between CKA-ic and Friedman show that the reaction model is not responsible for the inclination of the lines calculated under the isoconversion condition of both.

Table 18 shows for Rubber I, how the activation energies vary with the conversion into CKA-i (using the principle of isoconversion), for the other samples the information is found in Appendix K7 to K12. Contrasting these results with Table 13 (Friedman results) highlights the fact that the values between both methods differ by less than 7% for the activation energy and 10% for the natural logarithm of the preexponential factor.

Table 18 Results of the CKA-i method for the thermo-degradation reaction of Rubber I in an atmosphere of N₂ at 20 ml min⁻¹ and non-isothermal conditions at heating rates 5, 10, 15, 20, 30 and 40 ° C min⁻¹.

α	R ²	E _{α} (kJ mol ⁻¹)	$\gamma_{E\alpha}$	ln(A /min ⁻¹)	$\gamma_{\ln A}$
0.20	0.9979	581	13	95	2
0.25	0.9978	551	13	90	2
0.30	0.9975	534	13	87	2
0.35	0.9973	524	14	85	2
0.40	0.9971	517	14	84	2
0.45	0.9967	510	15	83	2
0.50	0.9962	505	16	82	2
0.55	0.9961	499	16	81	2
0.60	0.9958	492	16	79	3
0.65	0.9954	486	16	78	3
0.70	0.9953	478	16	77	3
0.75	0.9949	476	17	77	3
0.80	0.9944	471	18	76	3
0.85	0.9945	465	17	74	3
0.90	0.9943	462	17	74	3
0.95	0.9938	464	18	74	3
Average	\bar{E} (kJ mol ⁻¹)	501	$\gamma_{\bar{E}}$	33	
	ln(\bar{A} /min ⁻¹)	81	$\gamma_{\ln \bar{A}}$	6	

5.3.4.4.

Correction of the isoconversion CKA method (CKA-ic)

To better visualize the reason why the data is transformed into a flat surface, the plots of Figure 34 and Figure 35 is superimposed, resulting in Figure 36. This operation can also be expressed as the superposition of the CKA type curves with CKA-i. Similar results are seen in Appendix L1 to L6 for the 6 Rubbers.

Figure 36 allows several points to be made. The first, it is equally valid to consider the principle of isoconversion in CKA, since there is the linear trend of the graph when the heating rate is varied at a constant conversion (values of R²> 0.9938) as shown in Table 18. On the other hand, the 7% difference with Friedman's results validates this idea.

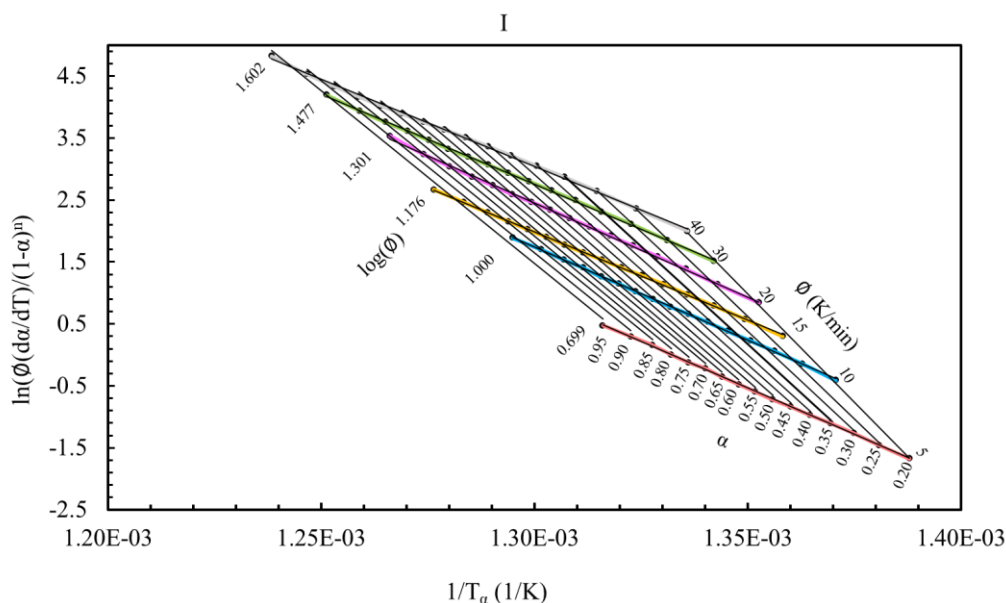


Figure 36 CKA method plot for Rubber I in an atmosphere of N_2 at 20 ml min^{-1} , under non-isothermal conditions at heating rates of 5, 10, 15, 20, 30 and $40 \text{ }^\circ\text{C min}^{-1}$. Analyzed under the isoconversion condition. Corresponding to the overlay of Figure 34 and Figure 35.

Figure 37 shows the comparison of Figure 35 of (CKA-i plot for Rubber I) with the shape of Figure 25 (OFW plot of Rubber I). Similarities between these models are appreciated. CKA-i is a plane that has been spatially rotated in the Cartesian plane, displacing the base of said plane (corresponding to the segment of conversions) with respect to the abscissa axis ($1/T$).

Suitably this displacement agrees with the inclination determined for CKA. Based on this fact and on space geometry it is possible to propose the subtraction of the tangents of CKA-i minus the average tangent of CKA, the resulting in a new plane would be made up of lines of the CKA method with the corrected isoconversion approximation (CKA-ic). This last CKA-ic plane would be aligning the axis of the abscissa with the base of the plane (conversion segment). In the same way, the cut-off point of both graphs can be adjusted, which corresponds to $\ln(A)$. Results of this approach to the subtraction of the slopes $\text{CKA-i} - \text{CKA} = \text{CKA-ic}$ are observed in Table 19. Similar results are shown in Appendix L7 to L12 for all Rubbers.

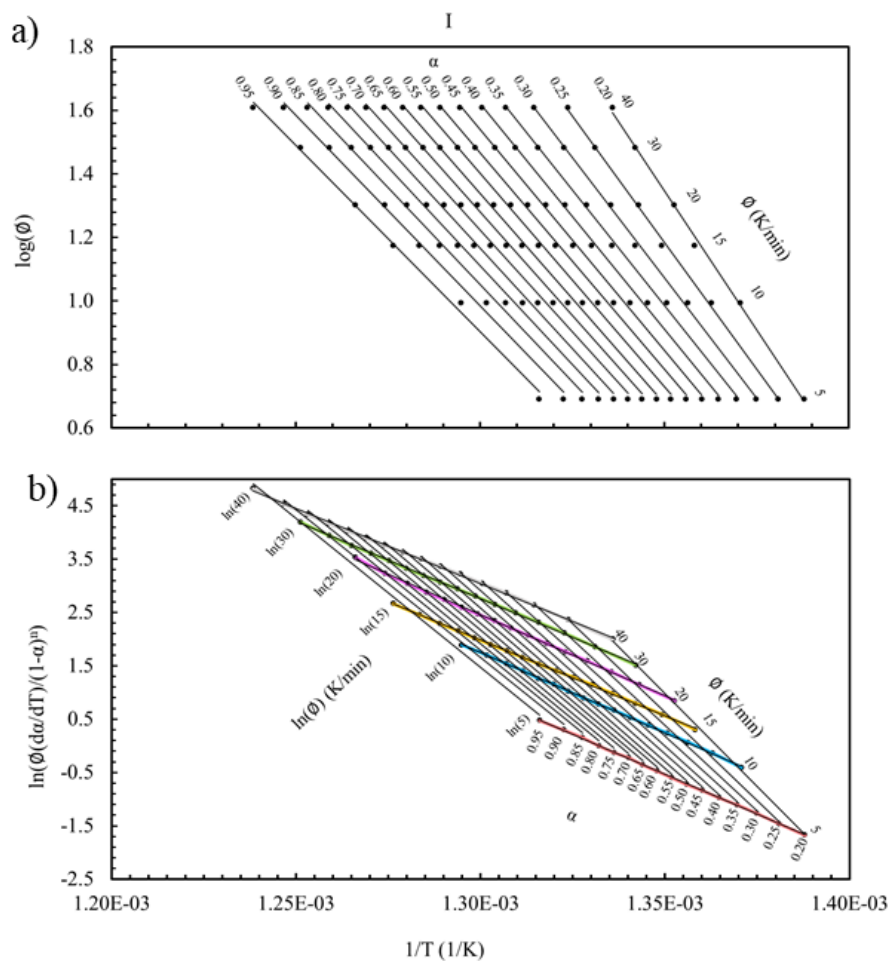


Figure 37 Comparison of OFW (a) with CKA-I (b) for the degradation of Rubber I in an atmosphere of N_2 at 20 ml min^{-1} , under non-isothermal conditions at heating rates of 5, 10, 15, 20, 30 and $40 \text{ }^\circ\text{C min}^{-1}$.

On the other hand, taking the data from Table 19 that contemplates the CKA-ic results can be compared with the OFW results (Table 11). Where the closeness of the values of both methods is noticeable, which differ by approximately 6% from each other.

Taking into account the mentioned points, it could be affirmed that CKA-ic represents the proof that there is between the differential and the integral methods. Formally, mathematicians know this as “Fundamental theorem of calculus”[101], and in this case it would be a particular application of the theorem. This statement can be understood in Figure 37 where at the ends of the plotted planes the values of $\log \phi$ are placed to identify the plane that is rotated on the Cartesian axis, it agrees with the OFW method

Table 19 CKA-ic results for Rubber I considering the isoconversion principle for the thermo-degradation reaction in an atmosphere of N₂ at 20 ml min⁻¹ and non-isothermal conditions at heating rates of 5, 10, 15, 20, 30 and 40 °C min⁻¹.

α	R ²	E (kJ mol ⁻¹)	γ_E	ln(A /min ⁻¹)	$\gamma_{\ln A}$
0.20	0.9979	337	20	55	3
0.25	0.9978	307	20	50	3
0.30	0.9975	290	20	47	3
0.35	0.9973	280	21	45	3
0.40	0.9971	273	21	44	3
0.45	0.9967	266	22	42	3
0.50	0.9962	261	23	41	3
0.55	0.9961	255	23	40	3
0.60	0.9958	248	23	39	3
0.65	0.9954	242	23	38	3
0.70	0.9953	234	23	37	3
0.75	0.9949	232	24	36	3
0.80	0.9944	227	25	35	4
0.85	0.9945	221	24	34	3
0.90	0.9943	218	24	34	3
0.95	0.9938	220	25	34	4
Average	\bar{E} (kJ mol ⁻¹)	257	$\gamma_{\bar{E}}$	33	
	ln(\bar{A} /min ⁻¹)	41	$\gamma_{\ln \bar{A}}$	6	

P. Budrugaec[46] has supported by mathematical proofs and simulations in his articles that there are differences between the results of the integral and differential methods.

P. Budrugaec et al.,[50] he has also expressed the need to be critical of methods that use the isoconversion approach. Considering that during the deduction of the mathematical expressions of the integral non-isothermal kinetic methods, the activation energy is an independent parameter of the conversion. P. Budrugaec et al.,[50] states that the mathematical results of activation energy as a conversion dependent variable are not correct. This suggestion is valid since, as demonstrated by the methods studied under the isoconversion approach in the rubbers of this work, the activation energy I and the frequency factor (A) are dependent on the

conversion. As an example, Figure 38 can be used as a reference. Additional results for all rubbers are in Appendix L13 to L18.

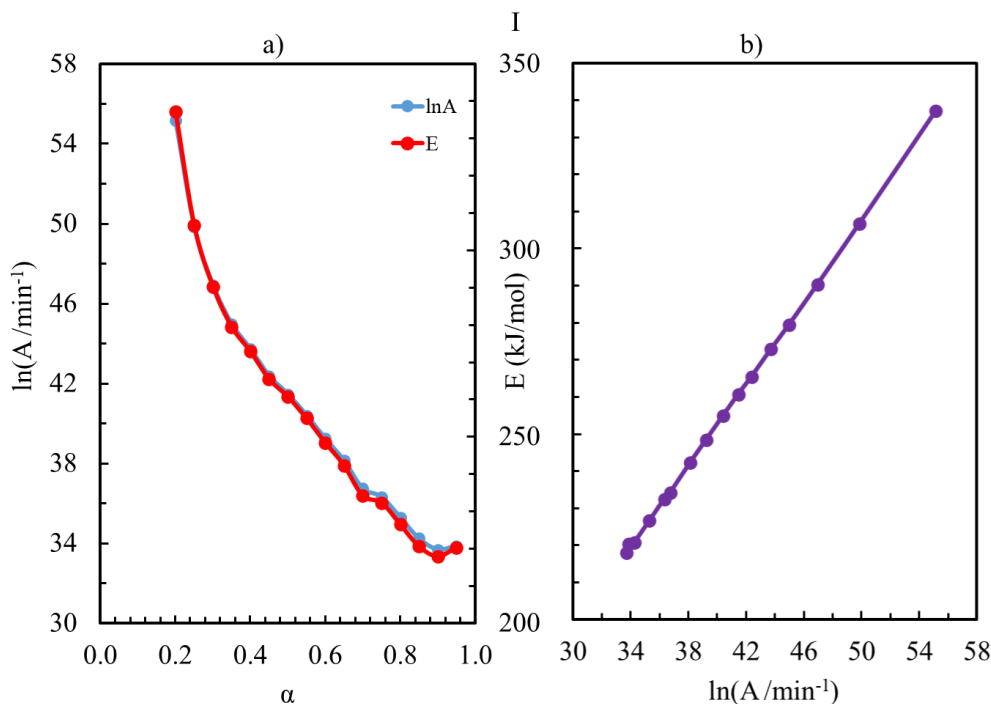


Figure 38 a) behavior of the activation energy and frequency factor at different conversions. B) variation of the activation energy with the frequency factor. For Rubber I. Obtained with the CKA-ic method under non-isothermal conditions at heating rates of 5, 10, 15, 20, 30 and 40 °C min⁻¹. Analyzed under the isoconversion condition.

Another approach to this idea is achieved by analyzing the fundamental mathematical expression of reaction rate equation (6). Understanding that for a single value of $\frac{d\alpha}{dt} = \frac{\emptyset d\alpha}{dT}$, only one value of E and A is accepted, $f(\alpha)$ being fixed. In general, it is observed in many works where the magnitudes of E and A vary with the conversion, the tendency to average as an attempt to compensate and report a single value. As an example, E is weighted in the works of Kalaei et al.,[29] or Gamlin et al.,[91] who present results with EPDM. But this could bring differences between results depending on the conversion rate approved by the author.

$$\frac{d\alpha}{dt} = \frac{\emptyset d\alpha}{dT} = A e^{-\frac{E}{RT}} f(\alpha) \quad (6)$$

5.4. Kinetic triplet

As defined above, the correct description of a degradation model of the EPDM jacket extracted from the ESP cables will depend on the estimation of the activation energy (E), the pre-exponential factor (A) and the order of reaction (n).

Therefore, in section 5.3 the selected methods are able to provide the results of these kinetic triplets (E, A and n) by using the correct approximations. For example, for the methods of: KMW and OFW it starts with the assumption that the order of reaction $n=1$. In Friedman's method the order of reaction is omitted by proposing that the reaction model is constant. Finally, in the method of CKA and CKA-ic require a reaction model $f(\alpha)$ that is validated or refuted by the results.

An important concept to take into account concerns apparent kinetic parameters. This terminology is used by authors such as J. Criado et al.,[102] to refer to the activation energy calculated by non-isothermal methods under the condition of isoconversion, referring precisely to the values of the activation energies that vary with the degree of conversion. V. Pistor et al.,[103] worked with a vulcanized elastomer using the apparent term to refer to the activation energies obtained in composite materials. Particular case where the measured experimental value of energy contemplates the sum of all the activation energies present in a process, being the consequence of physical-chemical phenomena presented in parallel and that cannot be measured individually. Then it is pertinent to clarify that all the values of the kinetic triplet of this study are considered apparent by the conditions that are analyzed.

Figure 39 shows a summary of the apparent activation energies obtained by the methods: KMW, OFW, Friedman, CKA and CKA-ic. Highlighting the methods: KMW, OFW, CKA and CKA-ic with values of the apparent activation energies ranging from 198 to 265 kJ mol^{-1} , while the apparent activation energy by Friedman's method is varying in values from 481 to 496 kJ mol^{-1} .

The results of apparent activation energy by the Friedman method are above the values of the other methods. Although this difference is high, it is not uncommon to see studies where the values presented differ by 30% when compared to other methods. Marinović-Cincović et al.,[104] report fluctuations in the

apparent activation energy for the thermodegradation of EPDM in the N_2 atmosphere from 70 to 450 kJ mol^{-1} when using KAS and Friedman whit conversion between 0.5 to 0.95. Results of this type suggest what has already been stated that by using the term EPDM a large number of possible formulations are covered, which are so called without giving more details. Although the adjustment of the data is mathematically consistent with Friedman's method there are no reports of activation energies of 500 kJ mol^{-1} . These values could be specific to the system. So, for Friedman's results they will be taken only as a reference value.

Experimental results from authors like Gamlin et al.,[91] who has reported an apparent activation energy ranging from 216 to 234 kJ mol^{-1} in thermodegradation of EPDM where ethylene content is varied. Kalae et al.,[29] show differences of apparent activation energy from 70 to 170 kJ mol^{-1} in EPDM mixtures with ZnO particles of various morphology, size and concentration.

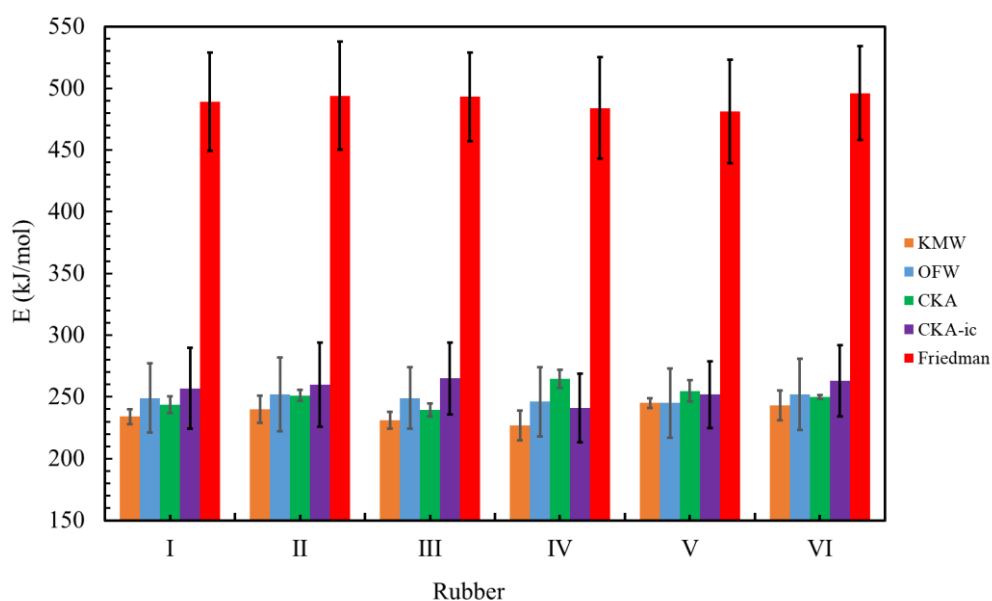


Figure 39 Summary plot of the apparent activation energies obtained by the different methods for the degradation of the 6 EPDM rubbers, under N_2 atmosphere, evaluated under non-isothermal conditions.

Table 22 shows the numerical values of the apparent activation energies computed with all the methods appreciating the uncertainty of each magnitude. Focusing the attention on the CKA-ic results, the proximity with OFW results is

noted. Reaffirming the feasibility of making calculations in the isoconversion condition.

Table 20 Summary of the apparent activation energies obtained by the different methods for all the EPDM rubbers extracted from the jackets.

Method	Rubber	I	II	III	IV	V	VI
KMW	E (kJ mol ⁻¹)	234	240	231	227	245	243
	γ_E	6	11	7	12	4	12
OFW	\bar{E} (kJ mol ⁻¹)	249	252	249	246	245	252
	$\gamma_{\bar{E}}$	28	30	25	28	28	29
CKA	\bar{E} (kJ mol ⁻¹)	244	251	240	265	255	250
	$\gamma_{\bar{E}}$	7	5	5	7	9	2
CKA-ic	\bar{E} (kJ mol ⁻¹)	257	260	265	241	252	263
	$\gamma_{\bar{E}}$	33	34	29	28	27	29
Friedman	\bar{E} (kJ mol ⁻¹)	489	494	493	484	481	496
	$\gamma_{\bar{E}}$	40	44	36	41	42	38

By listing the apparent activation energies individually for each rubber in the KMW, OFW, CKA and CKA-ic methods it is feasible to observe that the different values fall within the uncertainty range. The variation of approximately 5% can be interpreted as that the composition of the cables and variables such as pressure (proportional to depth) have no significant influence on the aging kinetics.

Again, it has to be understood that the differences in results observed between the different methods are based on:

Form that were developed: integrals or differentials. If an integral method is being used, the asymptotic approximations of P(x) proposed by each individual author must be considered.

Approaches such as assuming order of reaction $n=1$ or a reaction model of $f(\alpha) = (1 - \alpha)^n$.

Based on the results of FTIR and TGA where it can be seen that the composition of the polymeric matrix of the composite material is 54.3 % EPDM minimum. All samples can be analyzed together. The results of Table 20 show that the variations of the apparent activation energy of the 6 samples are very close among them, including deviations. This indicates that the aging process of the material in the studied well conditions is not intense enough to produce a degradation quantified by this method.

As already discussed, the reaction order for the KMW and OFW methods, it is more a variable set at $n=1$ than a calculated magnitude. This condition is necessary to calculate the frequency factor A . On the other hand, CKA allowed to have an apparent reaction order value of 0.95 on average. Very close to the unit. Therefore, the approximation of $n=1$ could be considered valid. C. Gamlin et al.,[39] reported in isothermal experiments reaction order values of 0.72 for thermodegradation of EPDM thus validating the results of this study.

Figure 40 summarizes the apparent results of the pre-exponential factor calculated by KMW, OFW, CKA, CKA-ic and Friedman. Emphasizing again the magnitude calculated by Friedman's method moves away from the results of the other methods. This variation may be due to the Friedman model hypothesis where the dependence of the reaction model on the kinetics of the thermodegradation of EPDM rubber is not included.

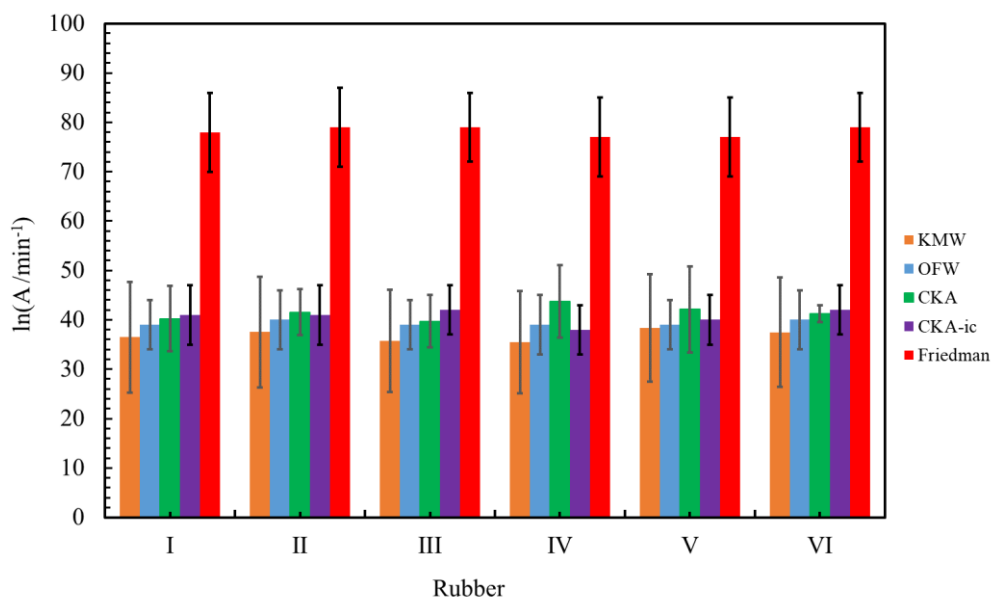


Figure 40 Apparent preexponential factor of degradation obtained by the different methods for the degradation of the 6 EPDM rubbers, under N_2 atmosphere, evaluated under non-isothermal conditions.

Table 21 shows the results of the $\ln A$ obtained by KMW, OFW, CKA, CKA-ic with an average being around a value of 40 and perceiving that CKA is one of the calculations with less uncertainty while CKA-ic predicts results. similar to OFW. C. Gamlin et al.,[39] report variation of the $\ln A$ from 30 to 36 when they

studied thermodegradation with EPDM with different polyethylene content in isothermal condition.

The activation energy data obtained by non-isothermal methods from various authors who worked with polyethylene and polypropylene are listed below: S. Zhong et al.,[105] with high-density polyethylene (HDPE) 263 kJ mol^{-1} , T. Yee et al.,[106] with low density polyethylene (LDPE) 280 kJ mol^{-1} , W. Hao et al.,[107] with polypropylene (PP) 190 kJ mol^{-1} . These data can be used to predict the influence of ethylene and propylene content on the degradation of a terpolymer such as EPDM. Of course, this estimate does not consider the contribution of diene, cross-links and typical EPDM characteristics.

In literature, different activation energy values are observed for the same EPDM thermodegradation reaction in the presence of N_2 gas, where variables such as additives, charges, ethylene/propylene ratios or the content of additives are evaluated.

C. Gamlin et al.,[91] modified the ethylene/propylene ratio in various mixtures when manufacturing different EPDM rubbers, obtaining mixtures that ranged between 40 and 75% ethylene and whose values of apparent activation energy calculated by FWO in non-isothermal condition ranges from 216 to 234 kJ mol^{-1} . C. Gamlin et al.,[39] also evaluated the same mixtures by isothermal methods, reporting values for the activation energy of 172 to 226 kJ mol^{-1} . They reported an increase in the stability of EPDM with the highest proportion of ethylene content in the copolymer. Another parameter reported by the authors is the preexponential factor that, expressed as $\ln A$, ranges between 25 and $36 \ln(\text{min}^{-1})$. In parallel, the reaction order that C. Gamlin et al.[39] reported by isothermal methods was in a range of 0.61 to 0.84.

According to Kalae et al.,[29] EPDM mixtures with zinc oxide particles of different size, morphology and concentration produce variations in the activation energy by thermally degrading in the presence of N_2 gas with values from 69 to 169 kJ mol^{-1} . They used the Kissinger and Friedman methods to do the calculations under non-isothermal conditions. The highest thermal stability is achieved with the smallest particle sizes of zinc oxide. In EPDM chains, a possible thermal insulation effect or limitation of chain movement is mentioned

Table 21 Summary of the apparent preexponential factor of degradation obtained by the different methods for all the EPDM rubbers extracted from the jackets.

Method	Rubber	I	II	III	IV	V	VI
Kissinger	$\ln(A / \text{min}^{-1})$	36	38	36	35	38	37
	$\gamma_{\ln A}$	11	11	10	10	11	11
OFW	$\ln(A / \text{min}^{-1})$	39	40	39	39	39	40
	$\gamma_{\ln A}$	5	6	5	6	5	6
CKA	$\ln(A / \text{min}^{-1})$	40	42	40	44	42	41
	$\gamma_{\ln A}$	1	1	1	1	2	1
CKA-ic	$\ln(A / \text{min}^{-1})$	41	41	42	38	40	42
	$\gamma_{\ln A}$	6	6	5	5	5	5
Friedman	$\ln(A / \text{min}^{-1})$	78	79	79	77	77	79
	$\gamma_{\ln A}$	8	8	7	8	8	7

When studying the cables individually per well and using the differently proposed kinetic methods it is possible to notice that there is a maximum variation of activation energy of 5%. therefore, the change with depth can be considered insignificant. In the case of the pre-exponential factor, the same trend is repeated. This would imply that for the 2 groups of cables, regardless of the composition of the filled, there is no effect on the degradation or aging kinetics.

The low variations of E and A between the different samples agree that the chemical changes in the EPDM matrix are not really strong under the aging conditions that the cables are exposed in the well. In other words, thermo oxidation and aging have an effect on a small fraction of the polymer chain (probably chain ends, amorphous portions, weak points of the chemical structure), keeping the chemical structure of the main chain intact.

Comparing the 5 methods KMW, OFW, Friedman, CKA and CKA-ic in an experimental approach it is possible to discern that each one has its benefits. For example, OFW, Friedman, and KMW omit the use of the reaction model ($f(\alpha)$), which can get complex, but can also lead to error, since these methods assume reaction order 1. Rather, The CKA method requires testing several reaction models to find the best fit, but has the advantage of providing the kinetic triplet.

To perform the calculation in each of these methods, it is necessary to plan different heating speeds to be able to draw straight lines in the graphs of each method. For example, in the literature it is possible to find suggestions for Kissinger

and OFW where standards such as ASTM E2890 and E698 suggest the use of 4 to 9 heating speeds for the calculation of the activation energy. This suggestion arises from the need to have enough points to allow the best trend line to be drawn between the experimental points found. This same logic can be applied to the Friedman and CKA-ic methods where the trend line trace is under the condition of isoconversion. The CKA method, on the other hand, although it requires posing reaction models ($f(\alpha)$) is not limited by the need to use multiple heating rates to draw the best trend line on your graph. Actually, the CKA method originally covers the entire conversion range of the experimental data, which implies that for every line drawn by regression under this method, there can be experimental points that easily exceed 1000 data. From the experience in the present work, for heating speeds of 40 and 5 °C min⁻¹, more than 1800 and 15000 data are obtained respectively. And since in a wide range of heating rates from 5 to 40 °C min⁻¹, the CKA method has shown that there is a low difference between the results of the activation energy, the reaction order and the pre-exponential factor, they could only be proposed 3 heating speeds, thus reducing the number of proposed experiments equivalent in time and resources.

5.5. Mechanical proprieties

The variation of mechanical properties with the aging of thermoplastics such as EPDM has been reported previously by Hamza [108] and Canaud et al.,[109] by studying the effects of aging on EPDM rubbers.

5.5.1. Shore D Hardness

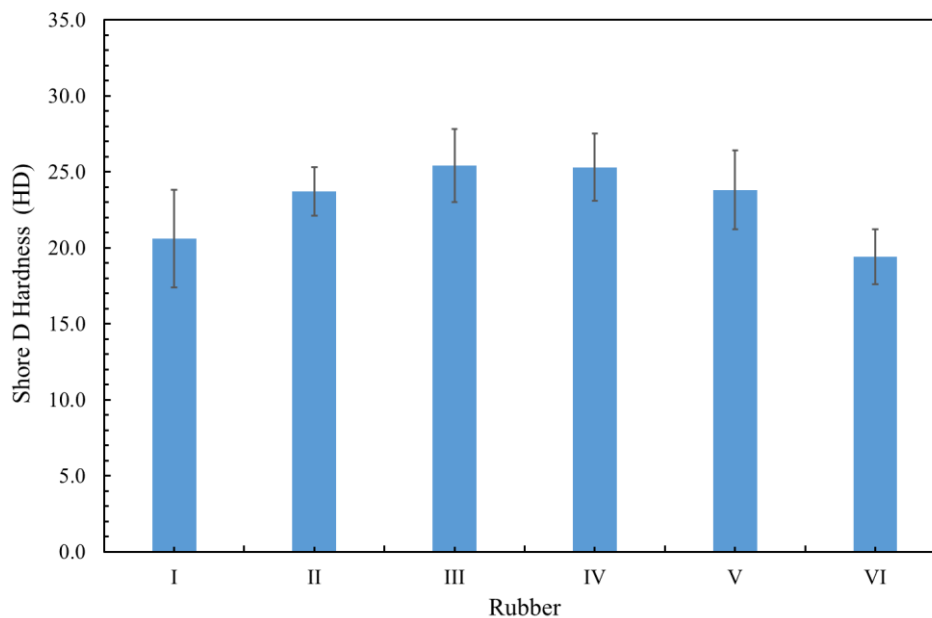
Table 22 and Figure 41 show the behavior of the Shore D hardness of the 6 rubbers, showing a variation between the samples within the range of the uncertainty of the measurements. It is shown the proximity of the Shore D hardness values for the aged III-VI rubbers with the reference samples I and II (virgin cables)

Table 22 Shore D Hardness for all EPDM samples.

Rubber	Depth (m)	Time (days)	Well	Hardness Shore D (HD)	$\gamma_{\text{Shore D}}$
I	0	0	N/A	20.6	3.2
II	0	0	N/A	23.7	1.6
III	760	1752	B17	25.4	2.4
IV	917	738	A28	25.3	2.2
V	1927	738	A29	23.8	2.6
VI	2170	1752	B17	19.4	1.8

In counterpart, Hamza et al.,[108] reported that properties such as hardness increase when the amount of charge increases (carbon black) and when aged under accelerated conditions for a short period of time (72 h max) within the temperature range from 120 to 180 °C.

Comparing EPDM from two different depths from the same well (rubbers III vs VI and IV vs V) there is a small tendency to decrease the Shore hardness D. For rubber III vs VI there is a 20% reduction in hardness. It is worth mentioning that the conditions of the cable VI were the most severe (the longest periods and the maximum depths).

**Figure 41** Shore D Hardness EPDM rubbers.

5.5.2. Tensile test

Figure 42 shows typical results obtained for rubber I using rectangular prism-shaped test bodies (Figure 8), extracted from the jacket of ESP cables. It is easy to appreciate that in the region of low deformations the curves of the same EPDM tend to coincide, allowing to obtain a low uncertainty in Young's modulus. The Yield Strength are obtained considering a secant line at 0.005 strain. It is also possible to observe oscillations in some curves due to slippage between the samples and the jaws. Finally, the maximum elongation has a large data dispersion due to phenomena of early breakage of the test bodies caused by irregularities in the surface of the samples itself caused by wearing the material. This phenomenon of formation of critical points is known as stress concentrators. Authors such as Yamamoto et al.,[110] explain how the presence of stress concentrators contributes to the early failure of the material. Appendix M1 to M6 includes the results of all the tests of all EPDM rubber specimens.

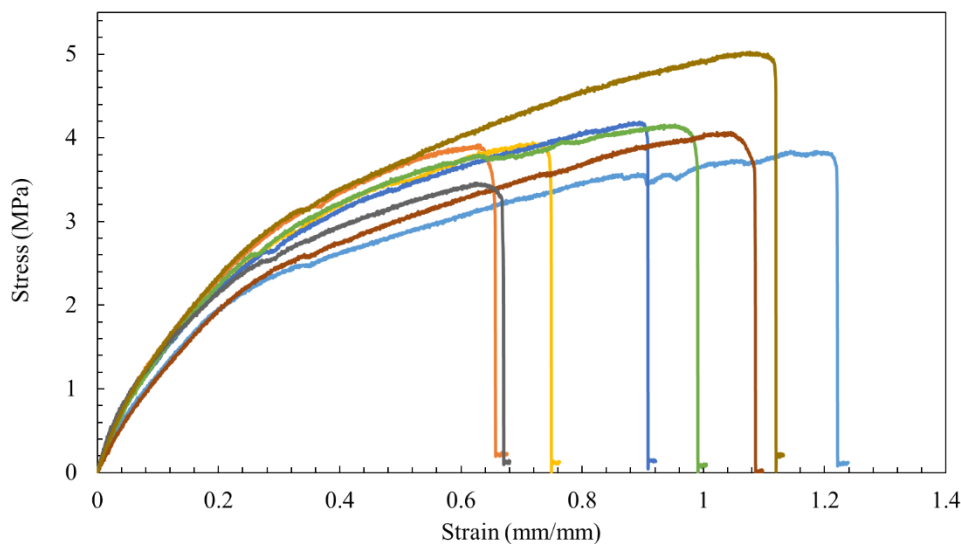


Figure 42 Stress-strain curve of Rubber I samples.

A summary of mechanical properties obtained by tensile tests is shown in Table 23. Figure 43 shows Young's modulus varying from 15 to 20 MPa in 6 EPDM

rubbers, highlighting again the specimen VI which is the only one that shows significant variation in respect to other specimens.

Table 23 A summary of mechanical properties evaluated by tensile tests

Rubber	Young's modulus (MPa)	γ_{Ym}	Yield Strength (MPa)	γ_{Ys}	Tensile Strength (MPa)	γ_{Ts}	Maximum Strain (%)	γ_{Ms}
I	20	2	0.6	0.1	4	0.5	78	20
II	19	1	0.5	0.2	3.2	0.1	82	10
III	19	3	0.6	0.3	3.4	0.8	92	56
IV	20	2	0.6	0.1	3.7	0.5	117	16
V	18	1	0.5	0.1	4.5	0.7	131	46
VI	15	1	0.5	0.1	6.1	0.7	207	46

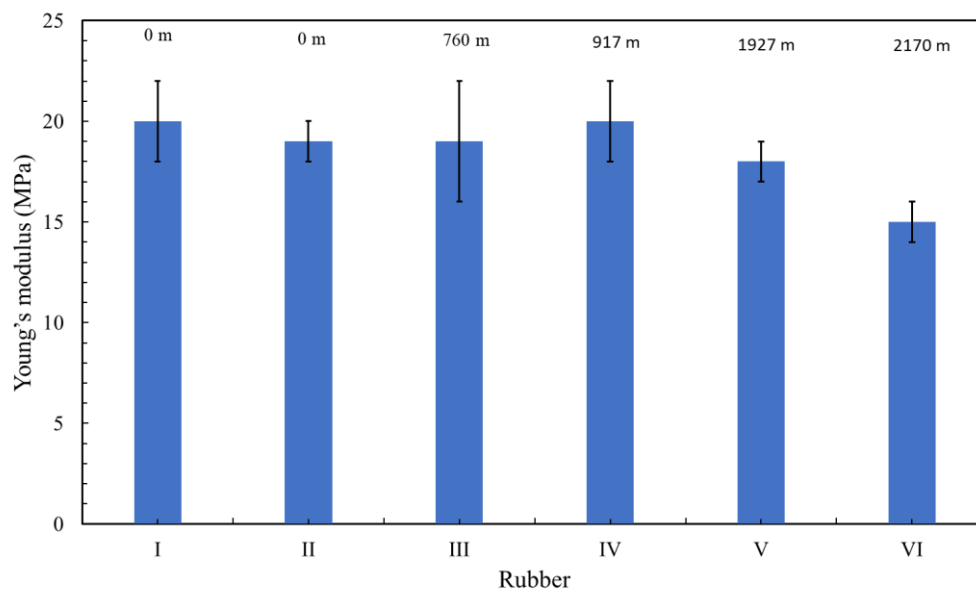


Figure 43 Young's modulus of EPDM rubbers.

The Yield Strength values are plotted in Figure 44, showing that their magnitudes can be considered constant for all rubbers.

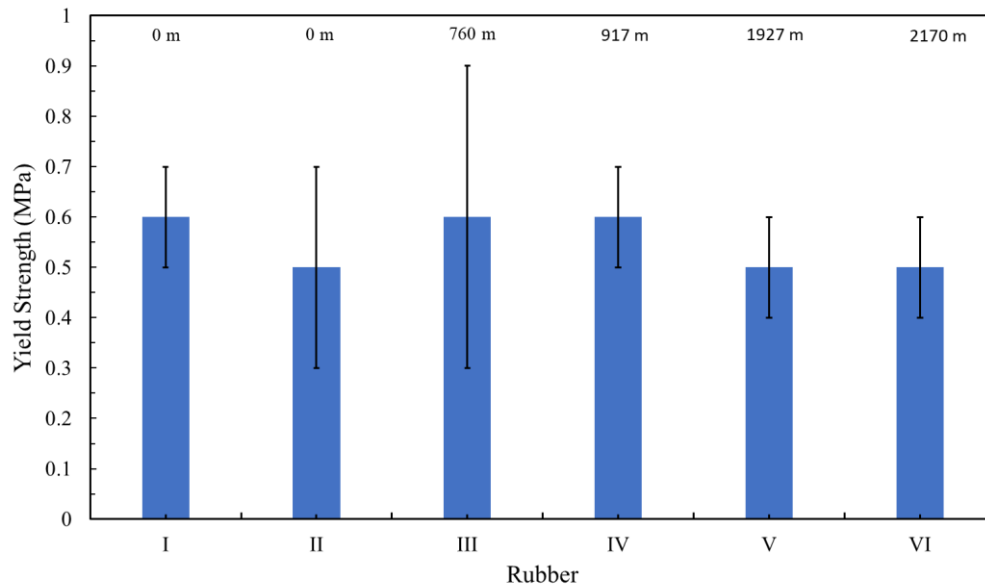


Figure 44 Yield Strength of EPDM rubbers.

In the case of Tensile Strength or Maximum Tensile Strength (UTS) the magnitudes are shown in Figure 45. One can notice a slight increase for rubber VI.

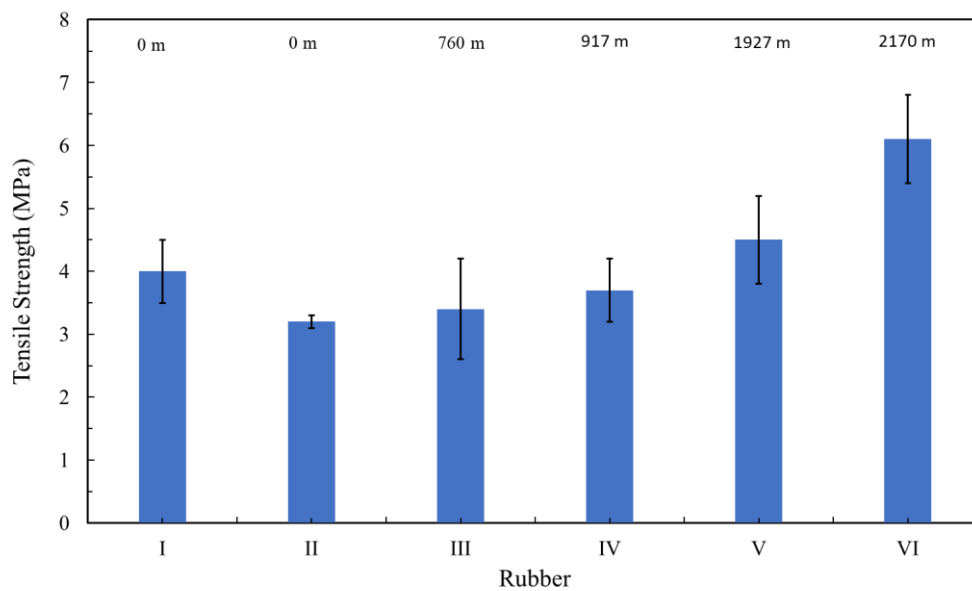


Figure 45 Tensile Strength of EPDM rubbers.

Assink et al.,[111] suggested that the increase of tensile strength and Young's modulus trend is justified by the increase in cross-linking. These authors performed

an aging study for 90 days at 140 °C for an EPDM formulation used for O-rings and with an initial Young's modulus as low as 7 MPa.

Among the four mechanical properties extracted from the uniaxial tensile stress tests it is evident that maximum strain, tensile strength and Young's modulus are the most sensitive to aging degradation. Another striking phenomenon is the subtle tendency of tensile strength and maximum strain to vary in parallel with depth (an information added at the top of each Figure from 42 to Figure 45).

Šarac et al.,[28] studied the accelerated aging of EPDM under radiation doses at temperatures from 25 to 85 °C, showing the sensitivity of the parameters such as maximum elongation and UTS. Phenomena of increased cross-linking compete with chain cleavage under the condition of accelerated aging by radiation and temperature, modifying the response of the material. Šarac's records agree that there is an increase in UST when the increase in cross-links dominates aging, reaching a maximum where the decrease is a consequence of chain cleavage. While the elongation at break experiences a decrease regardless of the phenomenon. This condition appears to be repeated in the real-time aging of the EPDM rubbers studied.

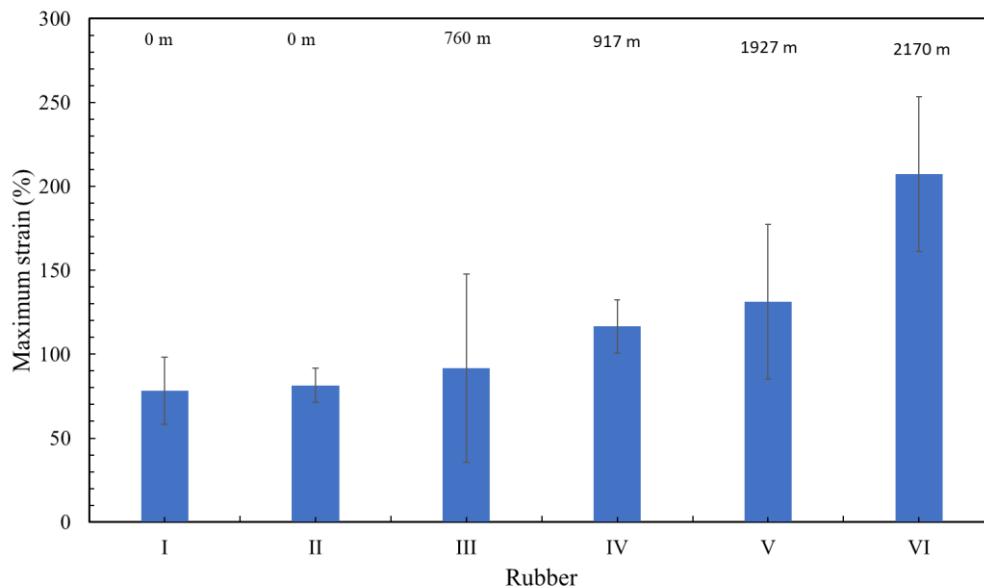


Figure 46 Maximum strain of EPDM rubbers.

5.6. Scanning Electron Microscope (SEM) coupled with energy dispersive X-ray spectrometer (EDX)

Table 24 presents a summary of the composition of the major elements obtained when analyzing the rubbers of the 6 samples by EDX.

C as the most widespread element, is presented in the range between 76.5 to 88.1 wt.%. Oxygen, silicon and aluminum agree with the presence of inorganic clay fillers. The elements such as sulfur and zinc can be recognized as part of the vulcanization additives added to the formulation mixture (Yuan et al. [112]).

An important finding by EDX is the aluminum-silicon proportion of the rubbers IV and V is that their proportions are very similar when Kaolin used as filler[113][114]. This can be better appreciated in the Figure 47. This ratio Al/Si can be used as an indicator to recognize the mineral source of the filler.

The EDX results again demonstrate the difference between the 2 groups of samples studied according to their filler (Metakaolin Group 1= rubbers I, II, III, VI or Kaolin Group 2= rubber IV and V) and they are used for possible changes in the degradation kinetics of the materials.

Table 24 Majority elemental composition determined by EDX

Rubber	Element	Carbon	Oxygen	Aluminum	Silicon	Sulfur	Zinc
I	Weight (%)	87.2	7.3	0.72	3.4	0.23	0.6
	γ_w	0.1	0.1	0.02	0.1	0.01	0.4
II	Weight (%)	85.8	9	0.76	3.1	0.19	0.6
	γ_w	0.8	1	0.02	0.1	0.01	0.5
III	Weight (%)	81.7	9.9	2.3	4.69	0.26	1.16
	γ_w	0.6	0.5	0.2	0.04	0.03	0.06
IV	Weight (%)	76.5	16.21	3.5	3.4	0.17	0.25
	γ_w	0.2	0.08	0.1	0.1	0.03	0.02
V	Weight (%)	81.1	12.02	3.43	3.1	0.101	0.08
	γ_w	0.3	0.04	0.07	0.2	0.001	0.08
VI	Weight (%)	88.1	7.4	0.51	2.5	0.21	0.6
	γ_w	0.2	0.2	0.02	0.1	0.04	0.5

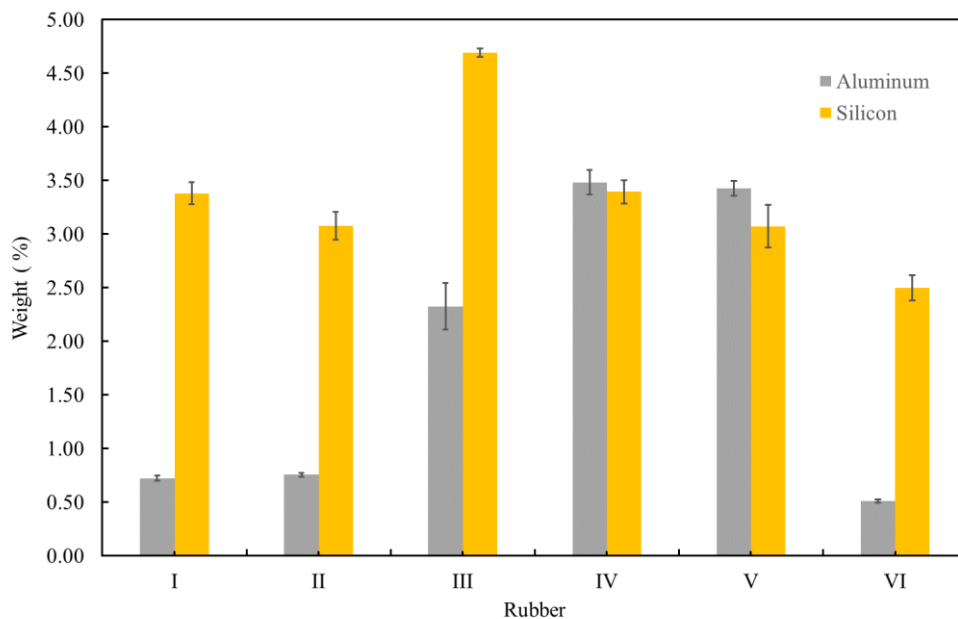


Figure 47 EDX Results for Aluminum and Silicon.

5.7. Crosslinked content

Table 25 and Figure 48 summarize the results of the cross-link fraction showing that the studied samples do not present important variations in cross-link fraction. It is normal to consider the increase in cross-linking in those formulations where there is an excess of vulcanizing agent (under the conditions of minimum reaction temperature) but as it appears that this is not the case. Rubber I and II reference samples have very similar values when compared to the aged samples.

Table 25 Cross-link fraction all rubbers.

Rubber	Well	Time (days)	Depth (m)	Cross-Link Fraction (w/w)	γ_{C-LF}
I		0	0	0.67	0.02
II		0	0	0.71	0.01
III	B-17	1752	760	0.72	0.004
IV	A-29	738	917	0.62	0.03
V	A-29	738	1927	0.72	0.002
VI	B-17	1752	2170	0.73	0.006

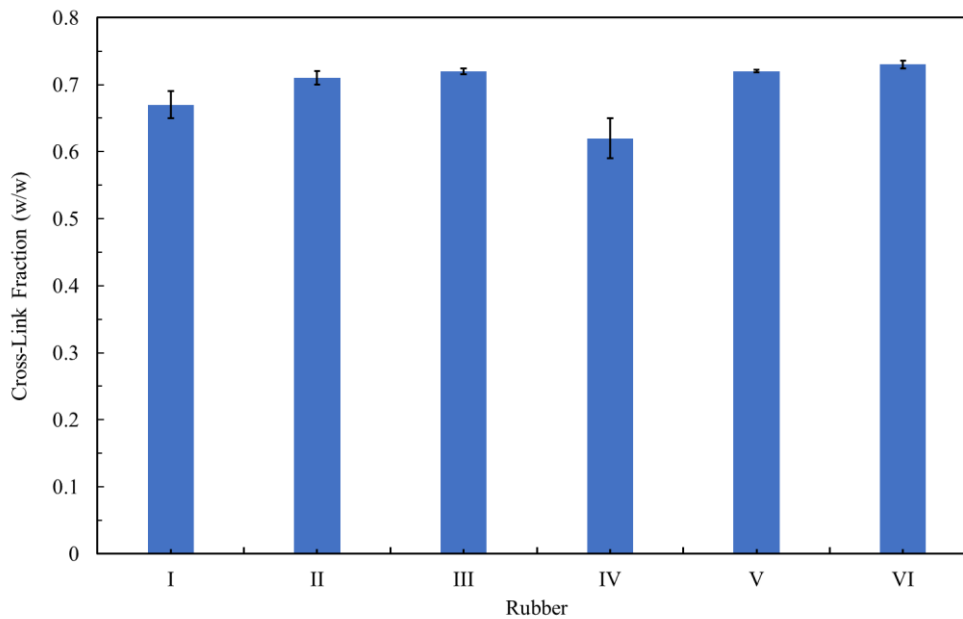


Figure 48 Cross-link fraction for EPDM rubbers.

Considering that the cross-link is constant and that the Young's modulus is decreasing, it is evident that other factors are responsible for this difference. This phenomenon occurs when substances such as plasticizers are added to a polymer mixture [115]. In this case, the formation of low molecular weight compounds will be caused by the degradation of the polymer matrix. Especially of the unvulcanized fraction of the rubber, starting with the amorphous regions [116] that are the most susceptible to thermal degradation. These new low molecular weight fractions can act as interchain plasticizers, reducing modulus and providing greater flexibility to the movement between chains facilitating the strain of the material.

Planes et al., [117] confirm that the amorphous regions of EPDM are the most likely to be degraded under gamma irradiation aging processes. Additionally, Planes et al. comments that the degradation of the crystalline regions is not ruled out, having its impact on the mechanical properties.

5.8. Absorption of Packer-Fluid+Safe-Scan

The behavior of the absorption of the Packer-Fluid+Safe-scan mixture in the six EPDM rubbers is shown in Figure 49. There is a small increase in mass over time of the six rubbers, showing that this material is susceptible to absorb the fluid. The curves obtained present some variations presumably produced during handling of the samples on drying or systematic errors in the balance. This explanation of small variations is typical for the technique suggested in ASTM D570[72].

Figure 49 highlights 2 groups of different adsorption rates. The first group with the highest slope corresponds to rubbers IV and V identified by FTIR as kaolin formulations. The second group that includes rubbers I, II, III and VI coincides with the material filled with Metakaolin.

Xiao et al.,[1] comment that EPDM can swell in the presence of various organic solvents, even in water to a lesser extent, and to prevent it from becoming embedded in the annular space, it is protected with Packer fluid. Table 26 shows the percentage of Packer-Fluid+Safe-scan absorbed at the end points of the study, being able to easily discriminate the rubbers by their response to adsorption.

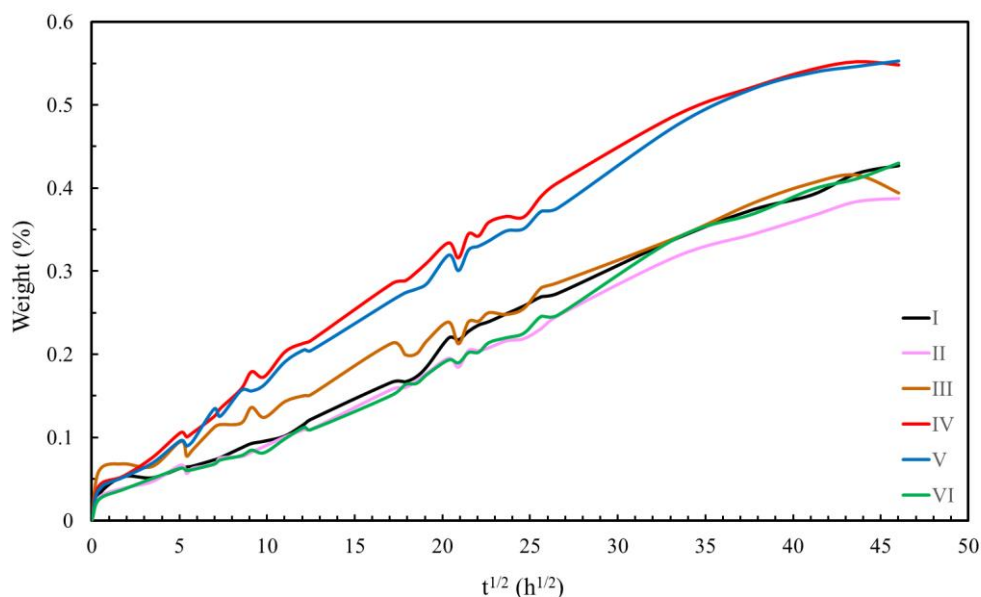


Figure 49 Percentage variation of mass for the all rubber immersed in Packer-Fluid+Safe-scan.

Table 26 Percentage end absorbed weight all rubbers.

Group	Rubber	% Absorbed weight	% Average absorbed weight	$\gamma_{\%Aaw}$
1	I	0.43	0.42	0.02
	II	0.39		
	III	0.41		
	VI	0.43		
2	IV	0.5524	0.5528	0.0004
	V	0.5531		

Figure 49 shows that the constant saturation level was not reached during the time that the absorption was evaluated. This could explain the difference in the magnitudes reported in Table 26. Based on the TGA results (Table 7), an approximation of the maximum amount of fluids absorbed can be predicted using mass losses in the range of 30 to 250 °C, these values correspond to 1.47 and 0.67 wt.% for groups 1 and 2 respectively.

6 Conclusions and future works

6.1. Conclusions

This work carried out a study of the physical, chemical and mechanical properties of the EPDM rubbers extracted from the Jacket of ESP cables that were used in the Peregrino field for periods of time of 738 days (2 years) and 1752 days (4.8 years), therefore, aged during that period of time under actual operating conditions.

The kinetic parameters studied allowed for evaluation of the kinetic triplet (apparent activation energy, pre-exponential factor and reaction order) for each material using non-isothermal methods (KMW, OFW, FR, CKA and CKA-ic).

CKA-ic is a new proposal for a kinetic computation method to evaluate non-isothermal systems under isoconversion conditions that shows results very similar to OFW for the calculation of the apparent activation energy and the pre-exponential factor. This new method responds to the gap found in the literature regarding the difference between integral and differential methods. When comparing CKA and CKA-ic, differences between methods with and without the isoconversion condition are explained.

The kinetic results validate a variation of approximately 5% in the activation energy between the 6 rubbers extracted from the Jacket covers of the ESP cables used in the Peregrino Field. Therefore, it can be considered that the activation energy is not influenced by the composition of the materials, or by the pressure (directly proportional to the depth) or any other operational condition. These variations show that the structure of the polymeric material is not so drastically affected despite having been used for 4.8 years.

Shore D hardness tests show that there is no variation in its magnitude in the investigated EPDM samples before and after aging.

Variations of 150 % of maximum deformation, 50 % of tensile strength and 20 % of Young's modulus were recorded in the uniaxial tensile tests when

comparing the rubber of the most extreme conditions (depth (2170 m) and time (4.8 years)) with rubber removed from cables that were deemed new or stock.

The adsorption results show that there is a clear dependence on the affinity of the material and the composition of the aluminosilicate filler. Showing that kaolin tends to absorb faster than metakaolin.

From our study it can be concluded that the EPDM-based layers of ESP cables suffer very slight aging under the operational conditions of the reservoir. The slight changes in the activation energy of the material during its thermodegradation reveal that its chemical structure is maintained over time, leaving no evidence of chain breaks or changes in crosslinking concentration.

According to what has been evaluated, the effect of aging in well conditions does not lead to destructive modifications of the EPDM rubber matrix. Therefore, it can be affirmed that the EPDM of the jackets are not weak links in the structure of modern ESP systems, although a greater number of ESP cables from different wells, naturally aged in conditions actual operating over periods of several years, and at different depths, it would be a mandatory requirement to acquire a more robust set of data and knowledge about the degradation processes within these cables.

6.2. Future works

To improve the values of the mechanical properties, it is necessary to consider increasing the number of samples and for this it is suggested to use longer lengths than the original cable samples.

CKA-ic proved to be a kinetic analysis method with results similar to OFW. In this case a thermodegradation reaction was analyzed using a single reaction model. To complete and validate its application, it is necessary to use reactions with reaction orders different of 1.

Taking into account the variety of operating conditions (temperature, pressure, well fluids) in ESP lifting systems and that there is a lack of data bases that consider the loss of properties of materials such as EPDM when they are used in these facilities. In the future, it would be interesting to work with a greater

number of cables from different wells, since in this way more reliable data on the effect of aging on the EPDM layer could be obtained.

7 References

- [1] J.J. Xiao, R.A. Lastra, B.A. Roth, S. Aramco, W. Lee, Material Overview for Electrical Submersible Pumps: Part I—Metallic and Ceramic Materials, *SPE Prod. Oper.* 35 (2020) 1–8. <https://doi.org/10.2118/190939-PA>.
- [2] E.B. Mano, *Introdução a polímeros 2a. edicao - Mano Eloisa Biasotto*, São Paulo, 2004.
- [3] M. Mahapatra, M. Karmakar, B. Mondal, N.R. Singha, Role of ZDC/S ratio for pervaporative separation of organic liquids through modified EPDM membranes: Rational mechanistic study of vulcanization, *RSC Adv.* 6 (2016) 69387–69403. <https://doi.org/10.1039/c6ra10104f>.
- [4] D. Harris, M. Banman, D. Malone, Design and qualification testing of ESP cable to improve ESP system run life, *Soc. Pet. Eng. - SPE Gulf Coast Sect. Electr. Submers. Pumps Symp. 2019, ESP 2019.* (2019).
- [5] IEA (2019), *World Energy Outlook 2019*, IEA, Paris <https://www.iea.org/reports/world-energy-outlook-2019>, n.d.
- [6] Ø. Kristoffersen, M. Stanko, A. Hoffmann, Short term production optimization using a model of the Peregrino Field, Brazil, *OTC Bras. 2017.* (2017) 767–779. <https://doi.org/10.4043/27995-ms>.
- [7] J.M. Ranjeva, E. Dahl, F. Martinho, B. Gonçalves, A. Ramos, Multilateral level-5 dual long horizontal openhole gravel pack completion on the peregrino field, *Proc. - SPE Annu. Tech. Conf. Exhib. 4* (2014) 2964–2979.
- [8] W. Honório, D. Lemos, R. De Lima, ESP control and monitoring system of heavy oil Peregrino field, *2015 SPE Artif. Lift Conf. - Lat. Am. Caribb.* (2015) 103–114. <https://doi.org/10.2118/173929-ms>.
- [9] A.J.S. Williams, D. Shipp, ESP downhole power quality - Do we have a healthy cardiovascular system?, *Soc. Pet. Eng. - SPE Gulf Coast Sect. Electr. Submers. Pumps Symp. 2019, ESP 2019.* (2019).
- [10] E.A. Snijders, A. Boersma, B. Van Baarle, P. Gijsman, Effect of dicumyl peroxide crosslinking on the UV stability of ethylene-propylene-diene

- (EPDM) elastomers containing 5-ethylene-2-norbornene (ENB), *Polym. Degrad. Stab.* 89 (2005) 484–491. <https://doi.org/10.1016/j.polymdegradstab.2005.02.002>.
- [11] V.M. Litvinov, P.A.M. Steeman, EPDM-carbon black interactions and the reinforcement mechanisms, as studied by low-resolution ^1H NMR, *Macromolecules*. 32 (1999) 8476–8490. <https://doi.org/10.1021/ma9910080>.
- [12] Grand View Research, Global Ethylene Propylene Diene Monomer Market Growth Report, 2025, (n.d.). <https://www.grandviewresearch.com/industry-analysis/ethylene-propylene-diene-monomer-epdm-market> (accessed February 14, 2021).
- [13] M. Ginic-Markovic, N.R. Choudhury, M. Dimopoulos, J.G. Matison, Weatherability of coated EPDM rubber compound by controlled UV irradiation, *Polym. Degrad. Stab.* 69 (2000) 157–168. [https://doi.org/10.1016/S0141-3910\(00\)00053-7](https://doi.org/10.1016/S0141-3910(00)00053-7).
- [14] G. van Doremaele, M. van Duin, M. Valla, A. Berthoud, On the Development of Titanium κ 1-Amidinate Complexes, Commercialized as Keltan ACETM Technology, Enabling the Production of an Unprecedented Large Variety of EPDM Polymer Structures, *J. Polym. Sci. Part A Polym. Chem.* 55 (2017) 2877–2891. <https://doi.org/10.1002/pola.28634>.
- [15] K.A.J. Dijkhuis, J.W.M. Noordermeer, W.K. Dierkes, The relationship between crosslink system, network structure and material properties of carbon black reinforced EPDM, *Eur. Polym. J.* 45 (2009) 3302–3312. <https://doi.org/10.1016/j.eurpolymj.2009.06.029>.
- [16] P. Sutanto, F. Picchioni, L.P.B.M. Janssen, K.A.J. Dijkhuis, W.K. Dierkes, J.W.M. Noordermeer, EPDM rubber reclaim from devulcanized EPDM, *J. Appl. Polym. Sci.* 102 (2006) 5948–5957. <https://doi.org/10.1002/app.25153>.
- [17] R. Chitta, A. Ginzburg, G. Van Doremaele, T. MacKo, R. Brüll, Separating ethylene-propylene-diene terpolymers according to the content of diene by HT-HPLC and HT 2D-LC, *Polymer (Guildf)*. 52 (2011) 5953–5960. <https://doi.org/10.1016/j.polymer.2011.10.050>.
- [18] A. De Almeida, L. Chazeau, G. Vigier, G. Marque, Y. Goutille, Influence of PE/PP ratio and ENB content on the degradation kinetics of γ -irradiated

- EPDM, *Polym. Degrad. Stab.* 110 (2014) 175–183.
<https://doi.org/10.1016/j.polymdegradstab.2014.08.029>.
- [19] S. Mitra, A. Ghanbari-Siahkali, P. Kingshott, H.K. Rehmeier, H. Abildgaard, K. Almdal, Chemical degradation of crosslinked ethylene-propylene-diene rubber in an acidic environment. Part II. Effect of peroxide crosslinking in the presence of a coagent, *Polym. Degrad. Stab.* 91 (2006) 81–93.
<https://doi.org/10.1016/j.polymdegradstab.2005.04.031>.
- [20] T. Nakamura, O. Chaikumpollert, Y. Yamamoto, Y. Ohtake, S. Kawahara, Degradation of EPDM seal used for water supplying system, *Polym. Degrad. Stab.* 96 (2011) 1236–1241.
<https://doi.org/10.1016/j.polymdegradstab.2011.04.007>.
- [21] Q. Zhao, X. Li, J. Gao, Aging of ethylene-propylene-diene monomer (EPDM) in artificial weathering environment, *Polym. Degrad. Stab.* 92 (2007) 1841–1846. <https://doi.org/10.1016/j.polymdegradstab.2007.07.001>.
- [22] Y.-D. Seo, H.-S. Lee, Y.-S. Kim, C. Song, A study on the aging degradation of ethylene-propylene-diene monomer (EPDM) under LOCA condition, *Nucl. Eng. Technol.* 43 (2011) 279–286.
<https://doi.org/10.5516/NET.2011.43.3.279>.
- [23] D. Bouguedad, A. Mekhaldi, O. Jbara, S. Rondot, A. Hadjadj, J. Douglade, P. Dony, Physico-chemical study of thermally aged EPDM used in power cables insulation, *IEEE Trans. Dielectr. Electr. Insul.* 22 (2015) 3207–3215.
<https://doi.org/10.1109/TDEI.2015.005227>.
- [24] M.M. Merrick, R. Sujanani, B.D. Freeman, Glassy polymers : Historical findings , membrane applications , and unresolved questions regarding physical aging, *Polymer (Guildf)*. 211 (2020) 123176.
<https://doi.org/10.1016/j.polymer.2020.123176>.
- [25] C. Li, Y. Ding, Z. Yang, Z. Yuan, L. Ye, Compressive stress-thermo oxidative ageing behaviour and mechanism of EPDM rubber gaskets for sealing resilience assessment, *Polym. Test.* 84 (2020) 106366.
<https://doi.org/10.1016/j.polymertesting.2020.106366>.
- [26] A. Kömmling, M. Jaunich, D. Wolff, Revealing effects of chain scission during ageing of EPDM rubber using relaxation and recovery experiment, *Polym. Test.* 56 (2016) 261–268.
<https://doi.org/10.1016/j.polymertesting.2016.10.026>.

- [27] Q. Zhao, X. Li, J. Gao, Aging behavior and mechanism of ethylene-propylene-diene monomer (EPDM) rubber in fluorescent UV/condensation weathering environment, *Polym. Degrad. Stab.* 94 (2009) 339–343. <https://doi.org/10.1016/j.polymdegradstab.2008.12.007>.
- [28] T. Šarac, J. Devaux, N. Quiévy, A. Gusarov, M.J. Konstantinović, The correlation between elongation at break and thermal decomposition of aged EPDM cable polymer, *Radiat. Phys. Chem.* 132 (2017) 8–12. <https://doi.org/10.1016/j.radphyschem.2016.10.017>.
- [29] M. Kalaei, S. Akhlaghi, S. Mazinani, A. Sharif, Y.C. Jarestani, M. Mortezaei, Effect of ZnO nanoparticles on kinetics of thermal degradation and final properties of ethylene–propylene–diene rubber systems, *J. Therm. Anal. Calorim.* 110 (2012) 1407–1414. <https://doi.org/10.1007/s10973-011-2097-1>.
- [30] N. Koga, Ozawa's kinetic method for analyzing thermoanalytical curves: History and theoretical fundamentals, *J. Therm. Anal. Calorim.* 113 (2013) 1527–1541. <https://doi.org/10.1007/s10973-012-2882-5>.
- [31] T. Ozawa, T. Sunose, T. Kaneko, Historical review on research of kinetics in thermal analysis and thermal endurance of electrical insulating materials, *J. Therm. Anal.* 44 (1995) 205–216. <https://doi.org/10.1007/BF02547149>.
- [32] H.E. Kissinger, Variation of peak temperature with heating rate in differential thermal analysis, *J. Res. Natl. Bur. Stand.* (1934). 57 (1956) 217. <https://doi.org/10.6028/jres.057.026>.
- [33] H.L. Friedman, Kinetics of thermal degradation of char-forming plastics from thermogravimetry. Application to a phenolic plastic, *J. Polym. Sci. Part C Polym. Symp.* 6 (2007) 183–195. <https://doi.org/10.1002/polc.5070060121>.
- [34] A.W. COATS, J.P. REDFERN, Kinetic Parameters from Thermogravimetric Data, *Nature.* 201 (1964) 68–69. <https://doi.org/10.1038/201068a0>.
- [35] M.J. Starink, The determination of activation energy from linear heating rate experiments: A comparison of the accuracy of isoconversion methods, *Thermochim. Acta.* 404 (2003) 163–176. [https://doi.org/10.1016/S0040-6031\(03\)00144-8](https://doi.org/10.1016/S0040-6031(03)00144-8).
- [36] S. Ding, A. Khare, M.T.K. Ling, C. Sandford, L. Woo, Polymer durability estimates based on apparent activation energies for thermal oxidative

- degradation, *Thermochim. Acta.* 367 (2001) 107–112. [https://doi.org/10.1016/S0040-6031\(00\)00677-8](https://doi.org/10.1016/S0040-6031(00)00677-8).
- [37] F. Shehzad, M.A. Al-Harhi, Graphite-LDH hybrid supported zirconocene for ethylene polymerization: Influence of the support on the crystallization kinetics and thermal stability of polyethylene, *Appl. Clay Sci.* (2020) 105947. <https://doi.org/10.1016/j.clay.2020.105947>.
- [38] J.D. Badia, A. Martinez-Felipe, L. Santonja-Blasco, A. Ribes-Greus, Thermal and thermo-oxidative stability of reprocessed poly(ethylene terephthalate), *J. Anal. Appl. Pyrolysis.* 99 (2013) 191–202. <https://doi.org/10.1016/j.jaap.2012.09.003>.
- [39] C. Gamlin, N. Dutta, N. Roy-Choudhury, D. Kehoe, J. Matisons, Influence of ethylene–propylene ratio on the thermal degradation behaviour of EPDM elastomers, *Thermochim. Acta.* 367–368 (2001) 185–193. [https://doi.org/10.1016/S0040-6031\(00\)00668-7](https://doi.org/10.1016/S0040-6031(00)00668-7).
- [40] T. Naruse, T. Hattori, Y. Yamaguchi, T. Kanai, T. Sekiya, Thermal degradation of chlorosulfonated polyethylene rubber and ethylene propylene diene terpolymer, *Mater. Des.* 42 (2012) 147–155. <https://doi.org/10.1016/j.matdes.2012.05.038>.
- [41] S. Vyazovkin, C.A. Wight, Isothermal and non-isothermal kinetics of thermally stimulated reactions of solids, *Int. Rev. Phys. Chem.* 17 (1998) 407–433. <https://doi.org/10.1080/014423598230108>.
- [42] T. Hatakeyama, *Thermal Analysis — Fundamentals and Applications to Polymer Science.*, 2nd Editio, 2000. [https://doi.org/10.1016/s0039-9140\(99\)00304-5](https://doi.org/10.1016/s0039-9140(99)00304-5).
- [43] J.R. Hulett, Deviations from the Arrhenius equation, *Q. Rev. Chem. Soc.* 18 (1964) 227–242. <https://doi.org/10.1039/qr9641800227>.
- [44] J.H. Flynn, L.A. Wall, A quick, direct method for the determination of activation energy from thermogravimetric data, *J. Polym. Sci. Part B Polym. Lett.* 4 (1966) 323–328. <https://doi.org/10.1002/pol.1966.110040504>.
- [45] C.D. Doyle, Series Approximations to the Equation of Thermogravimetric Data, *Nature.* 207 (1965) 290–291. <https://doi.org/10.1038/207290a0>.
- [46] P. Budrugaec, Differential non-linear isoconversional procedure for evaluating the activation energy of non-isothermal reactions, *J. Therm. Anal. Calorim.* 68 (2002) 131–139. <https://doi.org/10.1023/A:1014932903582>.

- [47] S. Vyazovkin, W. Linert, Reliability of conversion-time dependencies as predicted from thermal analysis data, *Anal. Chim. Acta.* 295 (1994) 101–107. [https://doi.org/10.1016/0003-2670\(94\)80339-0](https://doi.org/10.1016/0003-2670(94)80339-0).
- [48] R. Balart, D. Garcia-Sanoguera, L. Quiles-Carrillo, N. Montanes, S. Torres-Giner, Kinetic analysis of the thermal degradation of recycled acrylonitrile-butadiene-styrene by non- isothermal thermogravimetry, *Polymers (Basel)*. 11 (2019). <https://doi.org/10.3390/polym11020281>.
- [49] S. Vyazovkin, L. Vincent, N. Sbirrazzuoli, Thermal denaturation of collagen analyzed by isoconversional method, *Macromol. Biosci.* 7 (2007) 1181–1186. <https://doi.org/10.1002/mabi.200700162>.
- [50] P. Budrugaec, D. Homentcovschi, E. Segal, Critical analysis of the isoconversional methods for evaluating the activation energy. I. Theoretical background, *J. Therm. Anal. Calorim.* 63 (2000) 457–463. <https://doi.org/10.1023/A:1010148611036>.
- [51] T. Ozawa, Kinetic analysis of derivative curves in thermal analysis, *J. Therm. Anal.* 2 (1970) 301–324. <https://doi.org/10.1007/BF01911411>.
- [52] B.J. Lawner, A. Mattu, Cardiac Arrest, in: *Cardiovasc. Probl. Emerg. Med.*, Wiley-Blackwell, Oxford, UK, 2011: pp. 123–137. <https://doi.org/10.1002/9781119959809.ch9>.
- [53] H. Gu, J.M. He, J. Hu, Y.D. Huang, Thermal degradation kinetics of semi-aromatic polyamide containing benzoxazole unit, *J. Therm. Anal. Calorim.* 107 (2012) 1251–1257. <https://doi.org/10.1007/s10973-011-1778-0>.
- [54] A.K. Pal, V. Katiyar, Theoretical and analyzed data related to thermal degradation kinetics of poly (L-lactic acid)/chitosan-grafted-oligo L-lactic acid (PLA/CH-g-OLLA) bionanocomposite films, *Data Br.* 10 (2017) 304–311. <https://doi.org/10.1016/j.dib.2016.11.100>.
- [55] J. Farjas, P. Roura, Exact analytical solution for the Kissinger equation: Determination of the peak temperature and general properties of thermally activated transformations, *Thermochim. Acta.* 598 (2014) 51–58. <https://doi.org/10.1016/j.tca.2014.10.024>.
- [56] ASTM International, ASTM E698 “Standard Test Method for Kinetic Parameters for Thermally Unstable Materials Using Differential Scanning Calorimetry and the Flynn / Wall / Ozawa Method,” *Annu. B. ASTM Stand.* i (2019) 1–9. <https://doi.org/10.1520/E0698-18.ization>.

- [57] P. Budrugaec, A.L. Petre, E. Segal, Some problems concerning the evaluation of non-isothermal kinetic parameters, *J. Therm. Anal.* 47 (1996) 123–134. <https://doi.org/10.1007/bf01982692>.
- [58] J. Šesták, G. Berggren, Study of the kinetics of the mechanism of solid-state reactions at increasing temperatures, *Thermochim. Acta.* 3 (1971) 1–12. [https://doi.org/10.1016/0040-6031\(71\)85051-7](https://doi.org/10.1016/0040-6031(71)85051-7).
- [59] C.D. Gamlin, N.K. Dutta, N.R. Choudhury, Mechanism and kinetics of the isothermal thermodegradation of ethylene-propylene-diene (EPDM) elastomers, *Polym. Degrad. Stab.* 80 (2003) 525–531. [https://doi.org/10.1016/S0141-3910\(03\)00036-3](https://doi.org/10.1016/S0141-3910(03)00036-3).
- [60] I.M. Meththananda, S. Parker, M.P. Patel, M. Braden, The relationship between Shore hardness of elastomeric dental materials and Young's modulus, *Dent. Mater.* 25 (2009) 956–959. <https://doi.org/10.1016/j.dental.2009.02.001>.
- [61] A.N. Gent, On the Relation between Indentation Hardness and Young's Modulus, *Rubber Chem. Technol.* 31 (1958) 896–906. <https://doi.org/10.5254/1.3542351>.
- [62] C.M. Hansen, On predicting environmental stress cracking in polymers, *Polym. Degrad. Stab.* 77 (2002) 43–53. [https://doi.org/10.1016/S0141-3910\(02\)00078-2](https://doi.org/10.1016/S0141-3910(02)00078-2).
- [63] A.E. Vlastos, S.M. Gubanski, Surface Structural Changes of Naturally Aged Silicone and Epdm Composite Insulators, *IEEE Trans. Power Deliv.* 6 (1991) 888–900. <https://doi.org/10.1109/61.131149>.
- [64] R. Sundararajan, A. Mohammed, N. Chaipanit, T. Karcher, Z. Liu, In-service aging and degradation of 345 kV EPDM transmission line insulators in a coastal environment, *IEEE Trans. Dielectr. Electr. Insul.* 11 (2004) 348–361. <https://doi.org/10.1109/TDEI.2004.1285906>.
- [65] H. Olsen, K. Sheth, R.F. Pessoa, R. Okita, A. Crossley, I. Martinez, ESP assisted production allocation in peregrino field, *Proc. Annu. Offshore Technol. Conf.* 2 (2011) 923–933. <https://doi.org/10.4043/22579-ms>.
- [66] M.C.K. Oliveira, Composition of packer fluid for deep and ultra-deep wells in environments containing CO₂. Pub . No .: US 2011 /0160100 A1. PI 0905255-0. Assignee: PETROLEO BRASILEIRO S.A. - PETROBRA, Rio de Janeiro (BR). Appl. No 12/980,033. Dec. 28, 2009.

- [67] ASTM International, D2240-15 e1 “Standard Test Method for Rubber Property—Durometer Hardness”. West Conshohocken, PA; ASTM International, 2015., Annu. B. ASTM Stand. 05 (2010) 1–13. <https://doi.org/10.1520/D2240-15E01>.
- [68] T. Šarac, N. Quiévy, A. Gusarov, M.J. Konstantinović, The study of temperature and radiation induced degradation of cable polymers: A comparison between the mechanical properties of industrial and neat EPDM, *Procedia Struct. Integr.* 2 (2016) 2405–2414. <https://doi.org/10.1016/j.prostr.2016.06.301>.
- [69] ASTM International, D412-16 “Standard Test Methods for Vulcanized Rubber and Thermoplastic Elastomers—Tension”. West Conshohocken, PA; ASTM International, 2016., Annu. B. ASTM Stand. (2009) 1–14. <https://doi.org/10.1520/D0412-16>.
- [70] British Standards Institution, EN 60811-1-1:1995 “Insulating and sheathing materials of electric and optical cables — Common test methods — Part 1-1: General application — Measurement of thickness and overall dimensions — Tests for determining the mechanical properties”, ISBN: 0-580-250, Br. Stand. Inst. (1995) 307889–307915. <https://shop.bsigroup.com/>.
- [71] ASTM International., ASTM D2765 - 01, “Standart Test Methods for Determination of Gel Content and Swell Ratio of Crosslinked Ethylene Plastics”. West Conshohocken, PA; ASTM International, Annu. B. ASTM Stand. 01 (2006) 1–8. <https://doi.org/10.1520/D2765-01R06>.
- [72] ASTM International, ASTM D570-98 “Standard Test Method for Water Absorption of Plastics”. West Conshohocken, PA; ASTM International, 2018., Annu. B. ASTM Stand. 98 (2018) 1–4. <https://doi.org/10.1520/D0570-98R10E01.2>.
- [73] W.A. Lopes, M. Fascio, Flow chart for infrared spectra interpretation of organic compounds, *Quim. Nova.* 27 (2004) 670–673. <https://doi.org/10.1590/s0100-40422004000400025>.
- [74] J. Coates, Interpretation of Infrared Spectra, A Practical Approach, *Encycl. Anal. Chem.* (2006) 1–23. <https://doi.org/10.1002/9780470027318.a5606>.
- [75] ASTM International, D3677-10(2015) Standard Test Methods for Rubber—Identification by Infrared Spectrophotometry. West Conshohocken, PA; ASTM International, 2015., Annu. B. ASTM Stand. 211 (1987).

- <https://doi.org/10.1520/D3677-10R15>.
- [76] J.-R. Riba Ruiz, T. Canals, R. Cantero, Supervision of Ethylene Propylene Diene M-Class (EPDM) Rubber Vulcanization and Recovery Processes Using Attenuated Total Reflection Fourier Transform Infrared (ATR FT-IR) Spectroscopy and Multivariate Analysis, *Appl. Spectrosc.* 71 (2017) 141–151. <https://doi.org/10.1177/0003702816653131>.
- [77] S. Mitra, A. Ghanbari-Siahkali, P. Kingshott, S. Hvilsted, K. Almdal, An investigation on changes in chemical properties of pure ethylene-propylene-diene rubber in aqueous acidic environments, *Mater. Chem. Phys.* 98 (2006) 248–255. <https://doi.org/10.1016/j.matchemphys.2005.09.028>.
- [78] B. Ilic, A. Mitrovic, L. Milicic, Thermal treatment of kaolin clay to obtain metakaolin, *Hem. Ind.* 64 (2010) 351–356. <https://doi.org/10.2298/HEMIND100322014I>.
- [79] A. Elimbi, H.K. Tchakoute, M. Kondoh, J. Dika Manga, Thermal behavior and characteristics of fired geopolymers produced from local Cameroonian metakaolin, *Ceram. Int.* 40 (2014) 4515–4520. <https://doi.org/10.1016/j.ceramint.2013.08.126>.
- [80] F.J. López, S. Sugita, M. Tagaya, T. Kobayashi, Metakaolin-Based Geopolymers for Targeted Adsorbents to Heavy Metal Ion Separation, *J. Mater. Sci. Chem. Eng.* 02 (2014) 16–27. <https://doi.org/10.4236/msce.2014.27002>.
- [81] N.D. Bansod, B.P. Kapgate, P.K. Maji, A. Bandyopadhyay, C. Das, Functionalization of epdm rubber toward better silica dispersion and reinforcement, *Rubber Chem. Technol.* 92 (2019) 219–236. <https://doi.org/10.5254/rct.18.81564>.
- [82] S. Puligilla, P. Mondal, Co-existence of aluminosilicate and calcium silicate gel characterized through selective dissolution and FTIR spectral subtraction, *Cem. Concr. Res.* 70 (2015) 39–49. <https://doi.org/10.1016/j.cemconres.2015.01.006>.
- [83] T. Zaharescu, S.R. Scagliusi, A.M. Luchian, A.B. Lugão, Degradability Characterization of EPDM/IIR Blends by γ -irradiation, *J. Polym. Environ.* 26 (2018) 616–625. <https://doi.org/10.1007/s10924-017-0966-9>.
- [84] L. Jianwen, Z. Xiaochao, Z. Xiaoguang, J. Ouyang, H. Yang, Insight into the effect of crystallographic structure on thermal conductivity of kaolinite

- nanoclay, *Appl. Clay Sci.* 173 (2019) 12–18. <https://doi.org/10.1016/j.clay.2019.03.011>.
- [85] S. Zulfiqar, M.I. Sarwar, N. Rasheed, C.T. Yavuz, Influence of interlayer functionalization of kaolinite on property profile of copolymer nanocomposites, *Appl. Clay Sci.* 112–113 (2015) 25–31. <https://doi.org/10.1016/j.clay.2015.04.010>.
- [86] B.-L. Zhu, C.L. Qi, Y.H. Zhang, T. Bisson, Z. Xu, Y.J. Fan, Z.X. Sun, Synthesis, characterization and acid-base properties of kaolinite and metal (Fe, Mn, Co) doped kaolinite, *Appl. Clay Sci.* 179 (2019) 105138. <https://doi.org/10.1016/j.clay.2019.105138>.
- [87] M. Leśniak, J. Partyka, M. Gajek, M. Sitarz, FTIR and MAS NMR study of the zinc aluminosilicate ceramic glazes, *J. Mol. Struct.* 1171 (2018) 17–24. <https://doi.org/10.1016/j.molstruc.2018.05.101>.
- [88] J.J. Maurer, Advances In Thermogravimetric Analyses Of Elastomer Systems, *J. Macromol. Sci. Part A - Chem.* 8 (1974) 73–82. <https://doi.org/10.1080/00222337408065815>.
- [89] H. Liang, J.M. Hardy, D. Rodrigue, J. Brisson, EPDM recycled rubber powder characterization: Thermal and thermogravimetric analysis, *Rubber Chem. Technol.* 87 (2014) 538–556. <https://doi.org/10.5254/rct.14.87988>.
- [90] Z.S. Petrović, J. Milić, M. Ionescu, J.R. Halladay, EPDM rubber plasticized with polymeric soybean oil of different molecular weights, *Rubber Chem. Technol.* 90 (2017) 667–682. <https://doi.org/10.5254/rct.18.82690>.
- [91] C. Gamlin, M.G. Markovic, N.K. Dutta, N.R. Choudhury, J.G. Matison, Structural effects on the decomposition kinetics of EPDM elastomers by high-resolution TGA and modulated TGA, *J. Therm. Anal. Calorim.* 59 (2000) 319–336. <https://doi.org/10.1023/a:1010164702571>.
- [92] L.R. Caballero, M.D.D.M. Paiva, E.D.M.R. Fairbairn, R.D.T. Filho, Thermal, mechanical and microstructural analysis of metakaolin based geopolymers, *Mater. Res.* 22 (2019) 1–8. <https://doi.org/10.1590/1980-5373-MR-2018-0716>.
- [93] D.L. Bish, R.B. Von Dreele, Rietveld refinement of non-hydrogen atomic positions in kaolinite, *Clays Clay Miner.* 37 (1989) 289–296. <https://doi.org/10.1346/CCMN.1989.0370401>.
- [94] S.W. Rutherford, R.E. Kurtz, M.G. Smith, K.G. Honnell, J.E. Coons,

- Measurement and correlation of sorption and transport properties of ethylene-propylene-diene monomer (EPDM) elastomers, *J. Memb. Sci.* 263 (2005) 57–65. <https://doi.org/10.1016/j.memsci.2005.04.015>.
- [95] E.M. Redline, M.C. Celina, C.E. Harris, N.H. Giron, T. Sugama, T. Pyatina, Anomalous aging of EPDM and FEPM under combined thermo-oxidative and hydrolytic conditions, *Polym. Degrad. Stab.* 146 (2017) 317–326. <https://doi.org/10.1016/j.polymdegradstab.2017.09.010>.
- [96] X. Wen, Y. Wang, J. Gong, J. Liu, N. Tian, Y. Wang, Z. Jiang, J. Qiu, T. Tang, Thermal and flammability properties of polypropylene/carbon black nanocomposites, *Polym. Degrad. Stab.* 97 (2012) 793–801. <https://doi.org/10.1016/j.polymdegradstab.2012.01.031>.
- [97] H.H. Le, S. Ilisch, B. Jakob, H.J. Radusch, Online characterization of the effect of mixing parameters on carbon black dispersion in rubber compounds using electrical conductivity, *Rubber Chem. Technol.* 77 (2004) 147–160. <https://doi.org/10.5254/1.3547808>.
- [98] J. Málek, The kinetic analysis of non-isothermal data, *Thermochim. Acta.* 200 (1992) 257–269. [https://doi.org/10.1016/0040-6031\(92\)85118-F](https://doi.org/10.1016/0040-6031(92)85118-F).
- [99] P. Budrugeac, E. Segal, Non-isothermal kinetics of reactions whose activation energy depends on the degree of conversion, *Thermochim. Acta.* 260 (1995) 75–85. [https://doi.org/10.1016/0040-6031\(95\)90476-X](https://doi.org/10.1016/0040-6031(95)90476-X).
- [100] T. Ozawa, Applicability of Friedman plot, *J. Therm. Anal.* 31 (1986) 547–551. <https://doi.org/10.1007/BF01914230>.
- [101] E.W. Weisstein, “Fundamental Theorems of Calculus.” From MathWorld-- A Wolfram Web Resource. <https://mathworld.wolfram.com/FundamentalTheoremsOfCalculus.html>, (2020).
- [102] J.M. Criado, P.E. Sánchez-Jiménez, L.A. Pérez-Maqueda, Critical study of the isoconversional methods of kinetic analysis, *J. Therm. Anal. Calorim.* 92 (2008) 199–203. <https://doi.org/10.1007/s10973-007-8763-7>.
- [103] V. Pistor, F.G. Ornaghi, R. Fiorio, A.J. Zattera, P.J. Oliveira, C.H. Scuracchio, Desvulcanização do resíduo de terpolímero de etileno-propileno-dieno (EPDM-r) por micro-ondas, *Polimeros.* 20 (2010) 165–169. <https://doi.org/10.1590/S0104-14282010005000027>.
- [104] M. Marinović-Cincović, B. Janković, V. Jovanović, S. Samaržija-Jovanović,

- G. Marković, The kinetic and thermodynamic analyses of non-isothermal degradation process of acrylonitrile-butadiene and ethylene-propylene-diene rubbers, *Compos. Part B Eng.* 45 (2013) 321–332. <https://doi.org/10.1016/j.compositesb.2012.08.006>.
- [105] S. Zhong, B. Zhang, C. Liu, A. Shujaa aldeen, Mechanism of synergistic effects and kinetics analysis in catalytic co-pyrolysis of water hyacinth and HDPE, *Energy Convers. Manag.* 228 (2021) 113717. <https://doi.org/10.1016/j.enconman.2020.113717>.
- [106] T.G. Yee, O.H. Lin, K. Bindumadhavan, R. an Doong, Unveiling the thermal kinetics and scissoring mechanism of neolaty polyethylene/reduced graphite oxide nanocomposites, *J. Anal. Appl. Pyrolysis.* 123 (2017) 20–29. <https://doi.org/10.1016/j.jaap.2017.01.005>.
- [107] W. Hao, W. Li, W. Yang, L. Shen, Effect of silicon nitride nanoparticles on the crystallization behavior of polypropylene, *Polym. Test.* 30 (2011) 527–533. <https://doi.org/10.1016/j.polymertesting.2011.04.003>.
- [108] S.S. Hamza, Effect of Aging and Carbon Black on the Mechanical Properties of EPDM Rubber, *Polym. Test.* 17 (1998) 131–137. [https://doi.org/10.1016/S0142-9418\(97\)00039-1](https://doi.org/10.1016/S0142-9418(97)00039-1).
- [109] C. Canaud, L.L.Y. Visconte, R.C.R. Nunes, Propriedades mecânicas e de inflamabilidade de composições de borracha EPDM carregadas com negro de fumo e hidróxido de alumínio, *Polímeros.* 11 (2001) 35–40. <https://doi.org/10.1590/s0104-14282001000100009>.
- [110] G. Yamamoto, M. Onodera, K. Koizumi, J. Watanabe, H. Okuda, F. Tanaka, T. Okabe, Considering the stress concentration of fiber surfaces in the prediction of the tensile strength of unidirectional carbon fiber-reinforced plastic composites, *Compos. Part A Appl. Sci. Manuf.* 121 (2019) 499–509. <https://doi.org/10.1016/j.compositesa.2019.04.011>.
- [111] R.A. Assink, K.T. Gillen, B. Sanderson, Monitoring the degradation of a thermally aged EPDM terpolymer by ¹H NMR relaxation measurements of solvent swelled samples, *Polymer (Guildf).* 43 (2001) 1349–1355. [https://doi.org/10.1016/S0032-3861\(01\)00661-9](https://doi.org/10.1016/S0032-3861(01)00661-9).
- [112] Z. Yuan, W. Li, C. Li, L. Ye, Construction of multiple crosslinking networks in EPDM rubber: Synergistic reinforcing effect of graphene-zinc dimethacrylate on EPDM and improvement mechanism of sealing resilience,

- Compos. Part A Appl. Sci. Manuf. 121 (2019) 254–264.
<https://doi.org/10.1016/j.compositesa.2019.03.039>.
- [113] K. Srikrishna, G. Thomas, R. Martinez, M.P. Corral, S. De Aza, J.S. Moya, Kaolinite-mullite reaction series: a TEM study, *J. Mater. Sci.* 25 (1990) 607–612. <https://doi.org/10.1007/BF00714083>.
- [114] J.A. Torres-Luna, J.G. Carriazo, Porous aluminosilicic solids obtained by thermal-acid modification of a commercial kaolinite-type natural clay, *Solid State Sci.* 88 (2019) 29–35. <https://doi.org/10.1016/j.solidstatesciences.2018.12.006>.
- [115] R.T. Umemura, M.I. Felisberti, Plasticization of poly(3-hydroxybutyrate) with triethyl citrate: Thermal and mechanical properties, morphology, and kinetics of crystallization, *J. Appl. Polym. Sci.* (2020) 1–14. <https://doi.org/10.1002/app.49990>.
- [116] C. Eldsäter, B. Erlandsson, R. Renstad, A.C. Albertsson, S. Karlsson, The biodegradation of amorphous and crystalline regions in film-blown poly(ϵ -caprolactone), *Polymer (Guildf)*. 41 (2000) 1297–1304. [https://doi.org/10.1016/S0032-3861\(99\)00278-5](https://doi.org/10.1016/S0032-3861(99)00278-5).
- [117] E. Planes, L. Chazeau, G. Vigier, J.-M. Chenal, T. Stuhldreier, Crystalline microstructure and mechanical properties of crosslinked EPDM aged under gamma irradiation, *J. Polym. Sci. Part B Polym. Phys.* 48 (2010) 97–105. <https://doi.org/10.1002/polb.21848>.

Appendix

Appendix A Supplementary material to support Chapter 4.

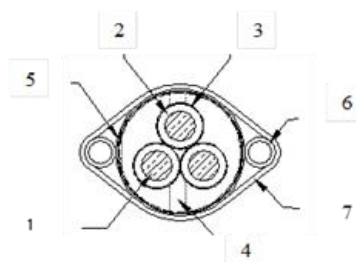
Appendix A1



CENTRILINE CEBER with CAPILLARY ROUND SPECIFICATION

Centrilift

PART NUMBER:	76011		
DESCRIPTION:	1/0SOLBC/5KV/90/HTFB/185/HGALV/2-3/8"STN'L TUBE-GALV-R		
1. CONDUCTOR:	1/0 AWG SOLID SOFT DRAWN BARE COPPER (SDBC)	DIA = 0.326"	8.28 mm
2. INSULATION:	EPDM DL90, 5KV HIGH DIELECTRIC, OIL RESISTANT 90 MIL NOMINAL THICKNESS 81 MIL MINIMUM THICKNESS	DIA = 0.512"	13.00 mm
3. BARRIER:	FLUORO BARRIER™, FEP PROTECTS THE INSULATION FROM FLUIDS AND CHEMICALS MINIMUM THICKNESS, 10MIL	DIA = 0.534"	13.56 mm
4. JACKET:	EPDM JACKET, CL-185, OIL RESISTANT, HIGH MODULUS EPDM 60 MIL NOMINAL THICKNESS 48 MIL MINIMUM THICKNESS NOMINAL DIAMETER OVER JACKET SPLINES =	1.342"	34.06mm
5. INNER ARMOR:	GALVANIZED STEEL ARMOR, 1/2" X .034" NOMINAL DIAMETER OVER ARMOR =	1.541"	39.14 mm
6. TUBE:	SPECIAL STAINLESS STEEL TUBES, 2 ea., 3/8" x .049" WALL Internal working PSI = 4,900; burst PSI = 19,600		
7. OUTER ARMOR:	GALVANIZED STEEL ARMOR, 1/2" X .025" COATED NOMINAL DIAMETER OVER ARMOR OVAL SHAPE =	1.666" x 2.416"	42.31 mm x 61.36mm
	NOMINAL WEIGHT PER FOOT =	3.57POUNDS	5.31kg/m
MARKER:	IDENTIFICATION TAPE PLACED PARALLEL UNDER ARMOR		
TEMPERATURE:	TEMPERATURE RATING CENTRILINE =	-32° C TO 204° C	-25° F TO 400° F
TESTED:	ICEA, IEEE 1018, AND CENTRILIFT SPECIFICATIONS		
	Materials and specifications are subject to change without notice.		



76011CEB.doc, JUNE 1, 2009,
KLM

Figure A1 Image modified from Centrilift Baker Hughes June 2009.

Appendix A2

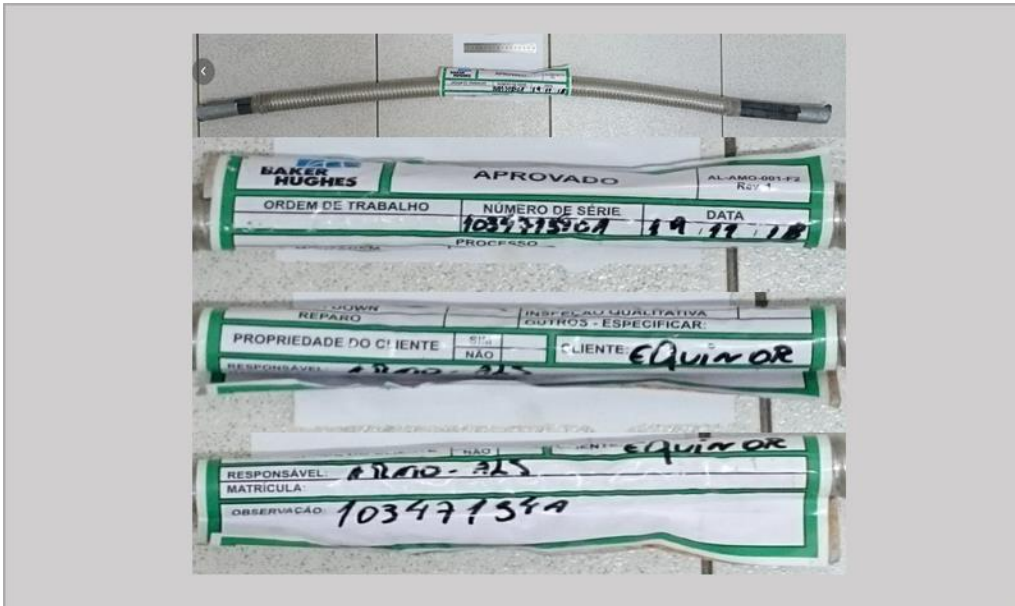


Figure A2 Image Cable I. Source of rubber I

Appendix A3

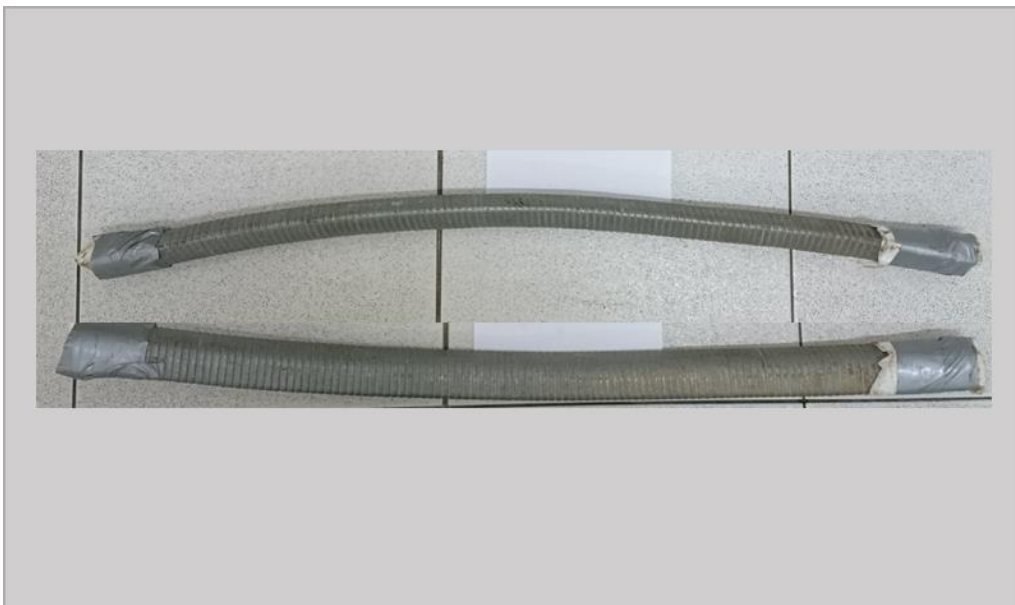


Figure A3 Image Cable II. Source of rubber II.

Appendix A4

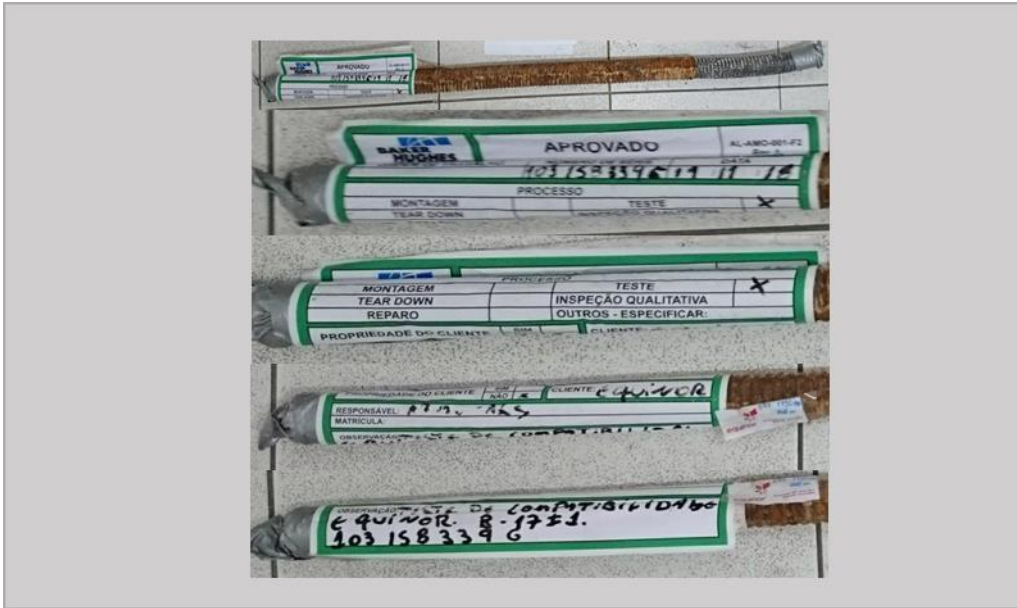


Figure A4 Image Cable III. Source of rubber III.

Appendix A5



Figure A5 Image Cable IV. Source of rubber IV.

Appendix A6



Figure A6 Image Cable V. Source of rubber V.

Appendix A7

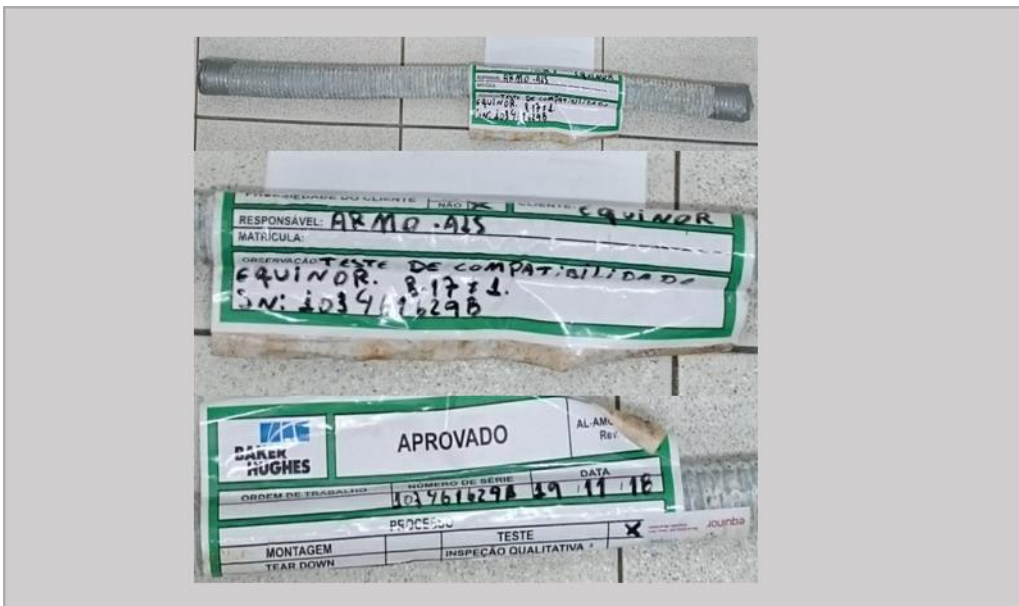
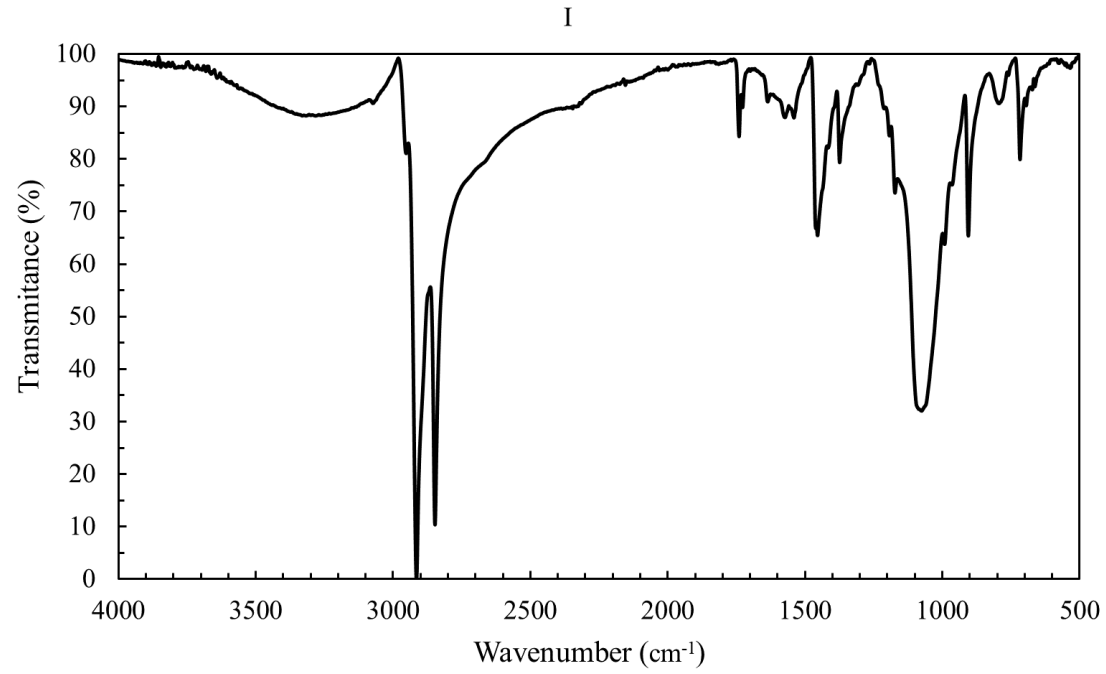


Figure A7 Image Cable VI. Source of rubber VI.

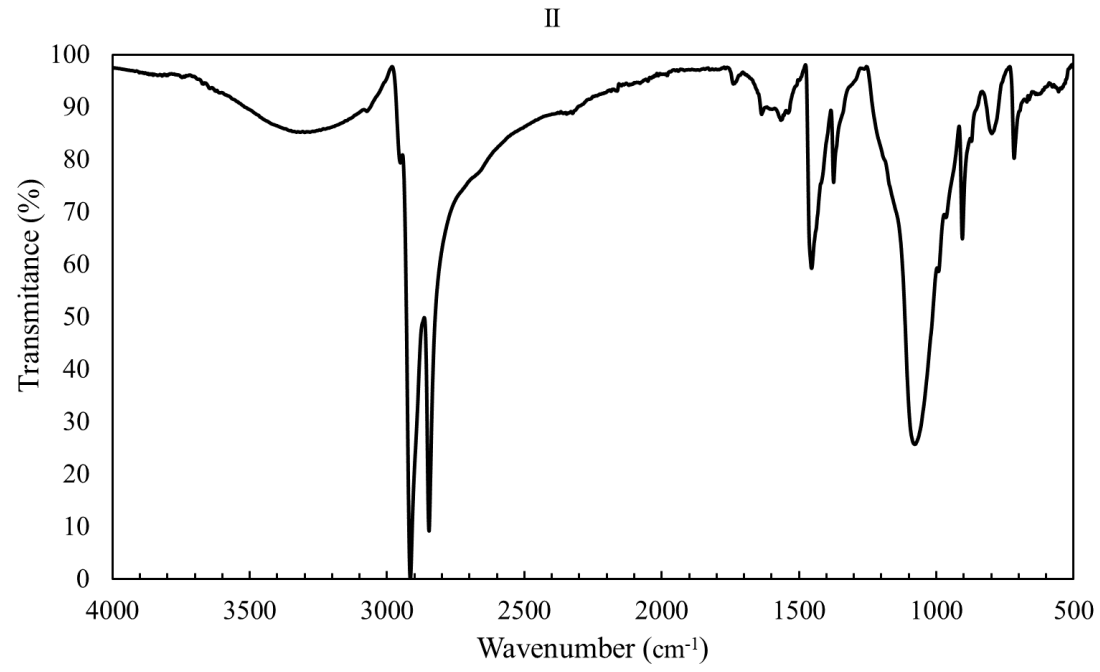
Appendix B Supplementary material to support Chapter 5.1.1.**Appendix B1**

PUC-Rio - Certificação Digital Nº 1821742/CA

**Figure B1** ATR plot of Rubber I.

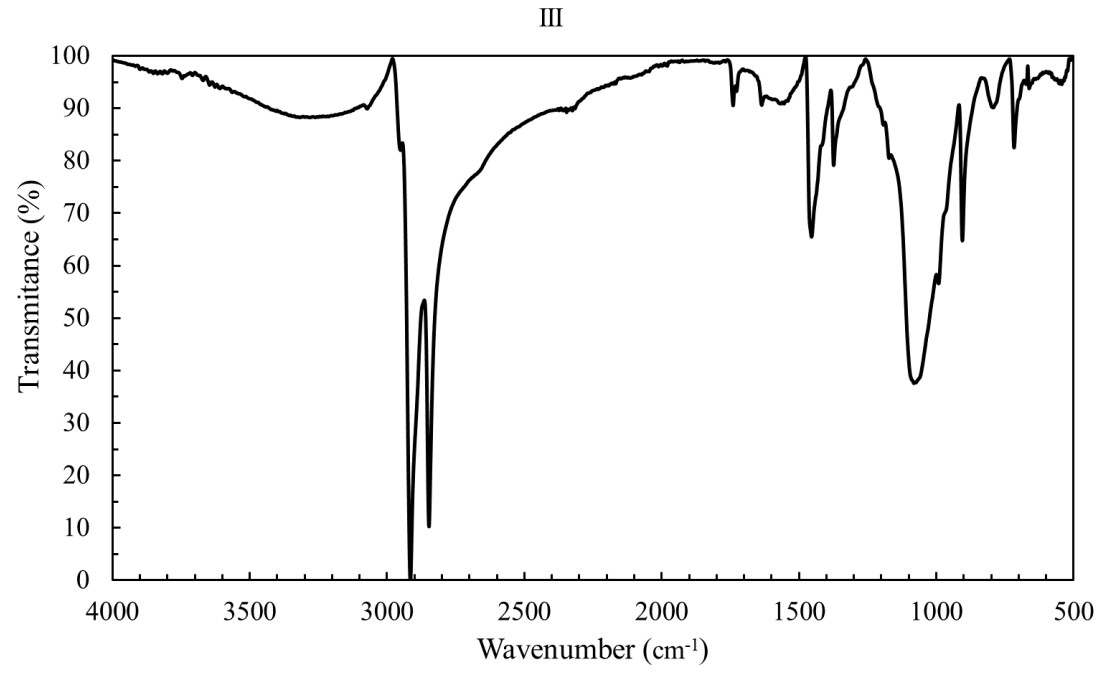
Appendix B2

PUC-Rio - Certificação Digital Nº 1821742/CA

**Figure B2** ATR plot of Rubber II.

Appendix B3

PUC-Rio - Certificação Digital Nº 1821742/CA

**Figure B3** ATR plot of Rubber III.

Appendix B4

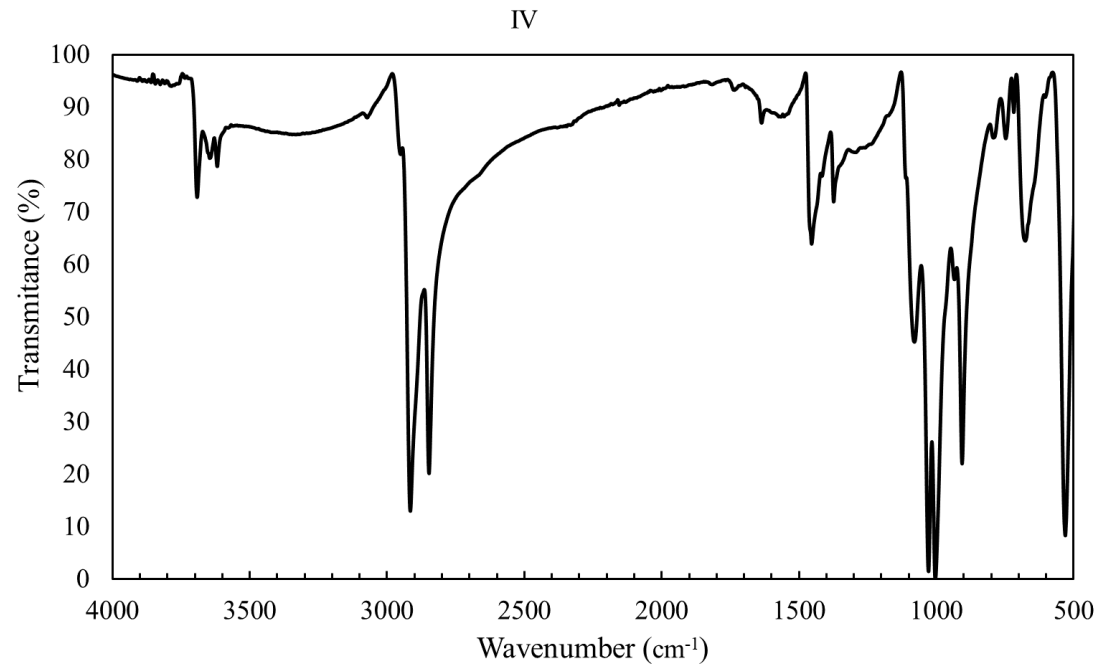


Figure B4 ATR plot of Rubber IV.

Appendix B5

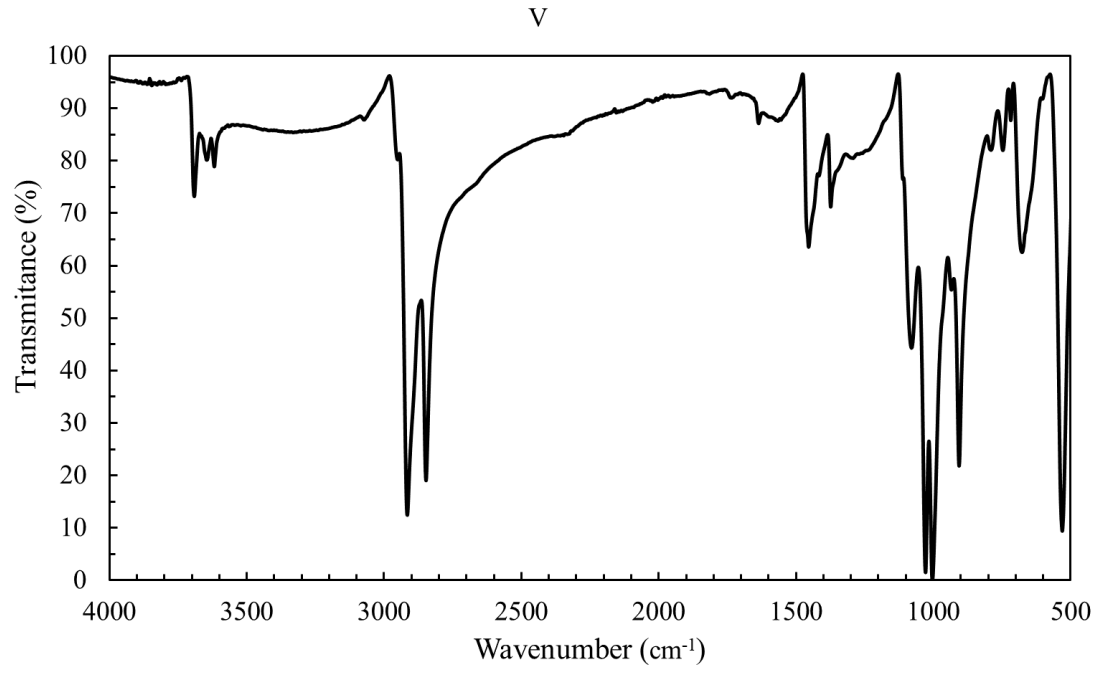
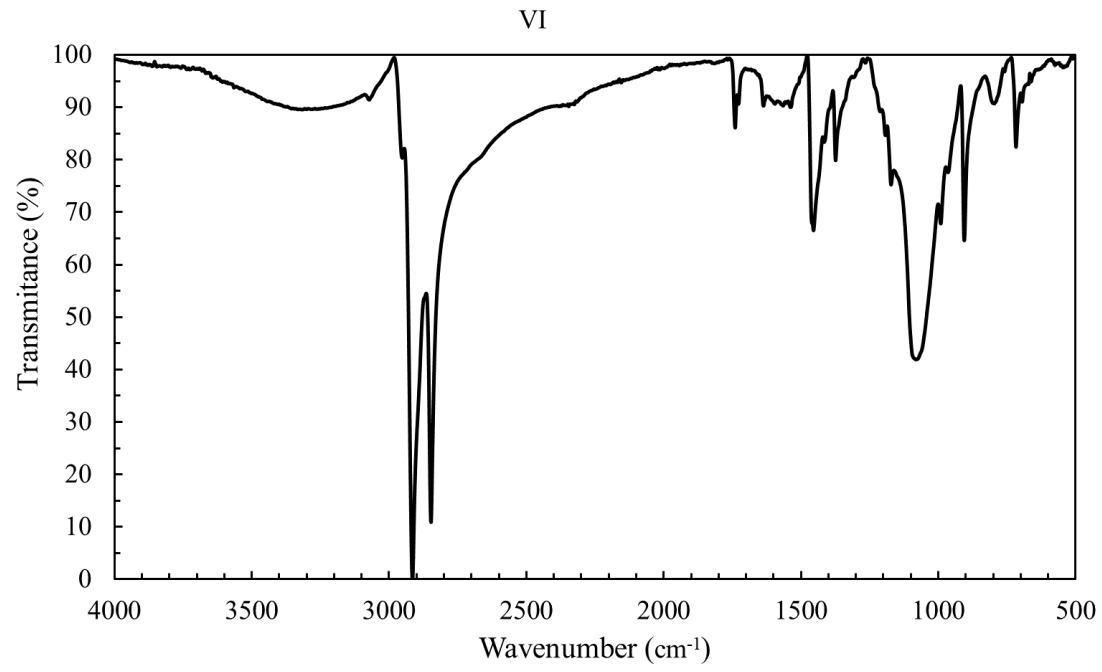


Figure B5 ATR plot of Rubber V.

Appendix B6

PUC-Rio - Certificação Digital Nº 1821742/CA

**Figure B6** ATR plot of Rubber VI.

Appendix C Supplementary material to support Chapter 5.2.1

Appendix C1

PUC-Rio - Certificação Digital Nº 1821742/CA

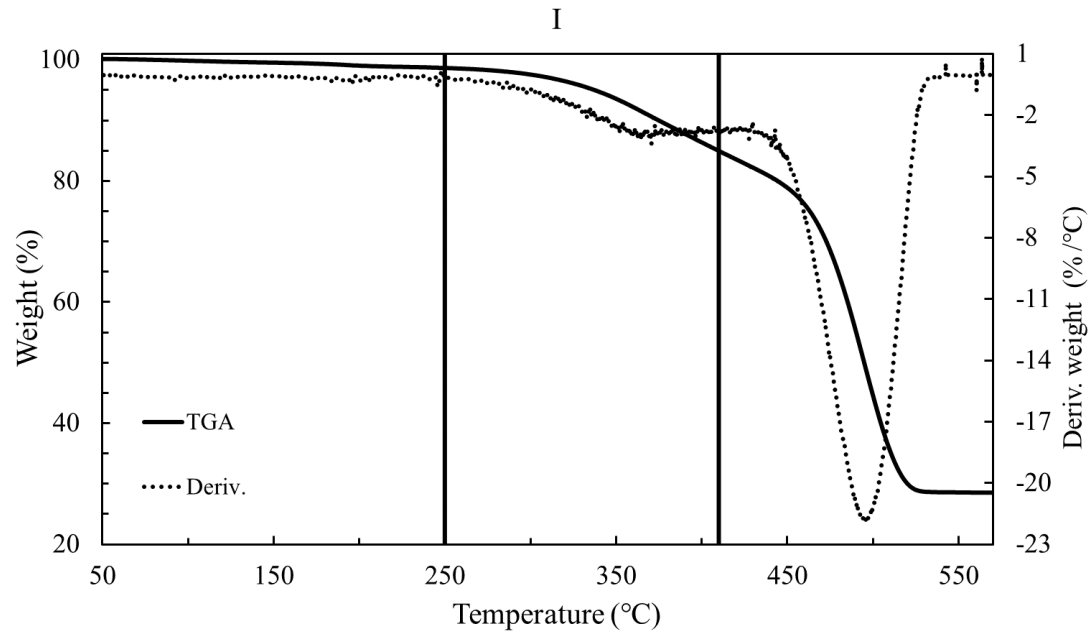


Figure C1 TGA plot for Rubber I at 20 °C min^{-1} with N_2 at 20 ml min^{-1} .

Appendix C2

PUC-Rio - Certificação Digital N° 1821742/CA

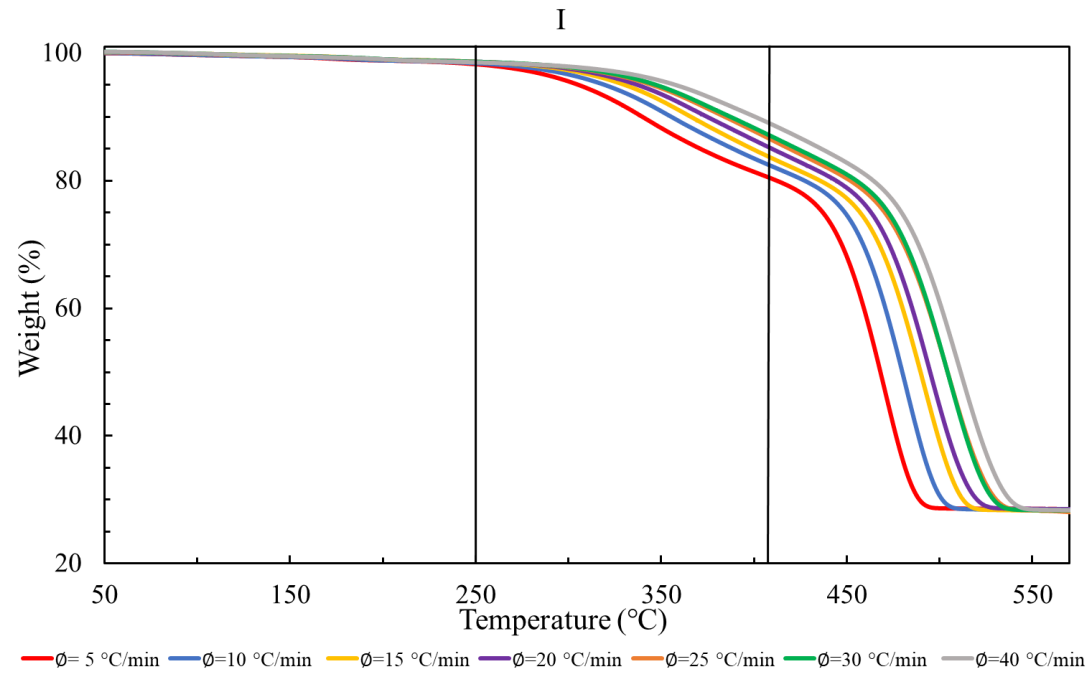


Figure C2 TGA plot for Rubber II at 20 °C min^{-1} with N_2 at 20 ml min^{-1} .

Appendix C3

PUC-Rio - Certificação Digital Nº 1821742/CA

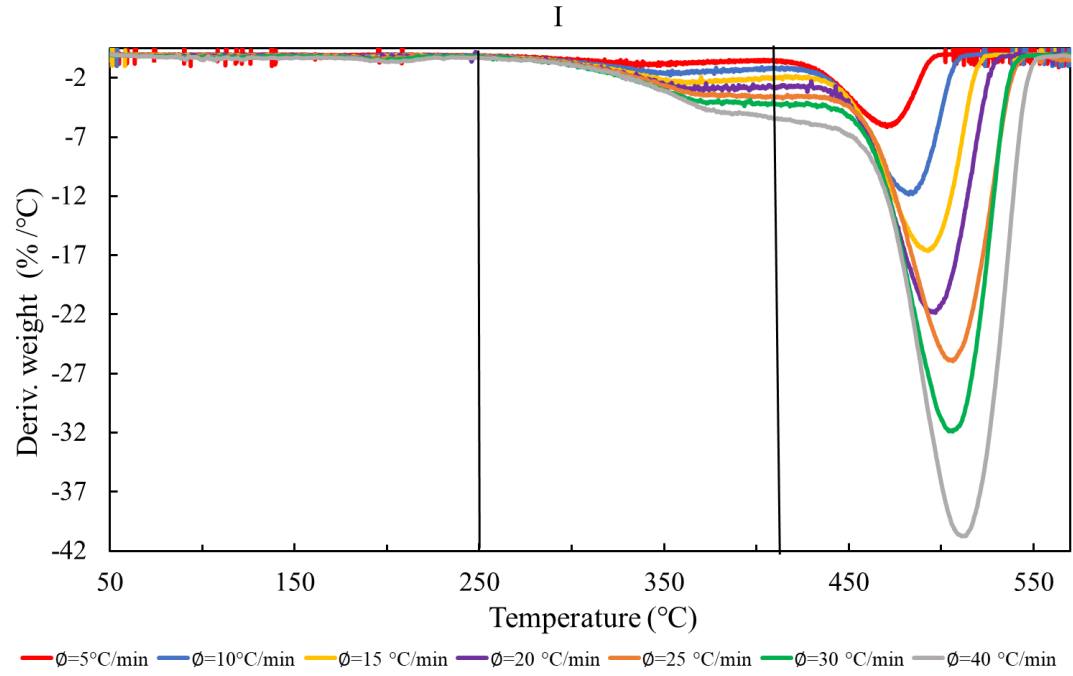


Figure C3 Derivative weight for Rubber I, under N_2 and 20 ml min^{-1} .

Appendix C4

PUC-Rio - Certificação Digital Nº 1821742/CA

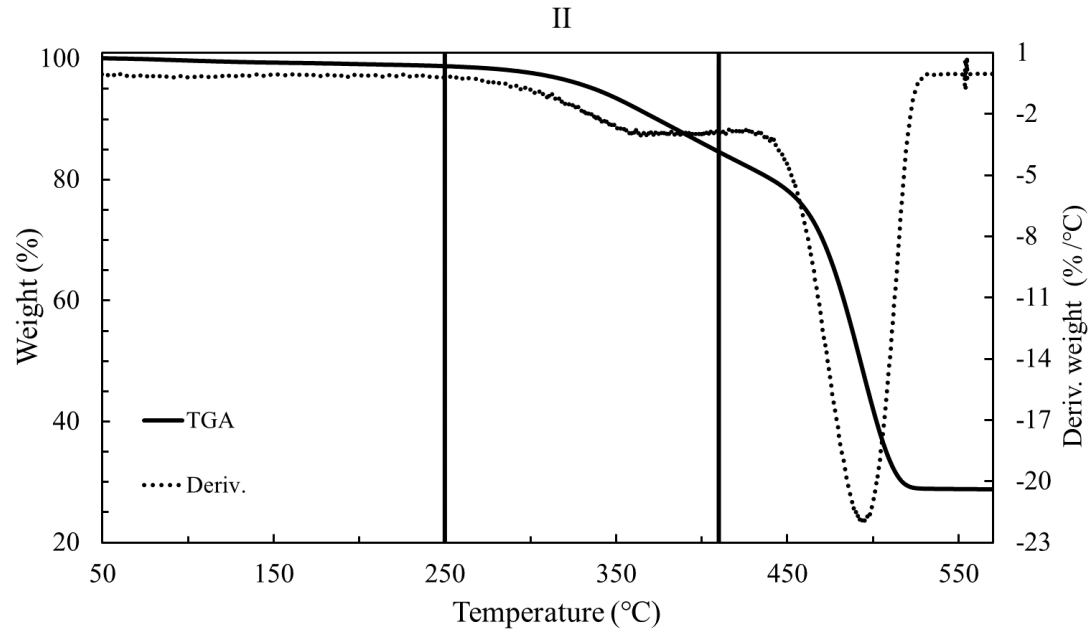


Figure C4 TGA plot for Rubber II at 20 °C min^{-1} with N_2 at 20 ml min^{-1} .

Appendix C5

PUC-Rio - Certificação Digital N° 1821742/CA

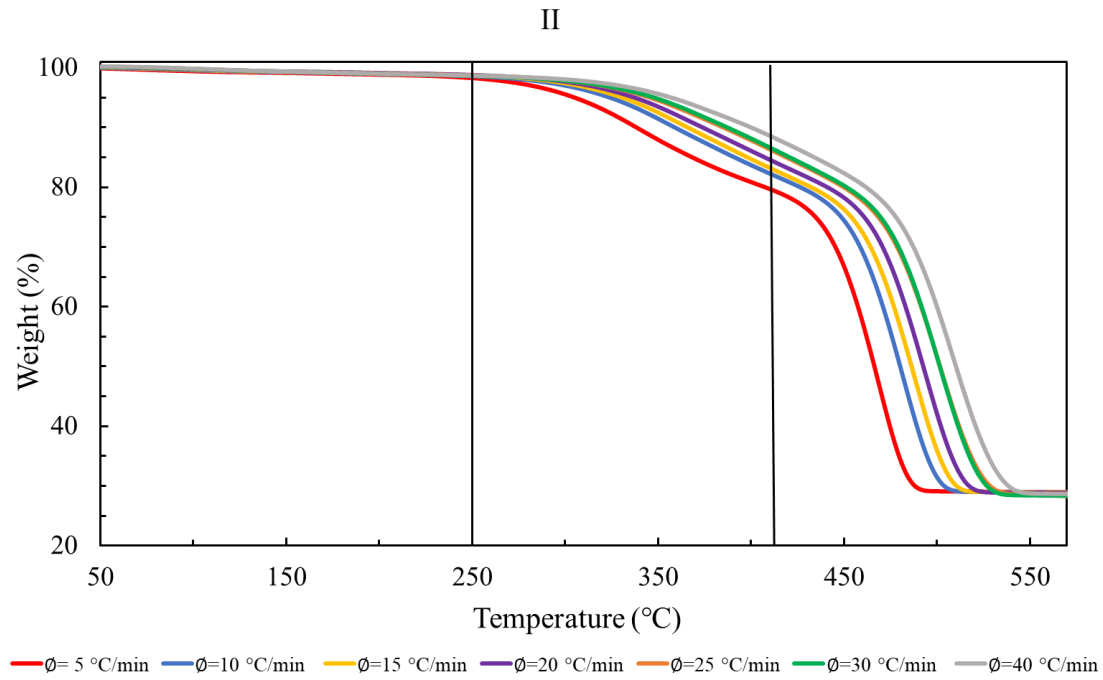


Figure C5 TGA plot for Rubber II, under N₂ at 20 ml min⁻¹.

Appendix C6

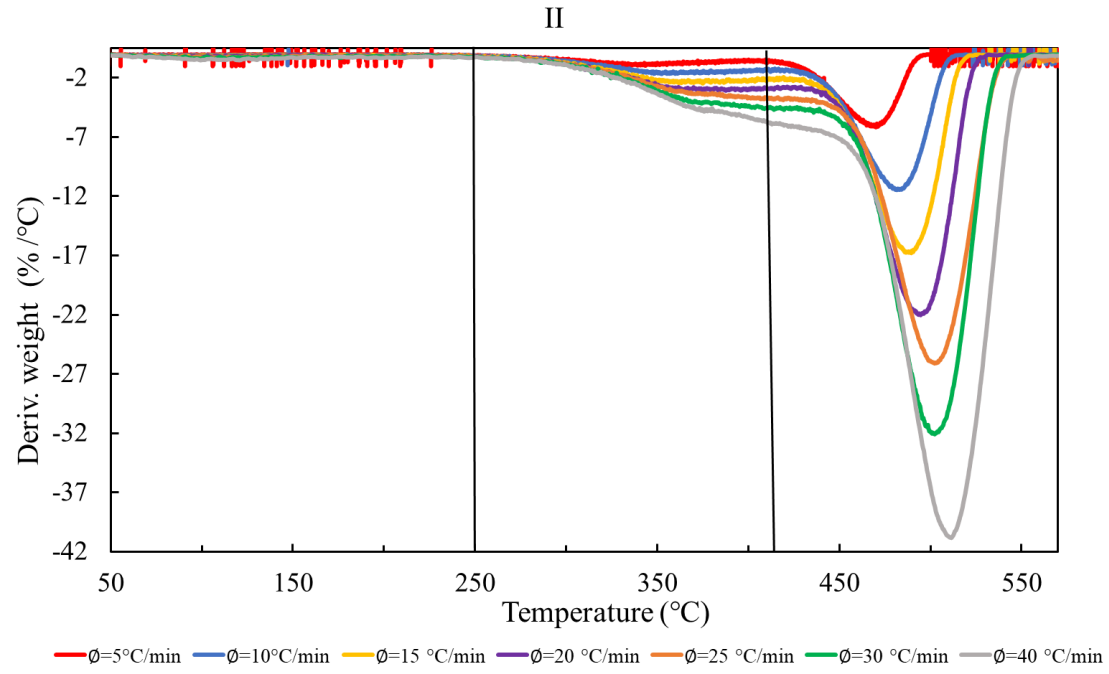


Figure C6 Derivative weight for Rubber I, under N_2 at 20 ml min^{-1} .

Appendix C7

PUC-Rio - Certificação Digital N° 1821742/CA

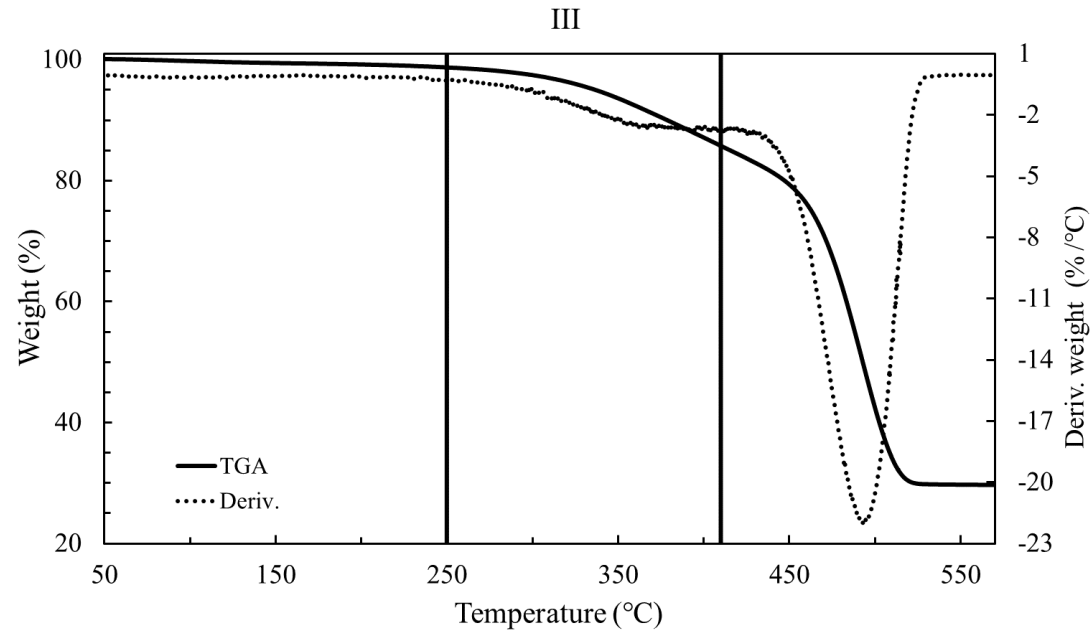
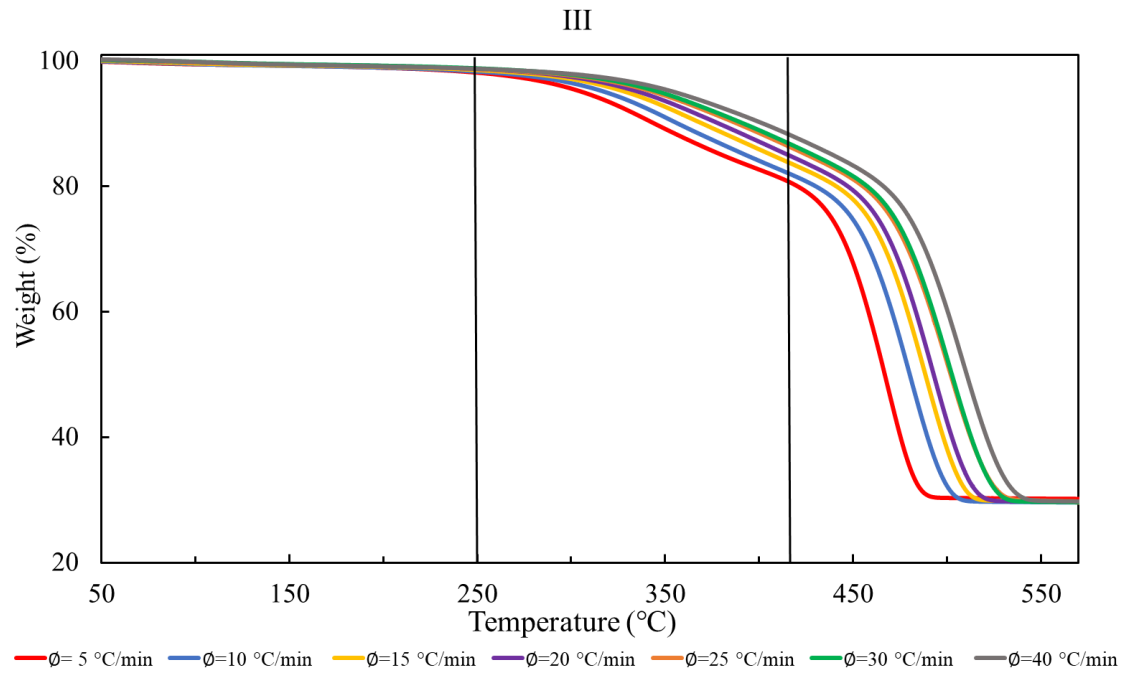


Figure C7 TGA plot for Rubber III at $20\text{ }^{\circ}\text{C min}^{-1}$ with N_2 at 20 ml min^{-1} .

Appendix C8

PUC-Rio - Certificação Digital Nº 1821742/CA

**Figure C8** TGA plot for rubber III, under N₂ at 20 ml min⁻¹.

Appendix C9

PUC-Rio - Certificação Digital Nº 1821742/CA

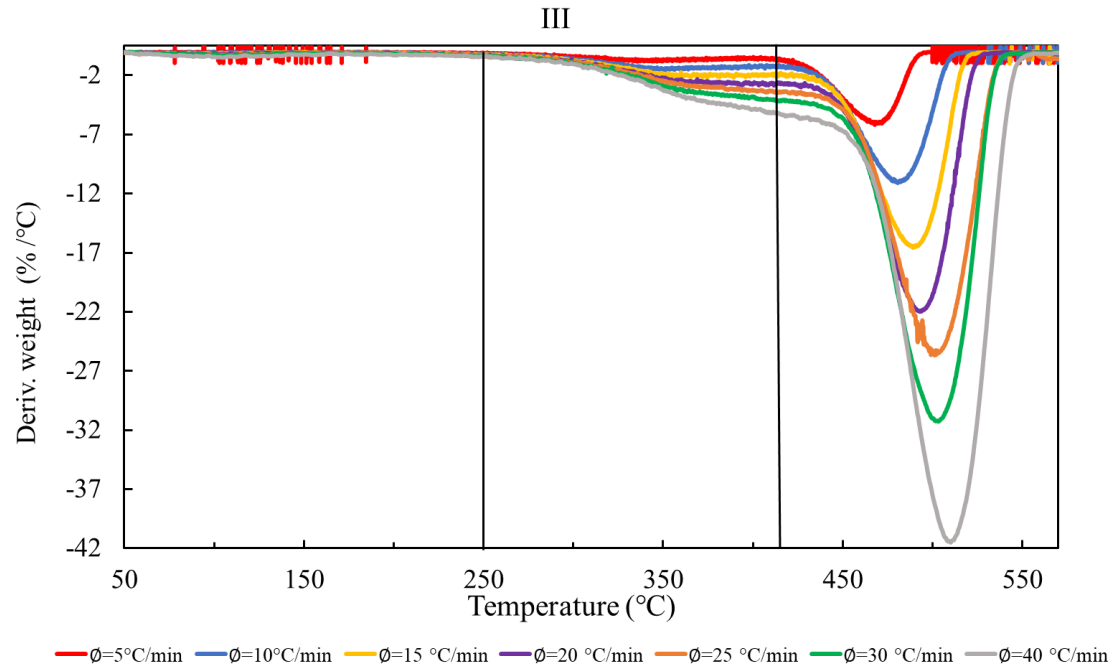


Figure C9 Derivative weight for rubber III, under N_2 at 20 ml min^{-1} .

Appendix C10

PUC-Rio - Certificação Digital N° 1821742/CA

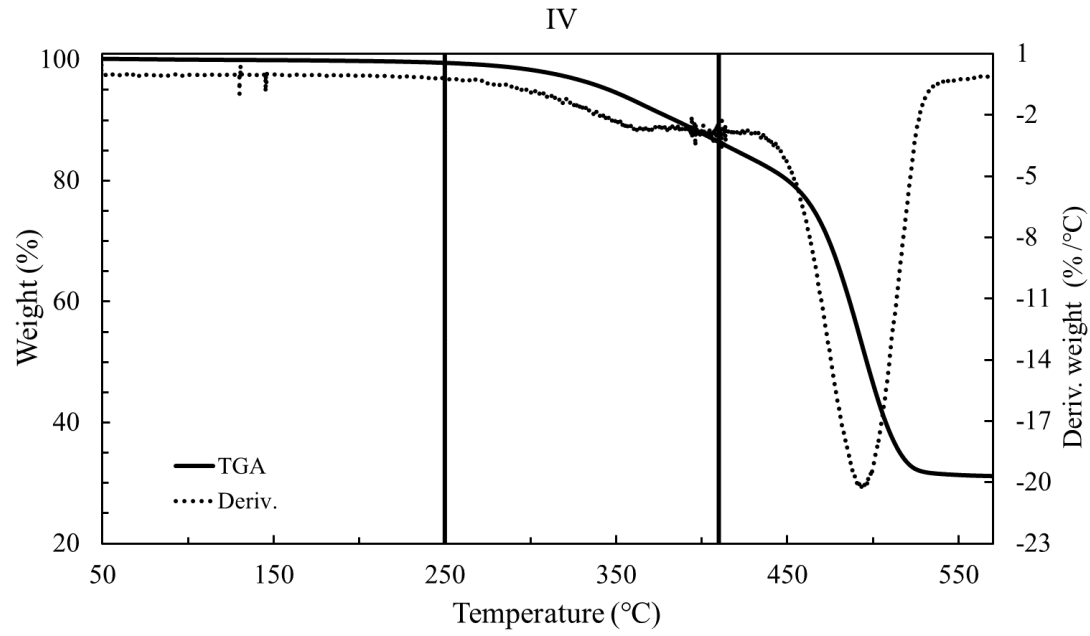
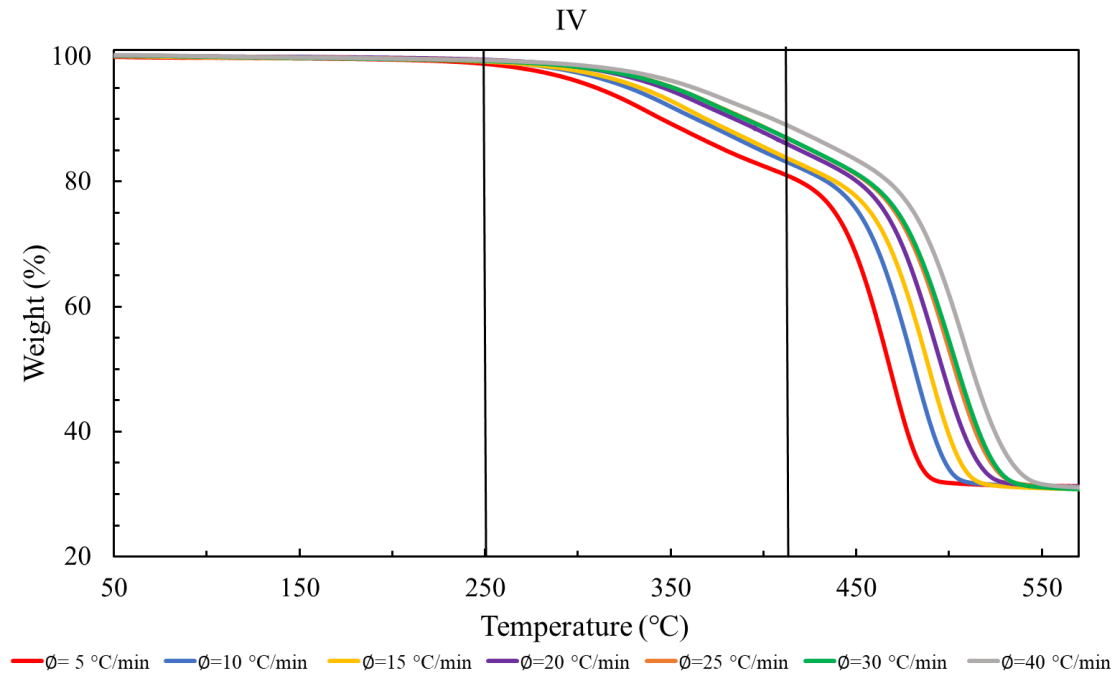


Figure C10 TGA plot for rubber IV at 20 °C min⁻¹, under N₂ at 20 ml min⁻¹.

Appendix C11

PUC-Rio - Certificação Digital N° 1821742/CA

**Figure C11** TGA plot for rubber IV, under N₂ at 20 ml min⁻¹.

Appendix C12

PUC-Rio - Certificação Digital N° 1821742/CA

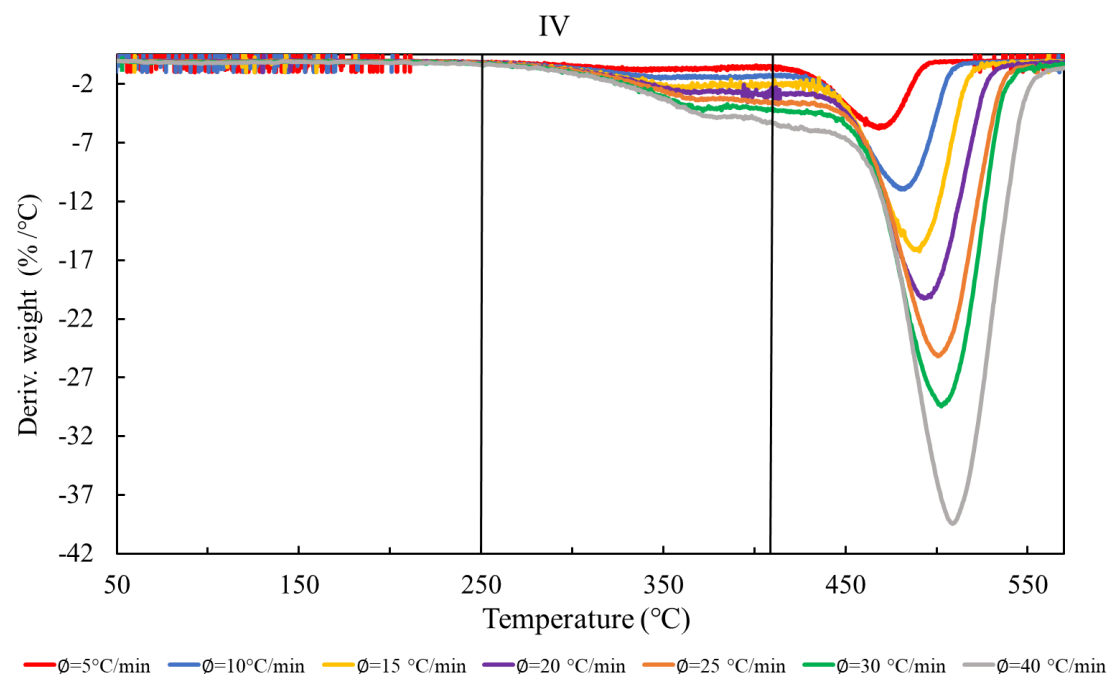


Figure C12 Derivative weight for rubber IV, under N_2 at 20 ml min^{-1} .

Appendix C13

PUC-Rio - Certificação Digital N° 1821742/CA

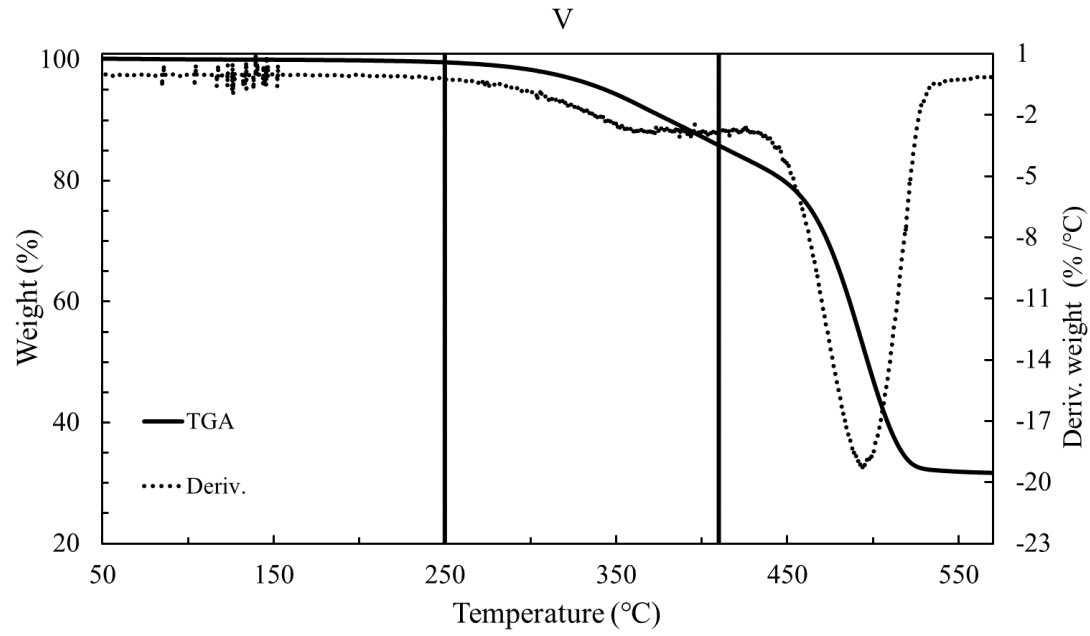
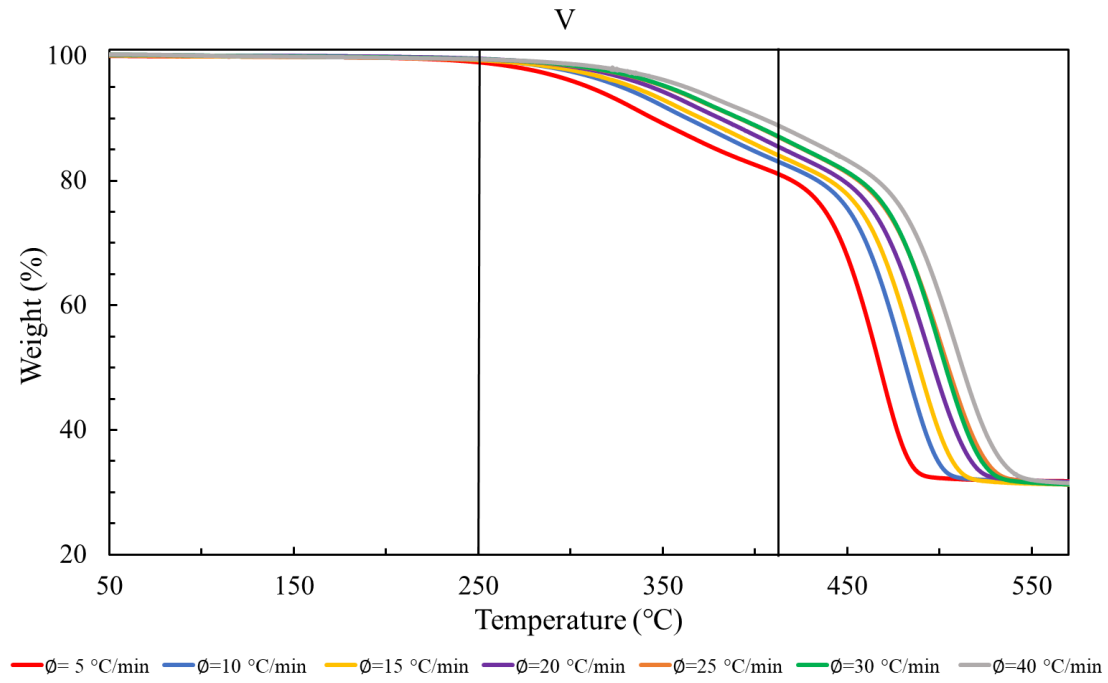


Figure C13 TGA for rubber V at 20 °C min⁻¹, under N₂ at 20 ml min⁻¹.

Appendix C14

PUC-Rio - Certificação Digital N° 1821742/CA

**Figure C14** TGA for rubber V, under N_2 at 20 ml min^{-1} .

Appendix C15

PUC-Rio - Certificação Digital Nº 1821742/CA

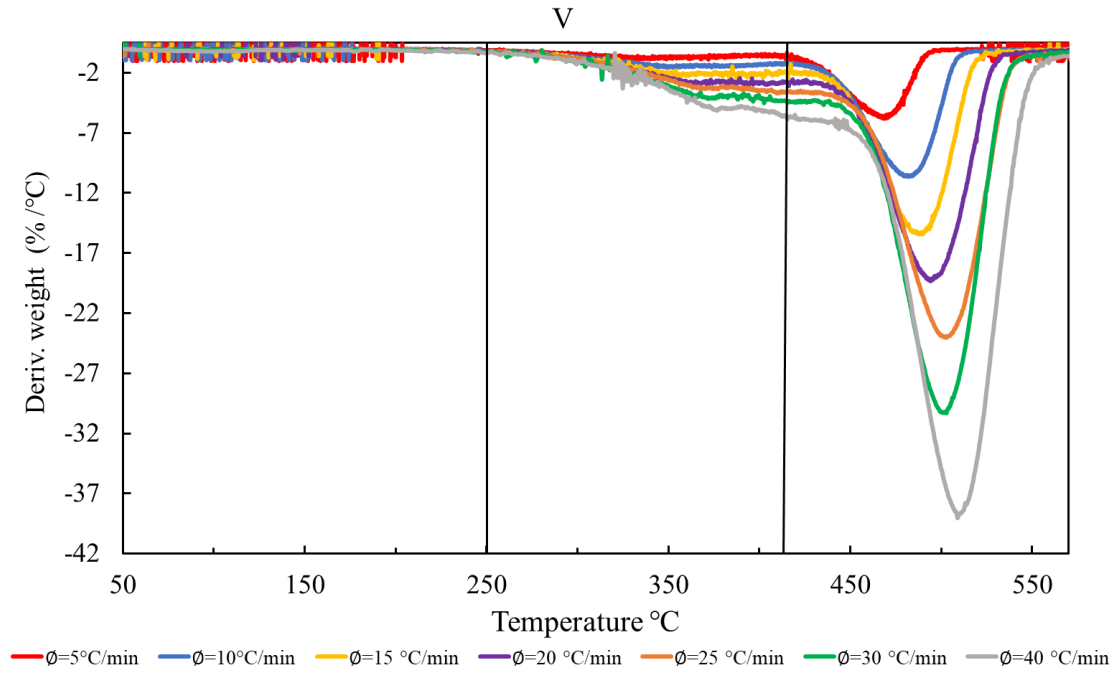


Figure C15 Derivative weight for rubber I, under N₂ at 20 ml min⁻¹.

Appendix C16

PUC-Rio - Certificação Digital Nº 1821742/CA

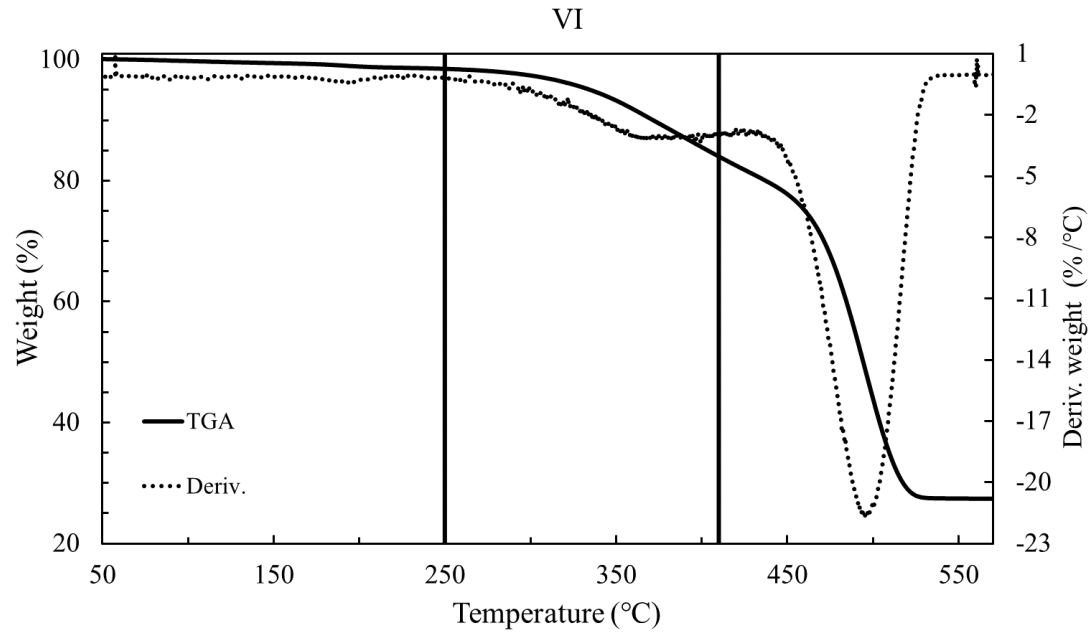
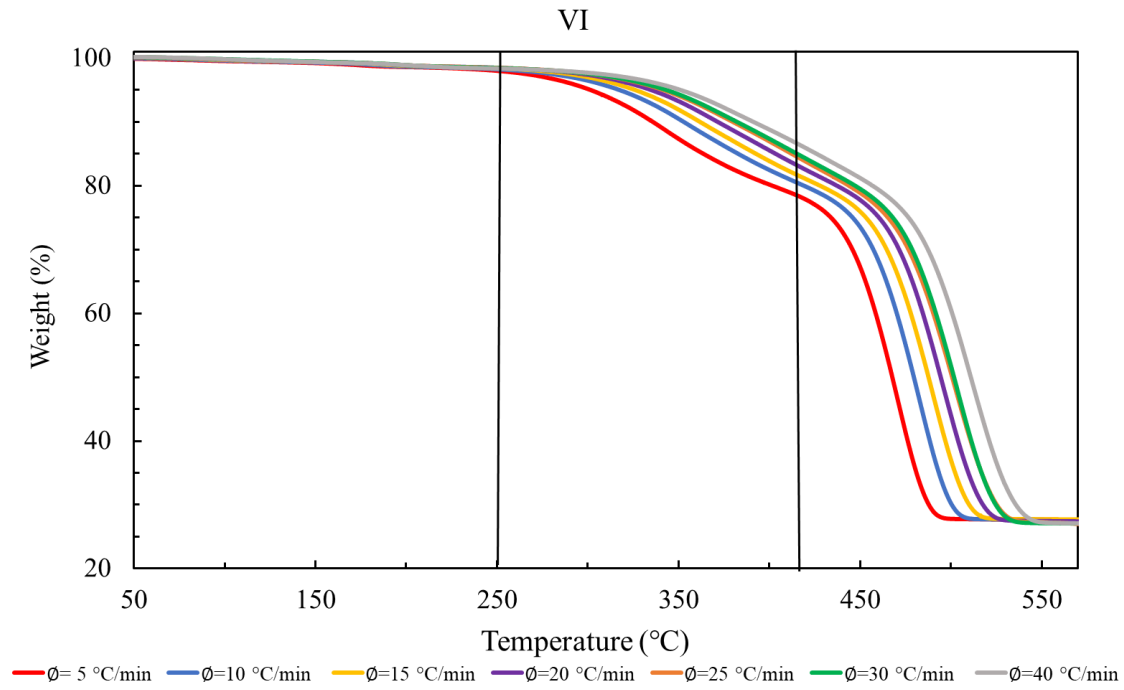


Figure C16 TGA plot for rubber VI at 20 °C min⁻¹, under N₂ at 20 ml min⁻¹.

Appendix C17

PUC-Rio - Certificação Digital Nº 1821742/CA

**Figure C17** TGA plot for rubber V, under N₂ at 20 ml min⁻¹.

Appendix C18

PUC-Rio - Certificação Digital N° 1821742/CA

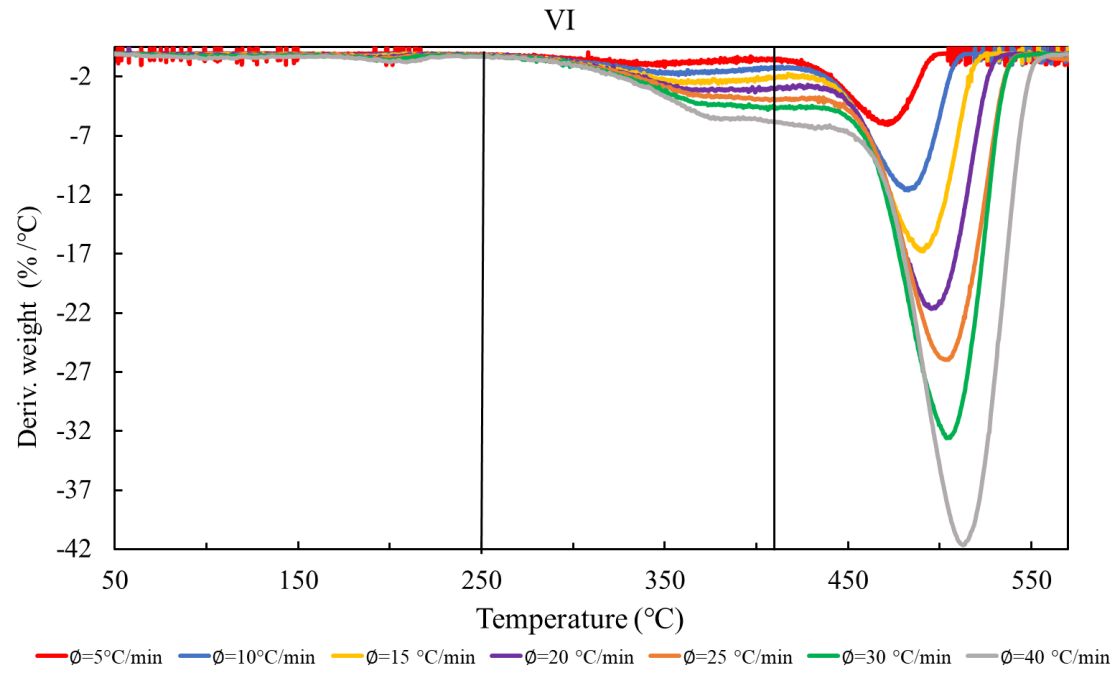


Figure C18 Derivative weight for rubber I, under N_2 at 20 ml min^{-1} .

Appendix C19

Heating rate (°C min ⁻¹)	% Weight lost 30-250 °C (Water)					
	I	II	III	IV	V	VI
5	1.733	1.731	1.856	1.178	0.998	1.970
10	1.574	1.407	1.691	0.720	0.576	1.736
15	1.350	1.272	1.447	0.810	0.669	1.566
20	1.334	1.231	1.269	0.518	0.425	1.508
25	1.371	1.293	1.266	0.614	0.569	1.521
30	1.350	1.355	1.176	0.720	0.504	1.557
40	1.434	1.322	1.242	0.611	0.528	1.625
Average	1.449	1.373	1.421	0.739	0.610	1.640
Standard deviation	0.139	0.155	0.240	0.200	0.173	0.152

Table C1 Percentage of weight water mass determined by TGA in N₂ atmosphere.

Heating rate (°C min ⁻¹)	% Weight lost 250-410 °C (Oil)					
	I	II	III	IV	V	VI
5	17.986	18.557	16.637	17.511	17.599	18.938
10	16.197	16.303	15.511	15.806	16.035	17.105
15	15.169	15.490	13.982	15.085	14.913	16.009
20	13.695	14.152	12.970	13.075	13.748	14.484
25	12.286	12.354	11.567	12.075	12.026	13.092
30	11.756	11.995	12.026	11.955	12.016	12.613
40	9.787	10.069	9.722	10.028	10.255	10.988
Average	13.840	14.131	13.081	13.648	13.799	14.747
Standard deviation	2.611	2.683	2.282	2.403	2.377	2.569

Table C2 Percentage of extender oils determined by TGA in N₂ atmosphere.

Appendix C20

Heating rate (°C min ⁻¹)	% Weight lost 410-570 °C (EPDM)					
	I	II	III	IV	V	VI
5	51.737	50.758	51.345	50.071	49.611	51.459
10	53.822	53.354	53.198	52.317	51.747	53.538
15	55.175	54.345	54.803	53.276	53.145	54.722
20	56.429	55.812	56.07	55.253	54.135	56.607
25	58.278	58.053	57.577	56.496	56.151	58.399
30	58.557	58.282	57.993	56.532	56.202	58.763
40	60.404	59.960	59.275	58.298	57.724	60.297
Average	56.343	55.795	55.754	54.606	54.102	56.255
Standard deviation	2.780	2.978	2.609	2.643	2.628	2.930

Table C3 Percentage of EPDM mass determined by TGA in N₂ atmosphere.

Heating rate (°C min ⁻¹)	% Residual mass in 570 °C (black carbon + Kaolin or Metakaolin)					
	I	II	III	IV	V	VI
5	28.543	28.954	30.162	31.240	31.792	27.633
10	28.407	28.936	29.600	31.157	31.642	27.621
15	28.306	28.893	29.768	30.829	31.273	27.703
20	28.542	28.805	29.691	31.154	31.692	27.401
25	28.065	28.300	29.588	30.815	31.254	26.988
30	28.337	28.368	29.641	30.793	31.278	27.067
40	28.375	28.649	29.761	31.063	31.493	27.090
Average	28.368	28.701	29.744	31.007	31.489	27.358
Standard deviation	0.151	0.251	0.183	0.176	0.208	0.283

Table C4 Percentage of black carbon + kaolin or metakaolin mass determined by TGA up 570 °C in N₂ atmosphere.

Appendix D Supplementary material to support Chapter 5.2.2

Appendix D1

PUC-Rio - Certificação Digital N° 1821742/CA

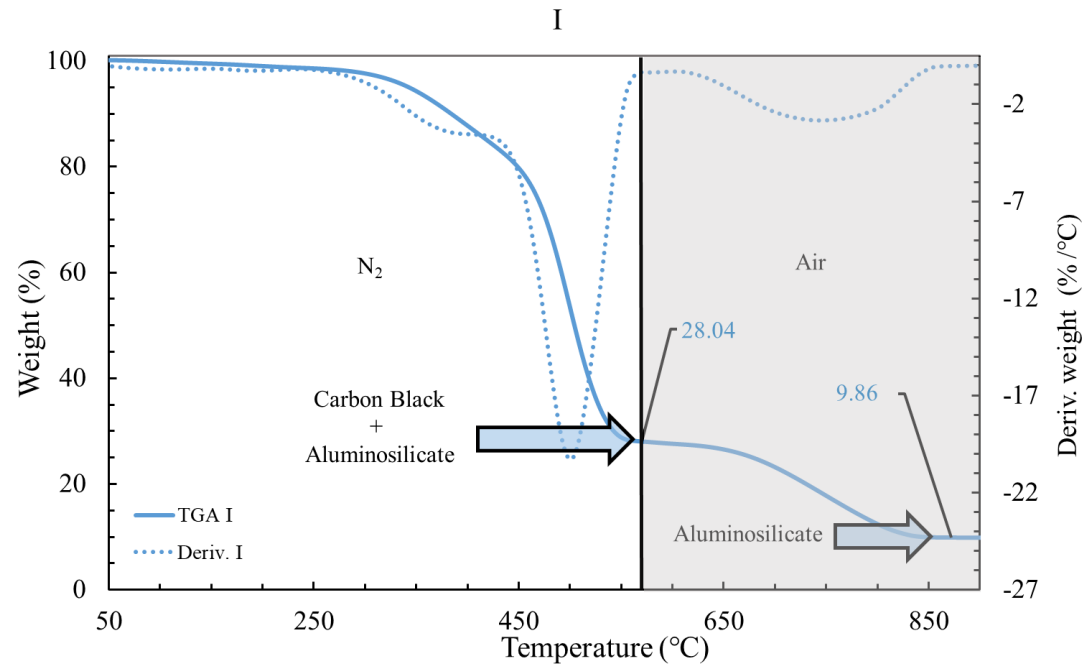


Figure D1 TGA at 25 °C min⁻¹ for Rubber I, under N₂ at 20 ml min⁻¹ from 30-570 °C and synthetic air 20 ml min⁻¹ from 570-900 °C.

Appendix D2

PUC-Rio - Certificação Digital N° 1821742/CA

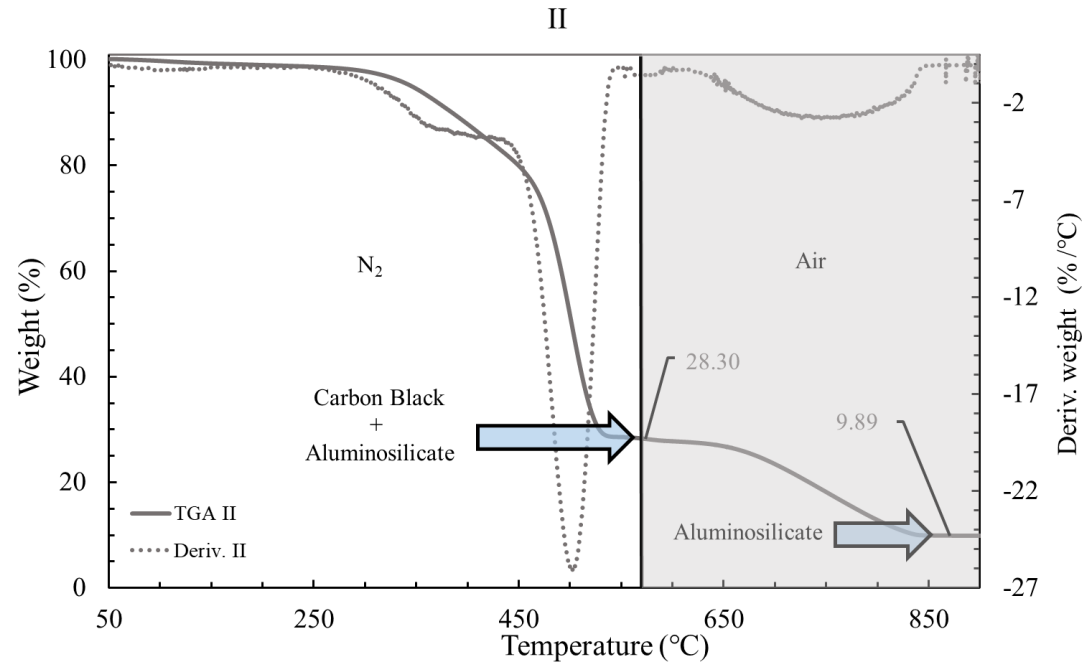


Figure D2 TGA at 25 °C min⁻¹ for Rubber II, under N₂ at 20 ml min⁻¹ from 30-570 °C and synthetic air 20 ml min⁻¹ from 570-900 °C.

Appendix D3

PUC-Rio - Certificação Digital N° 1821742/CA

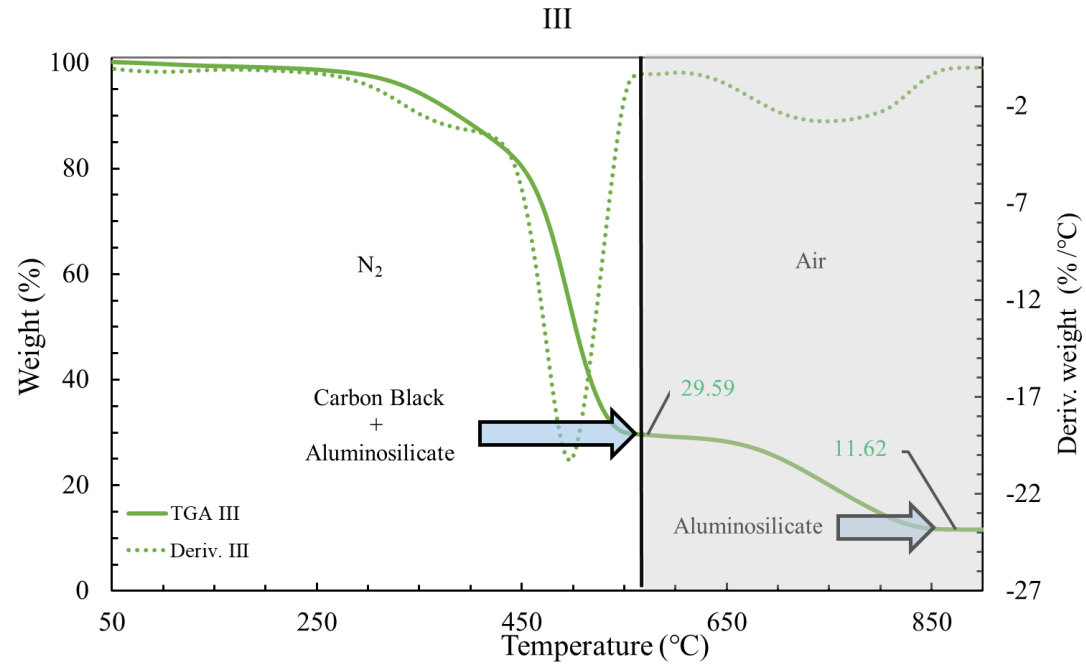


Figure D3 TGA at 25 °C min⁻¹ for Rubber III, under N₂ at 20 ml min⁻¹ from 30-570 °C and synthetic air 20 ml min⁻¹ from 570-900 °C.

Appendix D4

PUC-Rio - Certificação Digital N° 1821742/CA

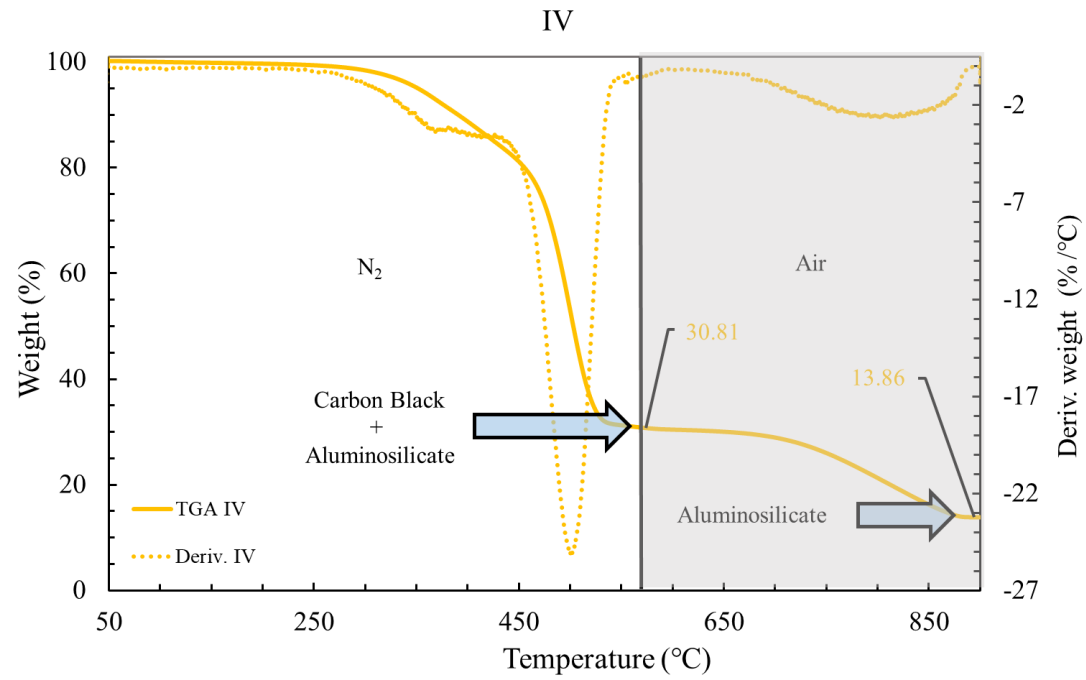


Figure D4 TGA at 25 °C min⁻¹ for Rubber IV, under N₂ at 20 ml min⁻¹ from 30-570 °C and synthetic air 20 ml min⁻¹ from 570-900 °C.

Appendix D5

PUC-Rio - Certificação Digital N° 1821742/CA

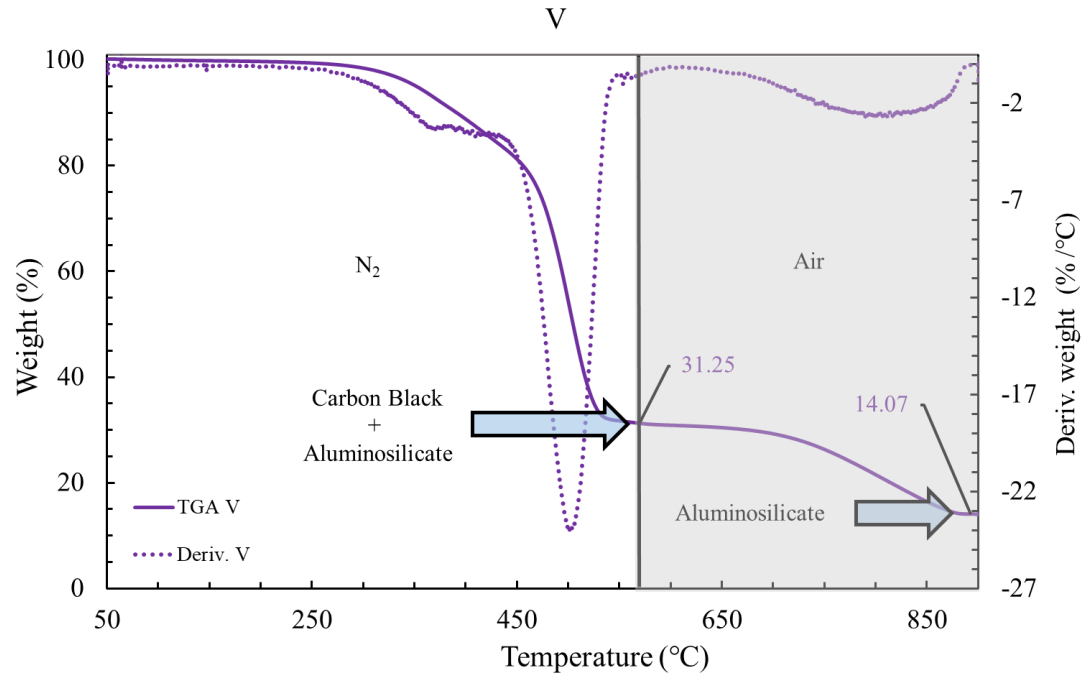


Figure D5 TGA at 25 °C min⁻¹ for Rubber V, under N₂ at 20 ml min⁻¹ from 30-570 °C and synthetic air 20 ml min⁻¹ from 570-900 °C.

Appendix D6

PUC-Rio - Certificação Digital N° 1821742/CA

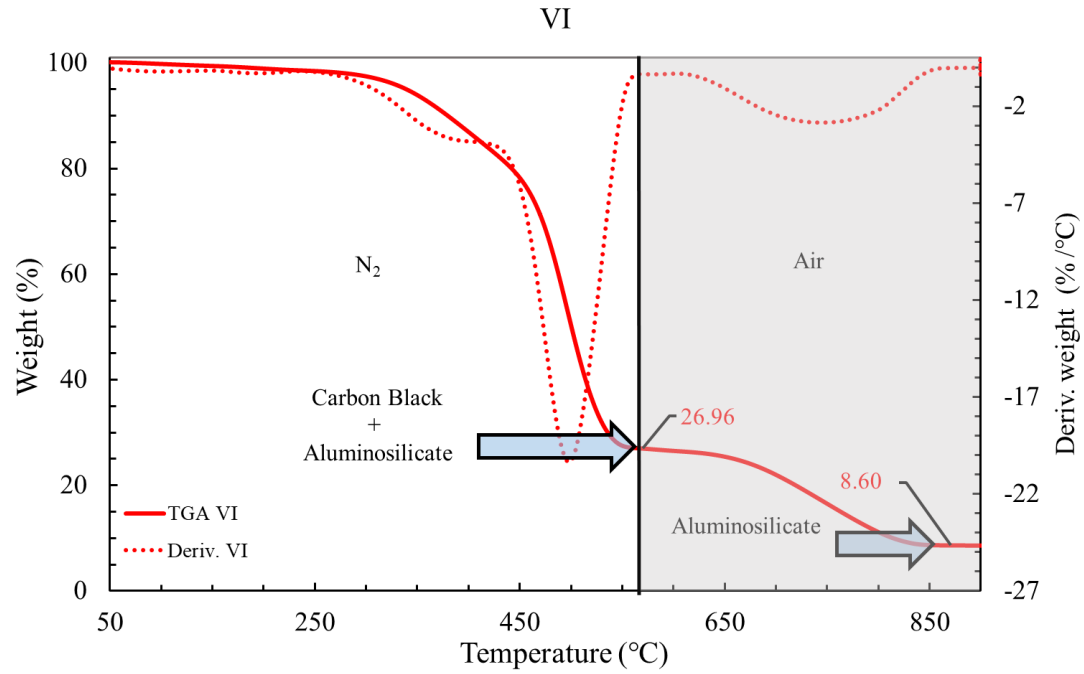


Figure D6 TGA at 25 °C min⁻¹ for Rubber VI, under N₂ at 20 ml min⁻¹ from 30-570 °C and synthetic air 20 ml min⁻¹ from 570-900 °C.

Appendix E Supplementary material to support Chapter 5.3

Appendix E1

PUC-Rio - Certificação Digital Nº 1821742/CA

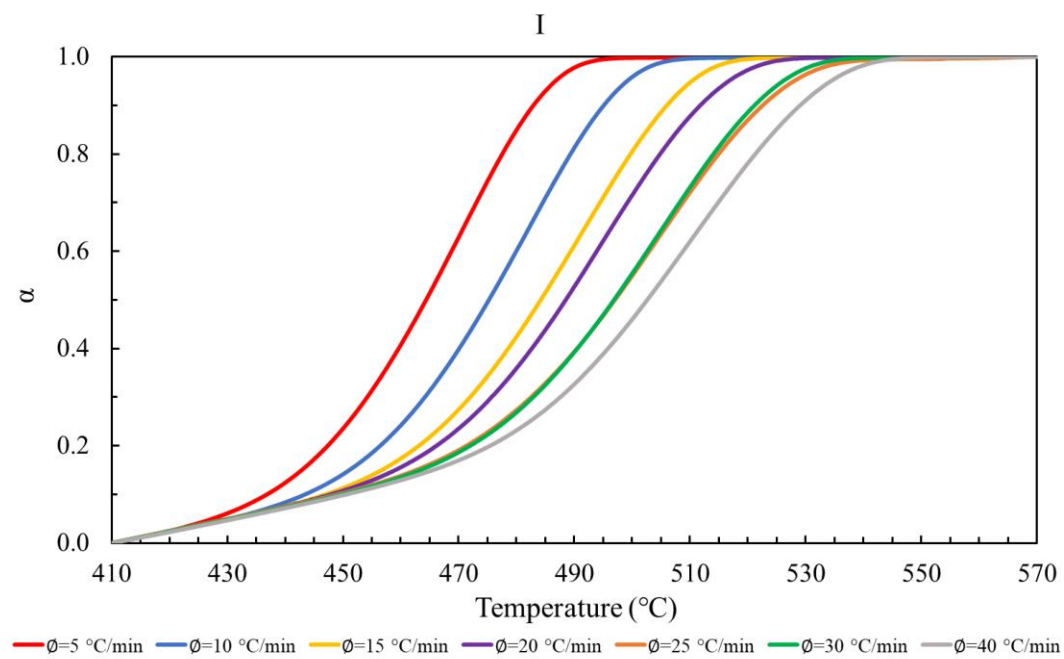


Figure E1 Conversion of EPDM degradation in Rubber I, at 20 ml min^{-1} , under N_2 atmosphere with different heating rates.

Appendix E2

PUC-Rio - Certificação Digital Nº 1821742/CA

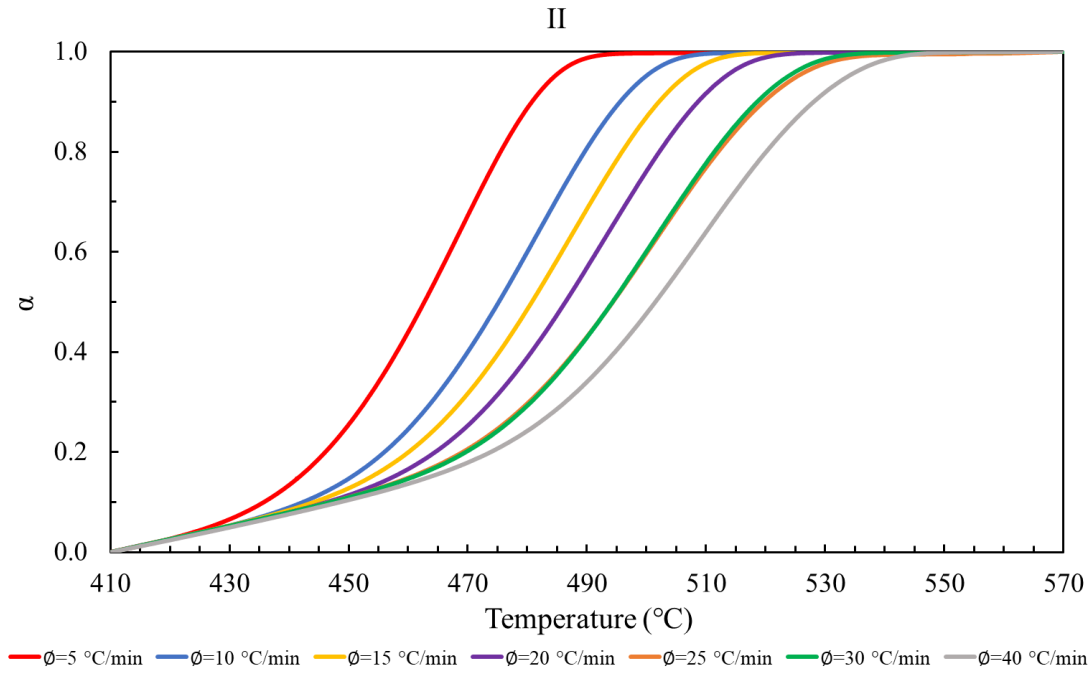


Figure E2 Conversion of EPDM degradation in Rubber II, at 20 ml min^{-1} , under N_2 atmosphere with different heating rates.

Appendix E3

PUC-Rio - Certificação Digital Nº 1821742/CA

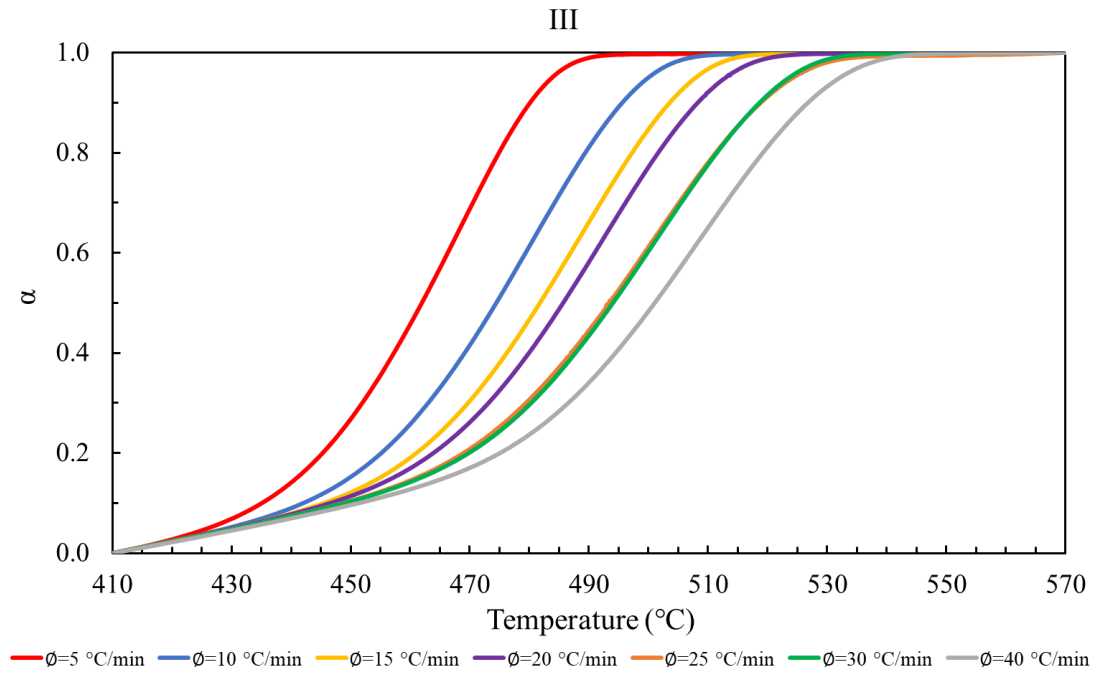


Figure E3 Conversion of EPDM degradation in Rubber III, at 20 ml min^{-1} , under N_2 atmosphere with different heating rates.

Appendix E4

PUC-Rio - Certificação Digital Nº 1821742/CA

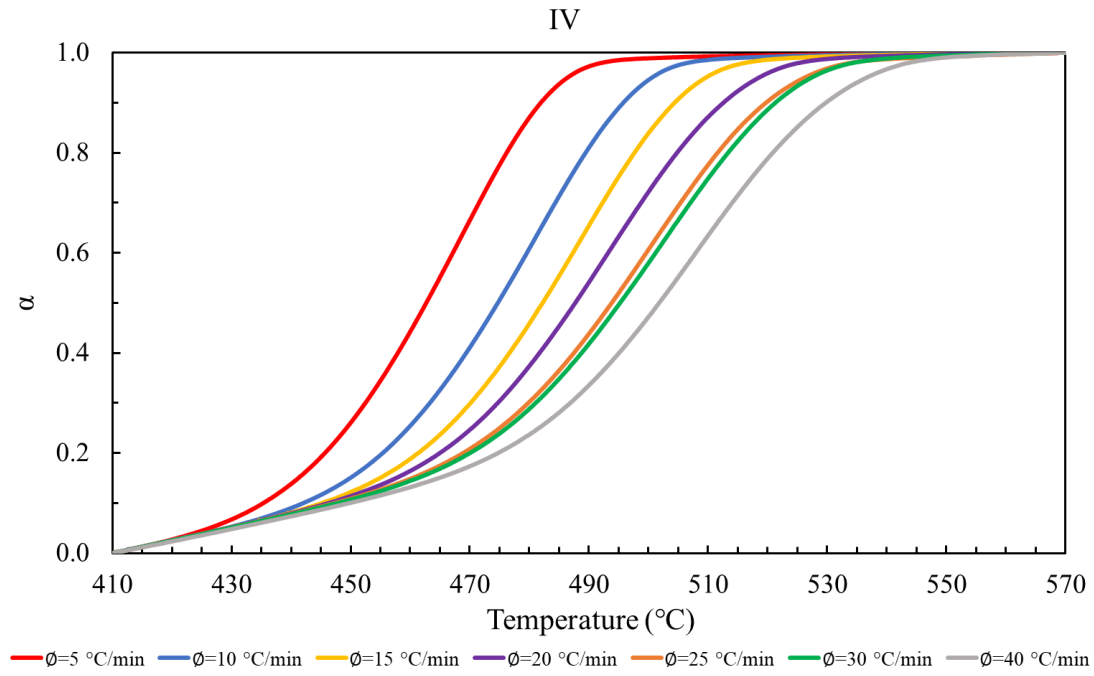


Figure E4 Conversion of EPDM degradation in Rubber IV, at 20 ml min^{-1} , under N_2 atmosphere with different heating rates.

Appendix E5

PUC-Rio - Certificação Digital Nº 1821742/CA

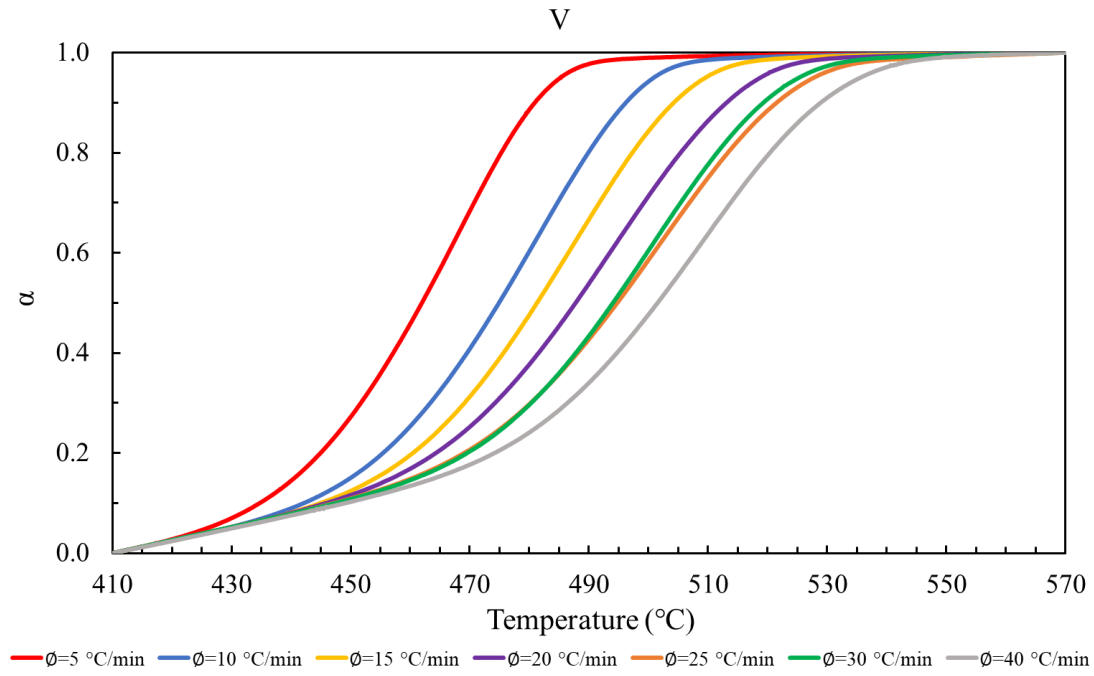


Figure E5 Conversion of EPDM degradation in Rubber V, at 20 ml min^{-1} , under N_2 atmosphere with different heating rates.

Appendix E6

PUC-Rio - Certificação Digital Nº 1821742/CA

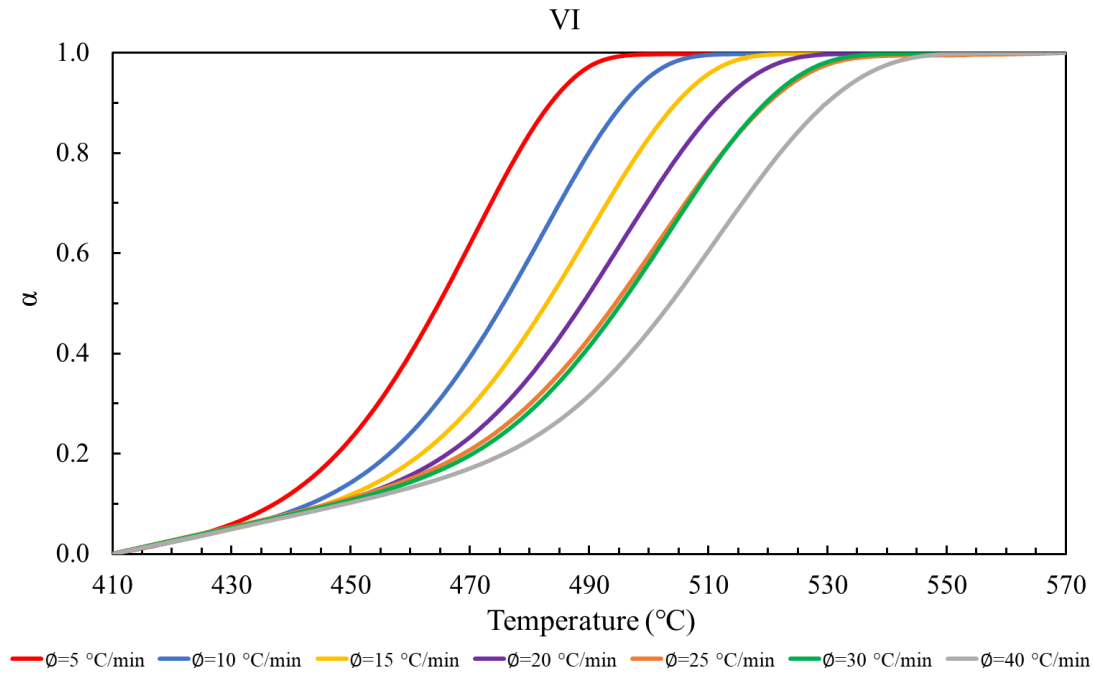


Figure E6 Conversion of EPDM degradation in Rubber VI, at 20 ml min^{-1} , under N_2 atmosphere with different heating rates.

Appendix F Supplementary material to support Chapter 5.3.1

Appendix F1

Rubber I				Rubber II			
\emptyset (K/min)	T_m (K)	α_m		\emptyset (K/min)	T_m (K)	α_m	
5	743.86	0.645		5	743.23	0.674	
10	755.58	0.654		10	754.69	0.633	
15	765.70	0.663		15	762.56	0.674	
20	770.05	0.658		20	767.67	0.657	
30	779.19	0.662		30	775.40	0.642	
40	784.92	0.649		40	784.60	0.664	
Slope	-28135	γ_S	721	Slope	-28869	γ_S	1292
Intercept	26	γ_I	1	Intercept	27	γ_I	2
R^2	0.9974			R^2	0.9920		
E (kJ/mol)	234	γ_E	6	E (kJ/mol)	240	γ_E	11
A (min ⁻¹)	6.83E+15	γ_A	72100	A (min ⁻¹)	2.01E+16	γ_A	156578
$k = 6.83 \times 10^{15} \text{ min}^{-1} e^{-\frac{233914 \frac{J}{mol}}{8.314 \frac{J}{mol K} T K}}$				$k = 2.01 \times 10^{15} \text{ min}^{-1} e^{-\frac{240019 \frac{J}{mol}}{8.314 \frac{J}{mol K} T K}}$			

Table F1

Data from Kissinger model plots of Rubber I and II. In N₂ atmosphere at 20 ml min⁻¹ and non-isothermal conditions at heating rates 5, 10, 15, 20, 30 and 40 °C min⁻¹ (assuming n=1).

Appendix F3

Rubber V				Rubber VI			
\emptyset (K/min)	T_m (K)	α_m		\emptyset (K/min)	T_m (K)	α_m	
5	742.20	0.661		5	744.80	0.656	
10	755.05	0.642		10	756.05	0.654	
15	762.80	0.660		15	764.36	0.664	
20	767.15	0.609		20	768.38	0.617	
30	775.93	0.655		30	776.81	0.646	
40	782.13	0.621		40	785.82	0.650	
Slope	-29459	γ_S	475	Slope	-29268	γ_S	1413
Intercept	28	γ_I	1	Intercept	28	γ_I	2
R^2		0.9990		R^2		0.9908	
E (kJ/mol)	245	γ_E	4	E (kJ/mol)	243	γ_E	12
A (min ⁻¹)	4.54E+16	γ_A	54862	A (min ⁻¹)	1.91E+16	γ_A	65195
$k = 4.54 \times 10^{16} \text{ min}^{-1} e^{-\frac{244919 \frac{J}{mol}}{8.314 \frac{J}{mol K} T K}}$				$k = 1.91 \times 10^{16} \text{ min}^{-1} e^{-\frac{243143 \frac{J}{mol}}{8.314 \frac{J}{mol K} T K}}$			

Table F3 Data from Kissinger model plots of Rubber V and VI. In N₂ atmosphere at 20 ml min⁻¹ and non-isothermal conditions at heating rates 5, 10, 15, 20, 30 and 40 °C min⁻¹ (assuming n=1).

Appendix G Supplementary material to support Chapter 5.3.2

Appendix G1

PUC-Rio - Certificação Digital N° 1821742/CA

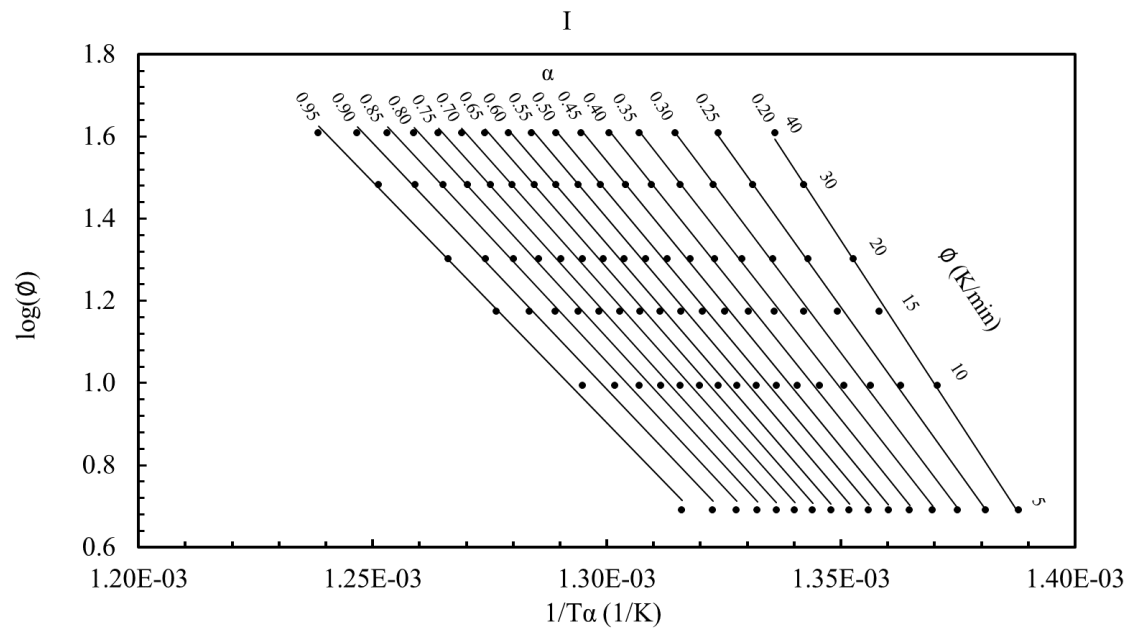


Figure G1 OFW method plot for Rubber I in N_2 atmosphere at 20 ml min^{-1} and non-isothermal conditions at heating rates $5, 10, 15, 20, 30$ and 40 °C min^{-1} Analyzed under isoconversion condition.

Appendix G2

PUC-Rio - Certificação Digital N° 1821742/CA

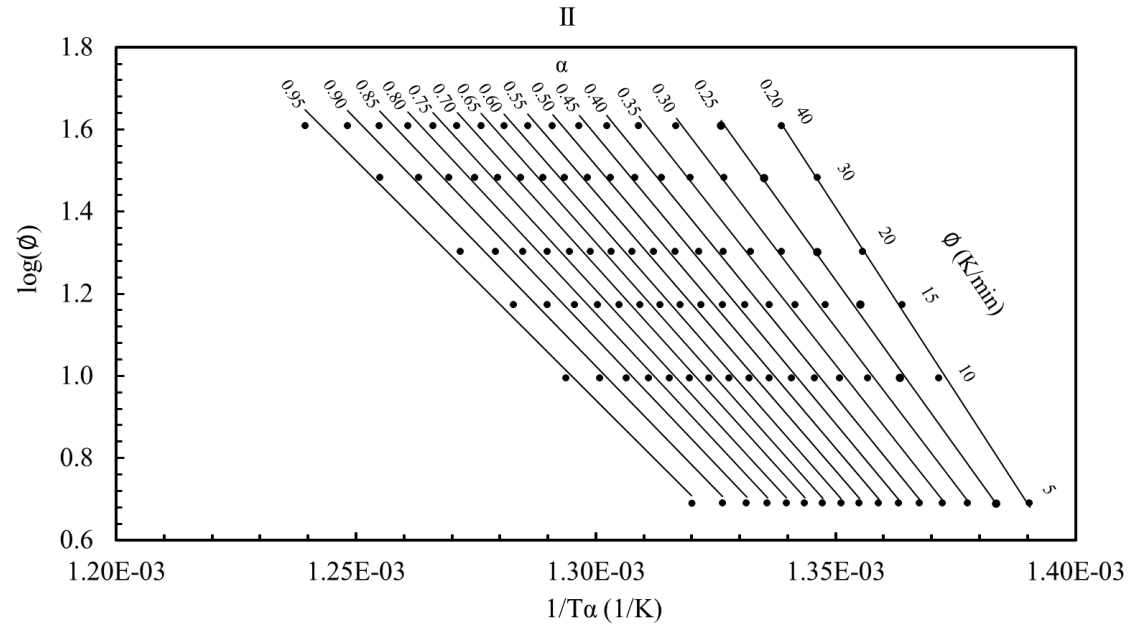


Figure G2 OFW method plot for Rubber II in N_2 atmosphere at 20 ml min^{-1} and non-isothermal conditions at heating rates 5, 10, 15, 20, 30 and $40 \text{ }^\circ\text{C min}^{-1}$. Analyzed under isoconversion condition.

Appendix G3

PUC-Rio - Certificação Digital N° 1821742/CA

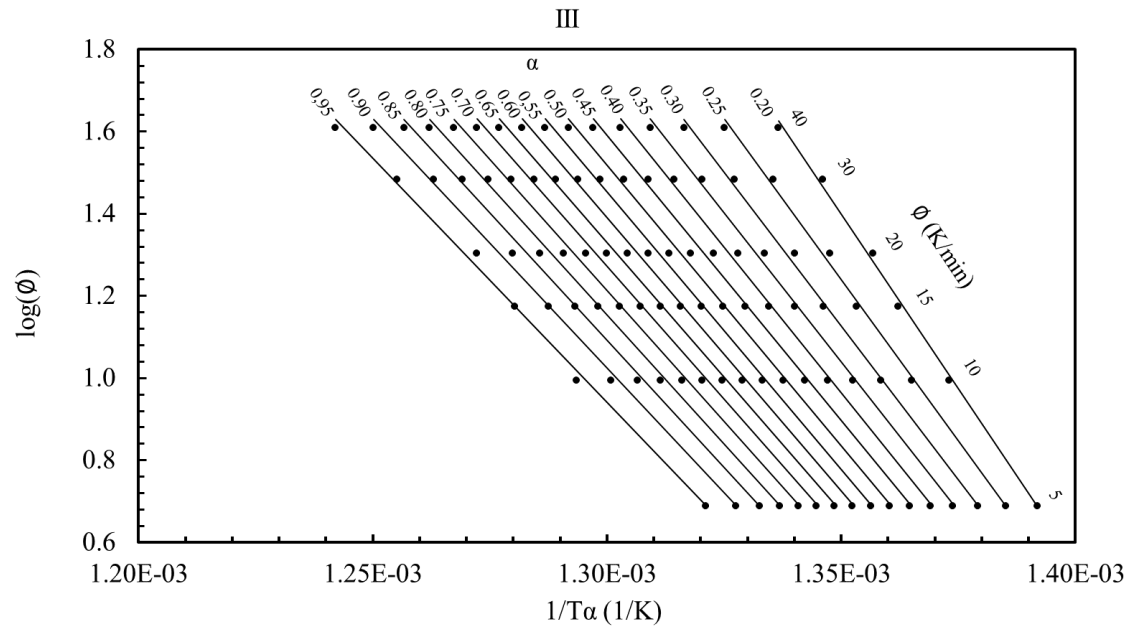


Figure G3 OFW method plot for Rubber III in N_2 atmosphere at 20 ml min^{-1} and non-isothermal conditions at heating rates 5, 10, 15, 20, 30 and $40 \text{ }^\circ\text{C min}^{-1}$ Analyzed under isoconversion condition.

Appendix G4

PUC-Rio - Certificação Digital N° 1821742/CA

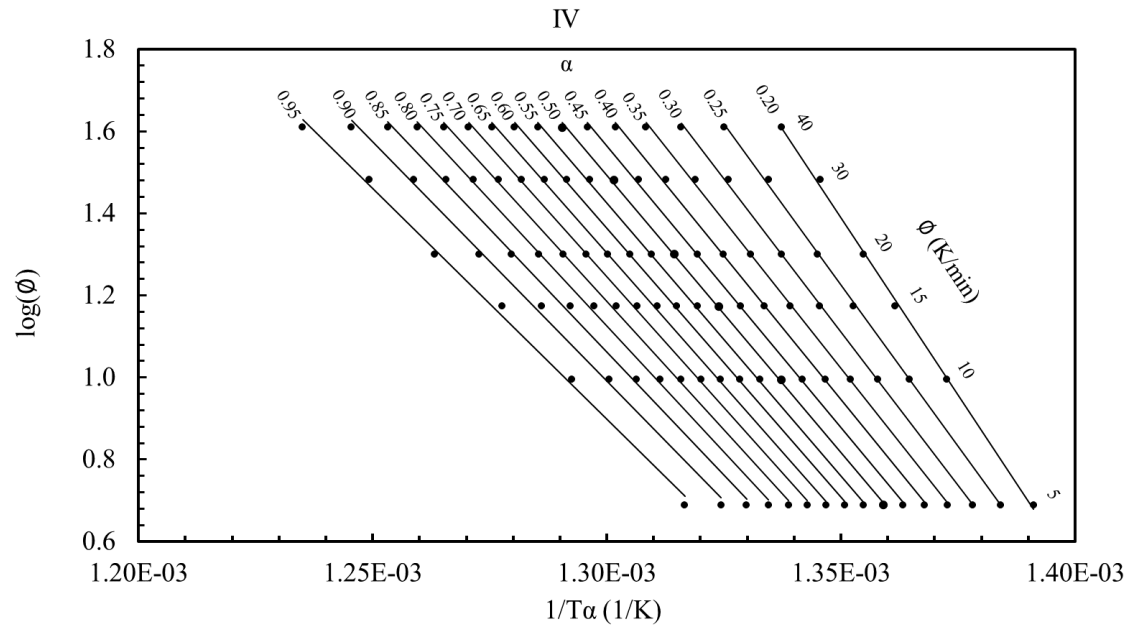


Figure G4 OFW method plot for Rubber IV in N_2 atmosphere at 20 ml min^{-1} and non-isothermal conditions at heating rates 5, 10, 15, 20, 30 and $40 \text{ }^\circ\text{C min}^{-1}$. Analyzed under isoconversion condition.

Appendix G5

PUC-Rio - Certificação Digital N° 1821742/CA

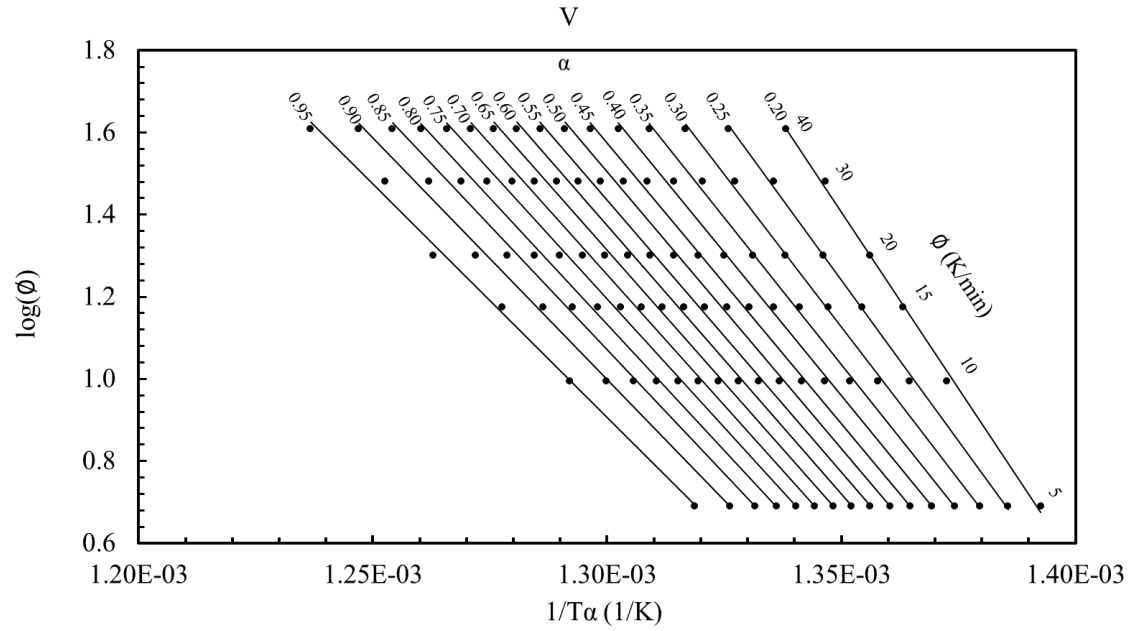


Figure G5 OFW method plot for Rubber V in N_2 atmosphere at 20 ml min^{-1} and non-isothermal conditions at heating rates 5, 10, 15, 20, 30 and 40 °C min^{-1} . Analyzed under isoconversion condition.

Appendix G6

PUC-Rio - Certificação Digital N° 1821742/CA

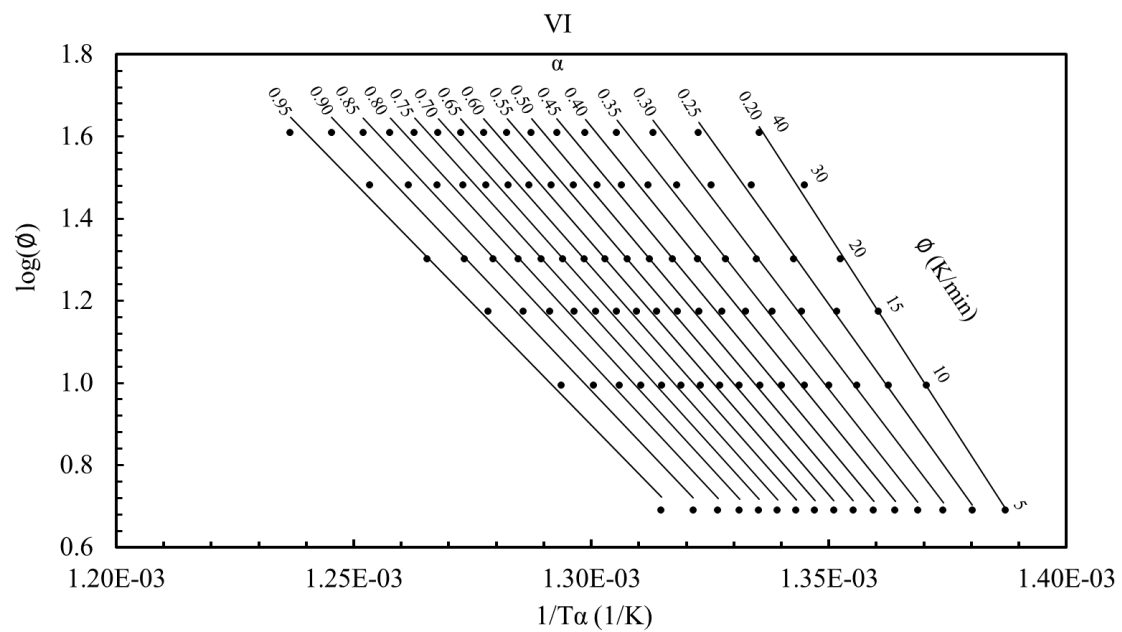


Figure G6 OFW method plot for Rubber VI in N_2 atmosphere at 20 ml min^{-1} and non-isothermal conditions at heating rates 5, 10, 15, 20, 30 and 40 °C min^{-1} . Analyzed under isoconversion condition.

Appendix G7

α	Slope	γ_s	Intercept	γ_I	R^2	E (kJ/mol)	γ_E	$\ln(A / \text{min}^{-1})$
0.20	-17480	401	24.9	0.5	0.9979	322	7	53
0.25	-15942	293	22.7	0.4	0.9986	293	5	48
0.30	-15122	282	21.5	0.4	0.9986	277	5	45
0.35	-14567	282	20.7	0.4	0.9985	266	5	43
0.40	-14203	280	20.1	0.4	0.9984	259	5	41
0.45	-13890	290	19.6	0.4	0.9983	253	5	40
0.50	-13635	295	19.2	0.4	0.9981	248	5	39
0.55	-13424	302	18.9	0.4	0.9980	244	5	38
0.60	-13216	309	18.5	0.4	0.9978	240	6	38
0.65	-13022	318	18.2	0.4	0.9976	237	6	37
0.70	-12814	327	17.9	0.4	0.9974	233	6	36
0.75	-12631	328	17.6	0.4	0.9973	230	6	35
0.80	-12428	334	17.3	0.4	0.9971	226	6	35
0.85	-12216	343	16.9	0.4	0.9969	222	6	34
0.90	-11994	342	16.6	0.4	0.9968	218	6	33
0.95	-11720	350	16.1	0.4	0.9964	213	6	32
Average	\bar{E} (kJ/mol)	249	γ_E	28	$\ln(\bar{A} / \text{min}^{-1})$	39	$\gamma_{\ln \bar{A}}$	5

Table G1 OFW method results for Rubber I, under N_2 atmosphere at 20 ml min^{-1} and non-isothermal conditions at heating rates 5, 10, 15, 20, 30 and $40 \text{ }^\circ\text{C min}^{-1}$. Analyzed under isoconversion condition.

Appendix G8

α	Slope	γ_s	Intercept	γ_I	R^2	E (kJ/mol)	γ_E	$\ln(A / \text{min}^{-1})$
0.20	-18011	397	25.7	0.5	0.9981	332	7	55
0.25	-16233	370	23.1	0.5	0.9979	298	7	49
0.30	-15347	394	21.8	0.5	0.9974	281	7	45
0.35	-14754	414	20.9	0.6	0.9969	270	8	43
0.40	-14346	430	20.3	0.6	0.9964	262	8	42
0.45	-14043	434	19.8	0.6	0.9962	256	8	41
0.50	-13773	449	19.4	0.6	0.9958	251	8	40
0.55	-13557	452	19.1	0.6	0.9956	247	8	39
0.60	-13341	454	18.7	0.6	0.9954	243	8	38
0.65	-13159	455	18.4	0.6	0.9953	240	8	37
0.70	-12940	462	18.1	0.6	0.9949	236	8	37
0.75	-12733	463	17.8	0.6	0.9947	232	8	36
0.80	-12520	467	17.4	0.6	0.9945	228	9	35
0.85	-12276	485	17.0	0.6	0.9938	224	9	34
0.90	-12011	499	16.6	0.6	0.9932	219	9	33
0.95	-11664	525	16.1	0.7	0.9920	212	10	32
Average	\bar{E} (kJ/mol)	252	γ_E	30	$\ln(\bar{A} / \text{min}^{-1})$	40	$\gamma_{\ln \bar{A}}$	6

Table G2 OFW method results for Rubber II, under N_2 atmosphere at 20 ml min^{-1} and non-isothermal conditions at heating rates 5, 10, 15, 20, 30 and $40 \text{ }^\circ\text{C min}^{-1}$. Analyzed under isoconversion condition.

Appendix G9

α	Slope	γ_s	Intercept	γ_I	R^2	E (kJ/mol)	γ_E	$\ln(A / \text{min}^{-1})$
0.20	-17002.40	430.40	24.35	0.59	0.9974	313	8	51
0.25	-15673.07	406.23	22.40	0.55	0.9973	288	7	47
0.30	-14961.29	381.70	21.33	0.51	0.9974	274	7	44
0.35	-14512.96	375.84	20.63	0.50	0.9973	265	7	43
0.40	-14179.35	367.79	20.11	0.49	0.9973	259	7	41
0.45	-13889.70	374.16	19.65	0.50	0.9971	253	7	40
0.50	-13676.70	363.29	19.30	0.48	0.9972	249	7	40
0.55	-13490.30	362.54	18.99	0.48	0.9971	245	7	39
0.60	-13294.99	353.52	18.67	0.46	0.9972	242	6	38
0.65	-13114.46	365.79	18.38	0.48	0.9969	239	7	37
0.70	-12943.09	355.31	18.10	0.46	0.9970	236	6	37
0.75	-12759.63	352.38	17.80	0.46	0.9970	232	6	36
0.80	-12579.06	360.82	17.51	0.47	0.9967	229	7	35
0.85	-12384.48	356.89	17.19	0.46	0.9967	225	6	35
0.90	-12149.67	358.08	16.82	0.46	0.9965	221	7	34
0.95	-11899.25	358.60	16.41	0.46	0.9964	217	7	33
Average	\bar{E} (kJ/mol)	249	γ_E	25	$\ln(\bar{A} / \text{min}^{-1})$	39	$\gamma_{\ln \bar{A}}$	5

Table G3 OFW method results for Rubber III, under N₂ atmosphere at 20 ml min⁻¹ and non-isothermal conditions at heating rates 5, 10, 15, 20, 30 and 40 °C min⁻¹. Analyzed under isoconversion condition.

Appendix G10

α	Slope	γ_s	Intercept	γ_I	R^2	E (kJ/mol)	γ_E	$\ln(A / \text{min}^{-1})$
0.20	-17252.13	310.26	24.68	0.42	0.9987	318	6	52
0.25	-15722.54	201.70	22.45	0.27	0.9993	289	4	47
0.30	-14919.91	170.11	21.25	0.23	0.9995	273	3	44
0.35	-14399.09	169.53	20.46	0.23	0.9994	263	3	42
0.40	-14046.10	158.47	19.91	0.21	0.9995	256	3	41
0.45	-13741.99	161.61	19.43	0.21	0.9994	250	3	40
0.50	-13504.48	158.57	19.05	0.21	0.9994	246	3	39
0.55	-13302.27	152.83	18.72	0.20	0.9995	242	3	38
0.60	-13105.38	155.91	18.40	0.20	0.9994	238	3	37
0.65	-12923.65	160.72	18.10	0.21	0.9994	235	3	37
0.70	-12728.92	173.16	17.79	0.23	0.9993	232	3	36
0.75	-12512.25	191.23	17.45	0.25	0.9991	228	3	35
0.80	-12267.40	215.75	17.07	0.28	0.9988	223	4	34
0.85	-11996.69	242.08	16.66	0.31	0.9984	218	4	33
0.90	-11666.00	280.49	16.16	0.36	0.9977	212	5	32
0.95	-11262.25	323.08	15.54	0.41	0.9967	205	6	31
Average	\bar{E} (kJ/mol)	246	γ_E	28	$\ln(\bar{A} / \text{min}^{-1})$	39	$\gamma_{\ln \bar{A}}$	6

Table G4 OFW method results for Rubber IV, under N₂ atmosphere at 20 ml min⁻¹ and non-isothermal conditions at heating rates 5, 10, 15, 20, 30 and 40 °C min⁻¹. Analyzed under isoconversion condition.

Appendix G11

α	Slope	γ_s	Intercept	γ_I	R^2	E (kJ/mol)	γ_E	$\ln(A / \text{min}^{-1})$
0.20	-17189.55	385.25	24.61	0.52	0.9980	317	7	52
0.25	-15654.21	284.52	22.37	0.38	0.9987	287	5	47
0.30	-14847.76	273.79	21.17	0.37	0.9986	272	5	44
0.35	-14329.45	301.43	20.38	0.40	0.9982	262	5	42
0.40	-13972.77	317.00	19.82	0.42	0.9979	255	6	41
0.45	-13684.39	328.03	19.37	0.44	0.9977	249	6	40
0.50	-13471.89	340.83	19.02	0.45	0.9974	245	6	39
0.55	-13257.53	348.49	18.67	0.46	0.9972	241	6	38
0.60	-13080.20	356.46	18.38	0.47	0.9970	238	6	37
0.65	-12894.02	371.55	18.07	0.49	0.9967	235	7	37
0.70	-12709.21	374.01	17.78	0.49	0.9965	231	7	36
0.75	-12519.78	385.14	17.47	0.50	0.9962	228	7	35
0.80	-12290.11	387.00	17.11	0.50	0.9960	224	7	34
0.85	-12044.18	398.87	16.73	0.51	0.9956	219	7	33
0.90	-11749.48	398.60	16.27	0.51	0.9954	214	7	32
0.95	-11352.85	389.96	15.66	0.50	0.9953	207	7	31
Average	\bar{E} (kJ/mol)	245	γ_E	28	$\ln(\bar{A} / \text{min}^{-1})$	39	$\gamma_{\ln \bar{A}}$	5

Table G5 OFW method results for Rubber V, under N_2 atmosphere at 20 ml min^{-1} and non-isothermal conditions at heating rates 5, 10, 15, 20, 30 and $40 \text{ }^\circ\text{C min}^{-1}$. Analyzed under isoconversion condition.

Appendix G12

α	Slope	γ_s	Intercept	γ_I	R^2	E (kJ/mol)	γ_E	$\ln(A / \text{min}^{-1})$
0.20	-17966.89	430.00	25.62	0.58	0.9977	332	8	54
0.25	-16159.00	462.74	23.01	0.62	0.9967	297	8	48
0.30	-15239.48	496.74	21.65	0.67	0.9958	279	9	45
0.35	-14682.50	489.87	20.81	0.65	0.9956	268	9	43
0.40	-14274.15	501.70	20.18	0.67	0.9951	261	9	42
0.45	-13959.63	503.11	19.69	0.67	0.9948	255	9	40
0.50	-13731.43	496.10	19.32	0.65	0.9948	250	9	40
0.55	-13524.97	489.32	18.99	0.64	0.9948	246	9	39
0.60	-13329.36	489.09	18.67	0.64	0.9946	242	9	38
0.65	-13153.76	489.61	18.38	0.64	0.9945	239	9	37
0.70	-12996.45	493.00	18.12	0.64	0.9943	237	9	37
0.75	-12808.96	498.85	17.82	0.65	0.9940	233	9	36
0.80	-12624.96	501.53	17.52	0.65	0.9937	230	9	35
0.85	-12418.16	508.35	17.19	0.65	0.9933	226	9	34
0.90	-12178.54	519.55	16.81	0.67	0.9928	222	9	34
0.95	-11852.02	535.01	16.30	0.68	0.9919	216	10	32
Average	\bar{E} (kJ/mol)	252	γ_E	29	$\ln(\bar{A} / \text{min}^{-1})$	40	$\gamma_{\ln\bar{A}}$	6

Table G6 OFW method results for Rubber VI, under N₂ atmosphere at 20 ml min⁻¹ and non-isothermal conditions at heating rates 5, 10, 15, 20, 30 and 40 °C min⁻¹. Analyzed under isoconversion condition.

Appendix G13

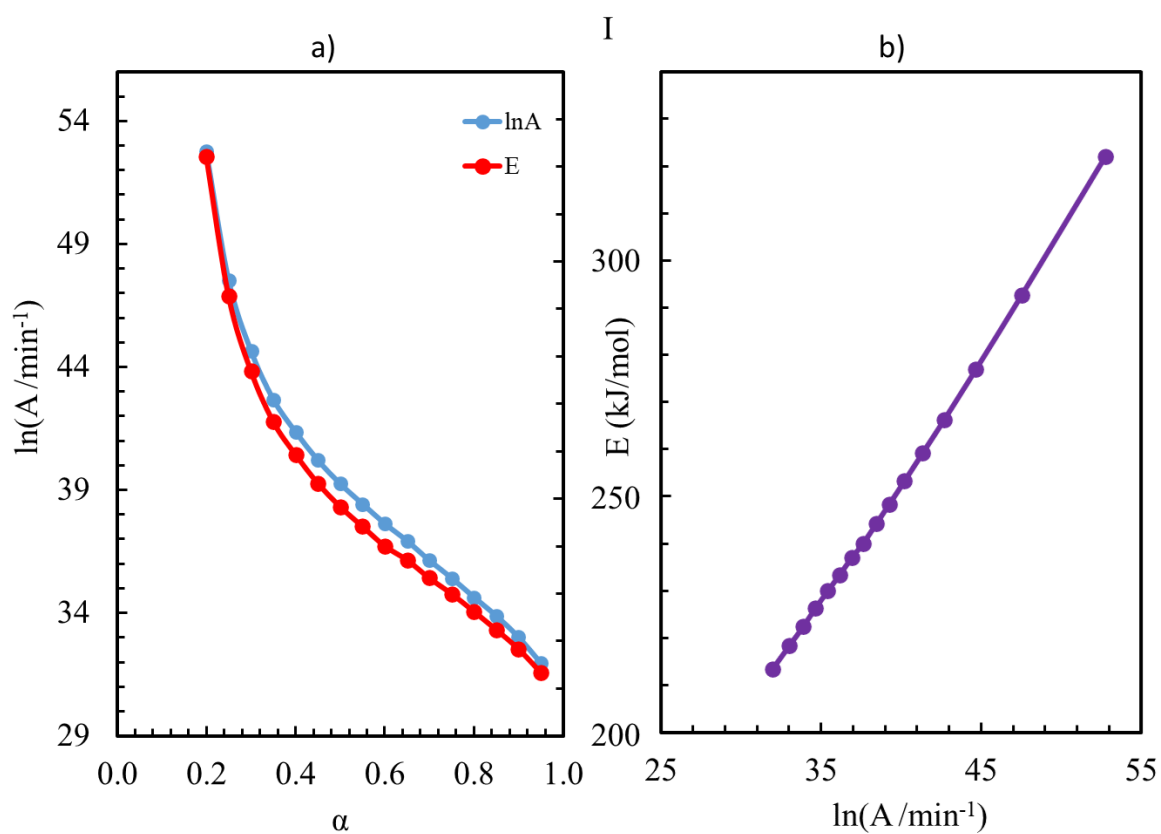


Figure G7 a) Behavior plot of the activation energy and frequency factor at different conversions. b) variation of the activation energy with the frequency factor for Rubber I. Obtained with the OFW method in non-isothermal conditions at heating speeds of 5, 10, 15, 20, 30 and 40 $^{\circ}\text{C min}^{-1}$. Analyzed under isoconversion condition.

Appendix G14

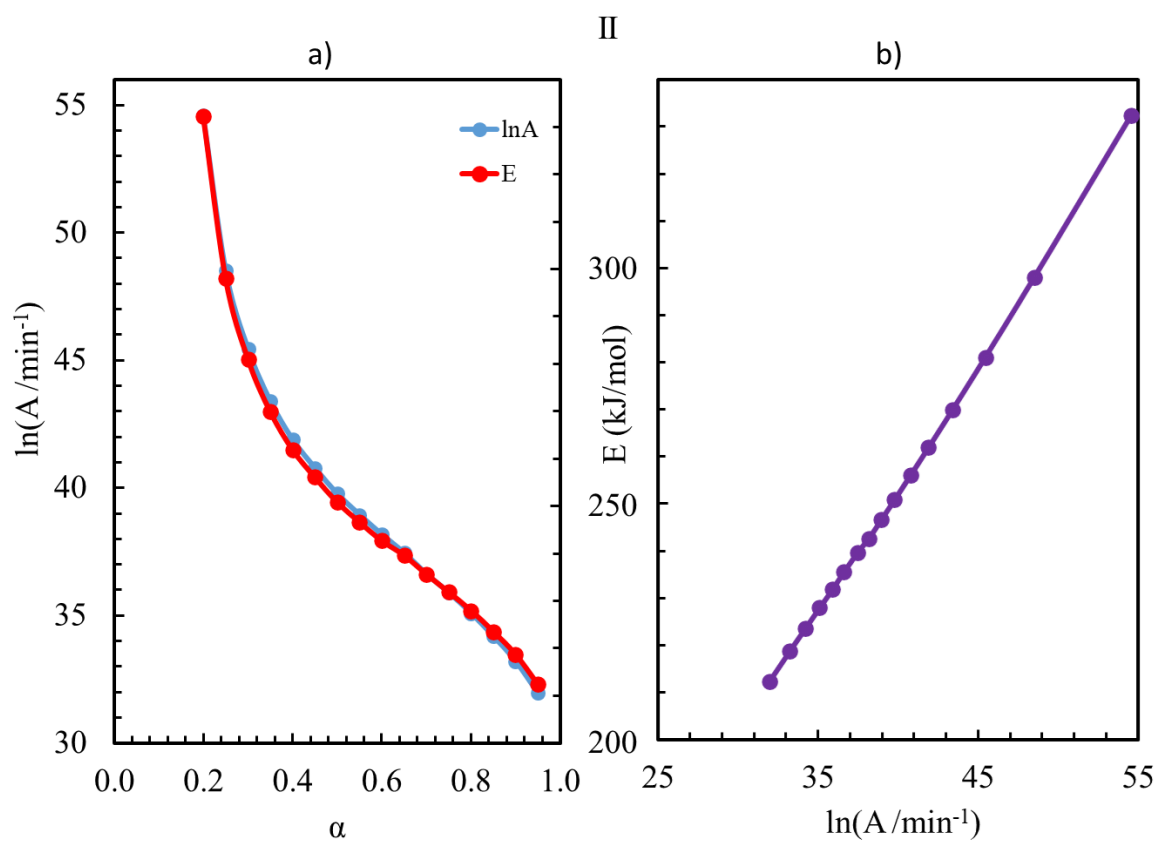


Figure G8 a) Behavior plot of the activation energy and frequency factor at different conversions. b) variation of the activation energy with the frequency factor for Rubber II. Obtained with the OFW method in non-isothermal conditions at heating speeds of 5, 10, 15, 20, 30 and 40 °C min⁻¹. Analyzed under isoconversion condition.

Appendix G15

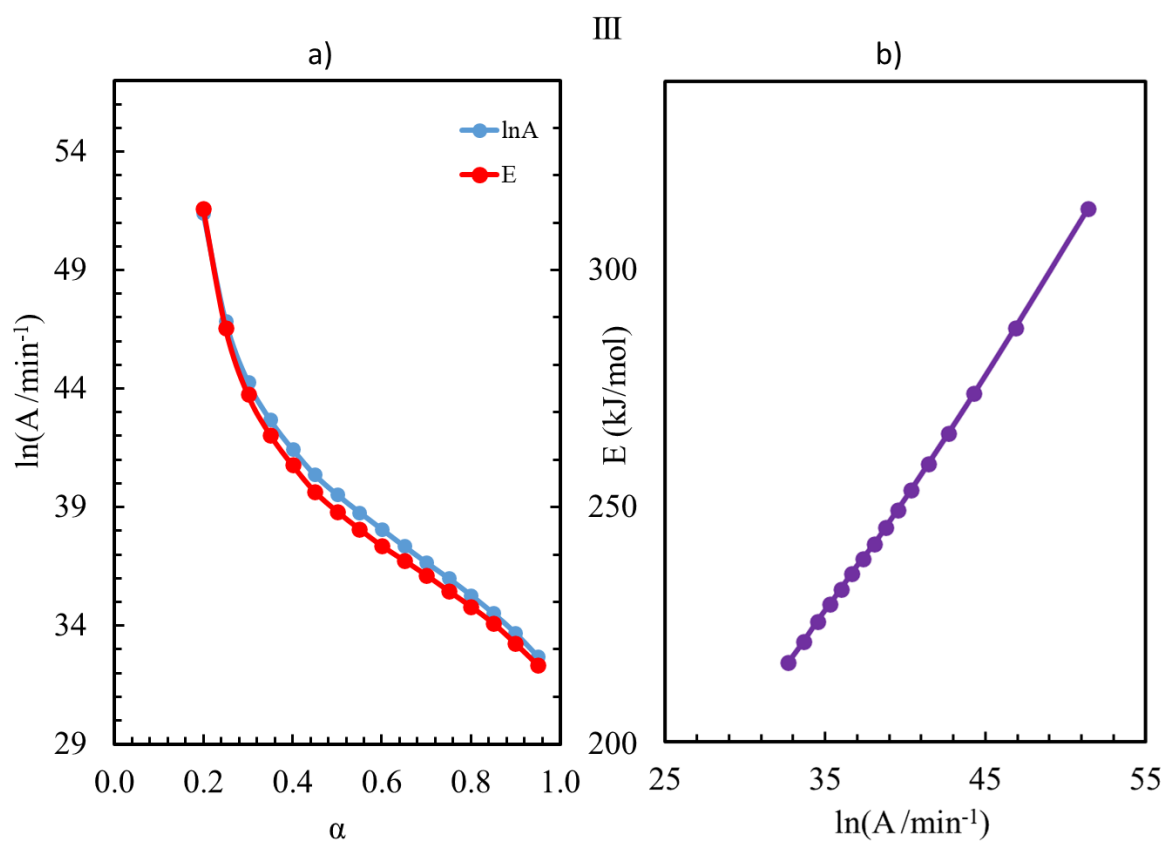


Figure G9 a) Behavior plot of the activation energy and frequency factor at different conversions. b) variation of the activation energy with the frequency factor for Rubber III. Obtained with the OFW method in non-isothermal conditions at heating speeds of 5, 10, 15, 20, 30 and 40 °C min⁻¹. Analyzed under isoconversion condition.

Appendix G16

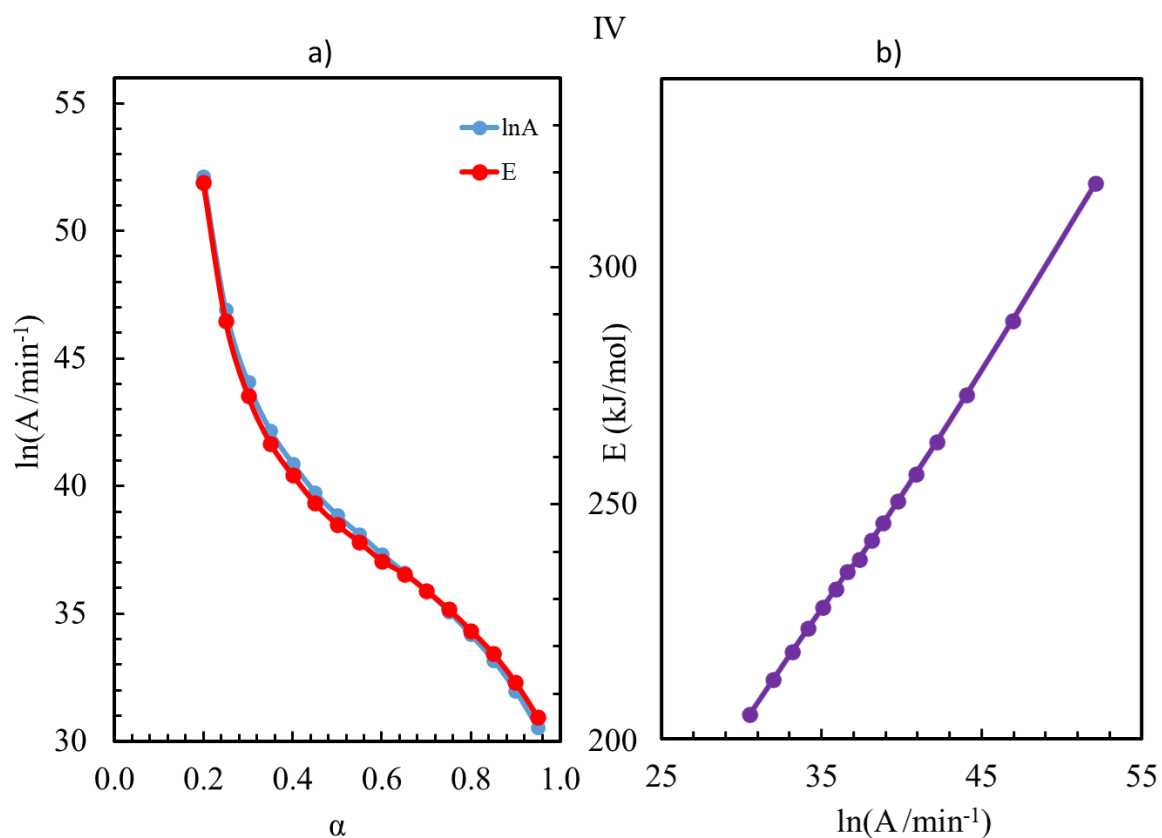


Figure G10 a) Behavior plot of the activation energy and frequency factor at different conversions. b) variation of the activation energy with the frequency factor for Rubber IV. Obtained with the OFW method in non-isothermal conditions at heating speeds of 5, 10, 15, 20, 30 and 40 °C min⁻¹. Analyzed under isoconversion condition.

Appendix G17

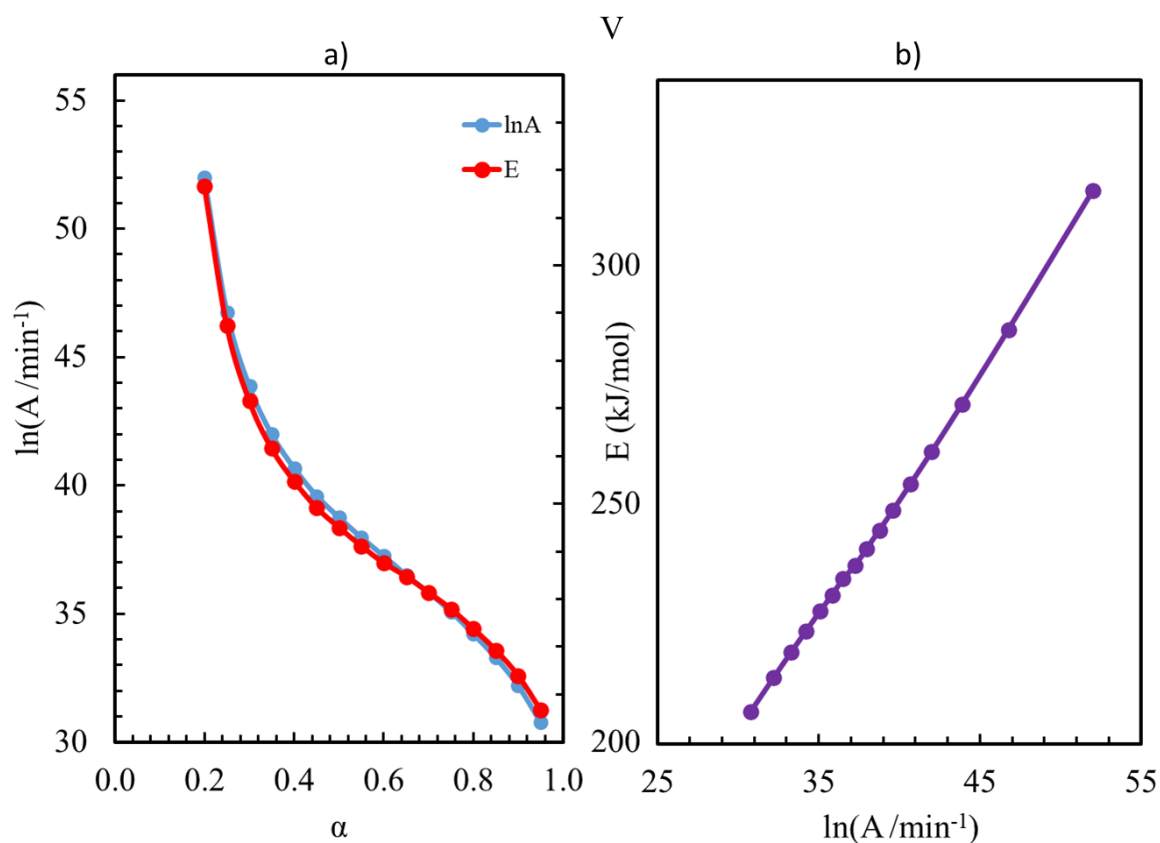


Figure G11 a) Behavior plot of the activation energy and frequency factor at different conversions. b) variation of the activation energy with the frequency factor for Rubber V. Obtained with the OFW method in non-isothermal conditions at heating speeds of 5, 10, 15, 20, 30 and 40 °C min⁻¹. Analyzed under isoconversion condition.

Appendix G18

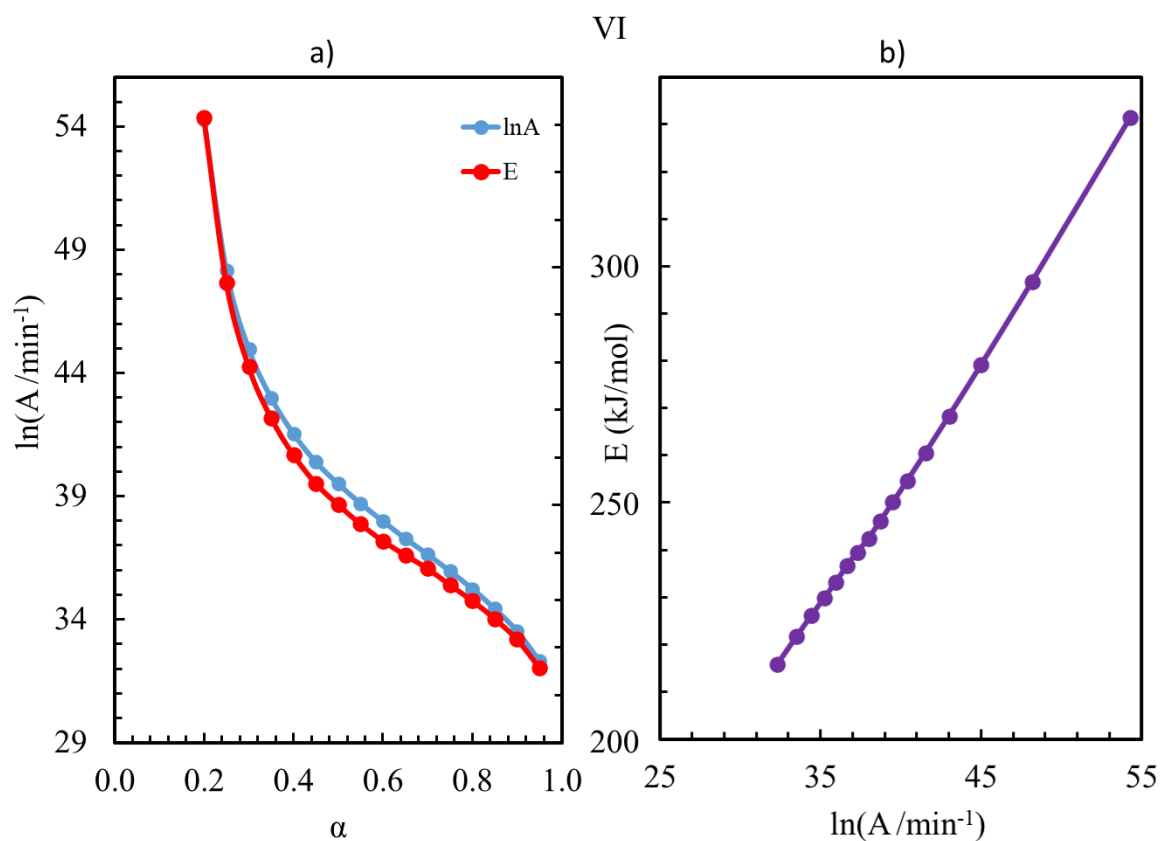


Figure G12 a) Behavior plot of the activation energy and frequency factor at different conversions. b) variation of the activation energy with the frequency factor for Rubber VI. Obtained with the OFW method in non-isothermal conditions at heating speeds of 5, 10, 15, 20, 30 and 40 °C min⁻¹. Analyzed under isoconversion condition.

Appendix H Supplementary material to support Chapter 5.3.3

Appendix H1

PUC-Rio - Certificação Digital N° 1821742/CA

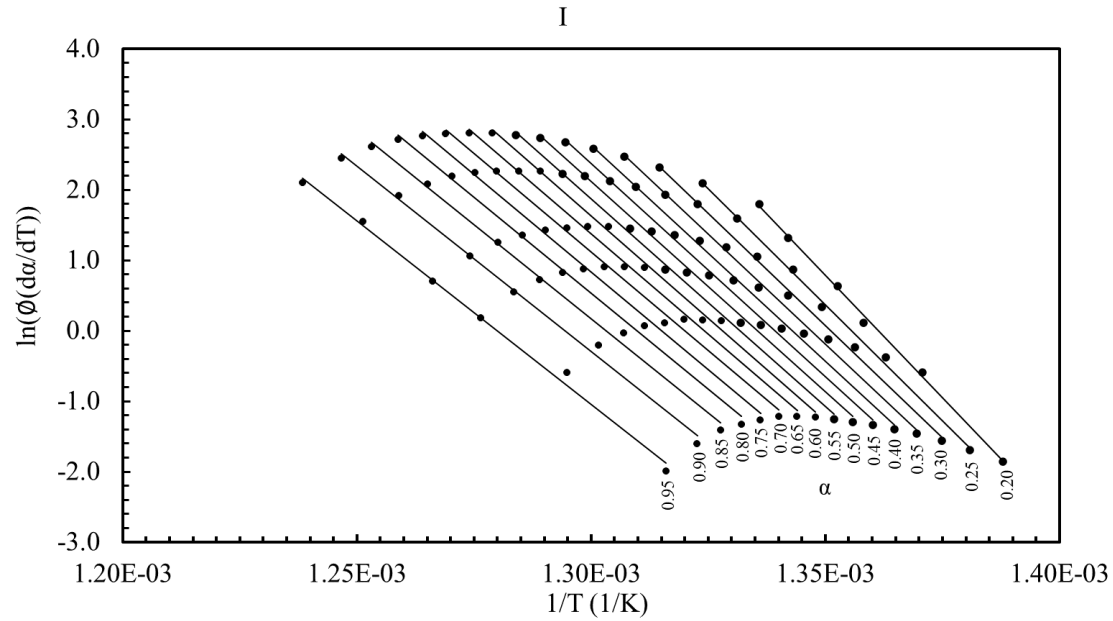


Figure H1 Friedman's method plot for Rubber I, under N_2 atmosphere at 20 ml min^{-1} and non-isothermal conditions at heating rates 5, 10, 15, 20, 30 and $40 \text{ }^\circ\text{C min}^{-1}$. Analyzed under isoconversion condition.

Appendix H2

PUC-Rio - Certificação Digital Nº 1821742/CA

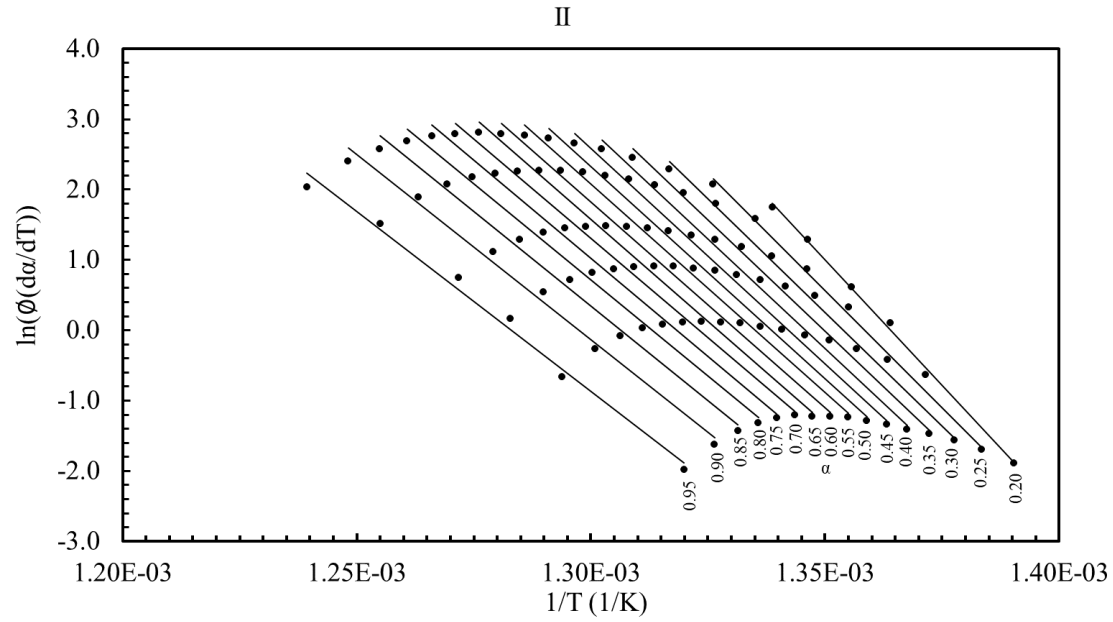


Figure H2 Friedman's method plot for Rubber II, under N_2 atmosphere at 20 ml min^{-1} and non-isothermal conditions at heating rates 5, 10, 15, 20, 30 and $40 \text{ }^\circ\text{C min}^{-1}$. Analyzed under isoconversion condition.

Appendix H3

PUC-Rio - Certificação Digital N° 1821742/CA

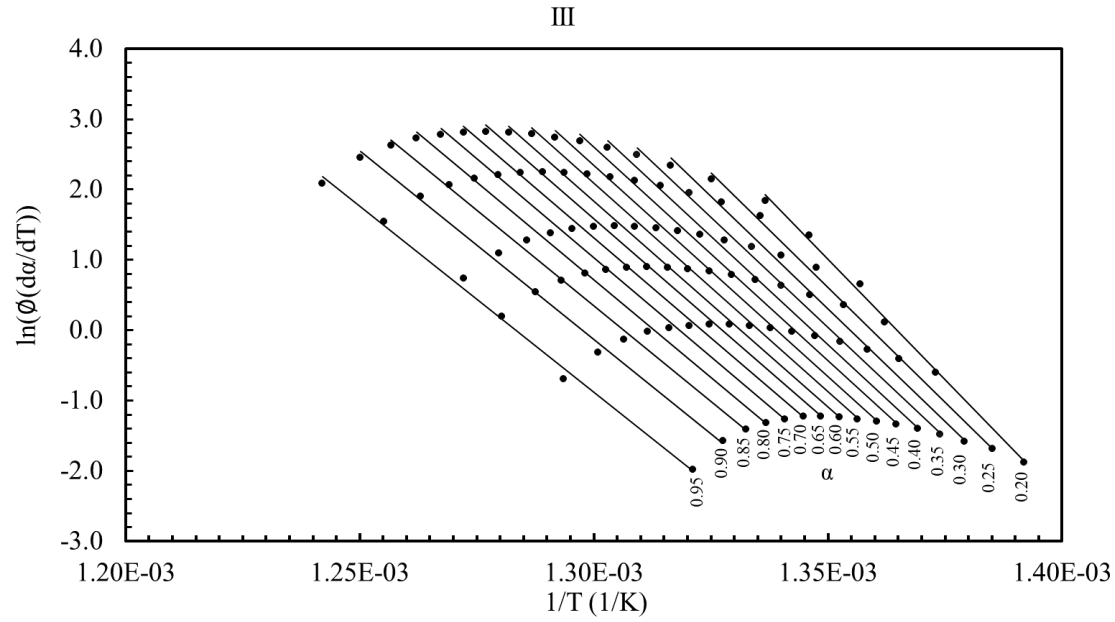


Figure H3 Friedman's method plot for Rubber III, under N_2 atmosphere at 20 ml min^{-1} and non-isothermal conditions at heating rates 5, 10, 15, 20, 30 and $40 \text{ }^\circ\text{C min}^{-1}$. Analyzed under isoconversion condition.

Appendix H4

PUC-Rio - Certificação Digital Nº 1821742/CA

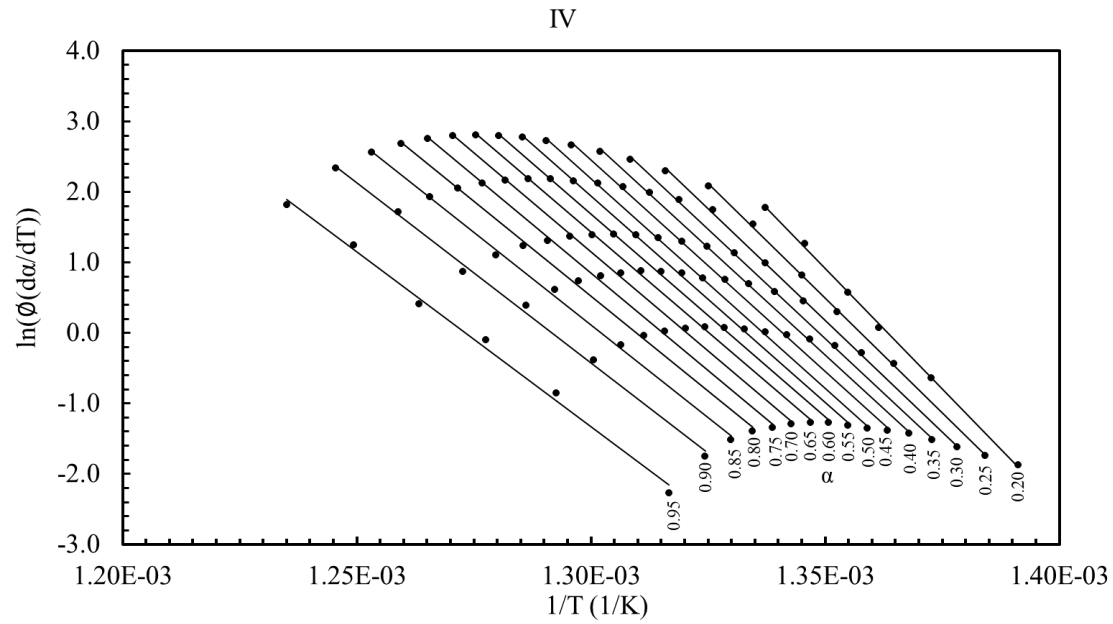


Figure H4 Friedman's method plot for Rubber VI, under N_2 atmosphere at 20 ml min^{-1} and non-isothermal conditions at heating rates 5, 10, 15, 20, 30 and $40 \text{ }^\circ\text{C min}^{-1}$. Analyzed under isoconversion condition.

Appendix H5

PUC-Rio - Certificação Digital N° 1821742/CA

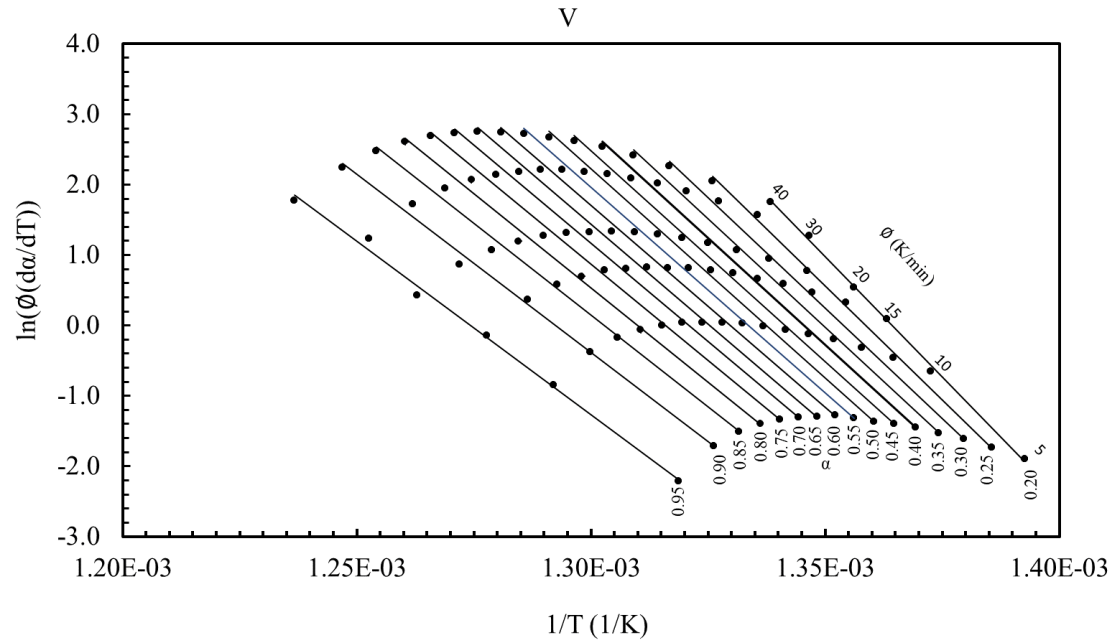


Figure H5 Friedman's method plot for Rubber V, under N_2 atmosphere at 20 ml min^{-1} and non-isothermal conditions at heating rates 5, 10, 15, 20, 30 and $40 \text{ }^\circ\text{C min}^{-1}$. Analyzed under isoconversion condition.

Appendix H6

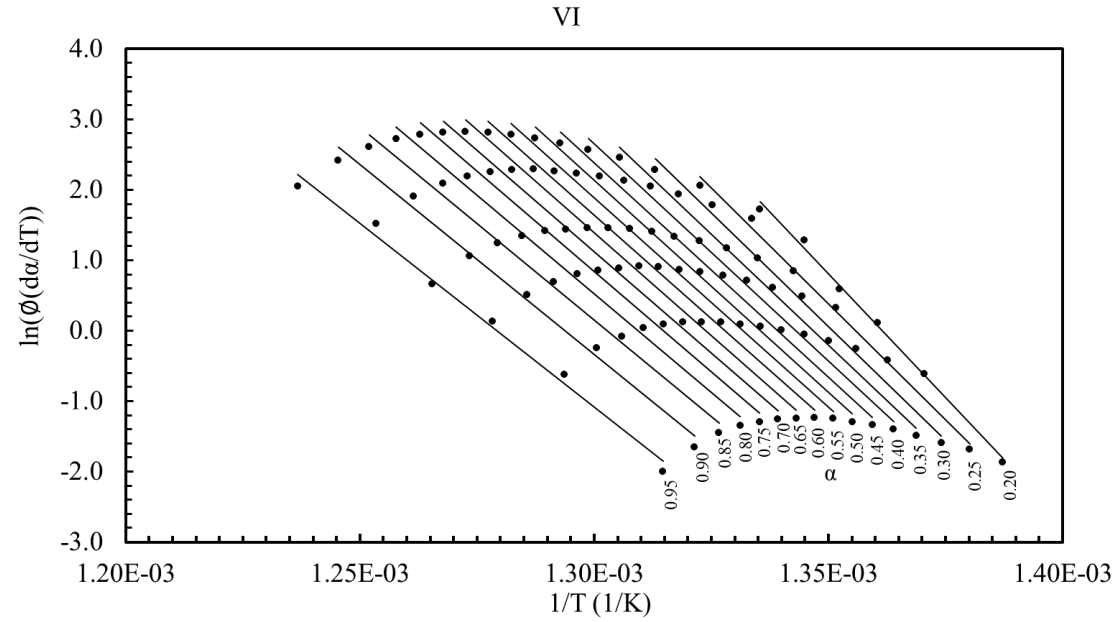


Figure H6 Friedman's method plot for Rubber VI, under N_2 atmosphere at 20 ml min^{-1} and non-isothermal conditions at heating rates 5, 10, 15, 20, 30 and $40 \text{ }^\circ\text{C min}^{-1}$. Analyzed under isoconversion condition.

Appendix H7

PUC-Rio - Certificação Digital N° 1821742/CA

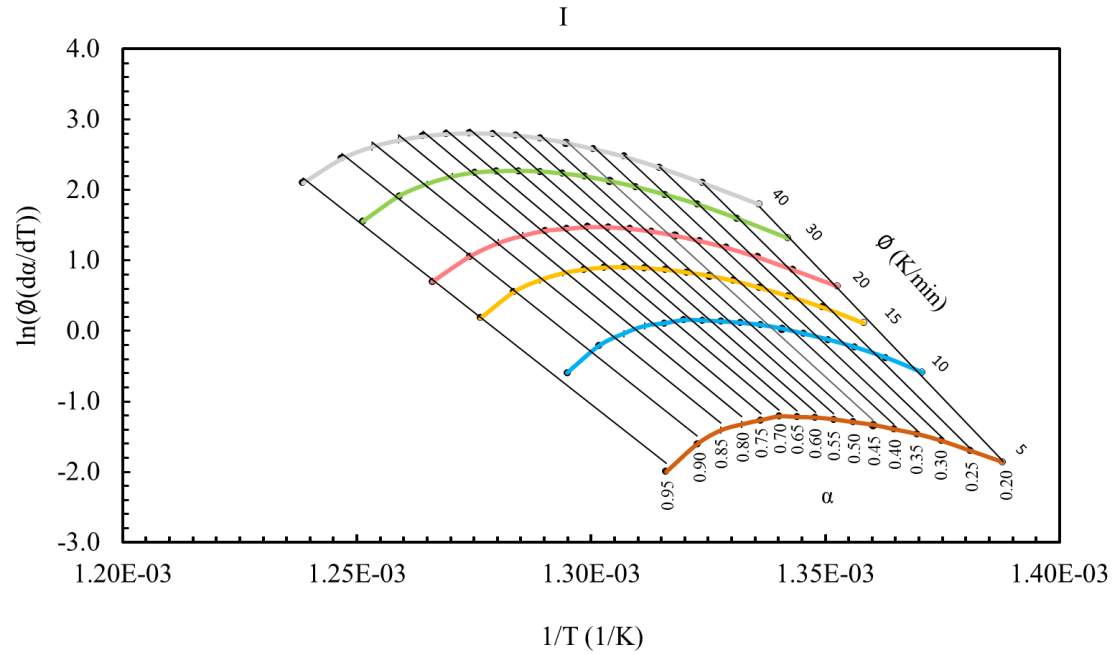


Figure H7 Friedman's method plot for Rubber I, under N_2 atmosphere at 20 ml min^{-1} and non-isothermal conditions at heating rates 5, 10, 15, 20, 30 and $40 \text{ }^\circ\text{C min}^{-1}$. Analyzed under isoconversion condition and superimposing the behavior at each heating speed.

Appendix H8

PUC-Rio - Certificação Digital Nº 1821742/CA

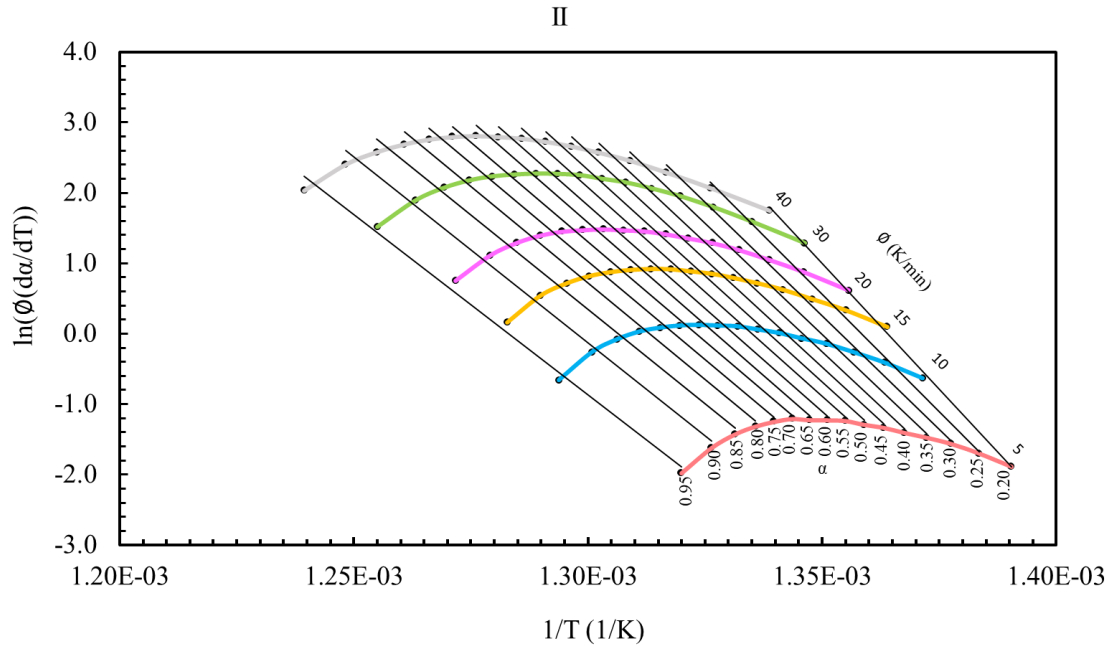


Figure H8 Friedman's method plot for Rubber II, under N_2 atmosphere at 20 ml min^{-1} and non-isothermal conditions at heating rates 5, 10, 15, 20, 30 and $40 \text{ }^\circ\text{C min}^{-1}$. Analyzed under isoconversion condition and superimposing the behavior at each heating speed.

Appendix H9

PUC-Rio - Certificação Digital N° 1821742/CA

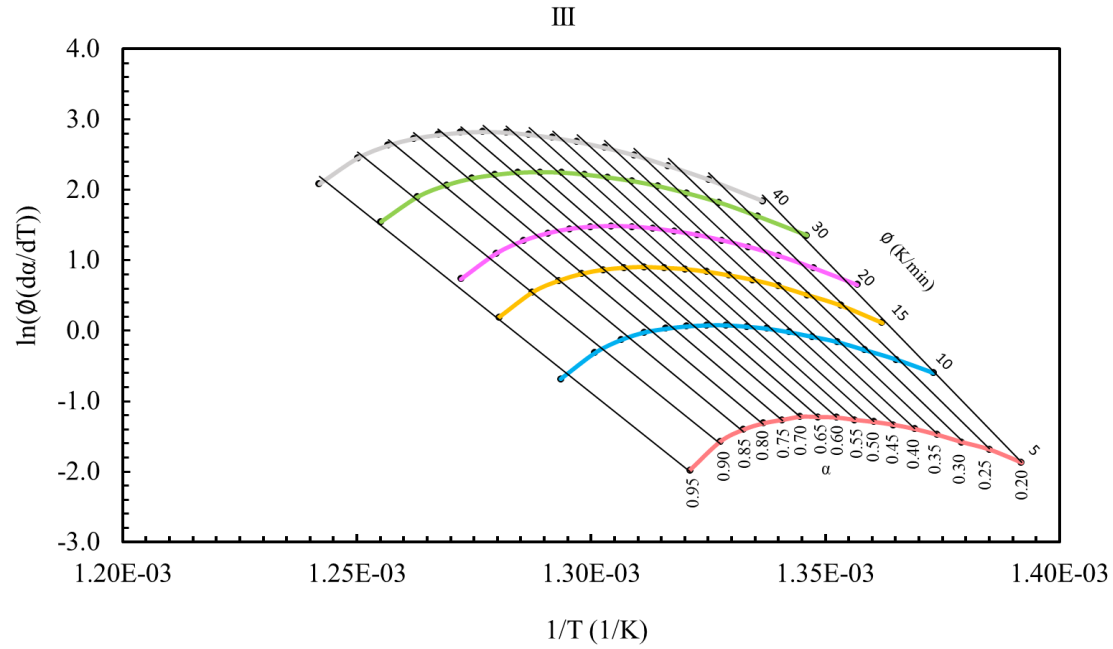


Figure H9 Friedman's method plot for Rubber III, under N_2 atmosphere at 20 ml min^{-1} and non-isothermal conditions at heating rates 5, 10, 15, 20, 30 and 40 °C min^{-1} . Analyzed under isoconversion condition and superimposing the behavior at each heating speed.

Appendix H10

PUC-Rio - Certificação Digital N° 1821742/CA

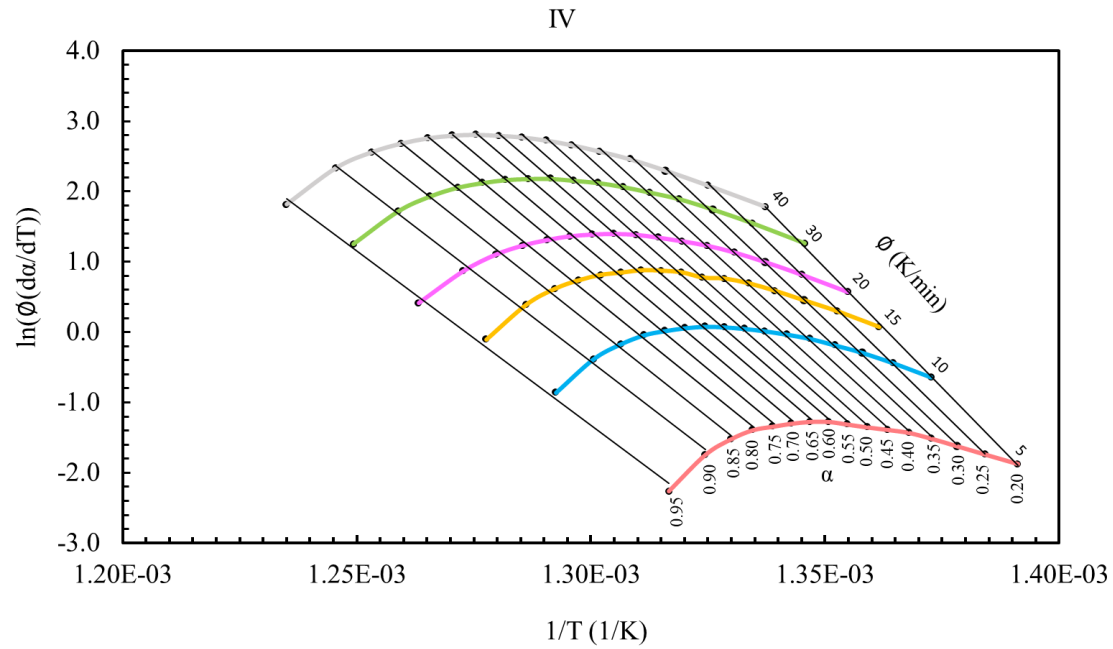


Figure H10 Friedman's method plot for Rubber IV, under N_2 atmosphere at 20 ml min^{-1} and non-isothermal conditions at heating rates $5, 10, 15, 20, 30$ and $40 \text{ }^\circ\text{C min}^{-1}$. Analyzed under isoconversion condition and superimposing the behavior at each heating speed.

Appendix H11

PUC-Rio - Certificação Digital N° 1821742/CA

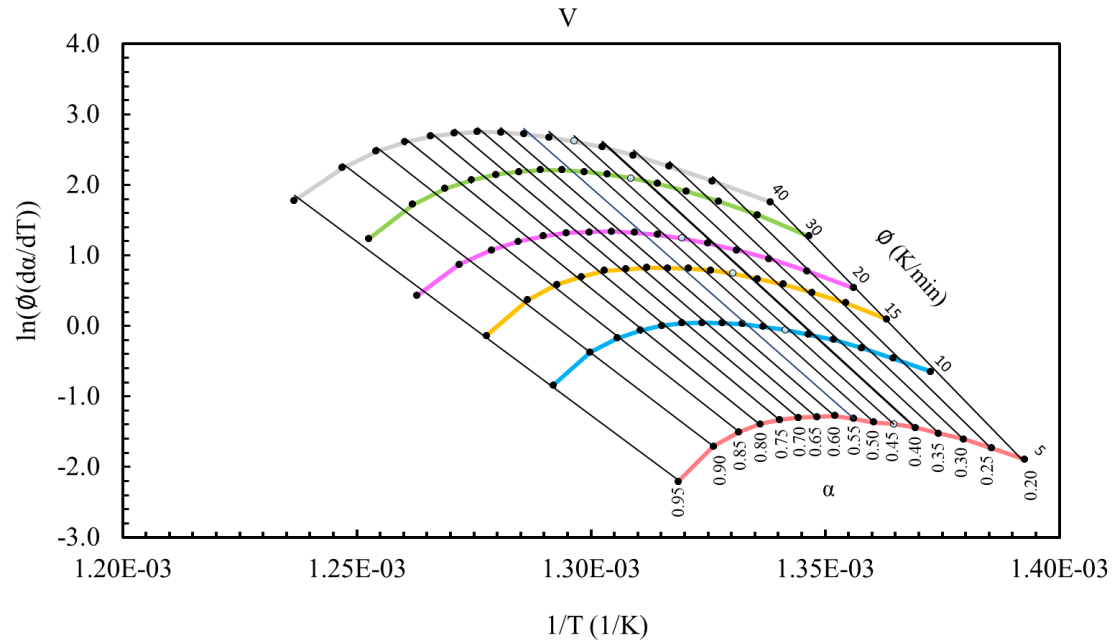


Figure H11 Friedman's method plot for Rubber V, under N_2 atmosphere at 20 ml min^{-1} and non-isothermal conditions at heating rates 5, 10, 15, 20, 30 and $40 \text{ }^\circ\text{C min}^{-1}$. Analyzed under isoconversion condition and superimposing the behavior at each heating speed.

Appendix H12

PUC-Rio - Certificação Digital Nº 1821742/CA

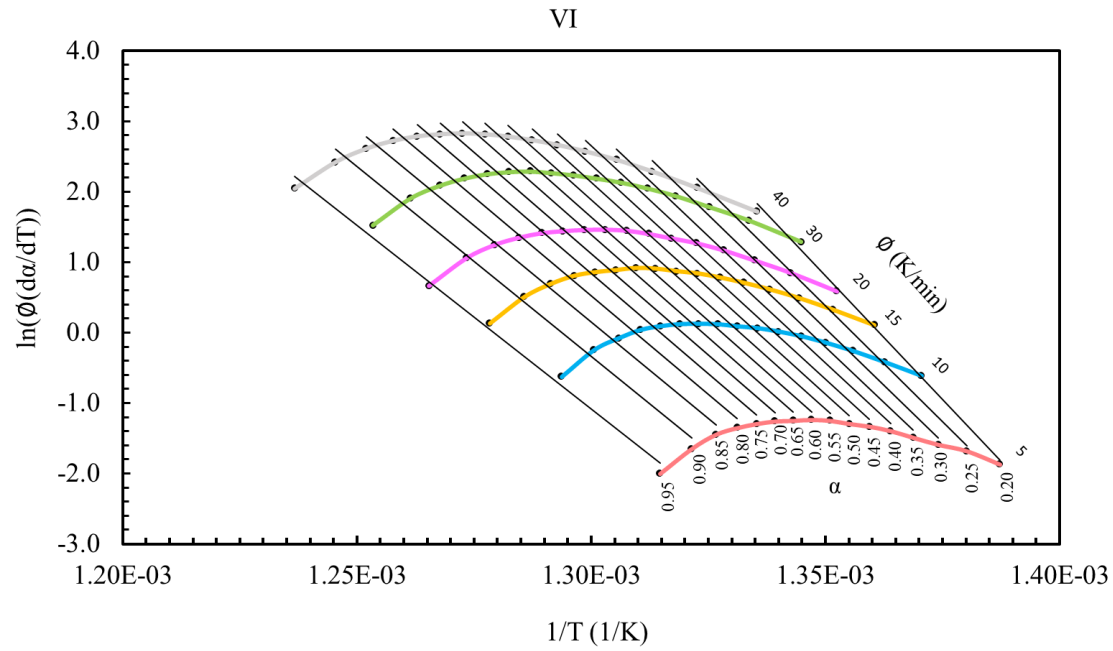


Figure H12 Friedman's method plot for Rubber VI, under N_2 atmosphere at 20 ml min^{-1} and non-isothermal conditions at heating rates 5, 10, 15, 20, 30 and $40 \text{ }^\circ\text{C min}^{-1}$. Analyzed under isoconversion condition and superimposing the behavior at each heating speed.

Appendix H13

\emptyset (K/min)	5	10	15	20	30	40					
α	($d\alpha/dT$)	($d\alpha/dT$)	($d\alpha/dT$)	($d\alpha/dT$)	($d\alpha/dT$)	($d\alpha/dT$)	R^2	E (kJ/mol)	γ_E	$\ln(A / \text{min}^{-1})$	$\gamma_{\ln A}$
0.20	0.0318	0.0560	0.0750	0.0940	0.1227	0.1482	0.9982	578	12	95	2
0.25	0.0374	0.0693	0.0940	0.1188	0.1626	0.2010	0.9981	547	12	89	2
0.30	0.0429	0.0803	0.1100	0.1422	0.1987	0.2497	0.9979	530	12	86	2
0.35	0.0473	0.0895	0.1240	0.1627	0.2279	0.2930	0.9977	518	12	84	2
0.40	0.0505	0.0972	0.1369	0.1791	0.2541	0.3260	0.9977	511	12	82	2
0.45	0.0539	0.1048	0.1466	0.1931	0.2758	0.3567	0.9974	502	13	81	2
0.50	0.0559	0.1104	0.1537	0.2047	0.2948	0.3801	0.9970	497	14	80	2
0.55	0.0581	0.1136	0.1599	0.2128	0.3070	0.3972	0.9971	490	13	78	2
0.60	0.0596	0.1161	0.1636	0.2174	0.3159	0.4052	0.9969	482	13	77	2
0.65	0.0600	0.1177	0.1655	0.2180	0.3182	0.4075	0.9966	474	14	76	2
0.70	0.0606	0.1182	0.1647	0.2128	0.3169	0.4039	0.9965	465	14	74	2
0.75	0.0574	0.1131	0.1598	0.2070	0.3108	0.3908	0.9962	461	14	73	2
0.80	0.0541	0.1089	0.1518	0.1929	0.2940	0.3695	0.9955	453	15	71	2
0.85	0.0498	0.0976	0.1373	0.1734	0.2646	0.3360	0.9958	444	14	70	2
0.90	0.0411	0.0820	0.1160	0.1434	0.2228	0.2843	0.9953	438	15	68	2
0.95	0.0277	0.0558	0.0802	0.1004	0.1556	0.2012	0.9951	433	15	67	2
Average		\bar{E} (kJ/mol)	489	γ_E	40	$\ln(\bar{A} / \text{min}^{-1})$	78	$\gamma_{\ln \bar{A}}$	8		

Table H1 Results of Friedman's method for Rubber I, under N_2 atmosphere at 20 ml min^{-1} and non-isothermal conditions at heating rates 5, 10, 15, 20, 30 and $40 \text{ }^\circ\text{C min}^{-1}$ Analyzed under isoconversion condition.

Appendix H14

\emptyset (K/min)	5	10	15	20	30	40					
α	(d α /dT)	(d α /dT)	(d α /dT)	(d α /dT)	(d α /dT)	(d α /dT)	R ²	E (kJ/mol)	γ_E	ln(A /min ⁻¹)	$\gamma_{\ln A}$
0.20	0.0310	0.0538	0.0740	0.0921	0.1193	0.1416	0.9975	594	15	97	2
0.25	0.0374	0.0670	0.0936	0.1196	0.1613	0.1951	0.9968	555	16	91	3
0.30	0.0429	0.0778	0.1097	0.1423	0.1987	0.2429	0.9963	536	16	87	3
0.35	0.0468	0.0876	0.1251	0.1638	0.2321	0.2872	0.9957	526	17	85	3
0.40	0.0502	0.0945	0.1371	0.1809	0.2590	0.3219	0.9951	518	18	84	3
0.45	0.0539	0.1021	0.1476	0.1932	0.2823	0.3517	0.9952	509	18	82	3
0.50	0.0563	0.1072	0.1567	0.2050	0.2972	0.3762	0.9948	501	18	81	3
0.55	0.0594	0.1120	0.1621	0.2138	0.3132	0.3933	0.9948	493	18	79	3
0.60	0.0600	0.1132	0.1669	0.2168	0.3188	0.4023	0.9944	486	18	78	3
0.65	0.0601	0.1143	0.1675	0.2200	0.3200	0.4079	0.9944	481	18	77	3
0.70	0.0611	0.1133	0.1654	0.2173	0.3159	0.4024	0.9943	470	18	75	3
0.75	0.0587	0.1099	0.1604	0.2126	0.3078	0.3883	0.9936	463	19	73	3
0.80	0.0549	0.1041	0.1516	0.2013	0.2909	0.3626	0.9928	455	19	72	3
0.85	0.0491	0.0935	0.1370	0.1814	0.2618	0.3248	0.9916	446	20	70	3
0.90	0.0405	0.0779	0.1152	0.1517	0.2182	0.2715	0.9905	438	21	68	3
0.95	0.0283	0.0523	0.0789	0.1056	0.1500	0.1879	0.9890	426	22	66	3
Average		\bar{E} (kJ/mol)	494	γ_E	44	ln(\bar{A} /min ⁻¹)	79	$\gamma_{\ln \bar{A}}$	8		

Table H2 Results of Friedman's method for Rubber II, under N₂ atmosphere at 20 ml min⁻¹ and non-isothermal conditions at heating rates 5, 10, 15, 20, 30 and 40 °C min⁻¹ Analyzed under isoconversion condition.

Appendix H15

\emptyset (K/min)	5	10	15	20	30	40					
α	(d α /dT)	(d α /dT)	(d α /dT)	(d α /dT)	(d α /dT)	(d α /dT)	R ²	E (kJ/mol)	γ_E	ln(A /min ⁻¹)	$\gamma_{\ln A}$
0.20	0.0314	0.0554	0.0749	0.0958	0.1274	0.1548	0.9966	571	17	94	3
0.25	0.0378	0.0672	0.0958	0.1215	0.1669	0.2094	0.9969	543	15	89	2
0.30	0.0421	0.0769	0.1110	0.1446	0.2034	0.2555	0.9966	532	15	87	3
0.35	0.0467	0.0864	0.1259	0.1638	0.2316	0.2973	0.9969	521	15	85	2
0.40	0.0507	0.0931	0.1378	0.1794	0.2560	0.3311	0.9970	513	14	83	2
0.45	0.0538	0.0993	0.1467	0.1935	0.2751	0.3600	0.9967	505	14	82	2
0.50	0.0561	0.1045	0.1545	0.2037	0.2895	0.3816	0.9969	499	14	80	2
0.55	0.0577	0.1074	0.1604	0.2121	0.3017	0.3988	0.9967	494	14	79	2
0.60	0.0597	0.1097	0.1631	0.2178	0.3100	0.4108	0.9967	487	14	78	2
0.65	0.0601	0.1094	0.1652	0.2191	0.3121	0.4150	0.9964	481	14	77	2
0.70	0.0603	0.1079	0.1635	0.2172	0.3098	0.4096	0.9963	473	14	75	2
0.75	0.0577	0.1043	0.1589	0.2105	0.3007	0.3969	0.9961	468	15	74	2
0.80	0.0549	0.0990	0.1502	0.1982	0.2857	0.3759	0.9960	461	15	73	2
0.85	0.0502	0.0890	0.1361	0.1788	0.2596	0.3411	0.9958	453	15	71	2
0.90	0.0423	0.0738	0.1156	0.1491	0.2202	0.2853	0.9953	445	15	69	2
0.95	0.0282	0.0508	0.0811	0.1038	0.1547	0.1974	0.9947	440	16	68	2
Average		\bar{E} (kJ/mol)	493	γ_E	36	ln(\bar{A} /min ⁻¹)	79	$\gamma_{\ln \bar{A}}$	7		

Table H3 Results of Friedman's method for Rubber III, under N₂ atmosphere at 20 ml min⁻¹ and non-isothermal conditions at heating rates 5, 10, 15, 20, 30 and 40 °C min⁻¹ Analyzed under isoconversion condition.

Appendix H16

\emptyset (K/min)	5	10	15	20	30	40					
α	(d α /dT)	(d α /dT)	(d α /dT)	(d α /dT)	(d α /dT)	(d α /dT)	R ²	E (kJ/mol)	γ_E	ln(A /min ⁻¹)	$\gamma_{\ln A}$
0.20	0.03	0.05	0.07	0.09	0.12	0.15	0.9993	568	7	93	1
0.25	0.04	0.07	0.09	0.11	0.15	0.20	0.9995	541	6	88	1
0.30	0.04	0.08	0.11	0.14	0.19	0.24	0.9995	526	6	86	1
0.35	0.04	0.08	0.12	0.16	0.22	0.29	0.9995	516	6	84	1
0.40	0.05	0.09	0.13	0.17	0.24	0.32	0.9996	505	5	82	1
0.45	0.05	0.10	0.14	0.18	0.26	0.35	0.9996	500	5	81	1
0.50	0.05	0.10	0.15	0.19	0.28	0.38	0.9996	495	5	80	1
0.55	0.06	0.11	0.16	0.20	0.28	0.39	0.9996	487	5	78	1
0.60	0.06	0.11	0.16	0.20	0.29	0.40	0.9996	479	5	77	1
0.65	0.06	0.11	0.16	0.20	0.29	0.41	0.9993	473	6	75	1
0.70	0.06	0.11	0.16	0.20	0.29	0.40	0.9992	467	6	74	1
0.75	0.05	0.10	0.15	0.19	0.28	0.39	0.9988	459	8	73	1
0.80	0.05	0.10	0.14	0.17	0.26	0.36	0.9985	447	9	70	1
0.85	0.04	0.09	0.12	0.15	0.23	0.32	0.9979	438	10	69	2
0.90	0.04	0.07	0.10	0.12	0.18	0.25	0.9968	426	12	66	2
0.95	0.02	0.04	0.06	0.08	0.12	0.15	0.9951	412	14	63	2
Average		\bar{E} (kJ/mol)	484	γ_E	41	ln(\bar{A} /min ⁻¹)	77	$\gamma_{\ln \bar{A}}$	8		

Table H4 Results of Friedman's method for Rubber IV, under N₂ atmosphere at 20 ml min⁻¹ and non-isothermal conditions at heating rates 5, 10, 15, 20, 30 and 40 °C min⁻¹ Analyzed under isoconversion condition.

Appendix H17

\emptyset (K/min)	5	10	15	20	30	40					
α	(d α /dT)	(d α /dT)	(d α /dT)	(d α /dT)	(d α /dT)	(d α /dT)	R ²	E (kJ/mol)	γ_E	ln(A /min ⁻¹)	$\gamma_{\ln A}$
0.20	0.03	0.05	0.07	0.09	0.12	0.14	0.9985	568	11	93	2
0.25	0.04	0.06	0.09	0.11	0.16	0.19	0.9977	538	13	88	2
0.30	0.04	0.07	0.11	0.13	0.19	0.24	0.9977	521	13	85	2
0.35	0.04	0.08	0.12	0.15	0.22	0.28	0.9973	512	13	83	2
0.40	0.05	0.09	0.13	0.16	0.25	0.31	0.9968	505	14	82	2
0.45	0.05	0.10	0.14	0.17	0.27	0.34	0.9965	497	15	80	2
0.50	0.05	0.10	0.15	0.18	0.28	0.36	0.9962	494	15	79	2
0.55	0.05	0.10	0.15	0.19	0.29	0.37	0.9960	485	15	78	2
0.60	0.06	0.11	0.15	0.19	0.30	0.38	0.9956	478	16	76	2
0.65	0.06	0.11	0.15	0.19	0.30	0.39	0.9950	472	17	75	3
0.70	0.06	0.11	0.15	0.19	0.29	0.38	0.9952	464	16	74	3
0.75	0.05	0.10	0.15	0.18	0.28	0.36	0.9944	456	17	72	3
0.80	0.05	0.10	0.13	0.17	0.26	0.34	0.9942	445	17	70	3
0.85	0.05	0.09	0.12	0.15	0.23	0.29	0.9933	434	18	68	3
0.90	0.04	0.07	0.10	0.12	0.19	0.23	0.9933	420	17	65	3
0.95	0.02	0.04	0.06	0.08	0.11	0.15	0.9948	409	15	63	2
Average		\bar{E} (kJ/mol)	481	γ_E	42	ln(\bar{A} /min ⁻¹)	77	$\gamma_{\ln \bar{A}}$	8		

Table H5 Results of Friedman's method for Rubber V, under N₂ atmosphere at 20 ml min⁻¹ and non-isothermal conditions at heating rates 5, 10, 15, 20, 30 and 40 °C min⁻¹ Analyzed under isoconversion condition.

Appendix H18

\emptyset (K/min)	5	10	15	20	30	40					
α	(d α /dT)	(d α /dT)	(d α /dT)	(d α /dT)	(d α /dT)	(d α /dT)	R ²	E (kJ/mol)	γ_E	ln(A /min ⁻¹)	$\gamma_{\ln A}$
0.20	0.03	0.06	0.07	0.09	0.12	0.14	0.9958	585	19	96	3
0.25	0.04	0.07	0.09	0.12	0.16	0.19	0.9949	549	20	89	3
0.30	0.04	0.08	0.11	0.14	0.20	0.24	0.9941	535	21	87	3
0.35	0.05	0.09	0.12	0.16	0.23	0.29	0.9940	524	20	85	3
0.40	0.05	0.10	0.14	0.18	0.26	0.32	0.9940	513	20	83	3
0.45	0.05	0.10	0.15	0.19	0.28	0.35	0.9940	505	20	81	3
0.50	0.06	0.11	0.16	0.20	0.29	0.38	0.9941	500	19	80	3
0.55	0.06	0.11	0.16	0.21	0.31	0.40	0.9946	494	18	79	3
0.60	0.06	0.11	0.17	0.22	0.32	0.41	0.9941	489	19	78	3
0.65	0.06	0.11	0.17	0.21	0.33	0.42	0.9933	485	20	77	3
0.70	0.06	0.11	0.16	0.21	0.32	0.41	0.9931	479	20	76	3
0.75	0.06	0.11	0.16	0.21	0.31	0.40	0.9926	473	20	75	3
0.80	0.05	0.11	0.15	0.19	0.29	0.37	0.9920	465	21	73	3
0.85	0.05	0.09	0.13	0.17	0.27	0.34	0.9920	456	21	71	3
0.90	0.04	0.08	0.11	0.14	0.22	0.28	0.9900	448	23	70	3
0.95	0.03	0.05	0.08	0.10	0.15	0.19	0.9897	434	22	67	3
Average		\bar{E} (kJ/mol)	496	γ_E	38	ln(\bar{A} /min ⁻¹)	79	$\gamma_{\ln \bar{A}}$	7		

Table H6 Results of Friedman's method for Rubber VI, under N₂ atmosphere at 20 ml min⁻¹ and non-isothermal conditions at heating rates 5, 10, 15, 20, 30 and 40 °C min⁻¹ Analyzed under isoconversion condition.

Appendix H19

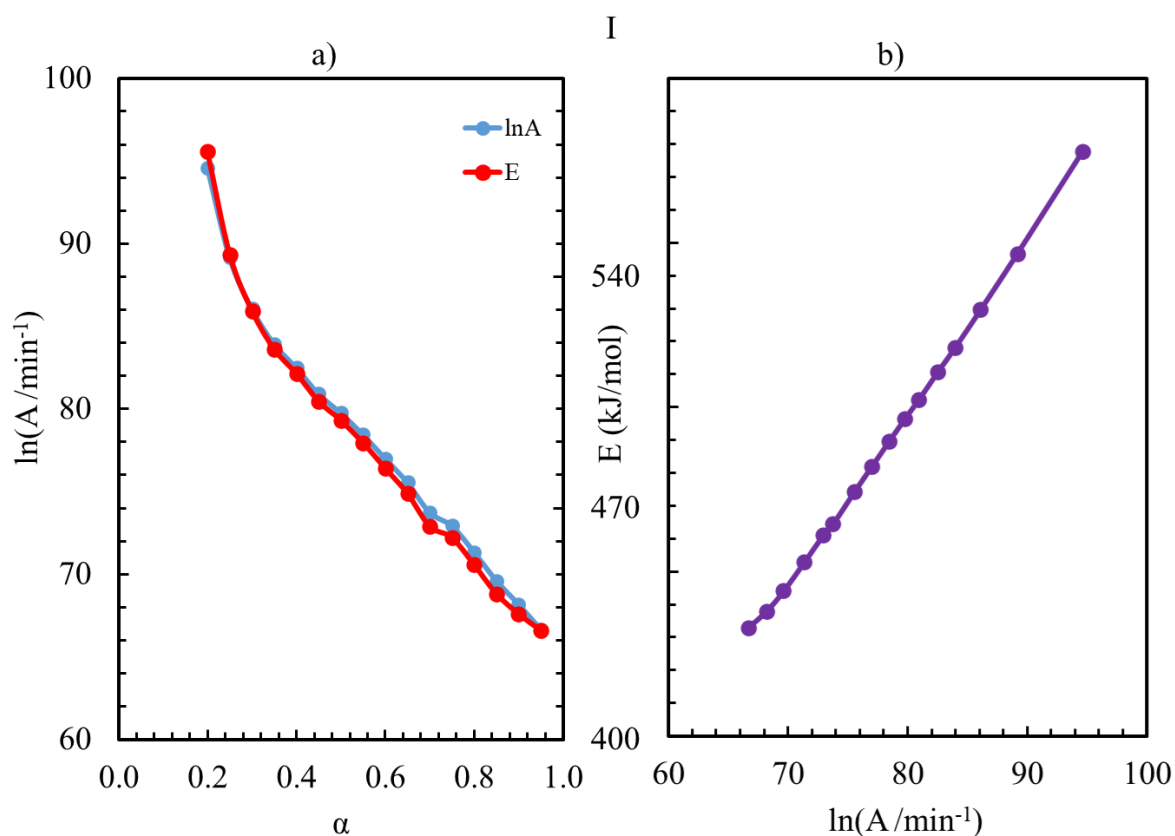


Figure H13 a) Behavior plot of the activation energy and frequency factor at different conversions. b) variation plot of the activation energy with the frequency factor for Rubber I. Obtained with Friedman's method in non-isothermal conditions at heating rates 5, 10, 15, 20, 30 and 40 °C min⁻¹. Analyzed under isoconversion condition.

Appendix H20

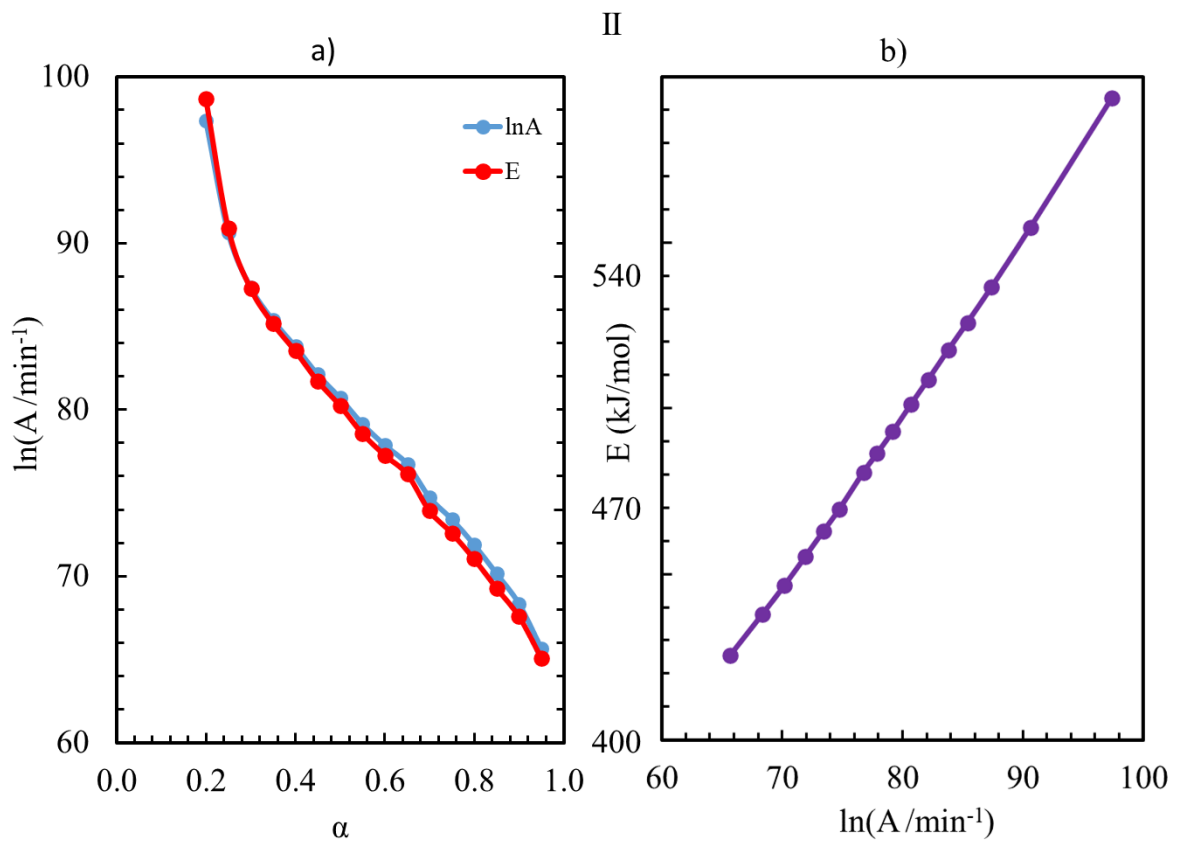


Figure H14 a) Behavior plot of the activation energy and frequency factor at different conversions. b) variation plot of the activation energy with the frequency factor for Rubber II. Obtained with Friedman's method in non-isothermal conditions at heating rates 5, 10, 15, 20, 30 and 40 °C min⁻¹. Analyzed under isoconversion condition.

Appendix H21

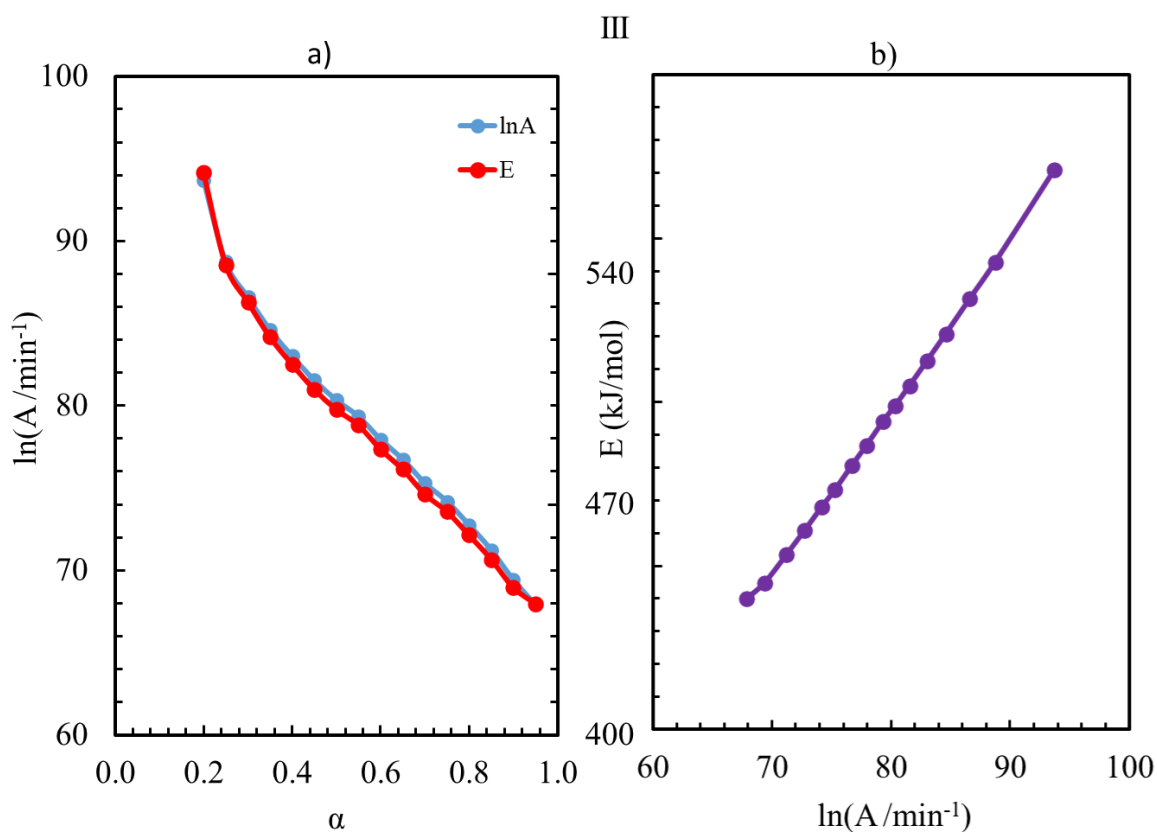


Figure H15 a) Behavior plot of the activation energy and frequency factor at different conversions. b) variation plot of the activation energy with the frequency factor for Rubber III. Obtained with Friedman's method in non-isothermal conditions at heating rates 5, 10, 15, 20, 30 and 40 °C min⁻¹. Analyzed under isoconversion condition.

Appendix H22

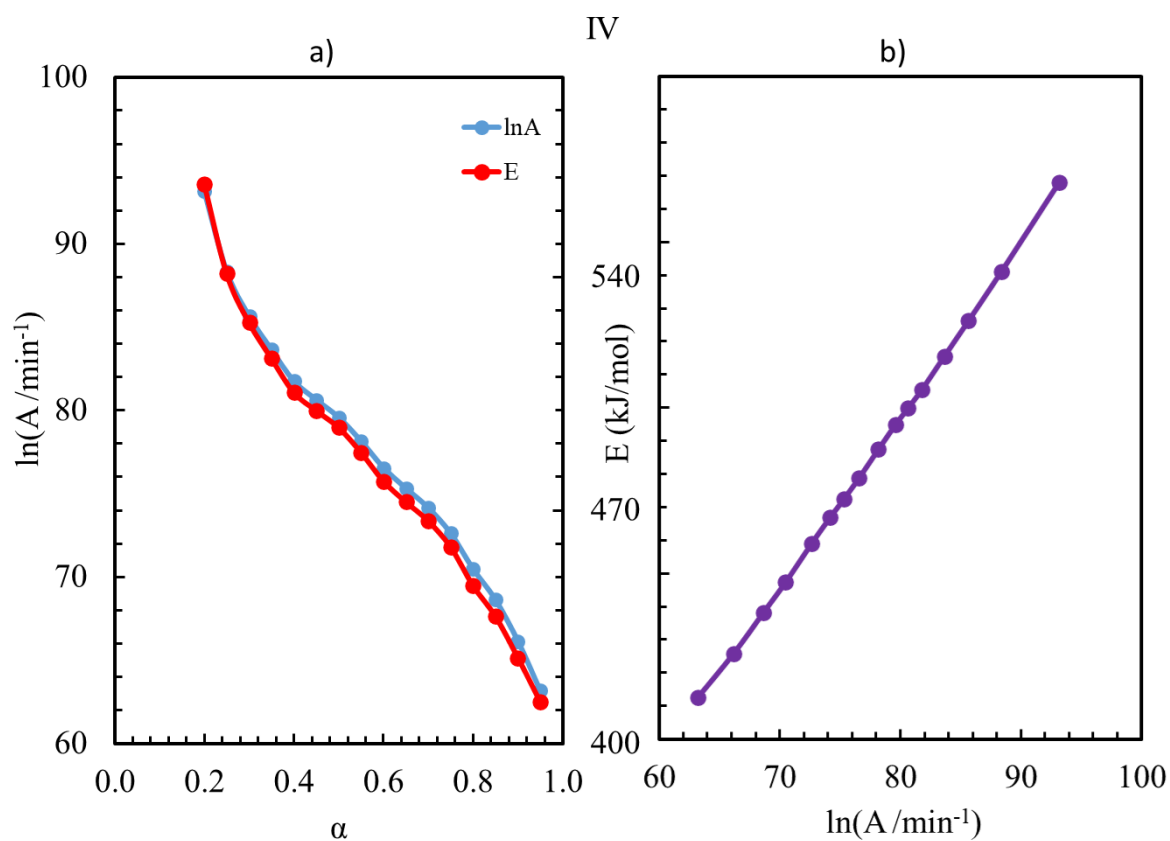


Figure H16 a) Behavior plot of the activation energy and frequency factor at different conversions. b) variation plot of the activation energy with the frequency factor for Rubber IV. Obtained with Friedman's method in non-isothermal conditions at heating rates 5, 10, 15, 20, 30 and 40 °C min⁻¹. Analyzed under isoconversion condition.

Appendix H23

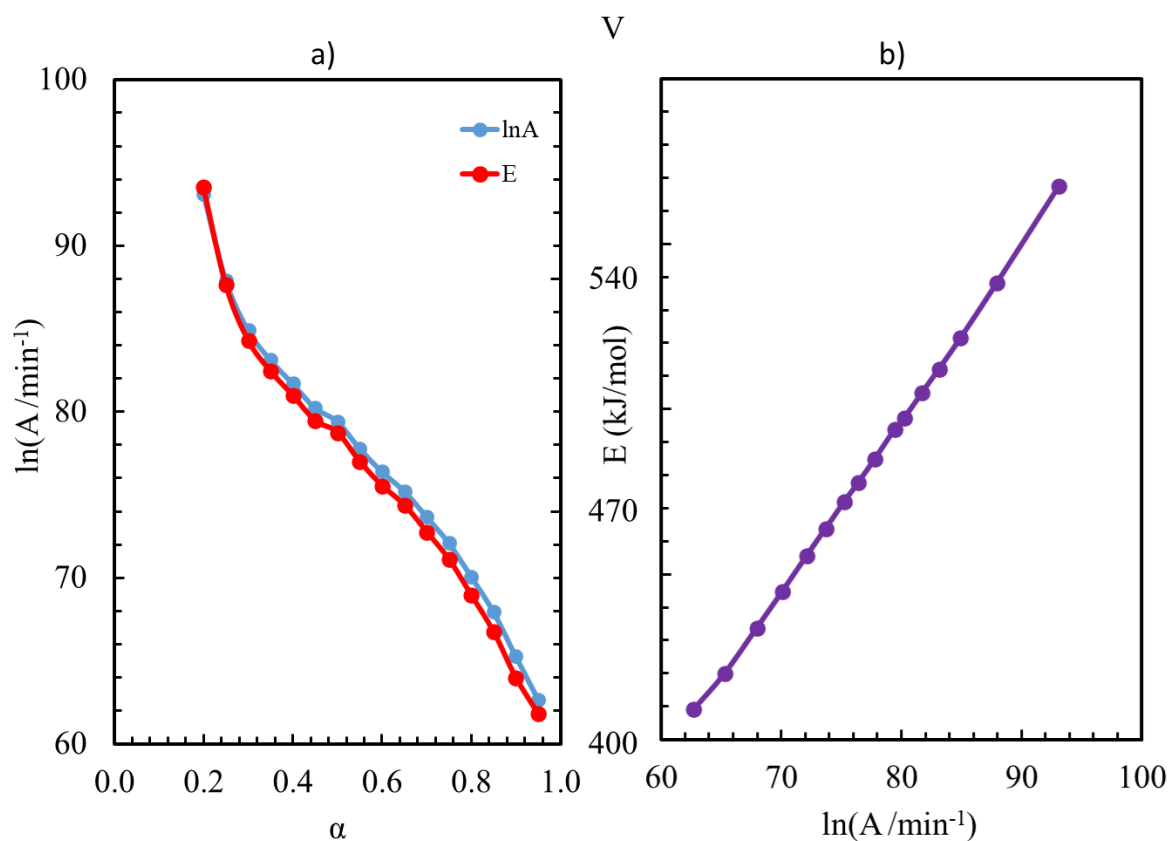


Figure H17 a) Behavior plot of the activation energy and frequency factor at different conversions. b) variation plot of the activation energy with the frequency factor for Rubber V. Obtained with Friedman's method in non-isothermal conditions at heating rates 5, 10, 15, 20, 30 and 40 °C min⁻¹. Analyzed under isoconversion condition.

Appendix H24

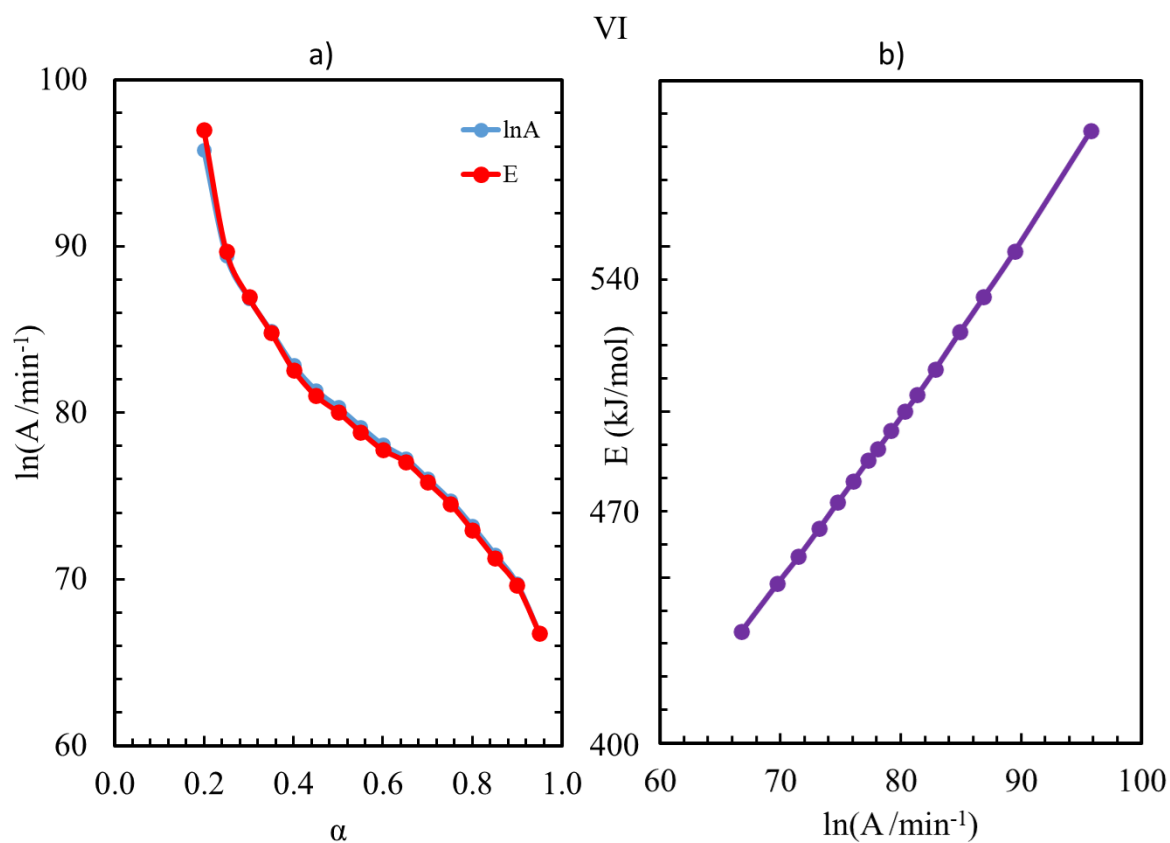


Figure H18 a) Behavior plot of the activation energy and frequency factor at different conversions. b) variation plot of the activation energy with the frequency factor for Rubber VI. Obtained with Friedman's method in non-isothermal conditions at heating rates 5, 10, 15, 20, 30 and 40 °C min⁻¹. Analyzed under isoconversion condition.

Appendix I Supplementary material to support Chapter 5.3.4.1

Appendix I1

PUC-Rio - Certificação Digital Nº 1821742/CA

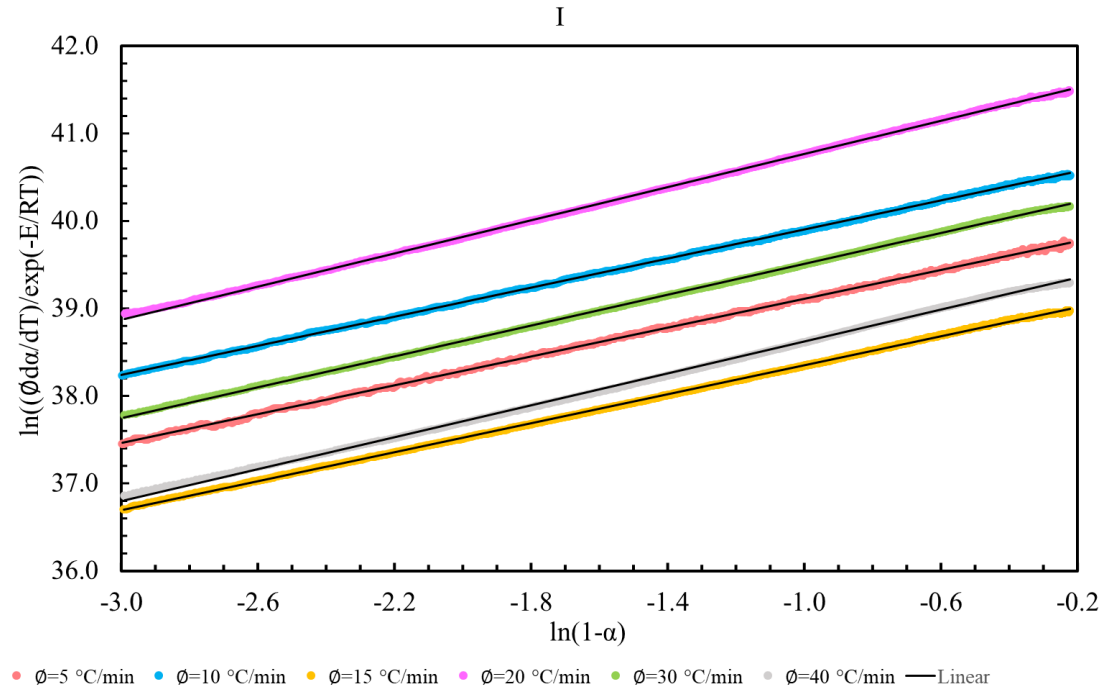


Figure I1 CKA method plot for calculating the reaction order of Rubber I, under N_2 atmosphere at 20 ml min^{-1} and non-isothermal conditions at heating rates 5, 10, 15, 20, 30 and 40 °C min^{-1} .

Appendix I2

PUC-Rio - Certificação Digital Nº 1821742/CA

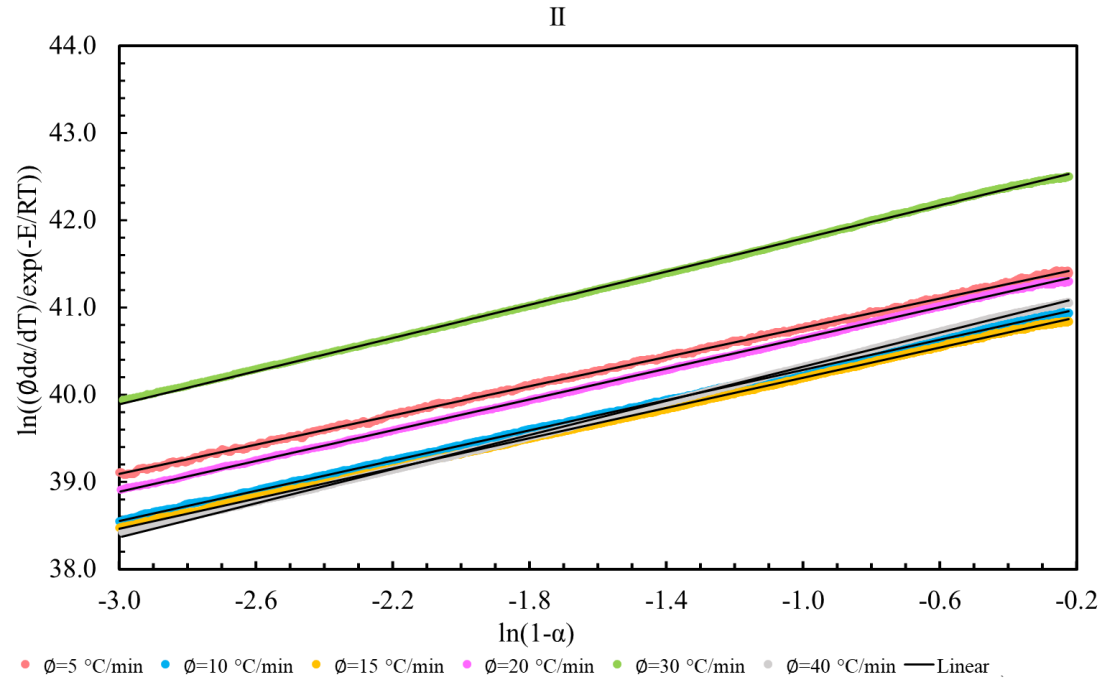


Figure I2 CKA method plot for calculating the reaction order of Rubber II, under N_2 atmosphere at 20 ml min^{-1} and non-isothermal conditions at heating rates 5, 10, 15, 20, 30 and 40 °C min^{-1} .

Appendix I3

PUC-Rio - Certificação Digital N° 1821742/CA

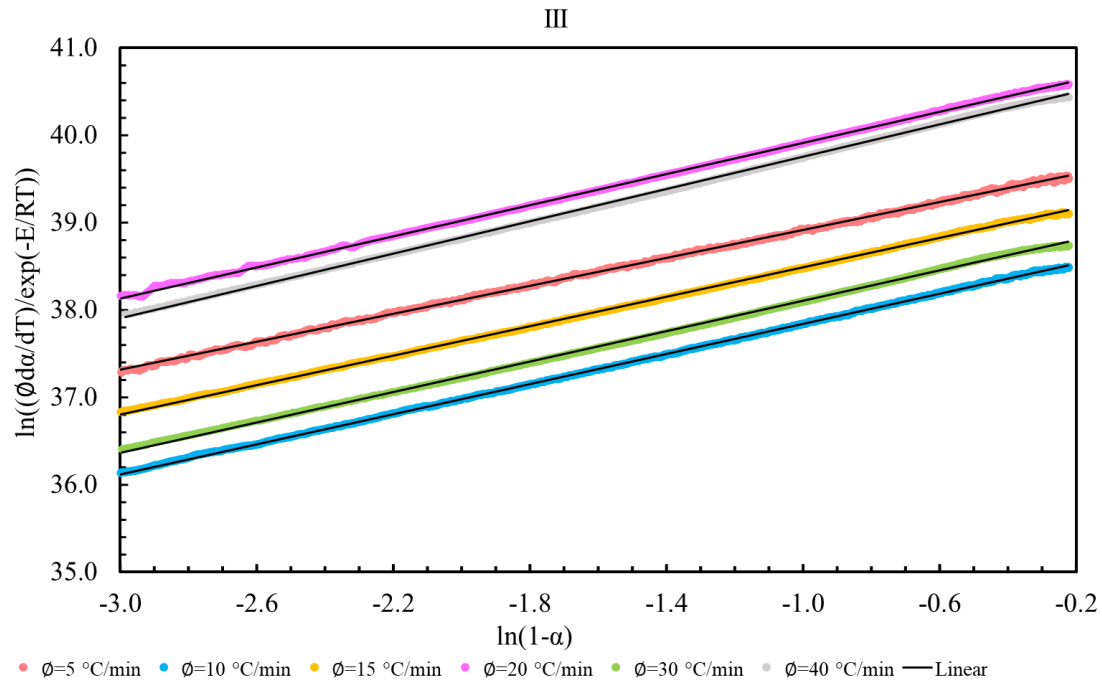


Figure I3 CKA method plot for calculating the reaction order of Rubber III, under N_2 atmosphere at 20 ml min^{-1} and non-isothermal conditions at heating rates 5, 10, 15, 20, 30 and 40 °C min^{-1} .

Appendix I4

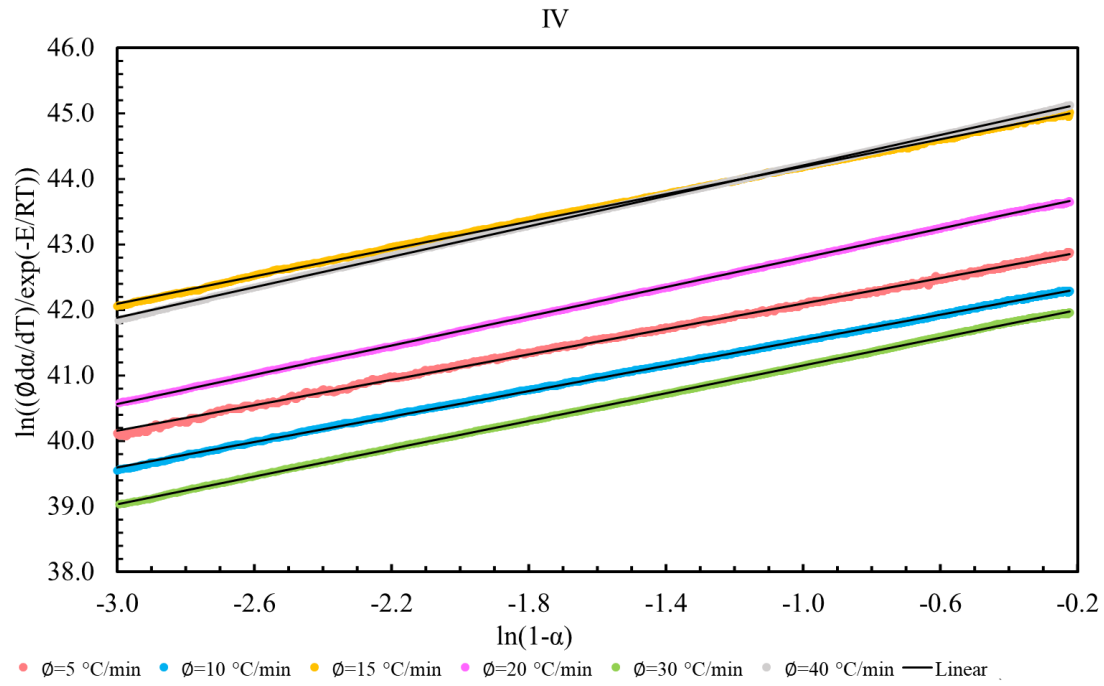


Figure I4 CKA method plot for calculating the reaction order of Rubber IV, under N_2 atmosphere at 20 ml min^{-1} and non-isothermal conditions at heating rates 5, 10, 15, 20, 30 and 40 °C min^{-1} .

Appendix I5

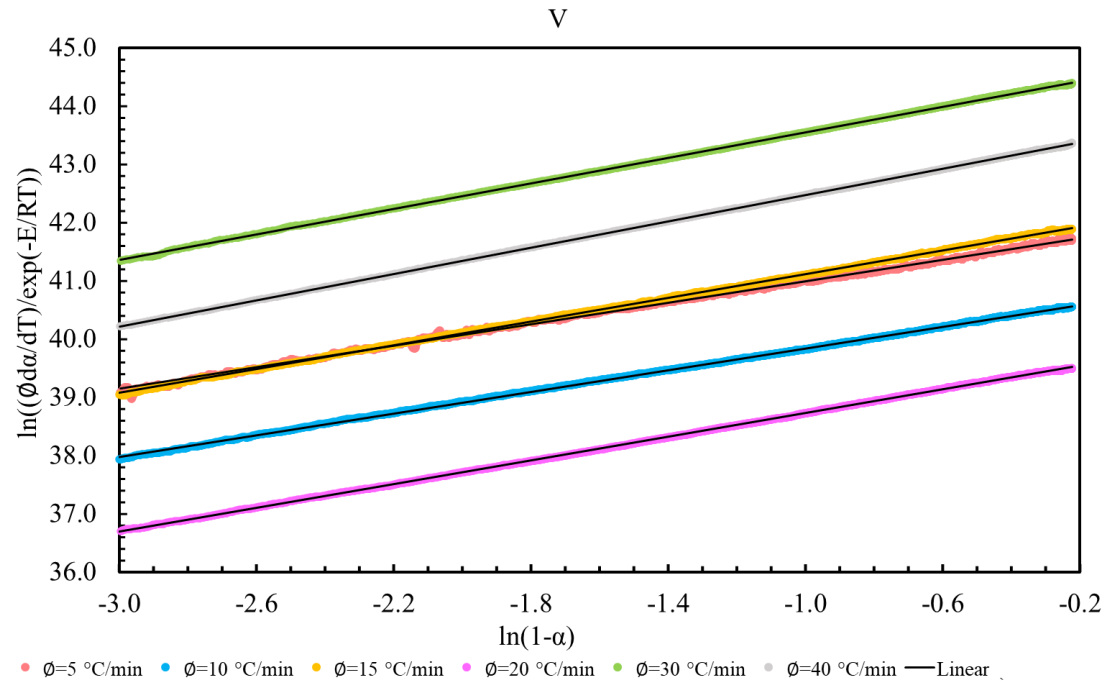


Figure I5 CKA method plot for calculating the reaction order of Rubber V, under N_2 atmosphere at 20 ml min^{-1} and non-isothermal conditions at heating rates 5, 10, 15, 20, 30 and 40 °C min^{-1} .

Appendix I6

PUC-Rio - Certificação Digital N° 1821742/CA

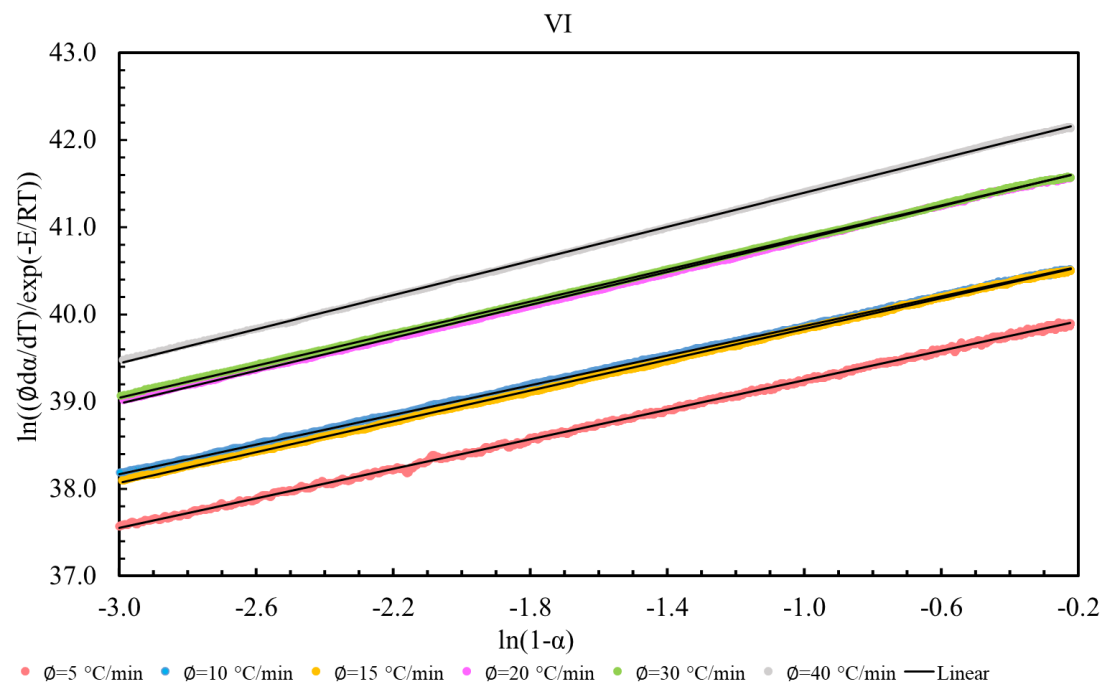


Figure I6 CKA method plot for calculating the reaction order of Rubber VI, under N₂ atmosphere at 20 ml min⁻¹ and non-isothermal conditions at heating rates 5, 10, 15, 20, 30 and 40 °C min⁻¹.

Appendix I7

\emptyset (K/min)	n	γ_n	$\ln(A / \text{min}^{-1})$	$\gamma_{\ln A}$	R^2
5	0.8251	0.0002	39.9350	0.0003	0.9997
10	0.8303	0.0003	40.7301	0.0003	0.9998
15	0.8301	0.0004	39.1810	0.0005	0.9996
20	0.9468	0.0005	41.7139	0.0006	0.9997
30	0.8832	0.0005	40.3928	0.0007	0.9997
40	0.9107	0.0010	39.5320	0.0013	0.9991
Average	\bar{n}	0.87	$\gamma_{\bar{n}}$	0.05	
	$\ln(\bar{A} / \text{min}^{-1})$	40.2	$\gamma_{\ln \bar{A}}$	0.8	

Table I1 Results of CKA method, for calculation of the reaction order of Rubber I, under N_2 atmosphere at 20 ml min^{-1} and non-isothermal conditions at heating rates 5, 10, 15, 20, 30 and $40 \text{ }^\circ\text{C min}^{-1}$.

Appendix I8

\emptyset (K/min)	n	γ_n	$\ln(A / \text{min}^{-1})$	$\gamma_{\ln A}$	R^2
5	0.8377	0.0002	41.6066	0.0003	0.9997
10	0.8661	0.0003	41.1533	0.0003	0.9998
15	0.8644	0.0004	41.0593	0.0005	0.9997
20	0.8820	0.0005	41.5298	0.0006	0.9996
30	0.9500	0.0007	42.7427	0.0009	0.9995
40	0.9762	0.0007	41.2942	0.0009	0.9996
Average	\bar{n}	0.90	$\gamma_{\bar{n}}$	0.05	
	$\ln(\bar{A} / \text{min}^{-1})$	41.6	$\gamma_{\ln \bar{A}}$	0.6	

Table I2 Results of CKA method, for calculation of the reaction order of Rubber II, under N_2 atmosphere at 20 ml min^{-1} and non-isothermal conditions at heating rates 5, 10, 15, 20, 30 and $40 \text{ }^\circ\text{C min}^{-1}$.

Appendix I9

\emptyset (K/min)	n	γ_n	$\ln(A / \text{min}^{-1})$	$\gamma_{\ln A}$	R^2
5	0.7996	0.0003	39.7135	0.0004	0.9996
10	0.8608	0.0003	38.7046	0.0004	0.9998
15	0.8414	0.0005	39.3295	0.0006	0.9996
20	0.8903	0.0004	40.8054	0.0006	0.9997
30	0.8679	0.0008	38.9721	0.0010	0.9992
40	0.9247	0.0007	40.6767	0.0009	0.9996
Average	\bar{n}	0.86	$\gamma_{\bar{n}}$	0.04	
	$\ln(\bar{A} / \text{min}^{-1})$	39.7	$\gamma_{\ln \bar{A}}$	0.8	

Table I3 Results of CKA method, for calculation of the reaction order of Rubber III, under N_2 atmosphere at 20 ml min^{-1} and non-isothermal conditions at heating rates 5, 10, 15, 20, 30 and $40 \text{ }^\circ\text{C min}^{-1}$.

Appendix I10

\emptyset (K/min)	n	γ_n	$\ln(A / \text{min}^{-1})$	$\gamma_{\ln A}$	R^2
5	0.9691	0.0004	43.0668	0.0006	0.9992
10	0.9710	0.0003	42.5129	0.0004	0.9998
15	1.0462	0.0004	45.2355	0.0006	0.9997
20	1.1177	0.0003	43.9142	0.0004	0.9999
30	1.0611	0.0005	42.2165	0.0006	0.9998
40	1.1604	0.0004	45.3650	0.0006	0.9999
Average	\bar{n}	1.05	$\gamma_{\bar{n}}$	0.07	
	$\ln(\bar{A} / \text{min}^{-1})$	43.7	$\gamma_{\ln \bar{A}}$	1.2	

Table I4 Results of CKA method, for calculation of the reaction order of Rubber IV, under N_2 atmosphere at 20 ml min^{-1} and non-isothermal conditions at heating rates 5, 10, 15, 20, 30 and $40 \text{ }^\circ\text{C min}^{-1}$.

Appendix I11

\emptyset (K/min)	n	γ_n	$\ln(A / \text{min}^{-1})$	$\gamma_{\ln A}$	R^2
5	0.9244	0.0005	41.9200	0.0007	0.9988
10	0.9317	0.0003	40.7737	0.0004	0.9997
15	1.0194	0.0004	42.1370	0.0005	0.9998
20	1.0179	0.0004	39.7492	0.0005	0.9998
30	1.0965	0.0004	44.6495	0.0005	0.9999
40	1.1274	0.0002	43.6012	0.0003	1.0000
Average	\bar{n}	1.02	$\gamma_{\bar{n}}$	0.08	
	$\ln(\bar{A} / \text{min}^{-1})$	42.1	$\gamma_{\ln \bar{A}}$	1.6	

Table I5 Results of CKA method, for calculation of the reaction order of Rubber V, under N_2 atmosphere at 20 ml min^{-1} and non-isothermal conditions at heating rates 5, 10, 15, 20, 30 and $40 \text{ }^\circ\text{C min}^{-1}$.

Appendix I12

\emptyset (K/min)	n	γ_n	$\ln(A / \text{min}^{-1})$	$\gamma_{\ln A}$	R^2
5	0.8467	0.0003	40.0923	0.0004	0.9996
10	0.8482	0.0002	40.7168	0.0003	0.9999
15	0.8830	0.0003	40.7168	0.0004	0.9998
20	0.9412	0.0005	41.8047	0.0006	0.9997
30	0.9184	0.0005	41.8028	0.0006	0.9998
40	0.9809	0.0005	42.3793	0.0006	0.9998
Average	\bar{n}	0.90	$\gamma_{\bar{n}}$	0.05	
	$\ln(\bar{A} / \text{min}^{-1})$	41.3	$\gamma_{\ln \bar{A}}$	0.8	

Table I6 Results of CKA method, for calculation of the reaction order of Rubber VI, under N_2 atmosphere at 20 ml min^{-1} and non-isothermal conditions at heating rates 5, 10, 15, 20, 30 and $40 \text{ }^\circ\text{C min}^{-1}$.

Appendix J Supplementary material to support Chapter 5.3.4.2

Appendix J1

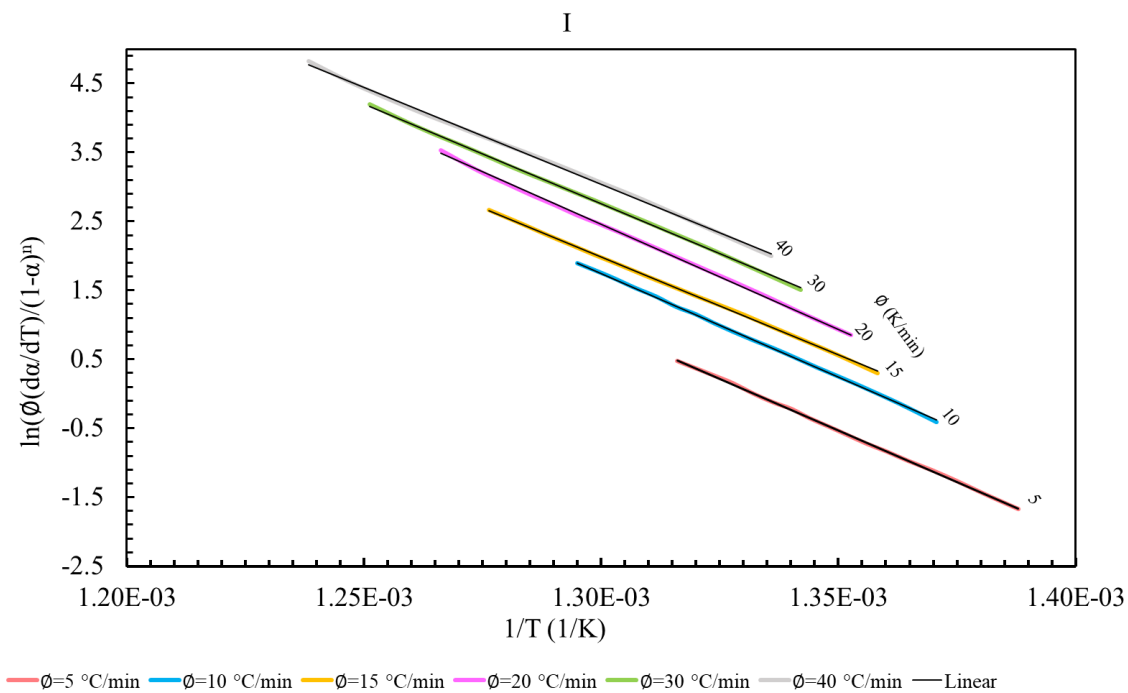


Figure J1 CKA plot method for calculation of activation energy of the thermodegradation reaction of Rubber I, under N_2 atmosphere at 20 ml min^{-1} and non-isothermal conditions at heating rates 5, 10, 15, 20, 30 and 40 °C min^{-1} .

Appendix J2

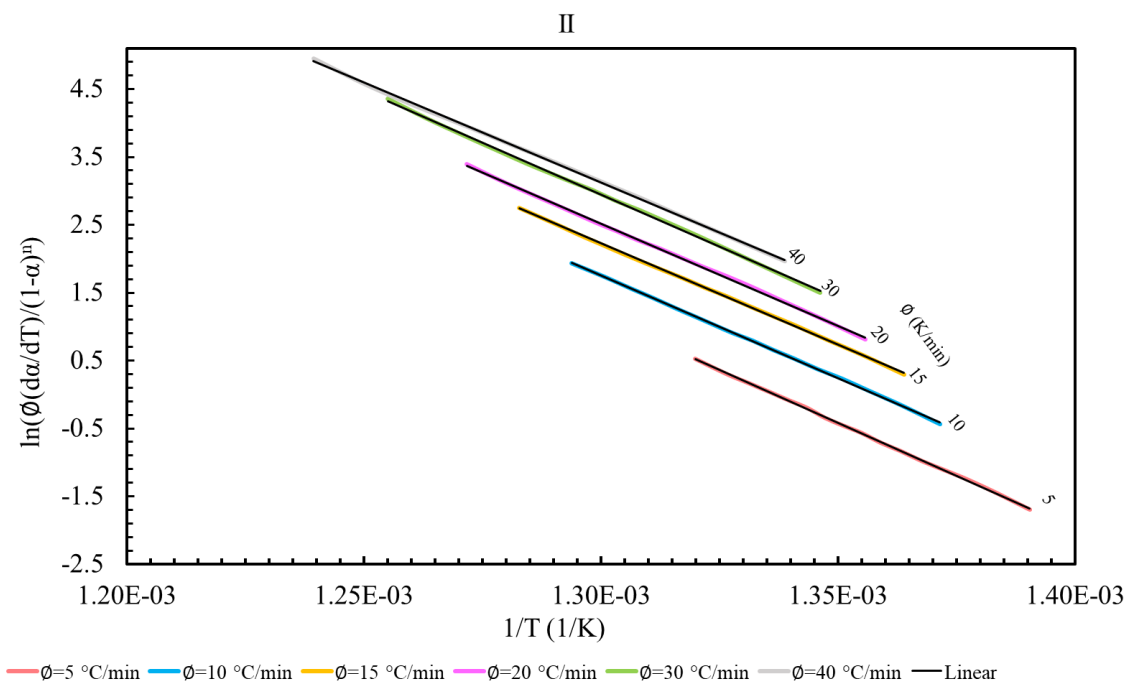


Figure J2 CKA plot method for calculation of activation energy of thermodegradation reaction of Rubber II, under N_2 atmosphere at 20 ml min^{-1} and non-isothermal conditions at heating rates 5, 10, 15, 20, 30 and 40 °C min^{-1}

Appendix J3

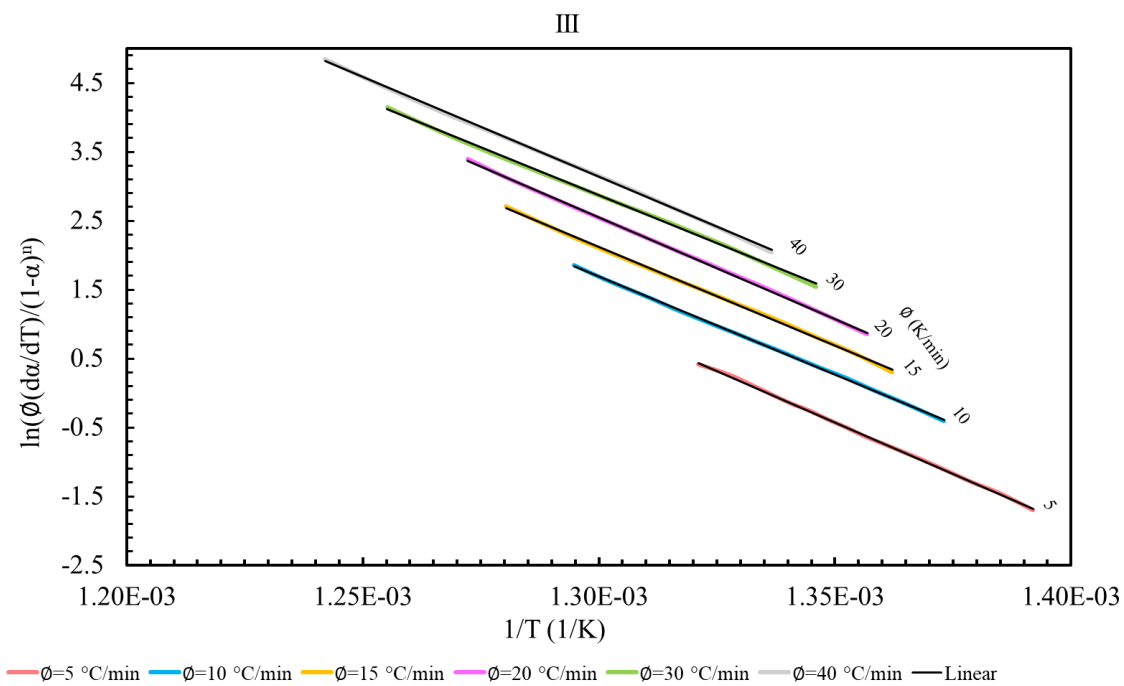


Figure J3 CKA plot method for calculation of activation energy of thermodegradation reaction of Rubber III, under N_2 atmosphere at 20 ml min^{-1} and non-isothermal conditions at heating rates 5, 10, 15, 20, 30 and $40 \text{ }^\circ\text{C min}^{-1}$.

Appendix J4

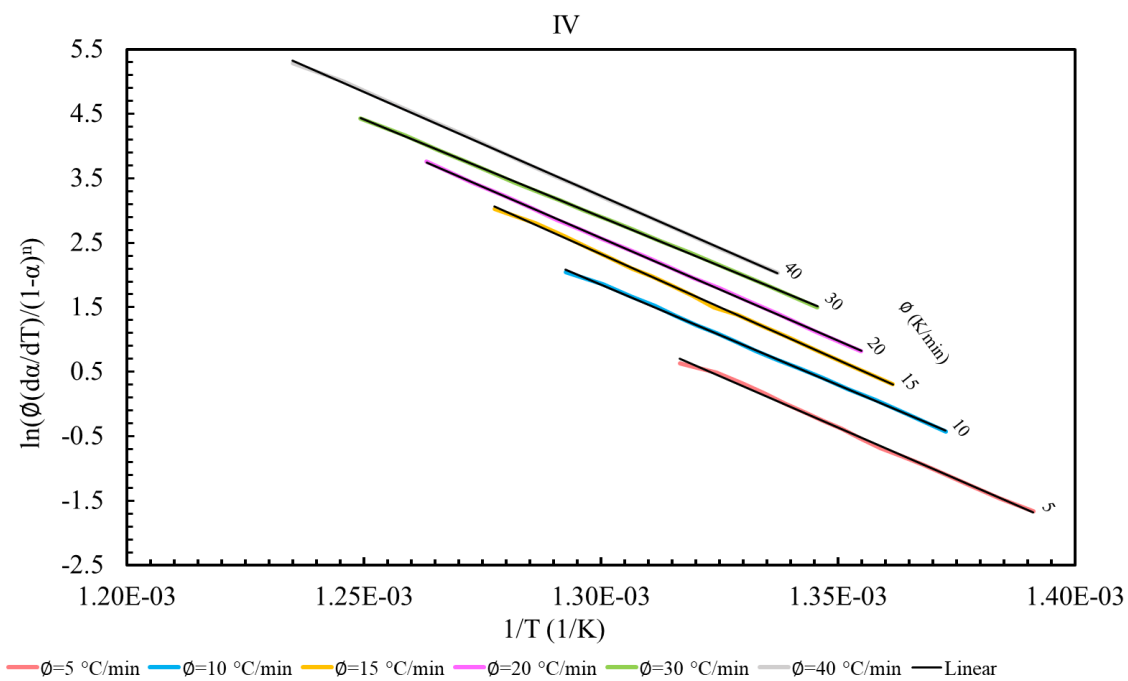


Figure J4 CKA plot method for calculation of activation energy of thermodegradation reaction of Rubber IV, under N_2 atmosphere at 20 ml min^{-1} and non-isothermal conditions at heating rates 5, 10, 15, 20, 30 and 40 °C min^{-1} .

Appendix J5

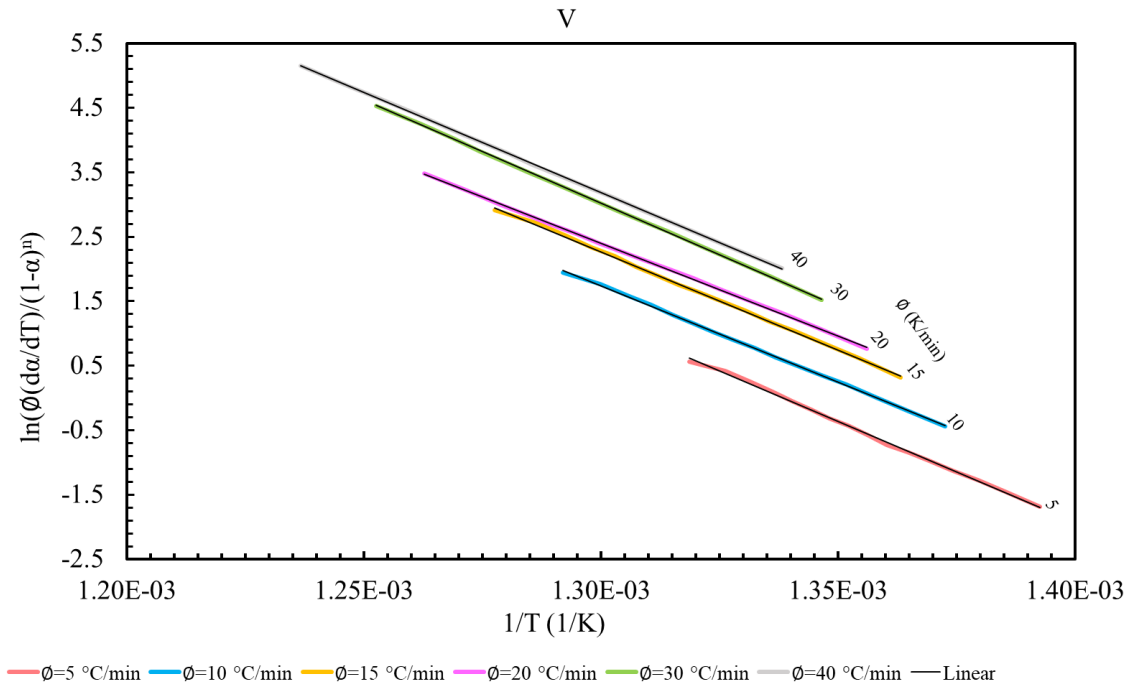


Figure J5 CKA plot method for calculation of activation energy of thermodegradation reaction of Rubber V, under N_2 atmosphere at 20 ml min^{-1} and non-isothermal conditions at heating rates 5, 10, 15, 20, 30 and $40 \text{ }^\circ\text{C min}^{-1}$.

Appendix J6

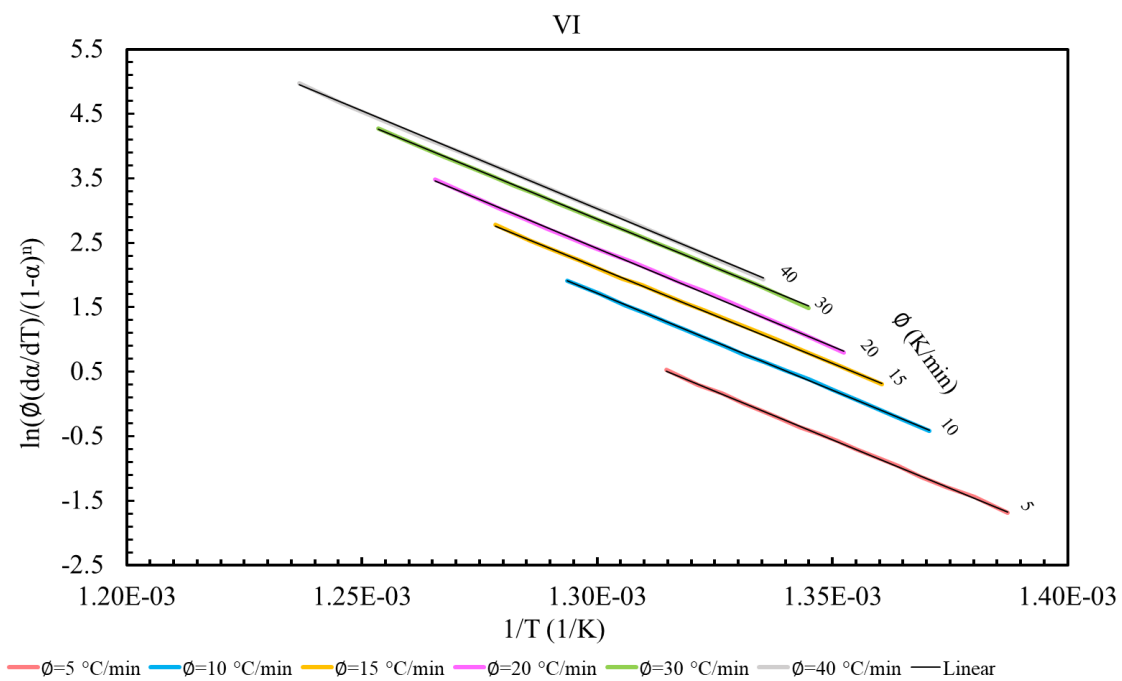


Figure J6 CKA plot method for calculation of activation energy of thermo-degradation reaction of Rubber VI, under N_2 atmosphere at 20 ml min^{-1} and non-isothermal conditions at heating rates 5, 10, 15, 20, 30 and 40 °C min^{-1} .

Appendix J7

\emptyset (K/min)	E (kJ/mol)	γ_E	$\ln(A / \text{min}^{-1})$	$\gamma_{\ln A}$	R^2
5	249.2	0.1	39.94	0.01	0.9997
10	249.3	0.1	40.73	0.01	0.9998
15	237.9	0.1	39.18	0.02	0.9997
20	251.1	0.1	41.71	0.02	0.9997
30	240.7	0.1	40.39	0.02	0.9998
40	233.4	0.2	39.53	0.03	0.9994
Average	\bar{E} (kJ/mol)	244	$\gamma_{\bar{E}}$	7	
	$\ln(\bar{A} / \text{min}^{-1})$	40.2	$\gamma_{\ln \bar{A}}$	0.8	

Table J1 Results of the CKA method for calculation of activation energy of Rubber I, under N_2 atmosphere at 20 ml min^{-1} and non-isothermal conditions at heating rates 5, 10, 15, 20, 30 and $40 \text{ }^\circ\text{C min}^{-1}$.

Appendix J8

\emptyset (K/min)	E (kJ/mol)	γ_E	$\ln(A / \text{min}^{-1})$	$\gamma_{\ln A}$	R^2
5	258.8	0.1	41.61	0.01	0.9997
10	252.0	0.1	41.15	0.01	0.9998
15	248.3	0.1	41.06	0.02	0.9998
20	249.5	0.1	41.53	0.02	0.9997
30	254.5	0.2	42.74	0.03	0.9996
40	244.1	0.2	41.29	0.02	0.9997
Average	\bar{E} (kJ/mol)	251	$\gamma_{\bar{E}}$	5	
	$\ln(\bar{A} / \text{min}^{-1})$	41.6	$\gamma_{\ln \bar{A}}$	0.6	

Table J2 Results of the CKA method for calculation of activation energy of Rubber II, under N_2 atmosphere at 20 ml min^{-1} and non-isothermal conditions at heating rates 5, 10, 15, 20, 30 and $40 \text{ }^\circ\text{C min}^{-1}$.

Appendix J9

\emptyset (K/min)	E (kJ/mol)	γ_E	$\ln(A / \text{min}^{-1})$	$\gamma_{\ln A}$	R^2
5	247.2	0.1	39.71	0.01	0.9996
10	236.7	0.1	38.70	0.01	0.9998
15	238.0	0.1	39.33	0.02	0.9996
20	244.7	0.1	40.81	0.02	0.9998
30	230.9	0.2	38.97	0.03	0.9994
40	240.1	0.2	40.68	0.03	0.9997
Average	\bar{E} (kJ/mol)	240	$\gamma_{\bar{E}}$	5	
	$\ln(\bar{A} / \text{min}^{-1})$	39.7	$\gamma_{\ln \bar{A}}$	0.8	

Table J3 Results of the CKA method for calculation of activation energy of Rubber III, under N_2 atmosphere at 20 ml min^{-1} and non-isothermal conditions at heating rates 5, 10, 15, 20, 30 and $40 \text{ }^\circ\text{C min}^{-1}$.

Appendix J10

\emptyset (K/min)	E (kJ/mol)	γ_E	$\ln(A / \text{min}^{-1})$	$\gamma_{\ln A}$	R^2
5	267.5	0.1	43.07	0.02	0.9991
10	260.0	0.1	42.51	0.01	0.9997
15	274.4	0.1	45.24	0.02	0.9997
20	264.4	0.1	43.91	0.01	0.9999
30	251.4	0.1	42.22	0.02	0.9998
40	269.5	0.1	45.37	0.02	0.9999
Average	\bar{E} (kJ/mol)	265	$\gamma_{\bar{E}}$	7	
	$\ln(\bar{A} / \text{min}^{-1})$	43.7	$\gamma_{\ln \bar{A}}$	1.2	

Table J4 Results of the CKA method for calculation of activation energy of Rubber IV, under N_2 atmosphere at 20 ml min^{-1} and non-isothermal conditions at heating rates 5, 10, 15, 20, 30 and $40 \text{ }^\circ\text{C min}^{-1}$.

Appendix J11

\emptyset (K/min)	E (kJ/mol)	γ_E	$\ln(A / \text{min}^{-1})$	$\gamma_{\ln A}$	R^2
5	260.4	0.1	41.92	0.02	0.9987
10	249.6	0.1	40.77	0.01	0.9997
15	254.9	0.1	42.14	0.02	0.9997
20	238.9	0.1	39.75	0.01	0.9998
30	266.2	0.1	44.65	0.02	0.9999
40	258.5	0.1	43.60	0.01	1.0000
Average	\bar{E} (kJ/mol)	255	$\gamma_{\bar{E}}$	9	
	$\ln(\bar{A} / \text{min}^{-1})$	42.1	$\gamma_{\ln \bar{A}}$	1.6	

Table J5 Results of the CKA method for calculation of activation energy of Rubber V, under N_2 atmosphere at 20 ml min^{-1} and non-isothermal conditions at heating rates 5, 10, 15, 20, 30 and $40 \text{ }^\circ\text{C min}^{-1}$.

Appendix J12

\emptyset (K/min)	E (kJ/mol)	γ_E	$\ln(A / \text{min}^{-1})$	$\gamma_{\ln A}$	R^2
5	250.3	0.1	40.09	0.01	0.9996
10	249.4	0.1	40.72	0.01	0.9999
15	246.8	0.1	40.72	0.01	0.9998
20	251.9	0.1	41.80	0.02	0.9997
30	249.0	0.1	41.80	0.02	0.9998
40	251.7	0.1	42.38	0.02	0.9999
Average	\bar{E} (kJ/mol)	250	$\gamma_{\bar{E}}$	2	
	$\ln(\bar{A} / \text{min}^{-1})$	41.3	$\gamma_{\ln \bar{A}}$	0.8	

Table J6 Results of the CKA method for calculation of activation energy of Rubber VI, under N_2 atmosphere at 20 ml min^{-1} and non-isothermal conditions at heating rates 5, 10, 15, 20, 30 and $40 \text{ }^\circ\text{C min}^{-1}$.

Appendix K Supplementary material to support Chapter 5.3.4.3

Appendix K1

PUC-Rio - Certificação Digital N° 1821742/CA

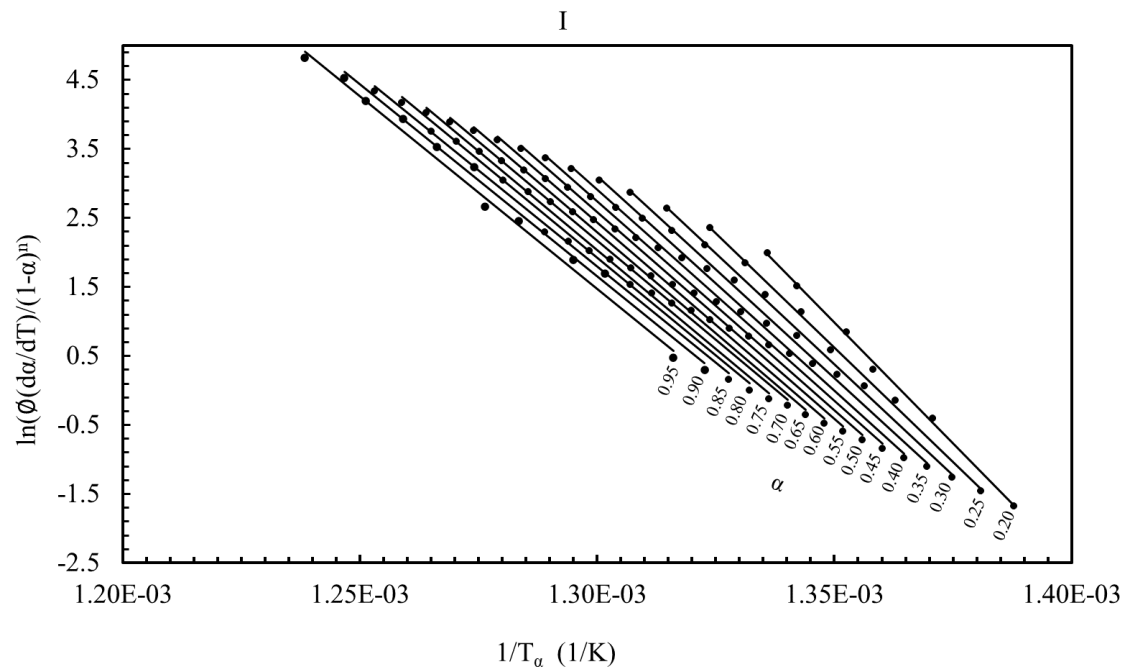


Figure K1 CKA-i method plot for Rubber I in an atmosphere of N_2 at 20 ml min^{-1} and non-isothermal conditions at heating rates 5, 10, 15, 20, 30 and 40 °C min^{-1} . Analyzed under the isoconversion condition

Appendix K2

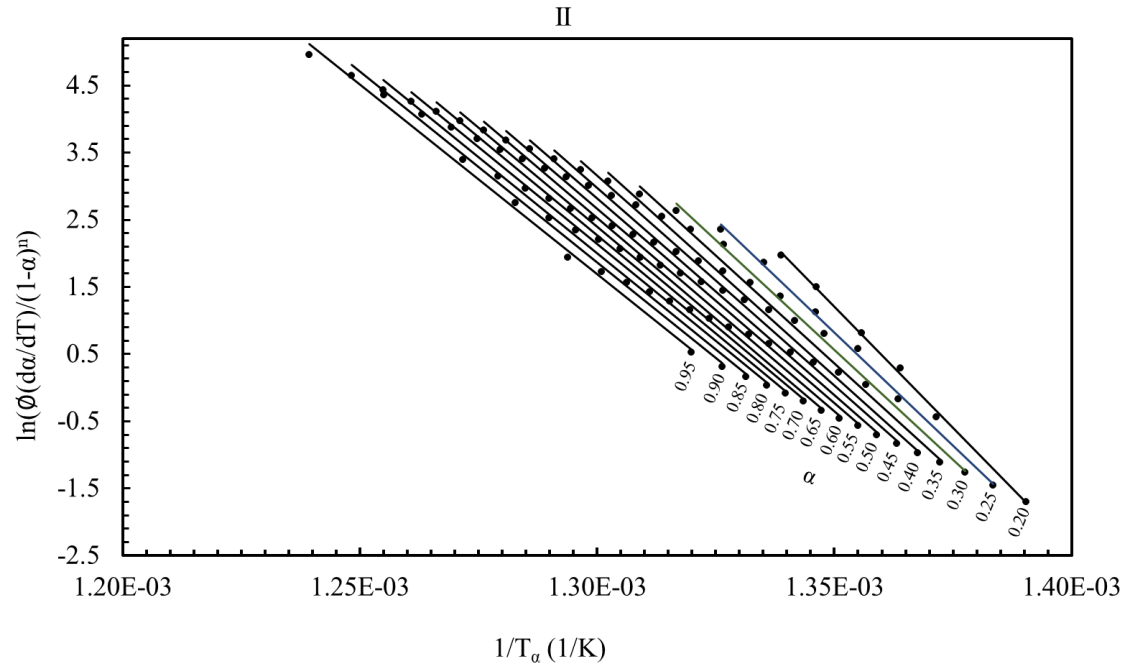


Figure K2 CKA-i method plot for Rubber II in an atmosphere of N_2 at 20 ml min^{-1} and non-isothermal conditions at heating rates 5, 10, 15, 20, 30 and $40 \text{ }^\circ\text{C min}^{-1}$. Analyzed under the isoconversion condition.

Appendix K3

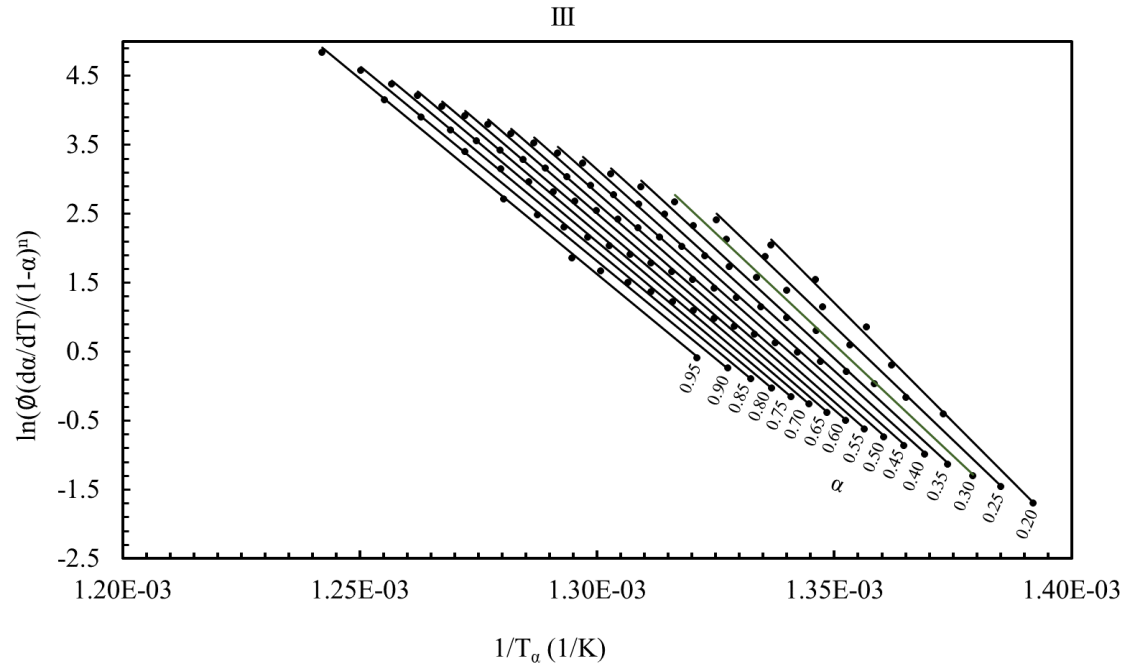


Figure K3 CKA-i method plot for Rubber III in an atmosphere of N_2 at 20 ml min^{-1} and non-isothermal conditions at heating rates 5, 10, 15, 20, 30 and $40 \text{ }^\circ\text{C min}^{-1}$. Analyzed under the isoconversion condition.

Appendix K4

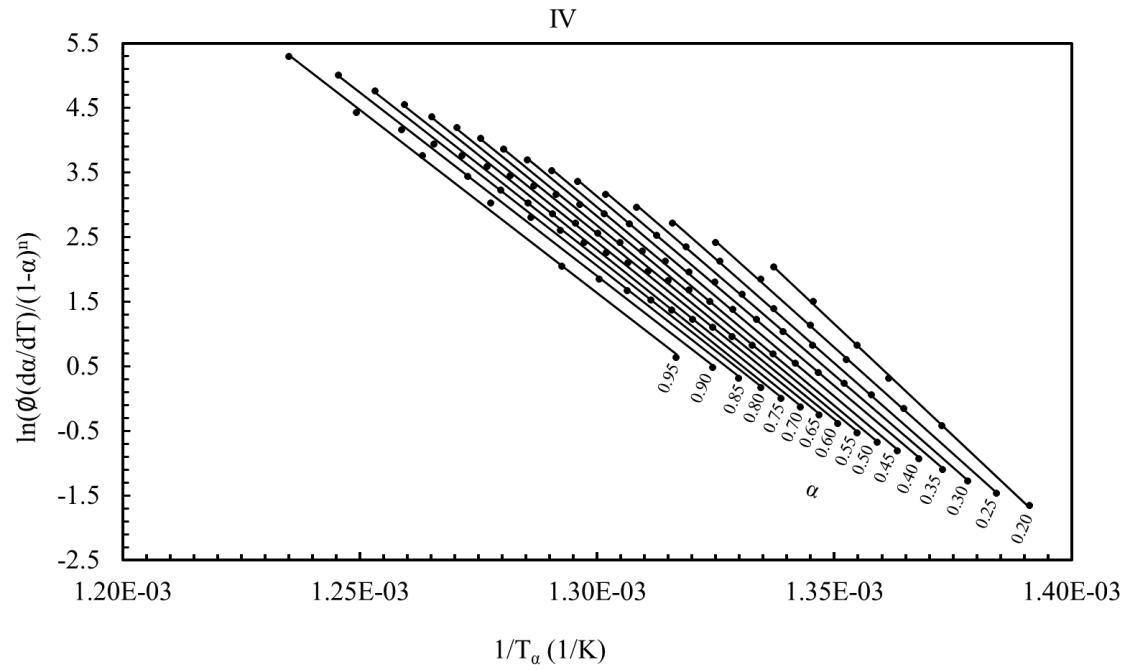


Figure K4 CKA-i method plot for Rubber IV in an atmosphere of N_2 at 20 ml min^{-1} and non-isothermal conditions at heating rates $5, 10, 15, 20, 30$ and 40 °C min^{-1} . Analyzed under the isoconversion condition.

Appendix K5

PUC-Rio - Certificação Digital Nº 1821742/CA

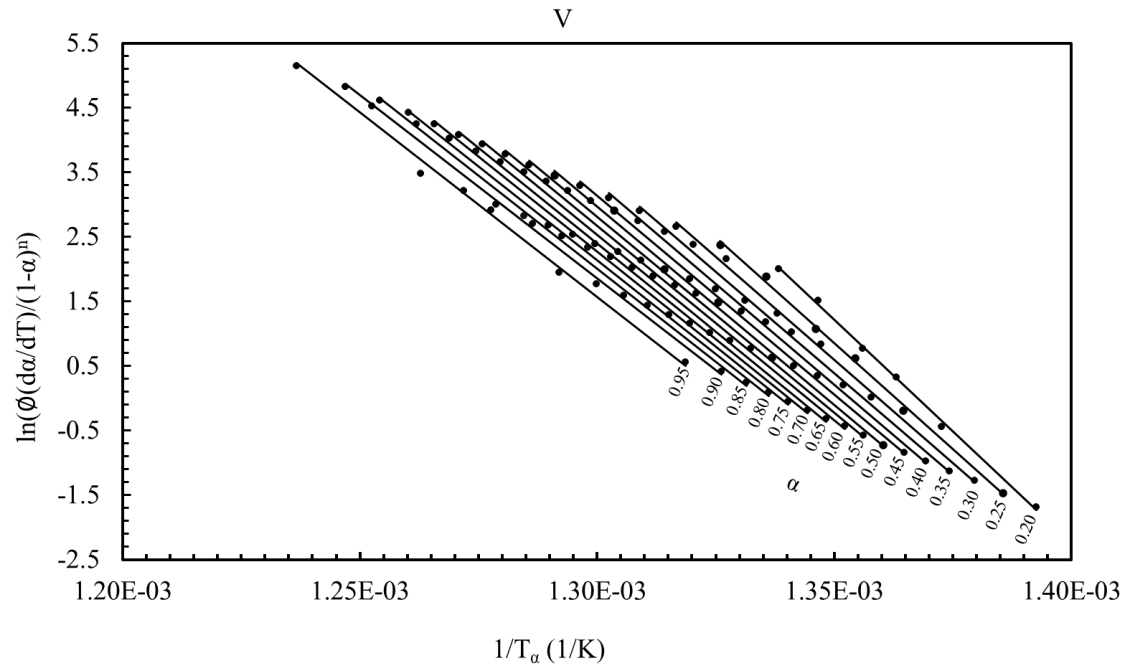


Figure K5 CKA-i method plot for Rubber V in an atmosphere of N_2 at 20 ml min^{-1} and non-isothermal conditions at heating rates 5, 10, 15, 20, 30 and $40 \text{ }^\circ\text{C min}^{-1}$. Analyzed under the isoconversion condition.

Appendix K6

PUC-Rio - Certificação Digital N° 1821742/CA

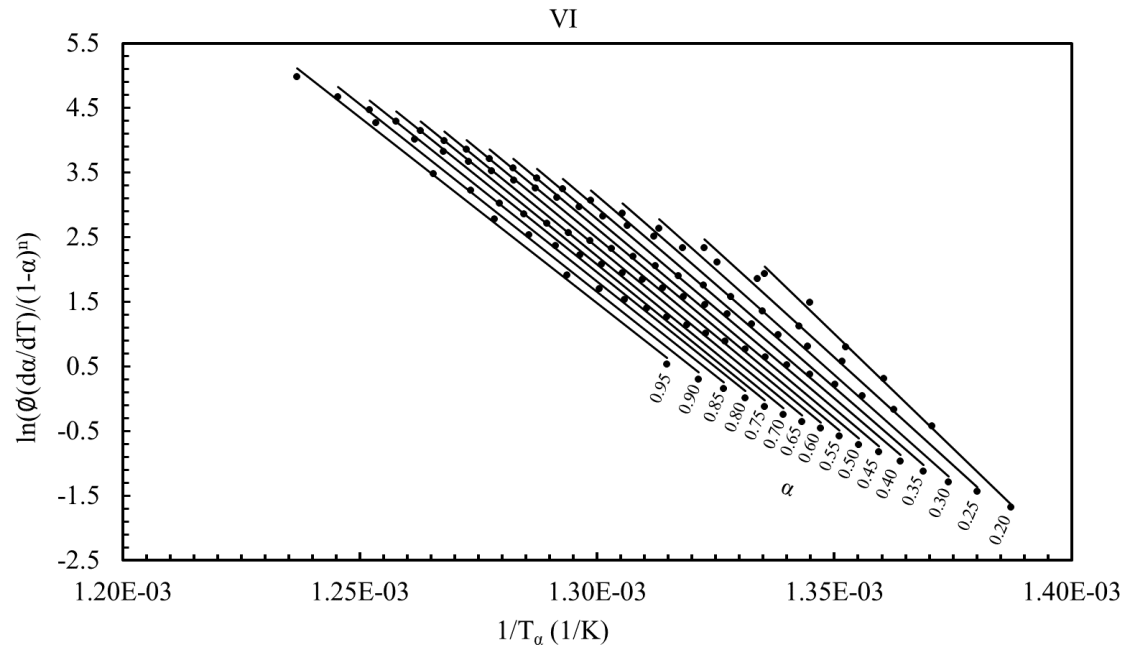


Figure K6 CKA-i method plot for Rubber VI in an atmosphere of N_2 at 20 ml min^{-1} and non-isothermal conditions at heating rates 5, 10, 15, 20, 30 and $40 \text{ }^\circ\text{C min}^{-1}$. Analyzed under the isoconversion condition.

Appendix K7

α	R^2	E_α (kJ/mol)	$\gamma_{E\alpha}$	$\ln(A / \text{min}^{-1})$	$\gamma_{\ln A}$
0.20	0.9979	581	13	95	2
0.25	0.9978	551	13	90	2
0.30	0.9975	534	13	87	2
0.35	0.9973	524	14	85	2
0.40	0.9971	517	14	84	2
0.45	0.9967	510	15	83	2
0.50	0.9962	505	16	82	2
0.55	0.9961	499	16	81	2
0.60	0.9958	492	16	79	3
0.65	0.9954	486	16	78	3
0.70	0.9953	478	16	77	3
0.75	0.9949	476	17	77	3
0.80	0.9944	471	18	76	3
0.85	0.9945	465	17	74	3
0.90	0.9943	462	17	74	3
0.95	0.9938	464	18	74	3
Average	\bar{E} (kJ/mol)	501	γ_E	33	
	$\ln(\bar{A} / \text{min}^{-1})$	81	$\gamma_{\ln \bar{A}}$	6	

Table K1 Results of the CKA-i method considering the isoconversion principle for the thermo-degradation reaction of Rubber I in an atmosphere of N_2 at 20 ml min^{-1} and non-isothermal conditions at heating rates of 5, 10, 15, 20, 30 and $40 \text{ }^\circ\text{C min}^{-1}$.

Appendix K8

α	R^2	E_α (kJ/mol)	$\gamma_{E\alpha}$	$\ln(A / \text{min}^{-1})$	$\gamma_{\ln A}$
0.20	0.9977	598	14	98	2
0.25	0.9972	560	15	92	2
0.30	0.9968	543	15	89	2
0.35	0.9964	534	16	87	3
0.40	0.9958	527	17	86	3
0.45	0.9961	519	16	84	3
0.50	0.9958	513	17	83	3
0.55	0.9959	506	16	82	3
0.60	0.9957	502	16	81	3
0.65	0.9959	498	16	80	3
0.70	0.9961	489	15	79	2
0.75	0.9957	485	16	78	2
0.80	0.9953	480	16	77	3
0.85	0.9949	476	17	76	3
0.90	0.9946	472	17	76	3
0.95	0.9944	470	18	75	3
Average	\bar{E} (kJ/mol)	511	$\gamma_{\bar{E}}$	34	
	$\ln(\bar{A} / \text{min}^{-1})$	83	$\gamma_{\ln \bar{A}}$	6	

Table K2 Results of the CKA-i method considering the isoconversion principle for the thermo-degradation reaction of Rubber II in an atmosphere of N_2 at 20 ml min^{-1} and non-isothermal conditions at heating rates of 5, 10, 15, 20, 30 and $40 \text{ }^\circ\text{C min}^{-1}$.

Appendix K9

α	R^2	E_α (kJ/mol)	$\gamma_{E\alpha}$	$\ln(A / \text{min}^{-1})$	$\gamma_{\ln A}$
0.20	0.9967	574	17	94	3
0.25	0.9970	547	15	90	2
0.30	0.9967	536	15	88	2
0.35	0.9970	527	15	86	2
0.40	0.9971	519	14	85	2
0.45	0.9968	513	14	83	2
0.50	0.9970	508	14	82	2
0.55	0.9968	504	14	82	2
0.60	0.9967	498	14	81	2
0.65	0.9965	493	15	80	2
0.70	0.9963	487	15	79	2
0.75	0.9962	484	15	78	2
0.80	0.9961	479	15	77	2
0.85	0.9960	475	15	76	2
0.90	0.9959	471	15	75	2
0.95	0.9962	471	15	75	2
Average	\bar{E} (kJ/mol)	505	$\gamma_{\bar{E}}$	29	
	$\ln(\bar{A} / \text{min}^{-1})$	82	$\gamma_{\ln \bar{A}}$	5	

Table K3 Results of the CKA-i method considering the isoconversion principle for the thermo-degradation reaction of Rubber III in an atmosphere of N_2 at 20 ml min^{-1} and non-isothermal conditions at heating rates of 5, 10, 15, 20, 30 and $40 \text{ }^\circ\text{C min}^{-1}$.

Appendix K10

α	R^2	E_α (kJ/mol)	$\gamma_{E\alpha}$	$\ln(A / \text{min}^{-1})$	$\gamma_{\ln A}$
0.20	0.9994	574	7	94	1
0.25	0.9997	549	5	90	1
0.30	0.9997	535	5	87	1
0.35	0.9997	526	4	86	1
0.40	0.9997	517	4	84	1
0.45	0.9997	514	4	83	1
0.50	0.9998	511	4	83	1
0.55	0.9995	505	5	82	1
0.60	0.9995	499	5	81	1
0.65	0.9993	495	6	80	1
0.70	0.9993	492	7	79	1
0.75	0.9990	488	8	79	1
0.80	0.9990	481	8	77	1
0.85	0.9986	476	9	77	1
0.90	0.9984	471	9	76	1
0.95	0.9980	470	10	75	2
Average	\bar{E} (kJ/mol)	506	$\gamma_{\bar{E}}$	28	
	$\ln(\bar{A} / \text{min}^{-1})$	82	$\gamma_{\ln \bar{A}}$	5	

Table K4 Results of the CKA-i method considering the isoconversion principle for the thermo-degradation reaction of Rubber IV in an atmosphere of N_2 at 20 ml min^{-1} and non-isothermal conditions at heating rates of 5, 10, 15, 20, 30 and $40 \text{ }^\circ\text{C min}^{-1}$.

Appendix K11

α	R^2	E_α (kJ/mol)	$\gamma_{E\alpha}$	$\ln(A / \text{min}^{-1})$	$\gamma_{\ln A}$
0.20	0.9982	575	12	95	2
0.25	0.9974	547	14	90	2
0.30	0.9974	532	14	87	2
0.35	0.9969	524	15	86	2
0.40	0.9964	519	16	84	3
0.45	0.9960	513	16	83	3
0.50	0.9955	512	17	83	3
0.55	0.9951	506	18	82	3
0.60	0.9944	501	19	81	3
0.65	0.9937	498	20	80	3
0.70	0.9936	493	20	80	3
0.75	0.9924	489	21	79	3
0.80	0.9917	483	22	78	3
0.85	0.9905	478	23	77	4
0.90	0.9900	472	24	76	4
0.95	0.9913	475	22	76	3
Average	\bar{E} (kJ/mol)	507	$\gamma_{\bar{E}}$	27	
	$\ln(\bar{A} / \text{min}^{-1})$	82	$\gamma_{\ln \bar{A}}$	5	

Table K5 Results of the CKA-i method considering the isoconversion principle for the thermo-degradation reaction of Rubber V in an atmosphere of N_2 at 20 ml min^{-1} and non-isothermal conditions at heating rates of 5, 10, 15, 20, 30 and $40 \text{ }^\circ\text{C min}^{-1}$.

Appendix K12

α	R^2	E_α (kJ/mol)	$\gamma_{E\alpha}$	$\ln(A / \text{min}^{-1})$	$\gamma_{\ln A}$
0.20	0.9963	590	18	97	3
0.25	0.9955	554	19	91	3
0.30	0.9948	541	20	88	3
0.35	0.9948	532	19	87	3
0.40	0.9950	522	19	85	3
0.45	0.9952	515	18	84	3
0.50	0.9953	512	17	83	3
0.55	0.9958	507	16	82	3
0.60	0.9958	504	16	81	3
0.65	0.9954	502	17	81	3
0.70	0.9955	498	17	80	3
0.75	0.9954	494	17	79	3
0.80	0.9954	489	17	78	3
0.85	0.9958	485	16	78	2
0.90	0.9951	482	17	77	3
0.95	0.9960	477	15	76	2
Average	\bar{E} (kJ/mol)	513	$\gamma_{\bar{E}}$	29	
	$\ln(\bar{A} / \text{min}^{-1})$	83	$\gamma_{\ln \bar{A}}$	5	

Table K6 Results of the CKA-i method considering the isoconversion principle for the thermo-degradation reaction of Rubber VI in an atmosphere of N_2 at 20 ml min^{-1} and non-isothermal conditions at heating rates of 5, 10, 15, 20, 30 and $40 \text{ }^\circ\text{C min}^{-1}$.

Appendix L Supplementary material to support Chapter 5.3.4.4

Appendix L1

PUC-Rio - Certificação Digital Nº 1821742/CA

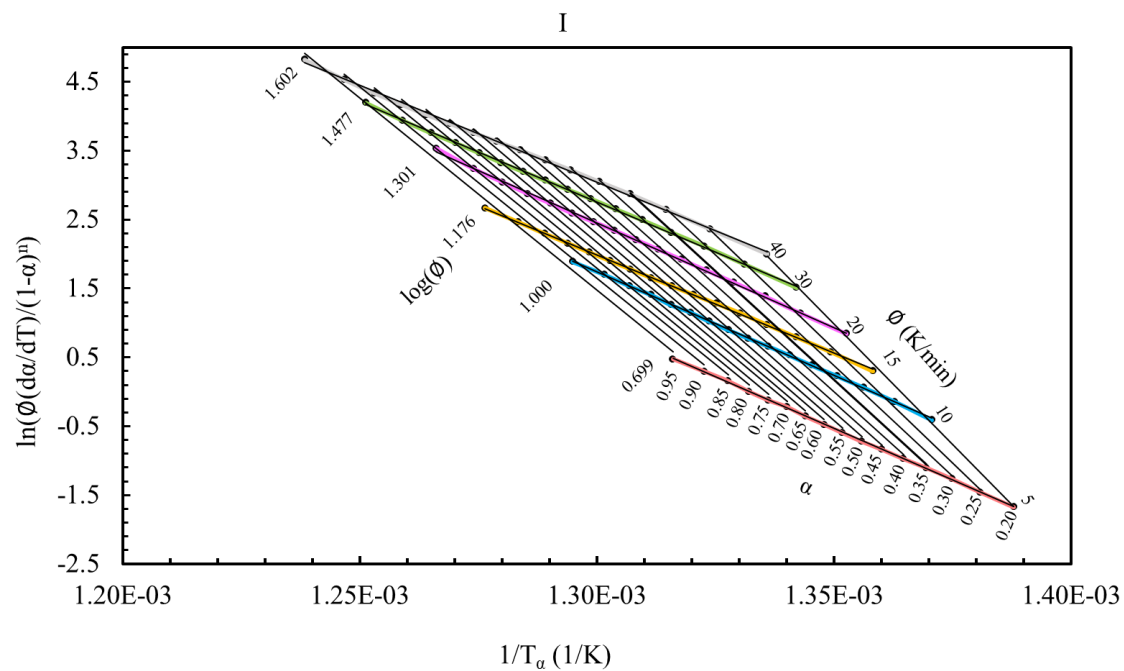


Figure L1 CKA method plot for Rubber I in an atmosphere of N_2 at 20 ml min^{-1} , under non-isothermal conditions at heating rates of 5, 10, 15, 20, 30 and $40 \text{ }^\circ\text{C min}^{-1}$. Analyzed under the isoconversion condition. Corresponding to the overlap of that of CKA and CKA-i.

Appendix L2

PUC-Rio - Certificação Digital N° 1821742/CA

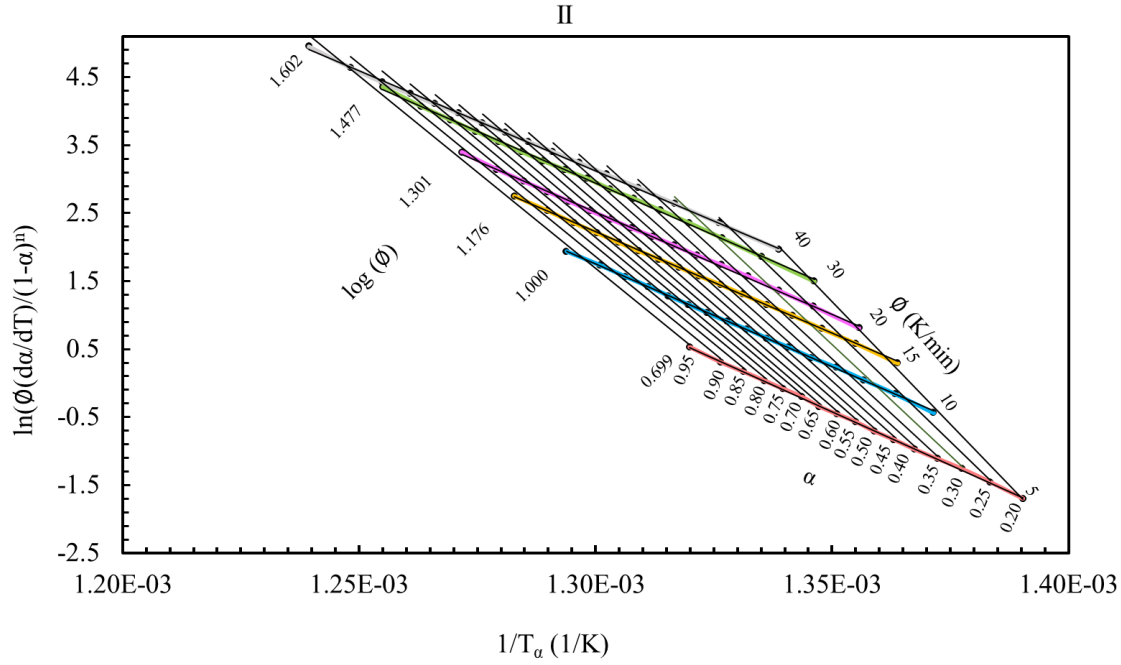


Figure L2 CKA method plot for Rubber II in an atmosphere of N₂ at 20 ml min⁻¹, under non-isothermal conditions at heating rates of 5, 10, 15, 20, 30 and 40 °C min⁻¹. Analyzed under the isoconversion condition. Corresponding to the overlap of that of CKA and CKA-i.

Appendix L3

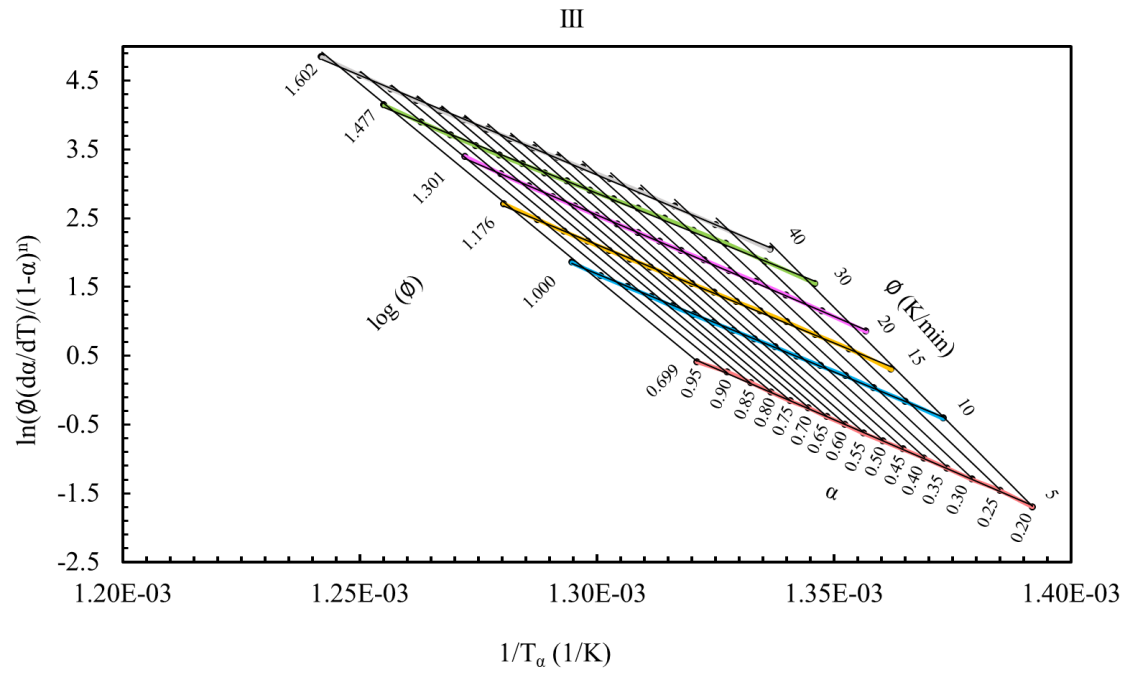


Figure L3 CKA method plot for Rubber III in an atmosphere of N_2 at 20 ml min^{-1} , under non-isothermal conditions at heating rates of 5, 10, 15, 20, 30 and 40 °C min^{-1} . Analyzed under the isoconversion condition. Corresponding to the overlap of that of CKA and CKA-i.

Appendix L4

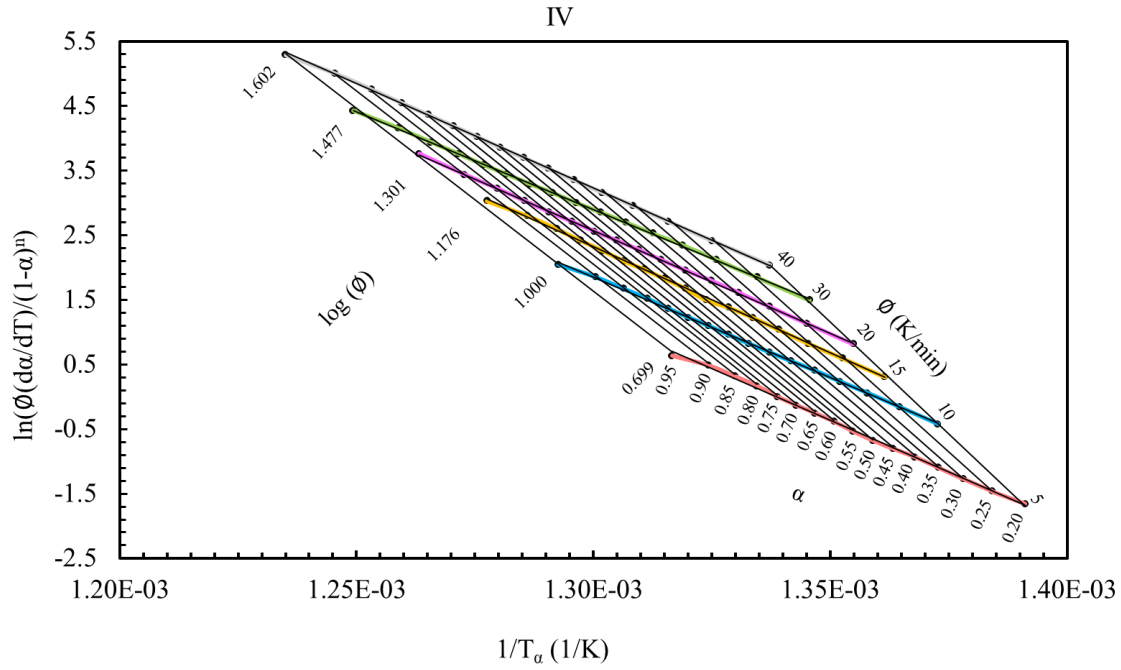


Figure L4 CKA method plot for Rubber IV in an atmosphere of N₂ at 20 ml min⁻¹, under non-isothermal conditions at heating rates of 5, 10, 15, 20, 30 and 40 °C min⁻¹. Analyzed under the isoconversion condition. Corresponding to the overlap of that of CKA and CKA-i.

Appendix L5

PUC-Rio - Certificação Digital N° 1821742/CA

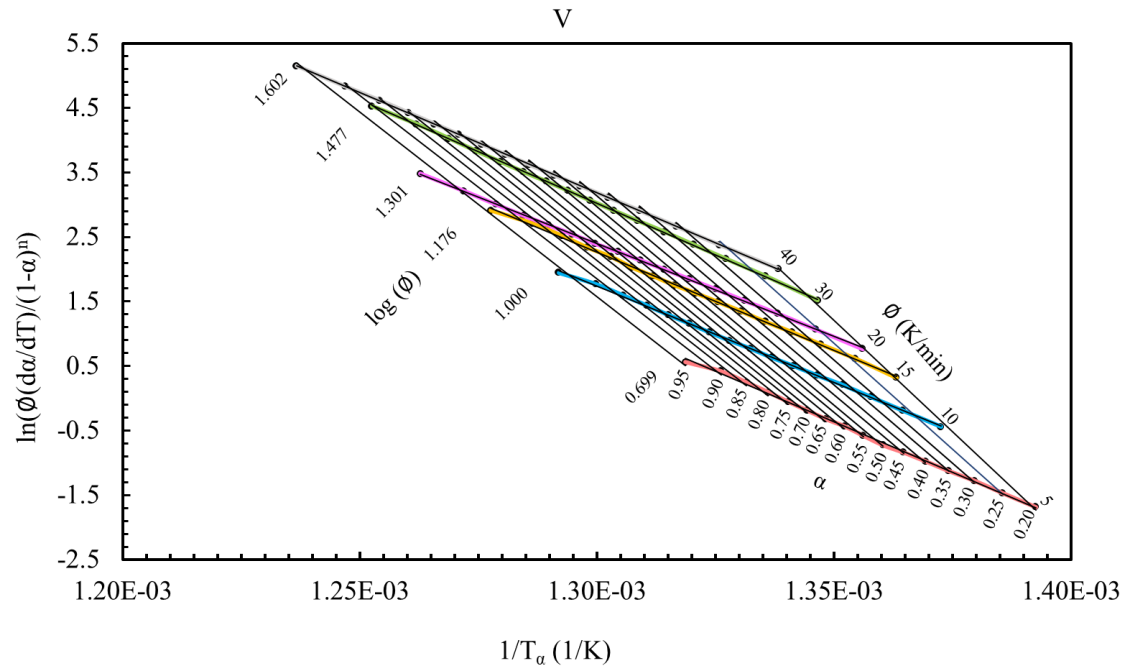


Figure L5 CKA method plot for Rubber V in an atmosphere of N_2 at 20 ml min^{-1} , under non-isothermal conditions at heating rates of 5, 10, 15, 20, 30 and $40 \text{ }^\circ\text{C min}^{-1}$. Analyzed under the isoconversion condition. Corresponding to the overlap of that of CKA and CKA-i.

Appendix L6

PUC-Rio - Certificação Digital N° 1821742/CA

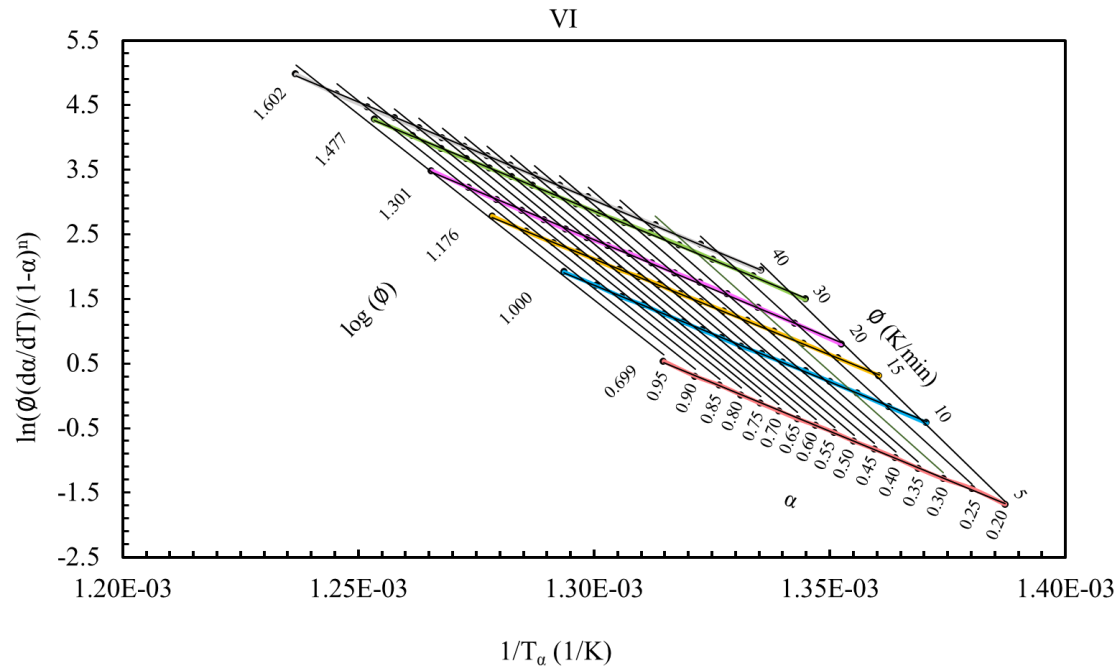


Figure L6 CKA method plot for Rubber VI in an atmosphere of N_2 at 20 ml min^{-1} , under non-isothermal conditions at heating rates of $5, 10, 15, 20, 30$ and 40 °C min^{-1} . Analyzed under the isoconversion condition. Corresponding to the overlap of that of CKA and CKA-i.

Appendix L7

α	R^2	E (kJ/mol)	γ_E	$\ln(A / \text{min}^{-1})$	$\gamma_{\ln A}$
0.20	0.9979	337	20	55	3
0.25	0.9978	307	20	50	3
0.30	0.9975	290	20	47	3
0.35	0.9973	280	21	45	3
0.40	0.9971	273	21	44	3
0.45	0.9967	266	22	42	3
0.50	0.9962	261	23	41	3
0.55	0.9961	255	23	40	3
0.60	0.9958	248	23	39	3
0.65	0.9954	242	23	38	3
0.70	0.9953	234	23	37	3
0.75	0.9949	232	24	36	3
0.80	0.9944	227	25	35	4
0.85	0.9945	221	24	34	3
0.90	0.9943	218	24	34	3
0.95	0.9938	220	25	34	4
Average	\bar{E} (kJ/mol)	257	γ_E	33	
	$\ln(\bar{A} / \text{min}^{-1})$	41	$\gamma_{\ln \bar{A}}$	6	

Table L1 CKA-ic results for Rubber I considering the isoconversion principle for the thermo-degradation reaction in an atmosphere of N_2 at 20 ml min^{-1} and non-isothermal conditions at heating rates of 5, 10, 15, 20, 30 and $40 \text{ }^\circ\text{C min}^{-1}$.

Appendix L8

α	R^2	E (kJ/mol)	γ_E	$\ln(A / \text{min}^{-1})$	$\gamma_{\ln A}$
0.20	0.9977	347	19	57	3
0.25	0.9972	309	20	50	3
0.30	0.9968	292	5	47	3
0.35	0.9964	283	5	45	3
0.40	0.9958	276	5	44	3
0.45	0.9961	268	5	43	3
0.50	0.9958	262	5	42	3
0.55	0.9959	255	5	40	3
0.60	0.9957	251	5	40	3
0.65	0.9959	247	5	39	3
0.70	0.9961	238	5	37	3
0.75	0.9957	234	5	37	3
0.80	0.9953	229	5	36	3
0.85	0.9949	225	5	35	3
0.90	0.9946	221	5	34	3
0.95	0.9944	219	5	34	3
Average	\bar{E} (kJ/mol)	260	γ_E	34	
	$\ln(\bar{A} / \text{min}^{-1})$	41	$\gamma_{\ln \bar{A}}$	6	

Table L2 CKA-ic results for Rubber II considering the isoconversion principle for the thermo-degradation reaction in an atmosphere of N_2 at 20 ml min^{-1} and non-isothermal conditions at heating rates of 5, 10, 15, 20, 30 and $40 \text{ }^\circ\text{C min}^{-1}$

Appendix L9

α	R^2	E (kJ/mol)	γ_E	$\ln(A / \text{min}^{-1})$	$\gamma_{\ln A}$
0.20	0.9967	334	22	55	4
0.25	0.9970	307	20	50	3
0.30	0.9967	296	20	48	3
0.35	0.9970	287	20	46	3
0.40	0.9971	279	19	45	3
0.45	0.9968	273	19	44	3
0.50	0.9970	268	19	43	3
0.55	0.9968	264	19	42	3
0.60	0.9967	258	19	41	3
0.65	0.9965	253	20	40	3
0.70	0.9963	247	20	39	3
0.75	0.9962	244	20	38	3
0.80	0.9961	239	20	37	3
0.85	0.9960	235	20	36	3
0.90	0.9959	231	20	36	3
0.95	0.9962	231	20	36	3
Average	\bar{E} (kJ/mol)	265	$\gamma_{\bar{E}}$	29	
	$\ln(\bar{A} / \text{min}^{-1})$	42	$\gamma_{\ln \bar{A}}$	5	

Table L3 CKA-ic results for Rubber III considering the isoconversion principle for the thermo-degradation reaction in an atmosphere of N_2 at 20 ml min^{-1} and non-isothermal conditions at heating rates of 5, 10, 15, 20, 30 and $40 \text{ }^\circ\text{C min}^{-1}$

Appendix L10

α	R^2	E (kJ/mol)	γ_E	$\ln(A / \text{min}^{-1})$	γ
0.20	0.9994	309	14	50	2
0.25	0.9997	284	12	46	2
0.30	0.9997	270	12	43	2
0.35	0.9997	261	11	42	2
0.40	0.9997	252	11	40	2
0.45	0.9997	249	11	39	2
0.50	0.9998	246	11	39	2
0.55	0.9995	240	12	38	2
0.60	0.9995	234	12	37	2
0.65	0.9993	230	13	36	2
0.70	0.9993	227	14	35	2
0.75	0.9990	223	15	35	2
0.80	0.9990	216	15	33	2
0.85	0.9986	211	16	33	2
0.90	0.9984	206	16	32	2
0.95	0.9980	205	17	31	3
Average	\bar{E} (kJ/mol)	241	$\gamma_{\bar{E}}$	28	
	$\ln(\bar{A} / \text{min}^{-1})$	38	$\gamma_{\ln \bar{A}}$	5	

Table L4 CKA-ic results for Rubber IV considering the isoconversion principle for the thermo-degradation reaction in an atmosphere of N_2 at 20 ml min^{-1} and non-isothermal conditions at heating rates of 5, 10, 15, 20, 30 and $40 \text{ }^\circ\text{C min}^{-1}$.

Appendix L11

α	R^2	E (kJ/mol)	γ_E	$\ln(A / \text{min}^{-1})$	$\gamma_{\ln A}$
0.20	0.9982	320	21	53	4
0.25	0.9974	292	23	48	4
0.30	0.9974	277	23	45	4
0.35	0.9969	269	24	44	4
0.40	0.9964	264	25	42	5
0.45	0.9960	258	25	41	5
0.50	0.9955	257	26	41	5
0.55	0.9951	251	27	40	5
0.60	0.9944	246	28	39	5
0.65	0.9937	243	29	38	5
0.70	0.9936	238	29	38	5
0.75	0.9924	234	30	37	5
0.80	0.9917	228	31	36	5
0.85	0.9905	223	32	35	6
0.90	0.9900	217	33	34	6
0.95	0.9913	220	31	34	5
Average	\bar{E} (kJ/mol)	252	$\gamma_{\bar{E}}$	27	
	$\ln(\bar{A} / \text{min}^{-1})$	40	$\gamma_{\ln \bar{A}}$	5	

Table L5 CKA-ic results for Rubber V considering the isoconversion principle for the thermo-degradation reaction in an atmosphere of N_2 at 20 ml min^{-1} and non-isothermal conditions at heating rates of 5, 10, 15, 20, 30 and $40 \text{ }^\circ\text{C min}^{-1}$.

Appendix L12

α	R^2	E (kJ/mol)	γ_E	$\ln(A / \text{min}^{-1})$	$\gamma_{\ln A}$
0.20	0.9963	340	20	55	4
0.25	0.9955	304	21	49	4
0.30	0.9948	291	22	47	4
0.35	0.9948	282	21	45	4
0.40	0.9950	272	21	43	4
0.45	0.9952	265	20	42	4
0.50	0.9953	262	19	41	4
0.55	0.9958	257	18	41	3
0.60	0.9958	254	18	40	3
0.65	0.9954	252	19	40	3
0.70	0.9955	248	19	39	3
0.75	0.9954	244	19	38	3
0.80	0.9954	239	19	37	3
0.85	0.9958	235	18	36	3
0.90	0.9951	232	19	36	3
0.95	0.9960	227	17	35	3
Average	\bar{E} (kJ/mol)	263	$\gamma_{\bar{E}}$	29	
	$\ln(\bar{A} / \text{min}^{-1})$	42	$\gamma_{\ln \bar{A}}$	5	

Table L6 CKA-ic results for Rubber VI considering the isoconversion principle for the thermo-degradation reaction in an atmosphere of N_2 at 20 ml min^{-1} and non-isothermal conditions at heating rates of 5, 10, 15, 20, 30 and $40 \text{ }^\circ\text{C min}^{-1}$.

Appendix L13

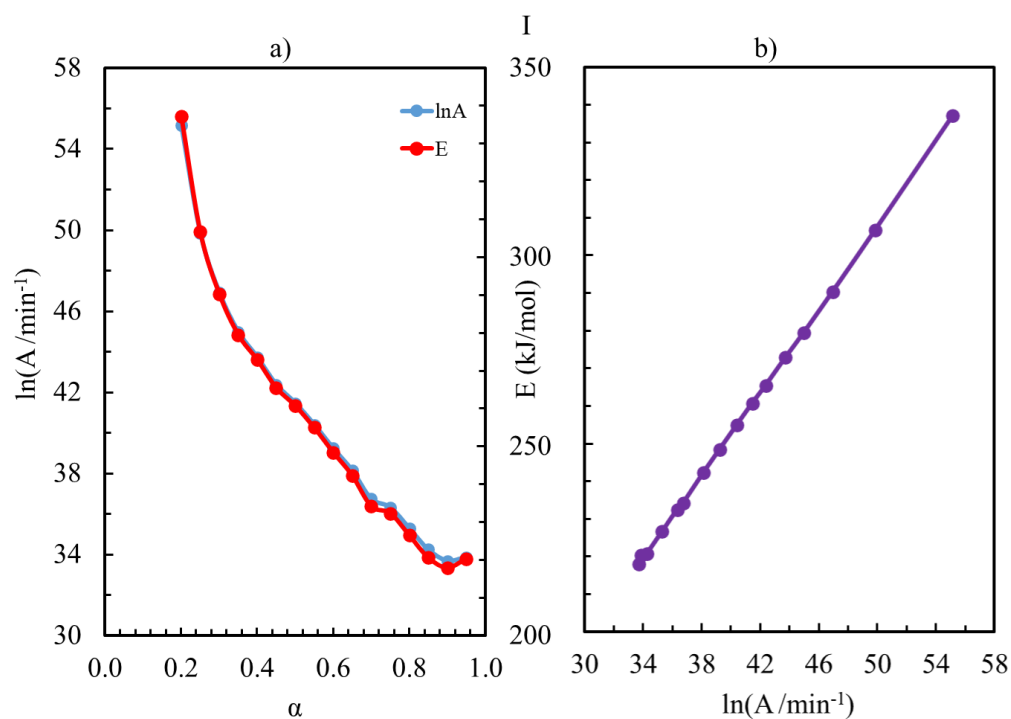


Figure L7 a) Behavior of the activation energy and frequency factor at different conversions. b) variation of the activation energy with the frequency factor. For Rubber I. Obtained with the CKA-ic method under non-isothermal conditions at heating rates of 5, 10, 15, 20, 30 and 40 $^{\circ}\text{C min}^{-1}$. for the thermo-degradation reaction in an atmosphere of N_2 at 20 ml min^{-1} .

Appendix L14

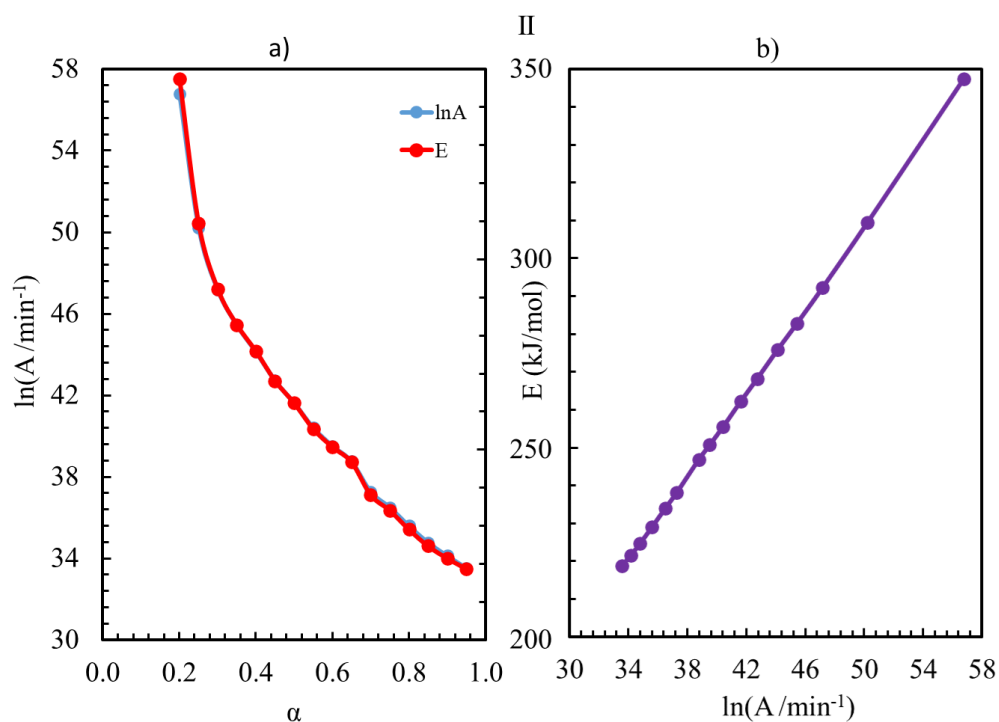


Figure L8 a) Behavior of the activation energy and frequency factor at different conversions. b) variation of the activation energy with the frequency factor. For Rubber II. Obtained with the CKA-ic method under non-isothermal conditions at heating rates of 5, 10, 15, 20, 30 and 40 $^{\circ}\text{C min}^{-1}$. for the thermo-degradation reaction in an atmosphere of N_2 at 20 ml min^{-1} .

Appendix L15

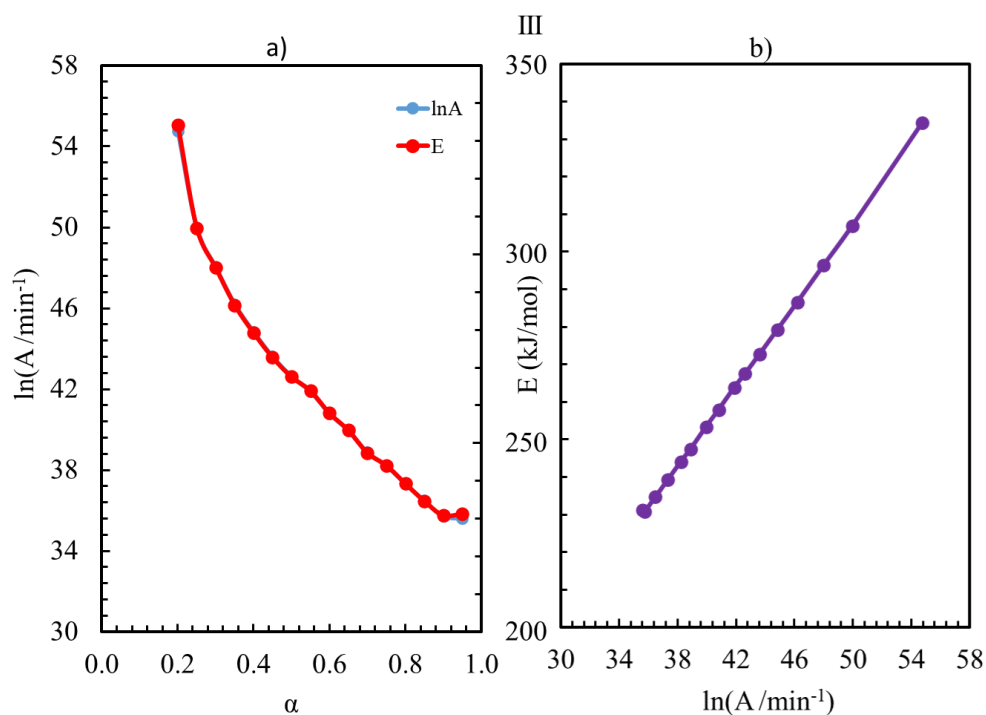


Figure L9 a) Behavior of the activation energy and frequency factor at different conversions. b) variation of the activation energy with the frequency factor. For Rubber III. Obtained with the CKA-ic method under non-isothermal conditions at heating rates of 5, 10, 15, 20, 30 and 40 °C min⁻¹. for the thermo-degradation reaction in an atmosphere of N₂ at 20 ml min⁻¹.

Appendix L16

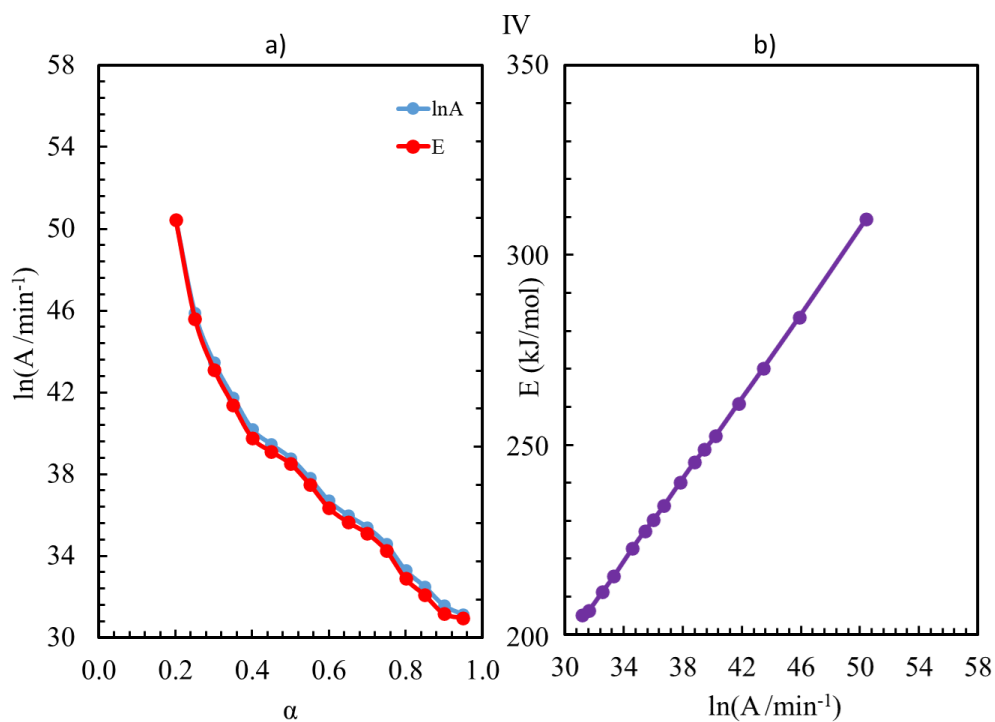


Figure L10 a) Behavior of the activation energy and frequency factor at different conversions. b) variation of the activation energy with the frequency factor. For Rubber IV. Obtained with the CKA-ic method under non-isothermal conditions at heating rates of 5, 10, 15, 20, 30 and 40 °C min⁻¹. for the thermo-degradation reaction in an atmosphere of N₂ at 20 ml min⁻¹.

Appendix L17

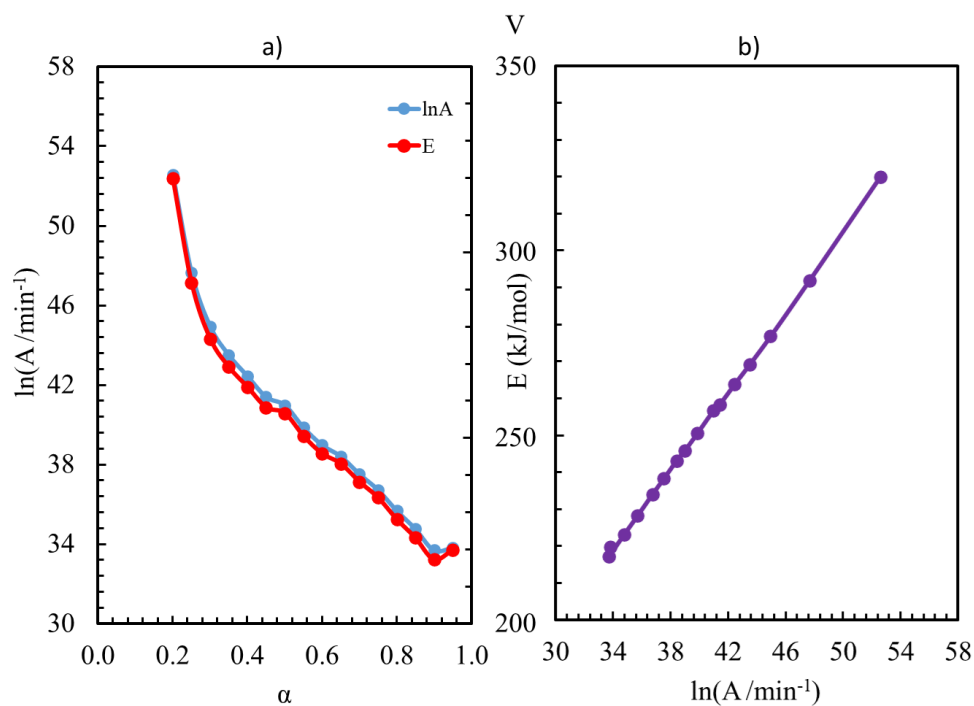


Figure L11 a) Behavior of the activation energy and frequency factor at different conversions. b) variation of the activation energy with the frequency factor. For Rubber V. Obtained with the CKA-ic method under non-isothermal conditions at heating rates of 5, 10, 15, 20, 30 and 40 °C min⁻¹. for the thermo-degradation reaction in an atmosphere of N₂ at 20 ml min⁻¹.

Appendix L18

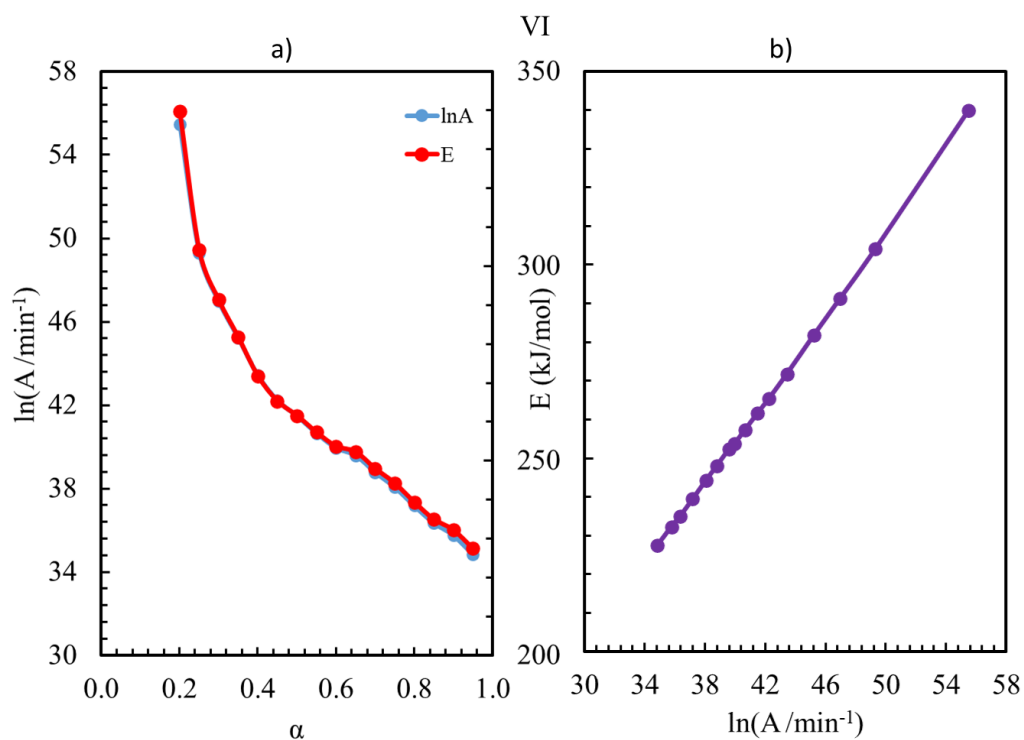
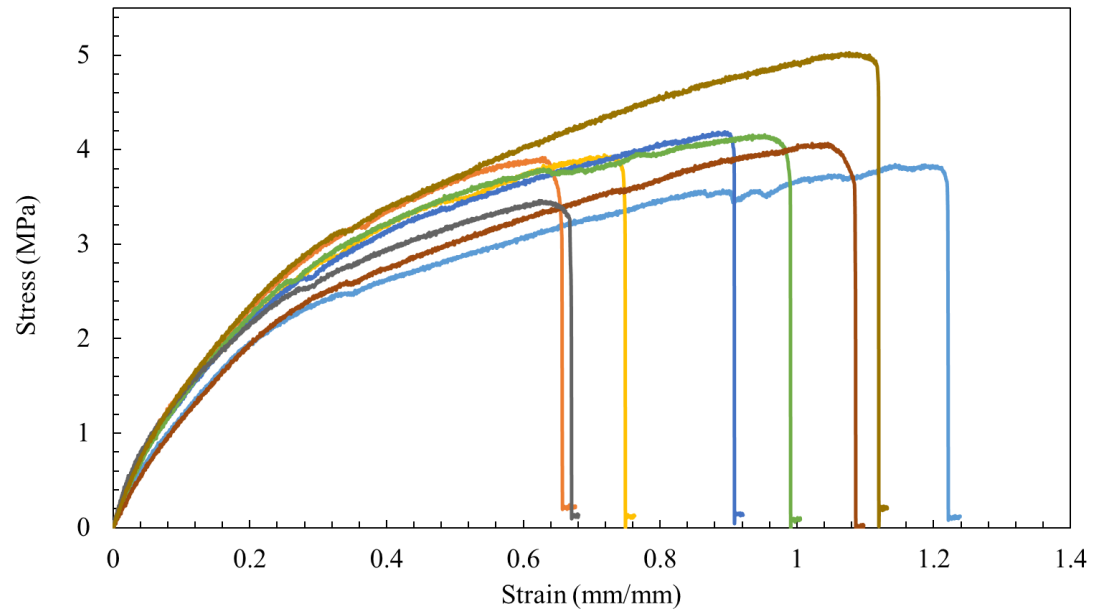


Figure L12 a) Behavior of the activation energy and frequency factor at different conversions. b) variation of the activation energy with the frequency factor. For Rubber VI. Obtained with the CKA-ic method under non-isothermal conditions at heating rates of 5, 10, 15, 20, 30 and 40 °C min⁻¹. for the thermo-degradation reaction in an atmosphere of N₂ at 20 ml min⁻¹.

Appendix M Supplementary material to support Chapter 5.5.2

Appendix M1

PUC-Rio - Certificação Digital Nº 1821742/CA

**Figure M1** Stress-strain curve Rubber I

Appendix M2

PUC-Rio - Certificação Digital Nº 1821742/CA

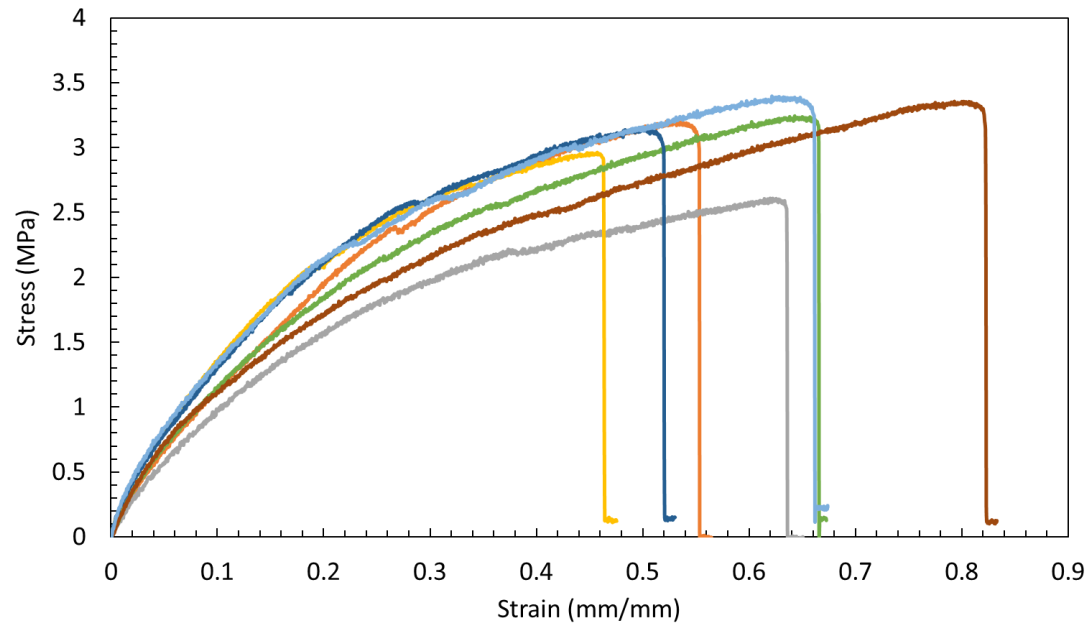


Figure M2 Stress-strain curve Rubber II

Appendix M3

PUC-Rio - Certificação Digital Nº 1821742/CA

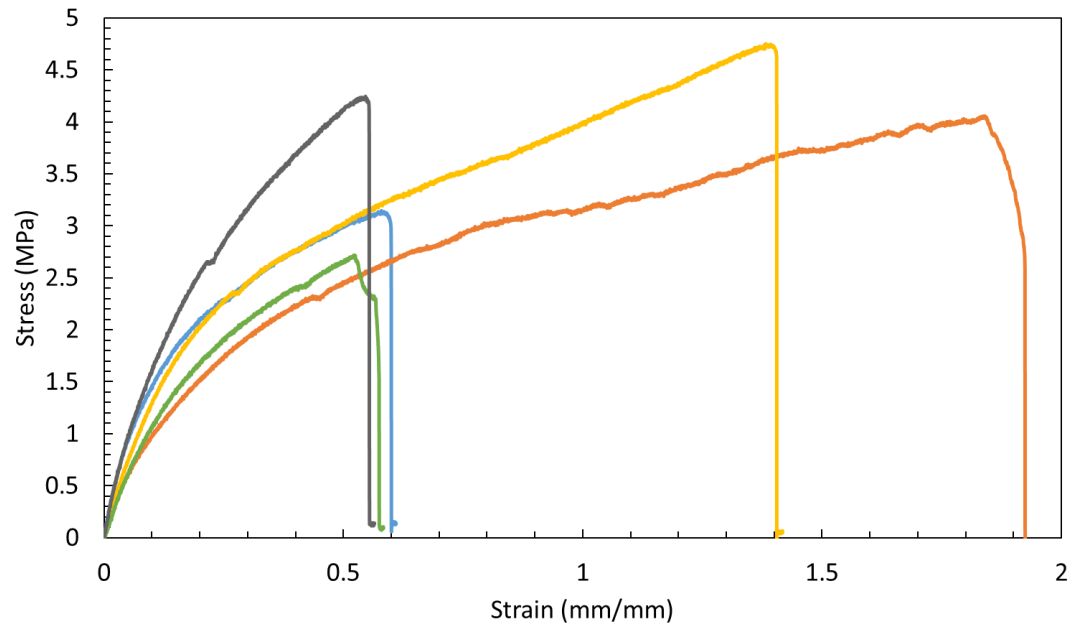


Figure M3 Stress-strain curve Rubber III

Appendix M4

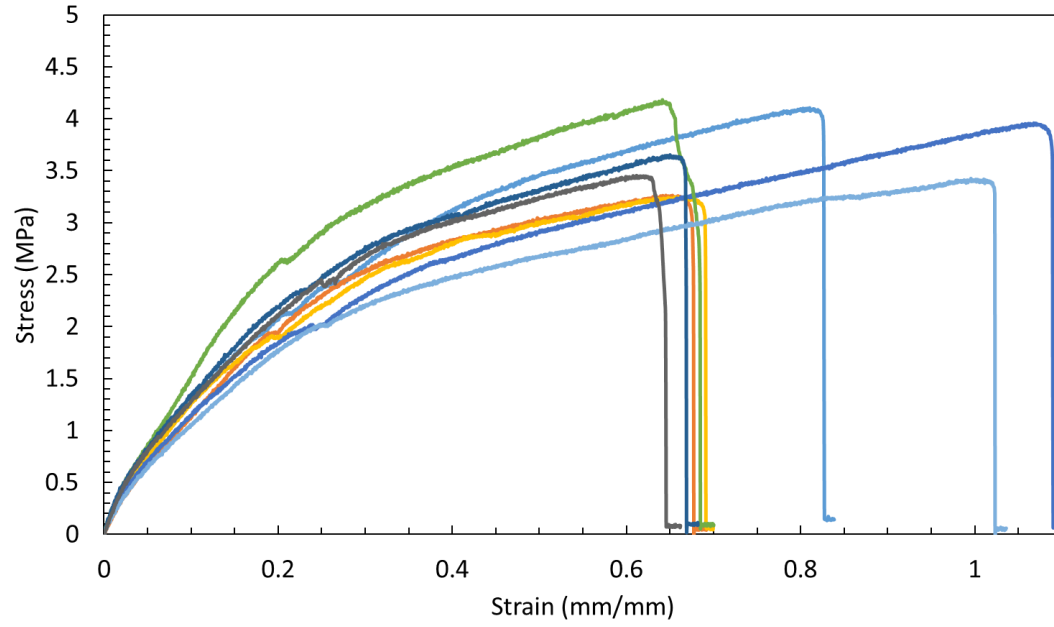


Figure M4 Stress-strain curve Rubber IV

Appendix M5

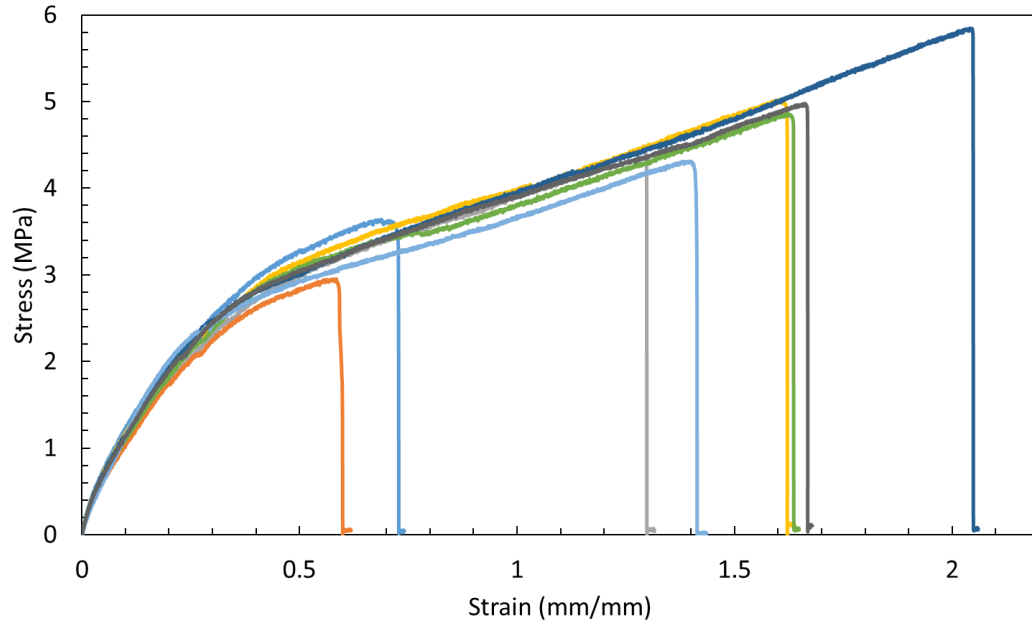


Figure M5 Stress-strain curve Rubber V

Appendix M6

PUC-Rio - Certificação Digital N° 1821742/CA

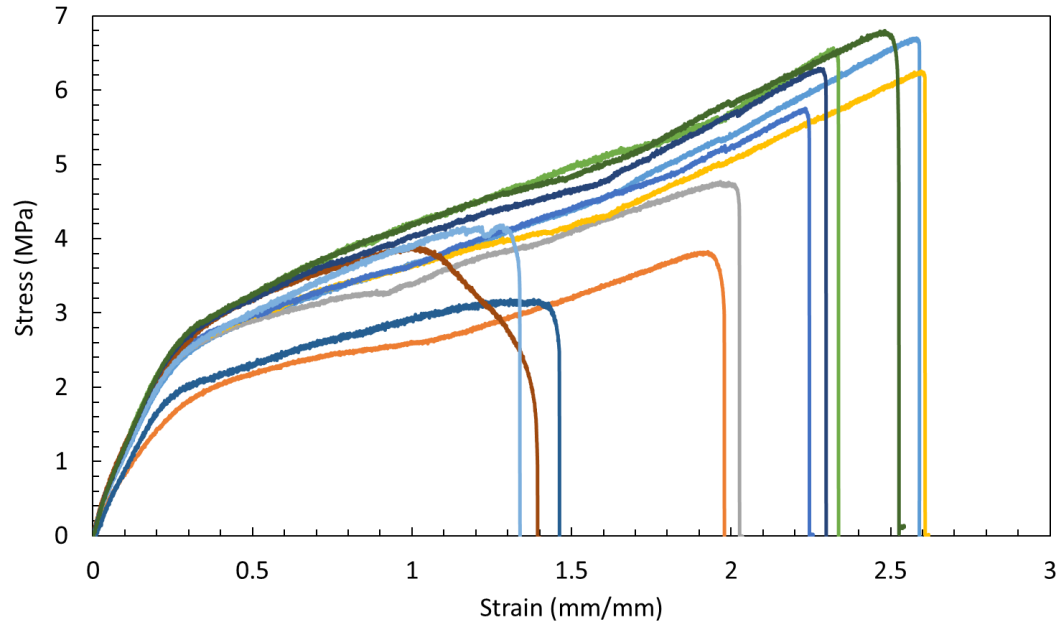


Figure M6 Stress-strain curve Rubber VI